
Exclusive Decays and Factorization in Flavour Physics

Gael Finauri

Vollständiger Abdruck der von der TUM School of Natural Sciences der Technischen Universität München zur Erlangung eines

Doktors der Naturwissenschaften (Dr. rer. nat.)

genehmigten Dissertation.

Vorsitz:

Prof. Dr. Peter Fierlinger

Prüfende der Dissertation:

1. Prof. Dr. Martin Beneke
2. Prof. Dr. Andreas Weiler

Die Dissertation wurde am 02.08.2024 bei der Technischen Universität München eingereicht und durch die TUM School of Natural Sciences am 17.10.2024 angenommen.

Abstract

We study the application of effective field theories to flavour physics. In particular we derive a factorization formula connecting the QCD light-cone distribution amplitude (LCDA) of a heavy meson to the universal LCDA defined in heavy quark effective theory (HQET). This formula allows to disentangle the perturbative heavy meson mass corrections from the hadronic physics at scales of order Λ_{QCD} . Our one-loop matching calculation allows to resum logarithms of the form $\alpha_s \ln(\Lambda_{\text{QCD}}/m_H)$, where m_H is the mass of a generic pseudoscalar heavy meson H . This is then applied, within the QCD factorization approach, to the \bar{B} and D meson LCDAs in the processes $W^\pm \rightarrow B^\pm \gamma$ and $\bar{B} \rightarrow DL$ respectively (L stands for a pseudoscalar light meson). The latter, in the so-called colour-suppressed tree topology, does not obey a factorization formula when $m_c \sim m_b$ is considered. Under the assumption $m_b \gg m_c \gg \Lambda_{\text{QCD}}$ we write down a factorization formula for colour-suppressed amplitudes which includes the D meson LCDA in QCD, allowing to provide theoretical predictions for such amplitudes.

Furthermore we extend the standard framework of QCD factorization for $\bar{B} \rightarrow D^{(*)+}L^-$ decays to include QED corrections by establishing a QED \times QCD factorization formula. The calculation of the one-loop hard-scattering kernels in QED allows us to give new numerical predictions for the colour-allowed tree topology effective amplitude $a_1(D^{(*)+}L^-)$. On top of the virtual corrections we also compute the effect of real ultrasoft photon radiation at the level of the decay rate. The latter turned out to be the dominant source of QED corrections.

In the last part we study the exotic possibility of having baryon number violation (BNV) in \bar{B} decays. Following a model independent approach we derive bounds on the BNV physical scale under the assumption that the new physics couples only to third generation quarks. The bounds are obtained from the experimental data on proton lifetime, computing the hypothetical proton decay mediated by a virtual b quark. With the derived bound on the BNV scale, a simple estimate excludes the possibility of observing BNV \bar{B} decays by a large margin.

Zusammenfassung

Wir untersuchen die Anwendung von effektiven Feldtheorien auf die Flavourphysik. Insbesondere leiten wir eine Faktorisierungsformel ab, die die QCD Lichtkegelverteilungsamplitude (LCDA) eines schweren Mesons mit der universellen LCDA verbindet, die in der Effektiven Theorie schwerer Quarks (HQET) definiert ist. Mit dieser Formel lassen sich die perturbativen Korrekturen der Masse schwerer Mesonen von der hadronischen Physik auf Skalen der Größenordnung Λ_{QCD} trennen. Unsere Ein-Schleifen-Matching-Berechnung ermöglicht die Resummation von Logarithmen der Form $\alpha_s \ln(\Lambda_{\text{QCD}}/m_H)$, wobei m_H die Masse eines generischen pseudoskalaren schweren Mesons H ist. Dies wird dann im Rahmen des QCD-Faktorisierungsansatzes auf die \bar{B} - und D -Meson-LCDAs in den Prozessen $W^\pm \rightarrow B^\pm \gamma$ und $\bar{B} \rightarrow DL$ (L steht für ein pseudoskalares leichtes Meson). Letztere, in der sogenannten farbunterdrückten Baumtopologie, gehorcht keiner Faktorisierungsformel, wenn $m_c \sim m_b$ betrachtet wird. Unter der Annahme $m_b \gg m_c \gg \Lambda_{\text{QCD}}$ schreiben wir eine Faktorisierungsformel für farbunterdrückte Amplituden auf, die die D -Meson LCDA in der QCD einbezieht und theoretische Vorhersagen für solche Amplituden ermöglicht.

Außerdem erweitern wir den Standardrahmen der QCD-Faktorisierung für $\bar{B} \rightarrow D^{(*)+}L^-$ -Zerfälle, um QED-Korrekturen einzubeziehen, indem wir eine QED \times QCD-Faktorisierungsformel aufstellen. Die Berechnung der Ein-Schleifen-Kerne der harten Streuung in der QED erlaubt es uns, neue numerische Vorhersagen für die effektive Amplitude $a_1(D^{(*)+}L^-)$ der farblich erlaubten Baumtopologie zu machen. Zusätzlich zu den virtuellen Korrekturen berechnen wir auch den Effekt der reellen ultraweichen Photonenstrahlung auf der Ebene der Zerfallsrate. Letztere erwies sich als die dominante Quelle der QED-Korrekturen.

Im letzten Teil untersuchen wir die exotische Möglichkeit einer Baryonenzahlverletzung (BNV) in \bar{B} -Zerfällen. Nach einem modellunabhängigen Ansatz leiten wir Grenzen für die physikalische Skala der BNV unter der Annahme, dass die neue Physik nur an Quarks der dritten Generation koppelt, ab. Die Grenzen werden aus den experimentellen Daten zur Protonenlebensdauer gewonnen, wobei der hypothetische Protonenzerfall, der durch ein virtuelles b -Quark vermittelt wird, berechnet wird. Mit der abgeleiteten Schranke für die BNV-Skala schließt eine einfache Schätzung die Möglichkeit der Beobachtung von BNV \bar{B} -Zerfällen mit großem Abstand aus.

Contents

I	Effective Field Theories in Flavour Physics	1
1	Introduction	2
1.1	Outline	5
2	Theoretical Framework and Effective Field Theories	6
2.1	Weak Effective Theory	6
2.2	Heavy Quark Effective Theory	7
2.2.1	Decay Constant Matching	9
2.3	Soft-Collinear Effective Theory	10
2.3.1	Method of Regions	10
2.3.2	Construction of the Leading Power SCET Lagrangian	14
2.3.3	Multipole Expansion	18
2.3.4	Arising of Non-Localities	18
2.3.5	Gauge Transformations	20
2.3.6	Wilson Lines	21
2.4	Boosted HQET	22
2.4.1	bHQET from HQET	24
2.4.2	bHQET from SCET	25
2.4.3	Soft-Collinear Fields	26
2.4.4	Decay Constant Matching in the Boosted Frame	27
2.5	Decoupling Transformations	28
2.5.1	In HQET and bHQET	29
2.5.2	In SCET	29
2.6	Reparametrization Invariance	30
2.7	Standard Model Effective Field Theory	31
2.8	Introduction to QCD Factorization	33
2.8.1	Factorization Formula for $\bar{B} \rightarrow M_1 M_2$	33
II	Mass Effects of Boosted Heavy Mesons	37
3	QCD Light-Cone Distribution Amplitudes for Heavy Mesons	38
3.1	The QCD LCDA	39

3.2	The HQET LCDA	41
3.2.1	Renormalization Group Evolution	41
3.2.2	Normalization and Cut-Off Moments	42
3.2.3	Asymptotic Behaviours	42
3.3	Matching	42
3.3.1	Peak Region	44
3.3.2	Tail Region	50
3.3.3	Merging of the Peak and Tail	54
3.4	Properties of the QCD LCDA	55
3.4.1	Endpoint Behaviour	56
3.4.2	Normalization	56
3.4.3	Evolution Equation	56
3.4.4	Comparison with Previous Works	58
3.5	Numerical Models for \bar{B} and D Meson QCD LCDAs	59
3.5.1	Input HQET LCDA and Evolution to the Matching Scale	59
3.5.2	QCD LCDA Initial Condition at the Matching Scale	61
3.5.3	Evolution to the Hard Scale	63
3.6	On the Normalization of the QCD LCDA	64
3.6.1	Log Analysis of the Cut-Off Moment	65
3.6.2	Improved Evolution	68
3.6.3	Numerical Comparisons of M_0	69
3.6.4	Large Meson Mass Limit	71
4	Branching Fraction of $W^\pm \rightarrow B^\pm \gamma$ Decays	74
4.1	Comparison with QCD Factorization	76
4.2	Comparison with HQET Factorization	77
4.2.1	Cross-Check with HQET Factorization	78
5	Colour-Suppressed $\bar{B} \rightarrow DL$ Decays	81
5.1	Power Counting of the Amplitudes	82
5.2	Region Analysis	84
5.2.1	Hard-Collinear Region	86
5.2.2	Anti-Hard-Collinear Region	86
5.2.3	Soft Region	86
5.2.4	Anti-Ultrasoft-Collinear Region	87
5.3	Factorization Formula for T and C Amplitudes	87
5.4	Phenomenology	89
5.4.1	D Meson LCDA Model Dependence	91
5.4.2	Comparison with Data	91

III	QED Corrections in B Decays	95
6	QED \times QCD Factorization in $\bar{B} \rightarrow D^{(*)}L$	96
6.1	Factorization Formula	97
6.1.1	Matching Equation	97
6.1.2	SCET \times HQET Renormalization Kernels	101
6.1.3	Hard-Scattering Kernels	103
6.1.4	Hadronic Matrix Elements	104
6.2	Semi-Leptonic $\bar{B} \rightarrow D^{(*)+}\ell^-\bar{\nu}_\ell$ Decay	105
6.2.1	Factorization Formula for Semi-Leptonic Decay	105
6.2.2	Physical Form Factor	107
7	Radiative Amplitude and Numerical Analysis	109
7.1	Ultrasoft Effects	109
7.2	Numerical Analysis	112
7.2.1	QED Corrections to Non-Radiative Amplitude	112
7.2.2	Non-Leptonic to Semi-Leptonic Decay Rates Ratios	115
IV	Baryon Number Violation	118
8	Possibility of Observing Baryon Number Violating B Decays?	119
8.1	Constraints on Light-Flavoured BNV Operators	121
8.2	Third Family BNV Operators	123
8.2.1	Operators with Left-Handed b Quark	123
8.2.2	Operators with Right-Handed b Quark	124
8.2.3	Operators Including Second Family Quarks	126
8.2.4	Weak Effective Hamiltonian	127
8.2.5	Local Six-Fermion Operators	127
8.3	Proton Decay Rate	128
8.3.1	Leptonic Decay: $p \rightarrow \ell^+\nu_\ell\bar{\nu}$	129
8.3.2	Two-Body Decay: $p \rightarrow \pi^+\bar{\nu}$	132
8.3.3	Two-Body Decay: $p \rightarrow \pi^0\ell^+$	134
8.3.4	Estimate of τ Mediated $p \rightarrow \ell^+\nu_\ell\bar{\nu}_\tau$ Decay	136
8.4	Inclusive BNV B Decays Estimates	138
V	Conclusions	140
9	Summary and Outlook	141

VI	Appendices	143
A	Numerical Inputs	144
B	Details of the SCET to bHQET Matching	148
	B.1 SCET Matrix Element	148
	B.2 bHQET Matrix Element	149
	B.3 Peak Region	150
	B.4 Tail Region	151
C	Details on QED Factorization	153
	C.1 Individual Diagrams for One-Loop Matching	153
	C.2 Convolutd Kernels	155
D	Pion and Proton Decay Matrix Elements	157
	D.1 Pseudoscalar Meson	157
	D.2 Proton	158
	Bibliography	159

Part I

Effective Field Theories in Flavour
Physics

Chapter 1

Introduction

Our understanding of the nature of fundamental interactions has undergone remarkable evolution over the past century. The Standard Model (SM) of particle physics [1–4] is the theory governing the dynamics of the electromagnetic, weak and strong interactions among particles. With the discovery of the Higgs boson [5, 6], in 2012, its last missing element found experimental evidence. Over the last decades the SM’s remarkable predictive power has aligned with experimental observations, yielding spectacular confirmations of its validity. However, crucial questions remain unanswered, necessitating an extension of the SM. By construction, gravity is not included in the SM, being irrelevant at the microscopic scale at the energies accessible in Earth-based experiments. Also, the observed matter-antimatter asymmetry in the Universe cannot be explained within the SM. Furthermore, several cosmological observations suggests that the particle content of the SM is only a small fraction of the total matter in the Universe, being dominated by dark matter [7]. While neutrinos are intrinsically massless particles in the SM, experimental evidences for their oscillation [8, 9] require a non-vanishing mass.

These compelling questions motivate the quest for New Physics (NP). The strategy for unraveling the nature of NP is twofold. A natural way would be to push the experimental energy ranges to so far unexplored regions, hoping for a direct detection of new particles. A second possibility is to indirectly detect NP by observing consistent deviations on known or rare processes between experimental measurements and SM predictions. In order to make this possible it is hence required that both the experimental and theoretical results are obtained with constantly increasing precision.

The intricacies of Quantum Field Theory (QFT) make the extraction of precise theoretical predictions a daunting task. When dealing with weakly coupled theories, the natural approach is to organize the calculation as a series expansion in the small coupling constants. However the magnitude of the coupling constants depends on the energy scale at which the physical process takes place. Indeed one of the biggest challenges comes from the intrinsic nature of Quantum Chromodynamics (QCD), governing the laws of the strong interaction, which becomes perturbative (i.e. small coupling constant) only for energies above a few times the proton mass. This phenomenon is called asymptotic freedom [10], and allows us to compute order by order in perturbation theory the strong interaction effects

between the fundamental particles: quarks and gluons. On the other hand, for energies of the order of the proton mass and below, the coupling constant α_s dangerously approaches unity, and the perturbative expansion is not a viable option anymore. This defines the non-perturbative regime of QCD, responsible for the confinement of quarks and gluons into colourless¹ hadrons.

Among the precision tests of the SM, flavour physics² is the study of the interactions between different particle generations, which in the unbroken phase of the SM is due solely to interactions with the Higgs field, the Yukawa interaction. In particular the phenomenology of hadrons involving the bottom quark b (B -physics), has proven to be an exciting field in recent years due to the increasing amount of experimental measurements from B -factories like BaBar [11], Belle [12] and Belle II [13] as well as the LHCb [14] experiment at CERN. During the last 10 years several observables started to present tensions with respect to their SM predictions, going under the name of “ B -anomalies” or in general “flavour anomalies” [15–18]. Although the striking lepton flavour universality tests, R_K and R_K^* [19], got resolved from the latest experimental update from LHCb [20, 21], other anomalies in $b \rightarrow c\tau\nu_\tau$ and purely hadronic decays persist [16, 22, 23] requiring further investigations. As theorists, our goal is to produce robust and reliable theoretical predictions to be compared with present and future experimental measurements, in order to either solve or enhance the significance of such anomalies. Having under control the SM contributions and sources of theoretical uncertainties is therefore a crucial and unavoidable step towards potential new discoveries.

The success of B -physics partly relies on the heavy mass $m_b = 4.8$ GeV [24] of the b quark, which provides an intrinsic perturbative scale, and also allows to perform a power expansion in Λ_{QCD}/m_b , where $\Lambda_{\text{QCD}} \approx \mathcal{O}(300$ MeV) is the hadronic scale at which α_s becomes formally infinite. Nevertheless, perturbation theory presents a well known issue when applied to multi-scale processes. Suppose we would like to compute the decay of a heavy particle of mass M into much lighter particles with mass $m \ll M$, as a perturbative expansion in the coupling constant α . In the perturbative series terms of the form³ $\alpha \ln(m/M)$ will appear to all orders, and for largely separated scales the *large logarithms* will spoil the convergence of the perturbative expansion. The solution to this problem is provided by the so-called renormalization group improved perturbation theory, which is the technique employed to resum such potential $\mathcal{O}(1)$ terms to all orders in the coupling constant. This procedure employs the renormalization group equations (RGEs) and goes under the name of *resummation*.

In order to gain a practical understanding of how this is applied to our example we need to introduce the concept of Effective Field Theories (EFTs) (see for example Refs. [25–27] and references therein). The purpose of EFTs is to disentangle the physics of different

¹The charge associated to the strong interaction is the *colour*.

²The SM matter content is divided into three copies sharing the same spin and gauge quantum numbers, which we call generations or families. With the term *flavour* we distinguish particles belonging to different generations.

³Even double logarithmic terms of the form $\alpha \ln^2(m/M)$ could be present, but the argumentation does not change.

scales by *integrating out* the high-energy degrees of freedom and describing the process only through the relevant low-energy degrees of freedom. In this sense, every physical theory from Newtonian mechanics to the SM is an EFT, given the absence of a complete theory of Nature. The effect of high-energy degrees of freedom is encoded in Wilson coefficients capturing the dependence from the hard scale that has been integrated out. The operation that fixes the Wilson coefficients, called *matching*, consists in comparing the same amplitude computed in the full theory and in the EFT and requiring that the two agree, in the regime of validity of the EFT. The power of EFTs is therefore employed for deriving *factorization theorems*, which in our simple example at the level of the scattering amplitude would take the form

$$i\mathcal{A}(M, m) = C(M, \mu) \times i\mathcal{A}_{\text{EFT}}(m, \mu) + \mathcal{O}\left(\frac{m}{M}\right), \quad (1.1)$$

where μ is the factorization scale coming from dimensional regularization⁴, and its dependence is cancelled⁵ between C and \mathcal{A}_{EFT} . As the EFT relies on an expansion in the region $m \ll M$, the result is valid up to *power corrections* of order $\mathcal{O}(m/M)$, which can be in principle systematically computed order by order. The Wilson coefficient $C(M, \mu)$, capturing the dependence on the hard scale M , can usually be computed in perturbation theory (if the scale M is in the perturbative regime of the full theory) and will contain terms of the form $\alpha \ln(\mu/M)$. Thus the matching has to be performed at a factorization scale $\mu = \mu_M \sim \mathcal{O}(M)$ to not spoil the convergence of the perturbative series. On the other hand the EFT matrix element $\mathcal{A}_{\text{EFT}}(m, \mu)$, carrying the dependence on the light scale m , would have to be evaluated at its natural scale $\mu = \mu_m \sim \mathcal{O}(m)$, in the regime of validity of the EFT. By computing and solving the RGE for $C(M, \mu)$ one can express the Wilson coefficient evaluated at the low scale μ_m in terms of the one evaluated at the high scale μ_M

$$C(M, \mu_m) = C(M, \mu_M)U(\mu_M, \mu_m), \quad (1.2)$$

where the evolution factor $U(\mu_M, \mu_m)$ contains the effects of the $\mathcal{O}(\alpha^n \ln^n(\mu_m/\mu_M))$ terms resummed to all orders. As a result the renormalization group improved expression for the factorized amplitude takes the form

$$i\mathcal{A}(M, m) = C(M, \mu_M)U(\mu_M, \mu_m) \times i\mathcal{A}_{\text{EFT}}(m, \mu_m) + \mathcal{O}\left(\frac{m}{M}\right), \quad (1.3)$$

where the convergence of the perturbative series is restored.

The works presented in this thesis heavily rely on the concepts outlined here, with appropriate generalizations to the specific EFTs and hierarchies of scales posed by the physical process under investigation.

⁴One could of course choose different regularizations, but dimensional regularization is the most convenient one for the topics discussed in this thesis and will be used in the following.

⁵For simplicity of the example we have considered a UV finite amplitude in the full theory, otherwise \mathcal{A} would also carry a dependence on a UV renormalization scale ν .

1.1 Outline

The outline of this thesis is as follows. In Chapter 2 we review some of the basic theoretical concepts and tools useful for the understanding of the works reported in the rest of the thesis. In Chapter 3 we perform a perturbative matching of the light-cone distribution amplitude (LCDA) of a generic heavy meson from QCD to heavy quark effective theory (HQET). This allows to factorize the heavy mass dependence into perturbatively calculable functions, leaving the non-perturbative physics to be encoded in the universal leading-twist HQET LCDA. The results are applied, in Chapter 4, to the process $W^\pm \rightarrow B^\pm \gamma$, where in QCD factorization the B meson LCDA appears. The works of both Chapter 3 and 4 were originally published in Ref. [28]. On the other hand, ongoing works on the application of the LCDA matching to two-body non-leptonic $\bar{B} \rightarrow DL$ decays in the colour-suppressed tree topology are presented in Chapter 5.

Changing topic to QED corrections, Chapter 6 presents the study on QED \times QCD factorization in $\bar{B} \rightarrow D^{(*)+} L^-$ decays, which together with the phenomenological analysis of Chapter 7, is published in Ref. [29]. We compute both virtual $\mathcal{O}(\alpha_{em})$ structure-dependent corrections from scales of the order of the bottom mass, and real radiation corrections coming from ultrasoft photons of energies much lower than the hadronic scale Λ_{QCD} .

In light of the flavour anomalies mentioned in the introduction, Chapter 8 investigates baryon number violation (BNV) in a scenario where the unknown new physics presents highly generation dependent couplings, in particular generating BNV interactions only when third family quarks are involved. Under this assumption we ask ourselves whether BNV B meson decays could be in the reach of experimental measurements in the near future. Based on the work published in Ref. [30], we find that the very tight constraints from proton stability indirectly induce sever bounds on the scale of new physics, making the direct observation of BNV B decays practically impossible.

A slightly off-topic work (published in Ref. [31]) on the extraction of $|V_{cb}|$ from inclusive semi-leptonic $\bar{B} \rightarrow X_c \ell^- \bar{\nu}_\ell$ decays, with the inclusion of the recently measured dilepton invariant mass moments [32, 33], is not included in this thesis.

We conclude and summarize in Chapter 9, while several appendices contain technical details which could be useful for a closer study of the material presented in this thesis.

Chapter 2

Theoretical Framework and Effective Field Theories

In this chapter we are going to summarize the construction and important features of the EFTs largely used in the rest of this work. Every EFT is characterized by one, or more, small power counting parameters allowing to systematically expand the effective Lagrangian to the desired order.

Depending on the background of the reader, some sections might be skipped.

2.1 Weak Effective Theory

In the broken phase of the SM, the weak interaction is the only one responsible for flavour changing processes, thus playing a pivotal role in flavour physics. In fact we are already facing a net hierarchy of scales between the electroweak scale set by the masses of the weak bosons W^\pm/Z , and the masses of the decaying hadrons. In the energy range typical of hadron decays, the weak bosons will only contribute as short-distance virtual particles, enabling us to integrate them out. The EFT resulting from the SM after having integrated out the weak bosons, together with the top quark and Higgs field, is the Weak Effective Theory (WET)¹ [34], the generalization of Fermi theory of weak interactions [35].

For simplicity we report here the effective Hamiltonian for processes mediated by the hadronic $b \rightarrow \bar{c}uq$ charged current ($q = \{d, s\}$)

$$\mathcal{H}_{\text{eff}} = \frac{G_F}{\sqrt{2}} V_{cb} V_{uq}^* (C_1 Q_1 + C_2 Q_2) + \text{h.c.}, \quad (2.1)$$

as it will be the relevant one for hadronic two-body $\bar{B} \rightarrow D^{(*)}$ decays studied in Chapters 5 and 6. We work in the CMM operator basis [36, 37]

$$\begin{aligned} Q_1 &= [\bar{c}\gamma^\mu(1 - \gamma^5)T^a b][\bar{q}\gamma_\mu(1 - \gamma^5)T^a u], \\ Q_2 &= [\bar{c}\gamma^\mu(1 - \gamma^5)b][\bar{q}\gamma_\mu(1 - \gamma^5)u], \end{aligned} \quad (2.2)$$

¹Also often referred to as the Low-Energy Effective Field Theory (LEFT).

which has the advantage of allowing to consistently use fully anticommuting γ^5 at any loop order, but at leading order in G_F . T^a are the SU(3) colour generators in the fundamental representation, and colour and spinor indices are implicitly contracted within the brackets. In (2.1) V_{ij} are the Cabibbo-Kobayashi-Maskawa (CKM) [38, 39] matrix elements, and [24]

$$G_F = \frac{\sqrt{2}g_2^2}{8m_W^2} = 1.1663788(6) \cdot 10^{-5} \text{ GeV}^{-2} \quad (2.3)$$

the Fermi constant, with g_2 being the SU(2) coupling constant. The scale-dependent Wilson coefficients C_1 and C_2 are known up to NNLO in QCD [40].

In the following we will make use of the chiral projectors

$$P_L = \frac{1 - \gamma^5}{2}, \quad P_R = \frac{1 + \gamma^5}{2}, \quad (2.4)$$

satisfying $P_L^2 = P_L$, $P_R^2 = P_R$ and $P_L P_R = P_R P_L = 0$.

2.2 Heavy Quark Effective Theory

In \bar{B} meson decays, one faces processes involving the interactions between a heavy quark² h and light degrees of freedom given by gluons and light quarks. The hard scale is now set by the heavy mass, $m_h \gg \Lambda_{\text{QCD}}$, and we would like to develop an effective theory where this scale is integrated out, i.e. taking the formal $m_h \rightarrow \infty$ limit. This theory, first constructed in 1990 [41, 42], is called Heavy Quark Effective Theory (HQET) and produced many important quantitative results over the last 35 years (see e.g. Refs. [43, 44] and references therein).

The peculiarity of this EFT is that we are not integrating out a particle, which therefore would not appear anymore in Feynman diagrams, but a *mode*. In particular we want to integrate out (freeze) the large momentum component of the heavy quark of order $\mathcal{O}(m_h)$. This results in a theory where the heavy quark is described by a velocity dependent static field. The concept of momentum modes will be crucial in the framework of Soft-Collinear Effective Theory (SCET), which we will treat in Section 2.3.

We now review the construction of the leading power³ (LP) HQET Lagrangian for the heavy quark field ψ_h . The idea is that the heavy quark bounded in the heavy hadron will be almost on-shell and move roughly with the hadron four-velocity v^μ . Therefore we would like to split the h momentum as

$$p_h^\mu = m_h v^\mu + k^\mu, \quad (2.5)$$

where k^μ is a residual momentum of order $\mathcal{O}(\Lambda_{\text{QCD}})$ and $v^2 = 1$. We now introduce two fields

$$h_v(x) = e^{im_h v \cdot x} \frac{1 + \not{v}}{2} \psi_h(x), \quad H_v(x) = e^{im_h v \cdot x} \frac{1 - \not{v}}{2} \psi_h(x), \quad (2.6)$$

²In the case of $b \rightarrow c$ transitions we typically also consider the c as a heavy quark, but the generalization from one to two heavy quarks is trivial.

³This corresponds to the limit $m_h \rightarrow \infty$, while finite mass corrections can be systematically computed as an expansion in Λ_{QCD}/m_h (power corrections) through the inclusion of higher-dimensional operators.

such that the full QCD field can be expressed as

$$\psi_h(x) = e^{-im_h v \cdot x} [h_v(x) + H_v(x)]. \quad (2.7)$$

At the level of the fields the splitting of the momentum is implemented through the exponential prefactor, which strips off the large momentum component from the full field

$$i\partial_\mu \psi_h(x) = m_h v_\mu \psi_h(x) + e^{-im_h v \cdot x} [i\partial_\mu h_v(x) + i\partial_\mu H_v(x)], \quad (2.8)$$

showing that parametrically $i\partial_\mu$ acting on the EFT fields scales like Λ_{QCD} . By construction, the fields satisfy the conditions

$$\not{v} h_v(x) = h_v(x), \quad \not{v} H_v(x) = -H_v(x), \quad (2.9)$$

suggesting that we are splitting the full field into its particle and anti-particle components with respect to the hard mode. We will show that the $H_v(x)$ field component is suppressed, and the goal is to integrate it out, leaving $h_v(x)$ as our degree of freedom in the low-energy EFT.

We express the QCD Lagrangian for the heavy quark in terms of the new fields

$$\begin{aligned} \mathcal{L}_{\text{QCD}} &= \bar{\psi}_h(x) (i\not{D} - m_h) \psi_h(x) = [\bar{h}_v(x) + \bar{H}_v(x)] (i\not{D} + m_h \not{v} - m_h) [h_v(x) + H_v(x)] \\ &= \bar{h}_v(x) i\nu \cdot D h_v(x) - \bar{H}_v(x) (i\nu \cdot D + 2m_h) H_v(x) \\ &\quad + \bar{H}_v(x) i\not{D}_\perp h_v(x) + \bar{h}_v(x) i\not{D}_\perp H_v(x), \end{aligned} \quad (2.10)$$

where $iD_\mu = i\partial_\mu + g_s A_\mu^a(x) T^a$ and $g_s = \sqrt{4\pi\alpha_s}$ is the SU(3) coupling constant. In (2.10) we used the projection properties of the EFT fields to simplify the expression, and in this context $D_\perp^\mu = D^\mu - v^\mu (v \cdot D)$. In order to derive the effective Lagrangian we can integrate out at tree level the H_v component using the equation of motion

$$(i\nu \cdot D + 2m_h) H_v(x) = i\not{D}_\perp h_v(x), \quad (2.11)$$

from which one can formally write

$$H_v(x) = \frac{1}{i\nu \cdot D + 2m_h} i\not{D}_\perp h_v(x), \quad \bar{H}_v(x) = -\bar{h}_v(x) i\overleftarrow{\not{D}}_\perp \frac{1}{-i\nu \cdot \overleftarrow{D} + 2m_h}, \quad (2.12)$$

where the arrow indicates that the covariant derivative is acting on the left. From (2.12) we can indeed deduce that $H_v(x)$ is suppressed by a factor of Λ_{QCD}/m_h with respect to the field $h_v(x)$. Inserting (2.12) into (2.10) we get

$$\begin{aligned} \mathcal{L}_{\text{HQET}} &= \bar{h}_v(x) i\nu \cdot D h_v(x) + \bar{h}_v(x) i\not{D}_\perp \frac{1}{i\nu \cdot D + 2m_h} i\not{D}_\perp h_v(x) \\ &= \bar{h}_v(x) i\nu \cdot D h_v(x) + \mathcal{O}\left(\frac{\Lambda_{\text{QCD}}}{m_h}\right), \end{aligned} \quad (2.13)$$

where the inverse derivative is associated to non-local terms, as we will explain in Section 2.3.4, but in this case can be expanded in a tower of local operators since $iD^\mu/m_h \sim \mathcal{O}(\Lambda_{\text{QCD}}/m_h)$.

The leading power HQET Lagrangian describes the interactions between a static field $h_v(x)$ and soft gluons with virtualities⁴ $\mathcal{O}(\Lambda_{\text{QCD}}^2)$. In other words the hard gluons have been integrated out together with the heavy mass, and the leftover soft interactions do not change the velocity v of the heavy quark. This modal interpretation will become clearer with the introduction of Soft-Collinear Effective Theory in Section 2.3.

2.2.1 Decay Constant Matching

As an example of application of HQET we consider the simple matching of the decay constant of a pseudoscalar heavy meson H from QCD [45]. The decay constants in QCD and HQET, f_H and $f_H^{\text{HQET}}(\mu)$ respectively, are defined through the matrix elements

$$\begin{aligned}\langle H(p_H) | \bar{\psi}_h(0) \gamma^\mu \gamma^5 q(0) | 0 \rangle &= -i f_H p_H^\mu, \\ \langle H(p_H) | \bar{h}_v(0) \gamma^\mu \gamma^5 q_s(0) | 0 \rangle &= -i f_H^{\text{HQET}}(\mu) m_H v^\mu,\end{aligned}\tag{2.14}$$

where we choose to use standard QCD normalization for the external states. The light-quark field q_s in HQET is a “soft field”, meaning that can have only momenta of order Λ_{QCD} or lower, since all the high-energy fluctuations $\mathcal{O}(m_h)$ of QCD have been integrated out. The one-loop matching gives a relation between the operators [44]

$$\bar{\psi}_h(0) \gamma^\mu \gamma^5 q(0) = C_V(\mu) \bar{h}_v(0) \gamma^\mu \gamma^5 q_s(0) + C_S(\mu) v^\mu \bar{h}_v(0) \gamma^5 q_s(0),\tag{2.15}$$

with Wilson coefficients

$$\begin{aligned}C_V(\mu) &= 1 - \frac{\alpha_s C_F}{4\pi} \left(\frac{3}{2} \ln \frac{\mu^2}{m_h^2} + 4 \right) + \mathcal{O}(\alpha_s^2), \\ C_S(\mu) &= 2 \frac{\alpha_s C_F}{4\pi} + \mathcal{O}(\alpha_s^2).\end{aligned}\tag{2.16}$$

Using the projection properties of the EFT field h_v we can show

$$\langle H(p_H) | \bar{h}_v(0) \gamma^5 q_s(0) | 0 \rangle = \langle H(p_H) | \bar{h}_v(0) \not{v} \gamma^5 q_s(0) | 0 \rangle = -i f_H^{\text{HQET}} m_H.\tag{2.17}$$

Finally taking the matrix element of the matching equation (2.15) between the vacuum and the H meson state, and employing (2.17), results in the well known relation [45]

$$f_H = f_H^{\text{HQET}}(\mu) \left[1 - \frac{\alpha_s C_F}{4\pi} \left(\frac{3}{2} \ln \frac{\mu^2}{m_h^2} + 2 \right) + \mathcal{O}(\alpha_s^2) \right].\tag{2.18}$$

⁴With “virtuality” of a particle of momentum p we mean the scaling of p^2 , and it usually refers to virtual particles.

2.3 Soft-Collinear Effective Theory

Precision physics in \bar{B} decays was the trigger for the development of Soft-Collinear Effective Theory (SCET) [46–52] in the early 2000s (for pedagogical reviews see e.g. Refs. [53, 54]). This theory describes collinear particles, namely energetic particles with “almost” light-like momenta, and their interactions. The remaining degrees of freedom are low-energy (soft) particles which are however unable to affect the directions of the collinear ones. In this sense one can draw a similarity with HQET where the leftover soft interactions cannot change the frozen velocity of the heavy quark. Since the first works in B -physics, the scope of applications of SCET has extended to collider physics, jet physics, electroweak resummation and only recently to soft theorems in gravity [55].

In this work we will only need two collinear directions, but the generalization to multiple directions is possible. The starting point is thus to define two light-like reference vectors n_-^μ and n_+^μ satisfying

$$n_-^2 = 0, \quad n_+^2 = 0, \quad n_- \cdot n_+ = 2, \quad (2.19)$$

which define the *collinear* (n_-) and *anti-collinear* (n_+) directions. A generic four-vector p^μ can hence be decomposed into

$$p^\mu = n_+ p \frac{n_-^\mu}{2} + p_\perp^\mu + n_- p \frac{n_+^\mu}{2}, \quad (2.20)$$

where $n_\pm p \equiv n_\pm \cdot p$ and the \perp does not need to be confused with the one in (2.10) related to the velocity in HQET. It will turn out useful to denote vectors in terms of their components with respect to the decomposition (2.20) in the form $p = (n_+ p, p_\perp, n_- p)$, from which, in the case of a momentum, one can easily compute the virtuality as

$$p^2 = (n_+ p)(n_- p) + p_\perp^2. \quad (2.21)$$

We now have to define the power counting parameter in order to consistently build the leading power SCET Lagrangian. However depending on the physical process under investigation, different variants of SCET might be needed. To illustrate this concept it is more instructive to first review the so-called *method of regions*.

2.3.1 Method of Regions

In order to pin down the correct EFT that will reproduce the infrared (IR) behaviour of the full theory, we rely on the powerful method of regions [56, 57]. The method of regions allows to decompose a dimensionally regulated multi-scale Feynman integral into single-scale integrals⁵ in a power expansion in the scales ratios. Whenever an integral depends on a hierarchy of scales, we might be interested only in the asymptotic behaviour of the result, namely in its expansion in the small ratios of scales. We would be therefore tempted to exchange the order of operations, first expanding the integrand and then solving a simpler

⁵This is true when all the scales are largely separated. By “single-scale integrals” we therefore intend here integrals where all their scales are parametrically of the same order.

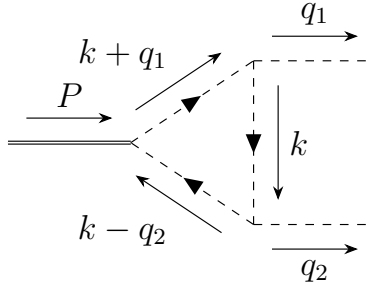


Figure 2.1: Triangle diagram corresponding to a heavy scalar (double line) decaying into two light scalars (dashed lines) through a loop of a massless charged scalar (dashed line with arrow).

integral. This would be however too naive as the integration variable spans all the possible scalings within the integration range, and the expansion of the integrand would therefore be ambiguous. A more formal way of seeing this is that the propagators make the integrand singular, hence integration and expansion do not commute in general.

The idea of the expansion by regions is that a loop integral will receive contributions only from a finite number of distinct *regions* in the loop momenta. A region is determined by a fixed scaling of the integration variables with respect to the external scales. Every region is computed separately by choosing a fixed scaling for the loop momenta, expanding the integrand accordingly (which now is a well defined operation), and only afterwards performing the integral over the whole integration range. The fact that we are expanding around a specific configuration of the loop momenta, but we still integrate over the whole integration range, is quite counter-intuitive. Nevertheless dimensional regularization (or any analytic regulator) allows this, given the vanishing of scaleless integrals (for a detailed explanation see Section 2.1 in [53]). The sum of all the regions will reproduce the result for the full integral, expanded in the scales ratios. This is where the power of the method of regions is, since it allows to evaluate the asymptotic expansion of a Feynman integral through the evaluation of simpler integrals. In this work we will mostly perform region analyses on one-loop integrals at leading power (LP), yet it's noteworthy that the method of regions finds application across a wider spectrum of contexts.

We illustrate the method through an explicit example with scalar fields for simplicity. A heavy particle of mass M is decaying into two light particles of mass m through a triangle loop diagram of a massless charged scalar (see Figure 2.1). The amplitude receives a contribution from the loop integral

$$\begin{aligned}
I_{\text{full}} &= -i \int \frac{d^d k}{(2\pi)^d} \frac{e^{\gamma_E \epsilon} (4\pi)^{2-\epsilon} \mu^{2\epsilon}}{[k^2 + i\eta][k^2 + 2q_1 \cdot k + m^2 + i\eta][k^2 - 2q_2 \cdot k + m^2 + i\eta]} \\
&= \frac{2}{M^2 \sqrt{1-4x^2}} \left[\text{Li}_2 \left(1 - \frac{1 - \sqrt{1-4x^2}}{2x^2} \right) - \text{Li}_2 \left(1 - \frac{1 + \sqrt{1-4x^2}}{2x^2} \right) \right] \\
&= \frac{1}{M^2} \left(\ln^2 x^2 + \frac{\pi^2}{3} + \mathcal{O}(x^2) \right), \tag{2.22}
\end{aligned}$$

where we defined the expansion parameter $x = m/M \ll 1$, and the full result of the

second line is given at leading power (in x) in the third line. The final state particles have back-to-back momenta, which scale as

$$q_1^\mu \sim M(1, x, x^2), \quad q_2^\mu \sim M(x^2, x, 1), \quad (2.23)$$

since $q_1^2 = q_2^2 = m^2$, $(q_1 + q_2)^2 = M^2$ and $q_1 \cdot q_2 \sim \mathcal{O}(M^2)$. The scaling of the perpendicular components $q_{1\perp}$ and $q_{2\perp}$ are fixed by requiring that q_1^2 and q_2^2 are homogeneous in x (see (2.21)). We call the scalings of q_1 and q_2 as *collinear* and *anti-collinear* modes respectively.⁶

We now apply the method of regions to the simple integral (2.22). In practice it means that we have to choose a scaling for the components of k , expand the integrand at LP in x and finally perform the integration. Whenever the integral, after the expansion of the integrand, results scaleless, we discard the region by noting that it does not contribute to the given loop integral. The sum of results from all the regions has to reproduce the full result (2.22) at LP.

Hard region

The hard region is defined by the homogeneous scaling

$$k \sim M(1, 1, 1), \quad (2.24)$$

which has therefore virtuality $k^2 \sim \mathcal{O}(M^2)$, and the integral in this region is given by

$$\begin{aligned} I_{\text{hard}} &= -i \int \frac{d^d k}{(2\pi)^d} \frac{e^{\gamma_E \epsilon} (4\pi)^{2-\epsilon} \mu^{2\epsilon}}{[k^2 + i\eta][k^2 + n_+ q_1 n_- k + i\eta][k^2 - n_- q_2 n_+ k + i\eta]} \\ &= \frac{e^{i\pi\epsilon}}{M^2} \left(\frac{\mu^2}{M^2} \right)^\epsilon \left(\frac{1}{\epsilon^2} - \frac{\pi^2}{12} + \mathcal{O}(\epsilon) \right), \end{aligned} \quad (2.25)$$

where we used $n_+ q_1 n_- q_2 = M^2 + \mathcal{O}(x^2)$. We can already notice some general features of region computations. The original integral (2.22) is finite, and has therefore no ϵ poles, however after the expansion of the integrand the new integral developed and infrared (IR) divergence that will cancel against poles from other regions. This is a general characteristic of the expansion by regions, where new intricate structures of ultraviolet (UV) and IR divergences arise in the single regions. Furthermore we emphasize that in the hard region the logarithms only depend on the hard scale M^2 , hinting at a first step towards the separation of scales. To perform such integrals a standard technique is to divide the integration measure in

$$\int d^d k = \frac{1}{2} \int_{-\infty}^{+\infty} d(n_+ k) \int_{-\infty}^{+\infty} d(n_- k) \int d^{d-2} k_\perp, \quad (2.26)$$

and performing first one of the one dimensional integrals with the residue theorem. This separation of the integration measure can sometimes lead to unregulated divergences in

⁶Technically in the applications to B -physics we would call these modes as *(anti-)hard-collinear*, as we will do from Chapter 3 on. We postpone this discussion to Section 2.8.1 where the distinction between hard-collinear and collinear modes will assume physical meaning.

the integrals over n_+k or n_-k , called rapidity divergences [58, 59], which need to be further regularized through an analytic regulator [60]. In this case the result has to first be expanded in the new analytic regulator and only afterwards in ϵ , as the expansions do not commute. When summing the contributions from the various regions the poles in the new regulator will cancel.

Collinear region

When k scales as the external momentum q_1 , we have the collinear region

$$k \sim M(1, x, x^2), \quad (2.27)$$

which gives the integral

$$\begin{aligned} I_c &= -i \int \frac{d^d k}{(2\pi)^d} \frac{e^{\gamma_E \epsilon} (4\pi)^{2-\epsilon} \mu^{2\epsilon}}{[k^2 + i\eta][k^2 + 2q_1 \cdot k + m^2 + i\eta][n_- q_2 n_+ k + i\eta]} \\ &= \frac{e^{i\pi\epsilon}}{M^2} \left(\frac{\mu^2}{m^2} \right)^\epsilon \left(-\frac{1}{\epsilon^2} + \frac{\pi^2}{12} + \mathcal{O}(\epsilon) \right), \end{aligned} \quad (2.28)$$

where now, since $k^2 \sim \mathcal{O}(m^2)$, the result depends only on the scale m^2 , except for the overall scaling $1/M^2$ which characterizes the LP contribution to the integral.

Anti-collinear region

Analogously to the collinear region, in the anti-collinear region the loop momentum scales as

$$k \sim M(x^2, x, 1), \quad (2.29)$$

giving

$$\begin{aligned} I_{\bar{c}} &= -i \int \frac{d^d k}{(2\pi)^d} \frac{e^{\gamma_E \epsilon} (4\pi)^{2-\epsilon} \mu^{2\epsilon}}{[k^2 + i\eta][n_+ q_1 n_- k + i\eta][k^2 - 2q_2 \cdot k + m^2 + i\eta]} \\ &= \frac{e^{i\pi\epsilon}}{M^2} \left(\frac{\mu^2}{m^2} \right)^\epsilon \left(-\frac{1}{\epsilon^2} + \frac{\pi^2}{12} + \mathcal{O}(\epsilon) \right) = I_c, \end{aligned} \quad (2.30)$$

which is expected from the symmetry of the process.

Soft region

There is an additional non-vanishing region, characterized by $q_i \cdot k \sim \mathcal{O}(m^2)$. This is the soft region, where k does not have a preferred direction, and its components are suppressed by m^2/M

$$k \sim M(x^2, x^2, x^2). \quad (2.31)$$

The integral in this region is

$$\begin{aligned}
I_{\text{soft}} &= -i \int \frac{d^d k}{(2\pi)^d} \frac{e^{\gamma_E \epsilon} (4\pi)^{2-\epsilon} \mu^{2\epsilon}}{[k^2 + i\eta][n_+ q_1 n_- k + m^2 + i\eta][n_- q_2 n_+ k + m^2 + i\eta]} \\
&= \frac{e^{i\pi\epsilon}}{M^2} \left(\frac{\mu^2 M^2}{m^4} \right)^\epsilon \left(\frac{1}{\epsilon^2} + \frac{\pi^2}{4} + \mathcal{O}(\epsilon) \right), \tag{2.32}
\end{aligned}$$

where again the result is a single-scale integral in which the contributions from the logarithms can be tamed by choosing $\mu = \mu_{\text{soft}} \sim \mathcal{O}(x^2 M)$.

Sum of the regions

The sum of the regions reads

$$I_{\text{hard}} + I_c + I_{\bar{c}} + I_{\text{soft}} = \frac{1}{M^2} \left(\ln^2 \frac{m^2}{M^2} + \frac{\pi^2}{3} \right), \tag{2.33}$$

which as expected agrees with the full result (2.22) expanded at LP in x , confirming that we found all the relevant regions of the integral under study.

With this example we have seen how the three relevant scales of the process are separated employing the strategy of regions. It is worth noting that naively one would have expected only two scales, given by M and m , nonetheless a third one is generated dynamically. This is also why a region analysis often helps in understanding the underlying physics of a given process.

The next step is the formulation of an EFT where the field content corresponds to the modes of the different regions, and the mode with higher virtuality (hard) is integrated out, since it does not appear in the external states. The EFT Feynman diagrams for a given process will then be in one-to-one correspondence with the regions of the full theory integral, except for the hard region which will be encapsulated into the Wilson coefficients (in this context also called *hard functions*).

Such an EFT can then be employed to derive factorization theorems to all orders in the perturbative expansion, which are an essential ingredient for employing the RGEs and thereby resumming the large logarithms.

2.3.2 Construction of the Leading Power SCET Lagrangian

We now want to tackle the problem of building an effective theory where the hard modes are integrated out. This theory, suited to reproduce the regions computation in presence of (anti-)collinear and soft modes, goes in the literature under the name of SCET_I. To be precise we should call the (anti-)collinear modes of this section as (anti-)hard-collinear, in contrast to the collinear modes of SCET_{II}. The distinction will be relevant in applications to B -physics in Section 2.8.1, where we will clarify the nomenclature. We imagine a process where the hard scale Q is set by the center of mass energy, and it is much larger than the

mass of the final state particles, denoted by m . This leads to a natural definition for a power counting parameter

$$\beta = \frac{m}{Q} \ll 1, \quad (2.34)$$

which is essential for a consistent construction of the EFT. The relevant modes of the full theory, pinned down from the region decomposition, are

$$\begin{aligned} \text{hard (h):} & \quad k^\mu \sim Q(1, 1, 1), \\ \text{collinear (c):} & \quad k^\mu \sim Q(1, \beta, \beta^2), \\ \text{anti-collinear (\bar{c}):} & \quad k^\mu \sim Q(\beta^2, \beta, 1), \\ \text{soft (s):} & \quad k^\mu \sim Q(\beta^2, \beta^2, \beta^2), \end{aligned} \quad (2.35)$$

but you will encounter more during the reading of this thesis. Albeit simpler and instructive, the construction of SCET for scalar particles would not be relevant for the works presented in this thesis, and can be found, for example, in Refs. [27, 53]. We hence start from the QCD Lagrangian, omitting ghost and gauge-fixing terms, for one massive and one massless quark fields, $\psi(x)$ and $q(x)$ respectively

$$\mathcal{L}_{\text{QCD}} = \bar{\psi}(i\not{D} - m)\psi + \bar{q}i\not{D}q - \frac{1}{4}G^{a,\mu\nu}G_{\mu\nu}^a, \quad (2.36)$$

where the gluon field strength tensor is

$$G_{\mu\nu}^a = \partial_\mu A_\nu^a - \partial_\nu A_\mu^a + g_s f^{abc} A_\mu^b A_\nu^c, \quad (2.37)$$

with f^{abc} the structure constants of SU(3). It is useful to introduce a matricial form of the gluon field

$$A^\mu(x) = A^{a,\mu}(x)T^a. \quad (2.38)$$

We now split the quarks and gluon fields into collinear (C), anti-collinear (\bar{C}) and soft (s) components

$$\psi = \psi_C + \psi_{\bar{C}}, \quad q = q_C + q_{\bar{C}} + q_s, \quad A^\mu = A_C^\mu + A_{\bar{C}}^\mu + A_s^\mu, \quad (2.39)$$

where each component describes only degrees of freedom with the respective momentum scaling. We are not including a soft component ψ_s for the massive field since the virtuality of its momentum would be $k^2 \sim \beta^4 Q^2 \ll m^2$, and therefore could not appear in on-shell external states. By inserting the decomposition (2.39) in the Lagrangian (2.36) we can schematically write

$$\mathcal{L}_{\text{QCD}} = \mathcal{L}_C + \mathcal{L}_{\bar{C}} + \mathcal{L}_s + \mathcal{L}_{\text{int}}, \quad (2.40)$$

where $\mathcal{L}_{C,\bar{C},s}$ are just a copies of \mathcal{L}_{QCD} with the field substitutions $\psi \rightarrow \psi_{C,\bar{C}}$, $q \rightarrow q_{C,\bar{C},s}$ and $A^\mu \rightarrow A_{C,\bar{C},s}^\mu$. The interaction Lagrangian \mathcal{L}_{int} contains the interaction terms between the different modes. The crucial point here is that we keep in \mathcal{L}_{int} only the terms allowed by momentum conservation, knowing that the EFT fields represent particles with a precise

momentum scaling. This means for example that all the interactions between collinear and anti-collinear particles are ruled out, as they would need to be mediated by a hard particle in order to conserve the total momentum. Therefore we can focus only on the collinear and soft sectors, as the anti-collinear sector will just be a copy of the collinear one with the replacements $C \rightarrow \bar{C}$ and $n_- \leftrightarrow n_+$.

If the theory would have been made by scalar fields only we could stop here. When dealing with fermions and gauge bosons, we encounter the additional challenge that the components of the collinear fields ψ_C , q_C and $A_C^{a,\mu}$ are not homogeneous in the power counting parameter β . The scaling of the fields can be derived from any kinetic term of the action by requiring

$$\int d^4x \mathcal{L}_{\text{kin}} \sim 1, \quad (2.41)$$

where $d^4x \sim k^{-4}$ and k is the total momentum associated to the operator in the Lagrangian. The gluon field scaling can be derived for example from

$$\int d^4x \frac{1}{2} \partial_\mu A_\nu^a(x) \partial^\nu A^{a,\mu}(x) \sim 1, \quad (2.42)$$

which shows that $A_\mu^a(x) \sim k_\mu$, hence

$$A_C^{a,\mu}(x) \sim Q(1, \beta, \beta^2), \quad A_s^{a,\mu}(x) \sim Q(\beta^2, \beta^2, \beta^2). \quad (2.43)$$

It is also useful to define (anti-)collinear and soft covariant derivatives

$$iD_C^\mu = i\partial^\mu + g_s A_C^\mu, \quad iD_{\bar{C}}^\mu = i\partial^\mu + g_s A_{\bar{C}}^\mu, \quad iD_s^\mu = i\partial^\mu + g_s A_s^\mu, \quad (2.44)$$

to separate the Lagrangian in its different sectors.

Lets turn now to the collinear fermion field ψ_C . We start by splitting it in two components, in analogy to (2.6), using the projectors induced by n_+ and n_-

$$\xi_C(x) = \frac{\not{n}_- \not{n}_+}{4} \psi_C(x), \quad \eta_C(x) = \frac{\not{n}_+ \not{n}_-}{4} \psi_C(x), \quad (2.45)$$

where $\psi_C(x) = \xi_C(x) + \eta_C(x)$ and $\not{n}_- \xi_C(x) = \not{n}_+ \eta_C(x) = 0$ due to the properties (2.19).

The Lagrangian for ψ_C in terms of the new fields is

$$\begin{aligned} \mathcal{L}_{\psi_C} &= \bar{\psi}_C (i\not{D} - m) \psi_C = (\bar{\xi}_C + \bar{\eta}_C) (i\not{D} - m) (\xi_C + \eta_C) \\ &= \bar{\xi}_C (in_- D) \frac{\not{n}_+}{2} \xi_C + \bar{\eta}_C (in_+ D) \frac{\not{n}_-}{2} \eta_C + \bar{\xi}_C (i\not{D}_{C,\perp} - m) \eta_C + \bar{\eta}_C (i\not{D}_{C,\perp} - m) \xi_C, \end{aligned} \quad (2.46)$$

where in the last line we have neglected the soft gluon fields in the covariant derivatives when they are subleading with respect to the collinear ones, due to the scaling (2.43). The only term where the soft gluon field survives is $in_- D = in_- \partial + g_s (n_- A_C + n_- A_s)$. This term will be the one responsible for the only leading power interactions between soft and collinear fields. From

$$\int d^4x \bar{\xi}_C(x) (in_- \partial) \frac{\not{n}_+}{2} \xi_C(x) \sim \beta^0, \quad \int d^4x \bar{\eta}_C(x) (in_+ \partial) \frac{\not{n}_-}{2} \eta_C(x) \sim \beta^0, \quad (2.47)$$

we derive the scalings

$$\xi_C(x) \sim \beta Q^{3/2}, \quad \eta_C(x) \sim \beta^2 Q^{3/2}, \quad (2.48)$$

showing that the η_C field is power suppressed with respect to ξ_C . For this reason, and because the action is quadratic, we can integrate out η_C exactly, employing the equations of motion. Formally solving the equations of motion with respect to $\bar{\eta}_C$ yields to

$$\eta_C(x) = \frac{1}{in_+ D_C} (i\not{D}_{C,\perp} + m) \frac{\not{h}_+}{2} \xi_C(x), \quad \bar{\eta}_C(x) = \bar{\xi}_C(x) \frac{\not{h}_+}{2} (i\overleftarrow{\not{D}}_{C,\perp} - m) \frac{1}{in_+ \overleftarrow{D}_C}, \quad (2.49)$$

and inserting it into the Lagrangian (2.46) we obtain

$$\mathcal{L}_{\xi_C} = \bar{\xi}_C \left[in_- D + (i\not{D}_{C,\perp} - m) \frac{1}{in_+ D_C} (i\not{D}_{C,\perp} + m) \right] \frac{\not{h}_+}{2} \xi_C. \quad (2.50)$$

We emphasize the fact that η_C has been integrated out exactly, which means that the collinear Lagrangian (2.50) is equivalent to the full QCD Lagrangian, in presence of only collinear modes. In other words we have rewritten the QCD Lagrangian in terms of new fields which scale homogeneously with respect to the large boost, but no expansion has been performed so far. Indeed \mathcal{L}_{ξ_C} does not suffer from power corrections, which is a consequence of boost invariance in QCD. The EFT expansion takes place in the interactions between the soft and collinear sectors.

The Lagrangian for the light collinear field q_C is simply obtained by taking $m = 0$ in (2.50). Since the soft modes have uniform scaling, the soft Lagrangian is just a copy of the QCD one with soft fields, from which one can easily derive

$$q_s(x) \sim \beta^3 Q^{3/2}. \quad (2.51)$$

To summarize, the SCET_I Lagrangian, for the theory (2.36), is

$$\mathcal{L}_{\text{SCET}} = \mathcal{L}_C + \mathcal{L}_{\bar{C}} + \mathcal{L}_s + \mathcal{L}_{s-C} + \mathcal{L}_{s-\bar{C}}, \quad (2.52)$$

where

$$\begin{aligned} \mathcal{L}_C &= -\frac{1}{4} G_C^{a,\mu\nu} G_{C,\mu\nu}^a + \bar{\xi}_C \left[in_- D_C + (i\not{D}_{C\perp} - m) \frac{1}{in_+ D_C} (i\not{D}_{C\perp} + m) \right] \frac{\not{h}_+}{2} \xi_C \\ &\quad + \bar{\xi}_C^q \left[in_- D_C + i\not{D}_{C\perp} \frac{1}{in_+ D_C} i\not{D}_{C\perp} \right] \frac{\not{h}_+}{2} \xi_C^q, \\ \mathcal{L}_{\bar{C}} &= \mathcal{L}_C \quad \text{with} \quad C \rightarrow \bar{C}, \quad n_- \leftrightarrow n_+, \\ \mathcal{L}_s &= -\frac{1}{4} G_s^{a,\mu\nu} G_{s,\mu\nu}^a + \bar{q}_s i\not{D}_s q_s, \end{aligned} \quad (2.53)$$

and $\xi_C^q(x) = (\not{h}_- \not{h}_+ / 4) q_C(x)$.

The determination of the interactions between the soft and collinear sectors, governed by \mathcal{L}_{s-C} and $\mathcal{L}_{s-\bar{C}}$, is a complicated topic [51]. However when restricting to leading power

it turns out to be quite simple, as the soft quark field is power suppressed. In fact, the total momentum associated to operators in $\mathcal{L}_{s-C}(\mathcal{L}_{s-\bar{C}})$ is (anti-)collinear, and therefore the leading power interaction terms in the Lagrangian must be $\mathcal{O}(\beta^4 Q^4)$. Given the scaling of the fields (2.43), (2.48) and (2.51), together with the projection properties of the fields, we conclude that soft quarks in \mathcal{L}_{int} can appear only at next-to-leading power (NLP).

The only LP interaction between collinear quarks and soft gluons comes from the first term in (2.50)

$$\mathcal{L}_{s-C} = g_s \bar{\xi}_C n_- A_s \frac{\not{n}_+}{2} \xi_C + g_s \bar{\xi}_C^q n_- A_s \frac{\not{n}_+}{2} \xi_C^q + \dots, \quad (2.54)$$

and the dots denote LP interactions between soft and collinear gluons, not relevant for the works discussed in this thesis. $\mathcal{L}_{s-\bar{C}}$ is obtained with the usual replacements.

This concludes the basic construction of the SCET Lagrangian for QCD, with obvious generalization to multiple quark flavours. For a complete list of the Feynman rules up to next-to-next-to-leading power (NNLP) we refer to Appendix A of Ref. [61].

2.3.3 Multipole Expansion

There is a subtlety regarding terms made by soft and collinear fields, like (2.54). When going to momentum space, only one component of the soft momentum is not power suppressed with respect to the corresponding collinear component. In order to have an homogeneous result in the power counting parameter in momentum space we would have to re-expand the EFT Feynman rules originating from the SCET Lagrangian, which would ruin the systematics of the effective theory. The way to implement this at the Lagrangian level is the so-called multipole expansion [51]. Whenever fields with soft and collinear scalings are combined, the space-time variable inherits the scaling $x^\mu \sim (\beta^{-2}, \beta^{-1}, 1)Q^{-1}$ ensuring $x \cdot p_C \sim \mathcal{O}(1)$. In order to have an homogeneous expression, the soft fields need to be expanded around the large space-time component $x_-^\mu \equiv (n_+ x) n_-^\mu / 2$ as follows [51]

$$A_s^\mu(x) = A_s^\mu(x_-) + x_\perp \cdot \partial_\perp A_s^\mu(x_-) + \frac{n_- x}{2} n_+ \partial A_s^\mu(x_-) = A_s^\mu(x_-) (1 + \mathcal{O}(\beta)). \quad (2.55)$$

In this way one is able to systematically achieve an homogeneous Lagrangian at any order in the power counting parameter, automatically keeping only the unsuppressed component (relative to the collinear one) of the soft momentum

$$p_s \cdot x_- = n_- p_s \frac{n_+}{2} x_\mu = p_{s+} \cdot x. \quad (2.56)$$

2.3.4 Arising of Non-Localities

When integrating out the hard modes, and performing a matching calculation, one has to build a complete basis of operators in the EFT at a given order in the power counting parameter. This is possible due to the fixed scaling of the fields and derivatives in the EFT. Derivatives acting on collinear fields scale as $i\partial_\mu \sim (1, \beta, \beta^2)Q$, showing that an arbitrary

number of derivatives along the light-cone direction of the collinear field does not yield a further suppression to the operator

$$\left(\frac{in_+\partial}{Q}\right)^k \xi_C(x) \sim \beta Q^{3/2}. \quad (2.57)$$

The inclusion of any number of such derivatives can be taken into account by spreading the collinear field along the light-cone direction

$$\xi_C(x + sn_+) = \sum_{k=0}^{\infty} \frac{s^k}{k!} (n_+\partial)^k \xi_C(x). \quad (2.58)$$

This translates into non-local operators, which instead of being multiplied by constant Wilson coefficients are convoluted with matching functions

$$\mathcal{L}_{\text{eff}} = \int ds_1 \dots ds_n C(s_1, \dots, s_n) \mathcal{O}(s_1, \dots, s_n), \quad (2.59)$$

where n is the number of collinear plus anti-collinear fields in the effective operator \mathcal{O} . In momentum space, the non-locality of the Wilson coefficient becomes

$$\begin{aligned} & \int ds_1 \dots ds_n C(s_1, \dots, s_n) \mathcal{O}(s_1, \dots, s_n) \\ &= \int \frac{d^4 p_1}{(2\pi)^4} \dots \frac{d^4 p_n}{(2\pi)^4} \int ds_1 \dots ds_n C(s_1, \dots, s_n) e^{-ip_1 \cdot (x+s_1 n_{\pm})} \dots e^{-ip_n \cdot (x+s_n n_{\pm})} \tilde{\mathcal{O}}(p_1, \dots, p_n) \\ &= \int \frac{d^4 p_1}{(2\pi)^4} \dots \frac{d^4 p_n}{(2\pi)^4} \tilde{C}(n_{\pm} p_1, \dots, n_{\pm} p_n) e^{-ix \cdot (p_1 + \dots + p_n)} \tilde{\mathcal{O}}(p_1, \dots, p_n), \end{aligned} \quad (2.60)$$

where $s_i n_{\pm}$ stands for $s_i n_+$ if p_i is collinear, and $s_i n_-$ if p_i is anti-collinear. So we see that the momentum space hard-function $\tilde{C}(n_{\pm} p_1, \dots, n_{\pm} p_n)$ depends on the large components of the collinear and anti-collinear momenta, which are indeed of the order of the hard scale.

The non-locality of the EFT operators finds a natural interpretation in terms of Feynman diagrams when comparing with the standard case of integrating out a heavy particle completely. In the latter case, we think about the EFT operators arising from diagrams where the virtual propagators of the heavy particle shrank to a point. This is because the dependence on the external momenta in the propagators of the heavy particle is a subleading effect, yielding to a local interaction after the expansion. Contrary to this in SCET the external (anti-)collinear particles still carry large momentum, but only in a specific direction, intuitively bringing the effective operators to be non-local in one dimension.

Another manifestation of non-locality is the presence of inverse derivatives in operators [53]. In fact we notice that the inverse derivative, with an infinitesimal $i\eta$ prescription in the denominator, can be rewritten as

$$\frac{i}{in_+\partial + i\eta} \xi(x) = \int_{-\infty}^0 ds \xi(x + sn_+), \quad (2.61)$$

which can be verified by applying the derivative to both sides of the equation, and using the fact that the fields vanish at infinity.

2.3.5 Gauge Transformations

Gauge invariance is an essential property of QCD which must be preserved by the EFT. Also the gauge transformations of QCD need to be split in soft and (anti-)collinear ones, to preserve the scaling of the EFT fields. In the following any discussion about collinear fields also applies to anti-collinear ones, with obvious replacements. Explicitly we build the two gauge transformation matrices as

$$V_C(x) = \exp[i\varepsilon_C^a(x)T^a], \quad V_s(x) = \exp[i\varepsilon_s^a(x)T^a], \quad (2.62)$$

where the dimensionless functions $\varepsilon_C^a(x)$ and $\varepsilon_s^a(x)$ governing the transformations have collinear and soft scalings respectively, namely

$$\partial_\mu \varepsilon_C^a(x) \sim (1, \beta, \beta^2)Q, \quad \partial_\mu \varepsilon_s^a(x) \sim (\beta^2, \beta^2, \beta^2)Q. \quad (2.63)$$

Not surprisingly, soft gauge transformations on soft fields act in the same way as in full QCD, since the Lagrangians have the same form

$$\begin{aligned} q_s(x) &\rightarrow V_s(x)q_s(x), \\ A_s^\mu(x) &\rightarrow V_s(x)A_s^\mu(x)V_s^\dagger(x) + \frac{i}{g_s}V_s(x)[\partial^\mu V_s^\dagger(x)], \end{aligned} \quad (2.64)$$

where the derivative in the last term acts only inside the square brackets. This ensures that the covariant derivative transforms as

$$iD_s^\mu \rightarrow iV_s(x)V_s^\dagger(x)\partial^\mu + iV_s(x)(\partial^\mu V_s^\dagger(x)) + g_s V_s(x)A_s^\mu(x)V_s^\dagger(x) = V_s(x)iD_s^\mu V_s^\dagger(x), \quad (2.65)$$

making the soft Lagrangian explicitly invariant under soft gauge transformations.

On the other hand collinear gauge transformations on soft fields are forbidden, as they would turn soft particles into collinear ones. Contrary to that, soft gauge transformations on collinear fields are non-trivial, as the small component of the collinear momentum is of the same order of the corresponding soft momentum component.

In light of the multipole expansion introduced in Section 2.3.3, the soft gauge transformation acts on the collinear fields as

$$\begin{aligned} \xi_C(x) &\rightarrow V_s(x_-)\xi_C(x), \\ A_C^\mu(x) &\rightarrow V_s(x_-)A_C^\mu(x)V_s^\dagger(x_-). \end{aligned} \quad (2.66)$$

Collinear gauge transformations on collinear fields are given by

$$\begin{aligned} \xi_C(x) &\rightarrow V_C(x)\xi_C(x), \\ A_C^\mu(x) &\rightarrow V_C(x)A_C^\mu(x)V_C^\dagger(x) + V_C(x)\left[\frac{i}{g_s}\partial^\mu + \frac{n_+^\mu}{2}n_-A_s(x_-), V_C^\dagger(x)\right]. \end{aligned} \quad (2.67)$$

Summarizing and putting everything together, one gets for the covariant derivative of the collinear Lagrangian

$$iD^\mu = i\partial^\mu + g_s A_C^\mu(x) + g_s \frac{n_+^\mu}{2} n_- A_s(x_-), \quad (2.68)$$

the transformations

$$\begin{cases} iD^\mu \rightarrow V_s(x_-)(iD^\mu)V_s^\dagger(x_-), \\ iD^\mu \rightarrow V_C(x)(iD^\mu)V_C^\dagger(x). \end{cases} \quad (2.69)$$

2.3.6 Wilson Lines

Non-local operators and the requirement of gauge invariance force us to introduce Wilson lines. A Wilson line, or gauge link, in QCD is defined as

$$[x, y] \equiv \mathbf{P} \exp \left[i g_s \int_y^x dz^\mu A_\mu(z) \right], \quad (2.70)$$

where \mathbf{P} is a path-ordering operator, which is essential as the group generators do not commute. The notation $[\cdot, \cdot]$ should not be confused with the commutator notation. The integral over z^μ is intended as a generic path, namely a function $z^\mu(t)$ with $z^\mu(0) = y^\mu$ and $z^\mu(1) = x^\mu$ such that the integral is changed into

$$\int_y^x dz^\mu = \int_0^1 dt \frac{dz^\mu}{dt}. \quad (2.71)$$

The Wilson line is crucial for building gauge invariant non-local currents, as its gauge transformation is given by

$$[x, y] \rightarrow V(x)[x, y]V^\dagger(y), \quad (2.72)$$

such that $\bar{\psi}(x)[x, y]\psi(y)$ is manifestly gauge invariant. Another important property of Wilson lines is that the covariant derivative along their integration path vanish

$$\frac{dx^\mu}{ds} iD_\mu[x, y] = \frac{dx^\mu}{ds} \left(i \frac{\partial}{\partial x^\mu} + g_s A_\mu(x) \right) [x, y] = 0, \quad (2.73)$$

where s is parametrizing the path. In our specific cases the paths will be straight lines and therefore dx^μ/ds will just be a constant vector.

In SCET we will need Wilson lines for dealing with non-localities along the light-cone directions, as seen in Section 2.3.4. It is useful to split the Wilson line in two by extending the integration path up to infinity on the light-like directions, and by using the parametrization $z^\mu = x^\mu + tn_+^\mu$. This brings us to the definition of a collinear Wilson line

$$W_C(x) = [x, -\infty n_+] = \mathbf{P} \exp \left[i g_s \int_{-\infty}^0 dt n_+ A_C(x + tn_+) \right], \quad (2.74)$$

which under collinear gauge transformations acts as

$$W_C(x) \rightarrow V_C(x)W_C(x)V_C^\dagger(-\infty n_+) = V_C(x)W_C(x), \quad (2.75)$$

where in the last equality we used the fact that gauge fields vanish at infinity. At this point one is able to write

$$[x, y]_C = W_C(x)W_C^\dagger(y), \quad (2.76)$$

where the conjugated Wilson line is defined with the anti-path ordering $\bar{\mathbf{P}}$. It is hence tempting to define collinear gauge invariant fields by “dressing” the SCET spinors with collinear Wilson lines

$$\chi(x) \equiv W_C^\dagger(x)\xi_C(x), \quad \bar{\chi}(x) \equiv \bar{\xi}_C(x)W_C(x). \quad (2.77)$$

2.4 Boosted HQET

We reviewed the basic concepts and constructions of two important effective theories, HQET and SCET, in Sections 2.2 and 2.3 respectively. In this Section we study the combination of the two: boosted HQET (bHQET). This theory is needed when dealing with heavy quarks, nearly on-shell, but boosted away from their rest frame. This can be the case for example of $t\bar{t}$ production at the LHC [62, 63], or a $W^\pm \rightarrow B^\pm\gamma$ radiative decay which we will study in more detail in Chapter 4.

In particular in this thesis we are interested in the application of bHQET to heavy mesons, produced in a hard process with large energy $Q \gg m_H$. Here m_H denotes the mass of a generic pseudoscalar meson H made by a heavy quark h of mass $m_h \sim \mathcal{O}(m_H)$ and a massless anti-quark \bar{q} .

In analogy to Section 2.3 we define the power counting parameter

$$\beta_h = \frac{m_H}{Q} \ll 1, \quad (2.78)$$

which quantifies how much the meson is boosted with respect to its rest frame. In fact we choose a reference frame \mathcal{S} where the meson four-momentum is

$$p_H^\mu = m_H v^\mu = Q \frac{n_-^\mu}{2} + \frac{m_H^2}{Q} \frac{n_+^\mu}{2}. \quad (2.79)$$

By calling \mathcal{S}^* the rest frame of the heavy meson, it is easy to show that a generic vector $V^{*\mu}$ in \mathcal{S}^* is written in terms of the components of V^μ in \mathcal{S} as

$$n_- V^* = \frac{1}{\beta_h} n_- V, \quad V_\perp^{*\mu} = V_\perp^\mu, \quad n_+ V^* = \beta_h n_+ V. \quad (2.80)$$

So far we only considered the large boost of the meson, which would lead us to the construction of SCET for a massive particle, as covered in Section 2.3. On top of that we

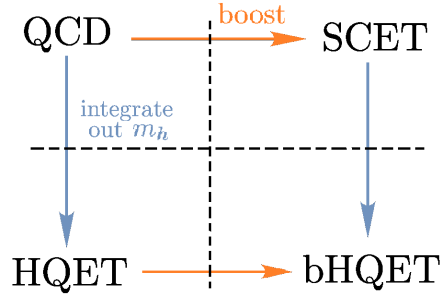


Figure 2.2: Abstract representation of the two possible paths in building bHQET from full QCD.

want to exploit the hierarchy $m_h \gg \Lambda_{\text{QCD}}$, as we do in HQET, and we therefore define a second natural power counting parameter

$$\lambda_h = \frac{\Lambda_{\text{QCD}}}{m_h} \ll 1. \quad (2.81)$$

With this definition we can express the momenta of the valence quarks of H in \mathcal{S}^*

$$p_h^* \sim (m_h, \Lambda_{\text{QCD}}, m_h) \sim (\beta_h, \lambda_h \beta_h, \beta_h) Q, \quad p_q^* \sim (\Lambda_{\text{QCD}}, \Lambda_{\text{QCD}}, \Lambda_{\text{QCD}}) \sim \lambda_h (\beta_h, \beta_h, \beta_h) Q, \quad (2.82)$$

where the presence of m_h induces virtual modes with homogeneous scaling

$$k_h^* \sim (m_h, m_h, m_h) \sim (\beta_h, \beta_h, \beta_h) Q. \quad (2.83)$$

By using the transformation (2.80) we derive the scalings for the relevant modes⁷ in \mathcal{S}

$$k_h \sim (1, \beta_h, \beta_h^2) Q \quad \text{“hard-collinear”}, \quad p_q \sim \lambda_h (1, \beta_h, \beta_h^2) Q \quad \text{“soft-collinear”}, \quad (2.84)$$

with virtualities $\mathcal{O}(m_h^2)$ and $\mathcal{O}(\Lambda_{\text{QCD}}^2)$ respectively.

Following the derivation of Section 2.2, we split the heavy quark momentum in the boosted frame as

$$p_h^\mu = m_h v^\mu + k^\mu, \quad (2.85)$$

where now v^μ and k^μ have acquired a preferred direction

$$v^\mu \sim (1/\beta_h, 1, \beta_h), \quad k^\mu \sim (1/\beta_h, 1, \beta_h) \Lambda_{\text{QCD}} \sim \lambda_h (1, \beta_h, \beta_h^2) Q, \quad (2.86)$$

realizing that the residual momentum of the heavy quark has to be now soft-collinear. Our goal is to write down a Lagrangian homogeneous in the power counting parameters β_h and λ_h . This can be achieved in two ways, depending on the order in which we perform the expansion, as it is pictorially depicted in Figure 2.2.

⁷We now proceed to call the modes with scaling $(1, \beta_h, \beta_h^2)$ as hard-collinear in this section, opposed to Section 2.3.

2.4.1 bHQET from HQET

In this section we derive the bHQET Lagrangian starting from the leading power (in λ_h) HQET one (2.13). We define the bHQET field as

$$h_n(x) = \sqrt{\frac{2}{n_+v}} e^{im_h v \cdot x} \frac{\not{n}_- \not{n}_+}{4} \psi_h(x), \quad (2.87)$$

where $\psi_h(x)$ is again the full QCD field. This definition first projects the full QCD field onto its large component $\xi_C(x)$ as done in (2.45), but also strips out the rapidly oscillating phase as in (2.6). The purpose of the prefactor is to make the scaling of h_n independent on the boost. As a result we can derive a relation between the HQET field $h_v(x)$ and the new $h_n(x)$ field

$$h_v(x) = \sqrt{\frac{n_+v}{2}} \frac{1 + \not{\psi}}{2} \left(1 - \frac{\not{n}_+ i \not{D}_\perp + m_h \not{\psi}_\perp - m_h}{2 i n_+ D + m_h n_+ v} \right) h_n(x), \quad (2.88)$$

where we used the equation of motion (2.49) and the covariant derivative scales now as a soft-collinear momentum. We now have to expand the relation (2.88) in λ_h and β_h , employing the projection properties

$$\frac{\not{n}_- \not{n}_+}{4} h_n(x) = h_n(x), \quad \not{n}_- h_n(x) = 0, \quad (2.89)$$

and paying attention to the structure of higher order terms

$$\begin{aligned} h_v(x) &= \sqrt{\frac{n_+v}{2}} \left[1 + \left(\frac{1 + \not{\psi}_\perp \not{n}_+}{n_+v} - \frac{i \not{D}_\perp}{2m_h} - \frac{1 - \not{\psi}_\perp i n_+ D}{2 m_h n_+ v} \right) + \mathcal{O}(\lambda_h^2, \lambda_h \beta_h) \right] h_n(x) \\ &= \sqrt{\frac{n_+v}{2}} \left[1 + \sum_{k=1}^{\infty} \mathcal{O}(\lambda_h^k) + \frac{\not{n}_+}{2} \mathcal{O}(\beta_h) \sum_{k=0}^{\infty} \mathcal{O}(\lambda_h^k) \right] h_n(x). \end{aligned} \quad (2.90)$$

We notice that up to a rescaling factor $\sqrt{n_+v/2}$ the bHQET and HQET fields, in the boosted frame \mathcal{S} , are the same at leading power in λ_h and β_h . The fact that only linear corrections in β_h affect the relation (2.90) deserves to be highlighted. This is because the relative scalings between the two terms in the denominator of (2.88) is of order λ_h , and the $\mathcal{O}(\beta_h)$ term from the projector $(1 + \not{\psi})/2$ vanish when acting on the power suppressed terms which are proportional to $\not{n}_+/2$. The situation is therefore familiar, because the same pattern is seen in the relation between the full QCD field and the collinear SCET spinor, as noticed in Section 2.3.

The $\mathcal{O}(\lambda_h)$ corrections between h_n and h_v are of a totally different kind, and can be seen as “artificial”, as they stem from our definition of the bHQET field. In fact one could absorb these power corrections in the definition of the EFT field as

$$h_n^{\text{new}}(x) = \sqrt{\frac{2}{n_+v}} \frac{\not{n}_- \not{n}_+}{4} h_v(x) = \sqrt{\frac{2}{n_+v}} e^{im_h v \cdot x} \frac{\not{n}_- \not{n}_+}{4} \frac{1 + \not{\psi}}{2} \psi_h(x), \quad (2.91)$$

which would lead to a small component spinor

$$\frac{\not{n}_+ \not{n}_-}{4} h_v(x) = \sqrt{\frac{n_+ v}{2}} \frac{1 + \not{\psi}_\perp}{n_+ v} \frac{\not{n}_+}{2} h_n^{\text{new}}(x), \quad (2.92)$$

and a relation

$$h_v(x) = \left(\frac{\not{n}_- \not{n}_+}{4} + \frac{\not{n}_+ \not{n}_-}{4} \right) h_v(x) = \sqrt{\frac{n_+ v}{2}} \left[1 + \frac{1 + \not{\psi}_\perp}{n_+ v} \frac{\not{n}_+}{2} \right] h_n^{\text{new}}(x), \quad (2.93)$$

free of corrections in λ_h . Obviously the difference in the definition of the bHQET field would result in a reorganization of the power corrections, but would not affect the leading-power theory. In some sense the definition (2.91) is more natural since the projector $(1 + \not{\psi})/2$, as in HQET, eliminates the small component (in λ_h) of the QCD spinor. Nevertheless (2.87) is used in the literature [64] since it makes matching computations from SCET easier.

Finally, by applying (2.90) to the HQET Lagrangian (2.13), we derive

$$\begin{aligned} \mathcal{L}_{\text{HQET}} &= \bar{h}_v(x) i v \cdot D h_v(x) = \frac{n_+ v}{2} \bar{h}_n(x) \left(1 + \frac{1 - \not{\psi}_\perp}{n_+ v} \frac{\not{n}_+}{2} \right) i v \cdot D \left(1 + \frac{1 + \not{\psi}_\perp}{n_+ v} \frac{\not{n}_+}{2} \right) h_n(x) \\ &= \bar{h}_n(x) i v \cdot D \frac{\not{n}_+}{2} h_n(x) (1 + \mathcal{O}(\lambda_h)), \end{aligned} \quad (2.94)$$

which defines the leading power bHQET Lagrangian [64]

$$\mathcal{L}_{\text{bHQET}} = \bar{h}_n(x) i v \cdot D \frac{\not{n}_+}{2} h_n(x). \quad (2.95)$$

As noted for the collinear SCET Lagrangian, we see that (2.94) does not have corrections of order $\mathcal{O}(\beta_h)$ as it arises from the suppressed terms in the field (2.90). As commented before, the corrections of order $\mathcal{O}(\lambda_h)$ are the ones coming from the definition of h_n , and could simply be eliminated by using instead the field (2.91).

Depending on the chosen definition for $h_n(x)$, the relationship between the leading-power Lagrangians (2.94) may exhibit power corrections in λ_h . However, incorporating all power corrections in HQET and consequently in (2.94) would establish equivalence between the two theories, as mandated by boost invariance. Indeed, one could alternatively circumvent the construction of the bHQET Lagrangian with the novel field h_n by employing standard HQET along with its Feynman rules [62,63]. While this approach yields the correct outcome, it introduces an inhomogeneous power counting in the parameter β_h , as the field $h_v(x)$ includes both large and small SCET fields.

2.4.2 bHQET from SCET

The bHQET Lagrangian can also be obtained by following the second path of Figure 2.2, namely by first rewriting the QCD Lagrangian in terms of a massive collinear spinor $\xi_C(x)$,

and then integrating out the heavy mass m_h . Using the definition (2.87) we can relate the SCET spinor $\xi_C(x)$ to the bHQET field

$$\xi_C(x) = \sqrt{\frac{n_+v}{2}} e^{-im_h v \cdot x} h_n(x). \quad (2.96)$$

Our starting point is therefore the massive collinear SCET Lagrangian (2.50), derived in Section 2.3. With the insertion of (2.96) we find [64]

$$\begin{aligned} \mathcal{L}_{\xi_C} &= \frac{n_+v}{2} \bar{h}_n(x) \left[m_h n_- v + i n_- D \right. \\ &\quad \left. + (m_h \not{v}_\perp - m_h + i \not{D}_\perp) \frac{1}{m_h n_+ v + i n_+ D} (m_h \not{v}_\perp + m_h + i \not{D}_\perp) \right] \frac{\not{v}_+}{2} h_n(x) \\ &= \bar{h}_n(x) \left[\frac{m_h}{2} n_- v n_+ v + i n_- D \frac{n_+v}{2} \right. \\ &\quad \left. + \frac{m_h}{2} (v_\perp^2 - 1) \left(1 - \frac{i n_+ D}{m_h n_+ v} \right) + i v_\perp \cdot D_\perp + \mathcal{O}(\beta_h \lambda_h^2 Q) \right] \frac{\not{v}_+}{2} h_n(x) \\ &= \bar{h}_n(x) i v \cdot D \frac{\not{v}_+}{2} h_n(x) (1 + \mathcal{O}(\lambda_h)), \end{aligned} \quad (2.97)$$

reproducing the same bHQET Lagrangian (2.95).

One could also go directly from QCD to bHQET by inverting the field relation (2.87), giving

$$\psi_h(x) = \sqrt{\frac{n_+v}{2}} e^{-im_h v \cdot x} \left(1 + \frac{m_h + m_h \not{v}_\perp + i \not{D}_\perp \not{v}_+}{m_h n_+ v + i n_+ D} \frac{\not{v}_+}{2} \right) h_n(x), \quad (2.98)$$

or with the definition (2.91)

$$\psi_h(x) = \sqrt{\frac{n_+v}{2}} e^{-im_h v \cdot x} \left[1 + \frac{i \not{D} - \not{v} i v \cdot D}{2 m_h + i v \cdot D} \right] \left[1 + \frac{1 + \not{v}_\perp \not{v}_+}{n_+ v} \frac{\not{v}_+}{2} \right] h_n(x), \quad (2.99)$$

which then have to be appropriately expanded in λ_h and β_h .

2.4.3 Soft-Collinear Fields

The bHQET field $h_n(x)$ is associated to particles with soft-collinear residual momentum, and only interacts with soft-collinear gluons, in absence of a true soft sector. It is hence useful to derive the scaling of the field from the kinetic term in the action

$$\int d^4x \bar{h}_n(x) i v \cdot \partial \frac{\not{v}_+}{2} h_n(x) \sim 1, \quad (2.100)$$

which implies

$$h_n(x) \sim \Lambda_{\text{QCD}}^{3/2}, \quad (2.101)$$

since $iv \cdot D \sim \Lambda_{\text{QCD}}$ and $d^4x \sim \Lambda_{\text{QCD}}^{-4}$. The purpose of the prefactor in (2.87) has become now clear, since it eliminates the dependence on the large component of the four-velocity from the field scaling. Indeed the standard HQET field in the boosted frame would scale like $h_v(x) \sim \sqrt{n_+ v} \Lambda_{\text{QCD}}^{3/2}$, as can be inferred from the relation (2.90).

To describe the light anti-quark in the boosted meson we need to introduce soft-collinear fields, as in the rest frame they would be described by soft fields. We hence split the QCD field $q(x)$ as

$$\xi_{sc}(x) = \frac{\not{n}_- \not{n}_+}{4} q(x), \quad \eta_{sc}(x) = \frac{\not{n}_+ \not{n}_-}{4} q(x) = \frac{i \not{D}_\perp}{in_+ D} \frac{\not{n}_+}{2} \xi_{sc}(x), \quad (2.102)$$

and in the same way as for the collinear Lagrangian (2.50) we integrate out the small field $\eta_{sc}(x)$. The resulting Lagrangian is \mathcal{L}_{ξ_C} with $C \rightarrow sc$. The scaling of the field can be inferred from

$$\int d^4x \bar{\xi}_{sc}(x) in_- D \frac{\not{n}_+}{2} \xi_{sc}(x) \sim 1, \quad (2.103)$$

where the covariant derivative scales as a soft-collinear momentum $iD^\mu \sim (1/\beta_h, 1, \beta_h) \Lambda_{\text{QCD}}$, hence

$$\xi_{sc}(x) \sim \sqrt{\frac{1}{\beta_h}} \Lambda_{\text{QCD}}^{3/2}, \quad \eta_{sc}(x) \sim \sqrt{\beta_h} \Lambda_{\text{QCD}}^{3/2}. \quad (2.104)$$

2.4.4 Decay Constant Matching in the Boosted Frame

As opposed to the QCD \rightarrow HQET matching briefly recalled in Section 2.2.1, we consider here the SCET \rightarrow bHQET decay constant matching, to better understand the connection between HQET and bHQET. We consider a boosted frame where $p_{H\perp} = 0$ for simplicity. As explained in Section 2.3, when going from QCD to purely collinear SCET we are simply rewriting the theory in terms of homogeneous objects in the boost power counting parameter, but the theories are equivalent. For this reason the matrix element of local two-particle collinear SCET operators are related to the QCD decay constant. In particular, by contracting (2.14) with $n_{+\alpha}$ and $n_{-\alpha}$, respectively, we can express f_H in two equivalent ways, as the matrix element of collinear currents in SCET [65]. This leads to the natural definition of the following two SCET operators,

$$\begin{aligned} \mathcal{O}_+^C &= \frac{1}{n_+ p_H} \bar{\xi}_C^{(h)}(0) \not{n}_+ \gamma^5 \xi_C(0), \\ \mathcal{O}_-^C &= -\frac{1}{n_- p_H} \bar{\xi}_C^{(h)}(0) \not{n}_+ \frac{m_h - i \overleftarrow{\not{D}}_\perp}{-in_+ \overleftarrow{D}} \frac{i \not{D}_\perp}{in_+ D} \gamma^5 \xi_C(0), \end{aligned} \quad (2.105)$$

where we have substituted the suppressed η_C field with (2.49). The hadronic matrix elements of the two operators (2.105) are by construction

$$\langle H(p_H) | \mathcal{O}_\pm^C | 0 \rangle = -i f_H. \quad (2.106)$$

The local SCET operators \mathcal{O}_\pm^C are matched to two bHQET bilinear operators

$$\begin{aligned}\mathcal{O}_+^h &= \frac{1}{m_H n_+ v} \sqrt{\frac{n_+ v}{2}} \bar{h}_n(0) \not{v}_+ \gamma^5 \xi_{sc}(0), \\ \mathcal{O}_-^h &= -\frac{1}{m_H} \sqrt{\frac{n_+ v}{2}} \bar{h}_n(0) \not{v}_+ \frac{i \not{D}_\perp}{i n_+ D} \gamma^5 \xi_{sc}(0),\end{aligned}\tag{2.107}$$

chosen such that the tree level matching is diagonal

$$\begin{pmatrix} \mathcal{O}_+^C \\ \mathcal{O}_-^C \end{pmatrix} = \left[1 + \frac{\alpha_s C_F}{4\pi} \begin{pmatrix} C_{++}^{(1)} & C_{+-}^{(1)} \\ C_{-+}^{(1)} & C_{--}^{(1)} \end{pmatrix} + \mathcal{O}(\alpha_s^2) \right] \begin{pmatrix} \mathcal{O}_+^h \\ \mathcal{O}_-^h \end{pmatrix}.\tag{2.108}$$

We define the bHQET decay constant $\tilde{f}_H(\mu)$ through the following matrix element

$$\langle H(p_H) | \mathcal{O}_+^h | 0 \rangle = -i \tilde{f}_H(\mu),\tag{2.109}$$

in analogy to the HQET one. Although probably true to all orders due to boost invariance, for our purposes it is sufficient to show at tree level that the matrix element $\langle H(p_H) | \mathcal{O}_-^h | 0 \rangle$ also equals $-i \tilde{f}_H$:

$$\begin{aligned}\langle H(p_H) | \mathcal{O}_-^h | 0 \rangle &= (1 + \mathcal{O}(\alpha_s)) \langle H(p_H) | \mathcal{O}_-^C | 0 \rangle = (1 + \mathcal{O}(\alpha_s)) \langle H(p_H) | \mathcal{O}_+^C | 0 \rangle \\ &= (1 + \mathcal{O}(\alpha_s)) \langle H(p_H) | \mathcal{O}_+^h | 0 \rangle = -i \tilde{f}_H(\mu) (1 + \mathcal{O}(\alpha_s)).\end{aligned}\tag{2.110}$$

It is sufficient to match only one of the SCET operators, the simpler \mathcal{O}_+^C , to determine the relation between the decay constants f_H and $\tilde{f}_H(\mu)$ at the one-loop order

$$\mathcal{O}_+^C = \left(1 - \frac{\alpha_s C_F}{4\pi} \left(\frac{3}{2} \ln \frac{\mu^2}{m_h^2} + 3 \right) \right) \mathcal{O}_+^h + \frac{\alpha_s C_F}{4\pi} \mathcal{O}_-^h.\tag{2.111}$$

Finally taking the hadronic matrix element of (2.111) leads to the relation between the decay constants

$$f_H = \tilde{f}_H(\mu) \left[1 - \frac{\alpha_s C_F}{4\pi} \left(\frac{3}{2} \ln \frac{\mu^2}{m_h^2} + 2 \right) + \mathcal{O}(\alpha_s^2) \right],\tag{2.112}$$

which confirms $\tilde{f}_H(\mu) = f_H^{\text{HQET}}(\mu)$, as we expected from boost invariance.

The fact that the basis of operators in bHQET is two-dimensional will be proven with a bottom-up approach in Section 3.3.2.

2.5 Decoupling Transformations

The modal effective theories presented here have a common feature which is crucial for proving factorization theorem to all orders in perturbation theory. At leading power, interactions with soft particles decouple, and can be relegated to only soft Wilson lines.

2.5.1 In HQET and bHQET

The simplest case is HQET. The interactions between the heavy quark field $h_v(x)$ and soft gluons can be eliminated from the LP Lagrangian by introducing a time-like soft Wilson line

$$Y_v(x) = \mathbf{P} \exp \left[ig_s \int_{-\infty}^0 dt v \cdot A_s(x + tv) \right], \quad (2.113)$$

and performing the non-local field-dependent field redefinition

$$h_v(x) = Y_v(x) h_v^{(0)}(x). \quad (2.114)$$

Due to the property (2.73) one can easily show

$$\mathcal{L}_{\text{HQET}} = \bar{h}_v(x) i v \cdot D h_v(x) = \bar{h}_v^{(0)}(x) Y_v^\dagger(x) i v \cdot D Y_v(x) h_v^{(0)}(x) = \bar{h}_v^{(0)}(x) i v \cdot \partial h_v^{(0)}(x), \quad (2.115)$$

therefore reducing leading power HQET to a free theory. At first sight this might look puzzling. However the theory remains non-trivial once external currents are considered. For example in presence of the weak heavy-to-light current, a tree level matching from QCD would give

$$\bar{q}(x) \gamma^\mu (1 - \gamma^5) b(x) \rightarrow \bar{q}_s(x) \gamma^\mu (1 - \gamma^5) h_v(x) = \bar{q}_s(x) \gamma^\mu (1 - \gamma^5) Y_v(x) h_v^{(0)}(x), \quad (2.116)$$

where the soft interactions between the heavy and light quark are now rewritten as interactions between a soft quark field $q_s(x)$ and a soft Wilson line $Y_v(x)$ which knows about the direction of motion of the heavy quark. The theories before and after decoupling are of course completely equivalent, however the advantage of the decoupling relies in the justification of the separation of matrix elements to all orders in the coupling constant. This point will become clearer when dealing with factorization theorems.

In bHQET the decoupling works in the same way, due to the similar form of the Lagrangian, with the only difference that we use a time-like soft-collinear Wilson line with $v^\mu \sim (1/\beta_h, 1, \beta_h)$.

2.5.2 In SCET

Now that we have understood how soft decoupling works in HQET we can extend it to SCET. The interaction of collinear quarks with a soft gluon comes from the term

$$\bar{\xi}_C(x) i n_- D \frac{\not{n}_+}{2} \xi_C(x) = \bar{\xi}_C(x) \left(i n_- \partial + g_s n_- A_s(x_-) + g_s n_- A_C(x) \right) \frac{\not{n}_+}{2} \xi_C(x), \quad (2.117)$$

in (2.50). The structure is very similar to the HQET one, with the replacement $v \rightarrow n_-$. Therefore we are encouraged to introduce light-like soft Wilson lines as

$$S_{n_\pm}(x) = \mathbf{P} \exp \left[ig_s \int_{-\infty}^0 dt n_\pm A_s(x + t n_\pm) \right], \quad (2.118)$$

and perform the fields redefinitions

$$\begin{aligned}\xi_C(x) &= S_{n_-}(x_-)\xi_C^{(0)}(x), \\ A_C(x) &= S_{n_-}(x_-)A_C^{(0)}(x)S_{n_-}^\dagger(x_-).\end{aligned}\tag{2.119}$$

By using

$$n_-^\mu \frac{\partial}{\partial x^\mu} = n_-^\mu \frac{\partial x_-^\nu}{\partial x^\mu} \frac{\partial}{\partial x_-^\nu} = n_-^\mu n_{+\mu} \frac{n_-^\nu}{2} \frac{\partial}{\partial x_-^\nu} = n_-^\nu \frac{\partial}{\partial x_-^\nu},\tag{2.120}$$

and the property (2.73), we can show

$$(in_-\partial + g_s A_s(x_-))S_n(x_-) = S_n(x_-)in_-\partial,\tag{2.121}$$

which therefore leads us to

$$\bar{\xi}_C(x)in_-D \frac{\not{n}_+}{2}\xi_C(x) = \bar{\xi}_C^{(0)}(x)in_-D_C^{(0)} \frac{\not{n}_+}{2}\xi_C^{(0)}(x),\tag{2.122}$$

with $iD_{C_\mu}^{(0)} = i\partial_\mu + g_s A_{C_\mu}^{(0)}(x)$. In this way we have decoupled soft gluons from collinear quarks. The same transformation also removes interactions between soft and collinear gluons, showing that, at leading power, soft and collinear sectors can be completely disentangled. The same caveat as in HQET applies here, where, in the presence of external currents, interactions with soft gluons will be represented by soft Wilson lines.

2.6 Reparametrization Invariance

A common feature of HQET, SCET and bHQET is the introduction of fixed reference vectors, v^μ and n_\pm^μ , which are used to split the momenta in different components. This introduces a redundancy in the theories. Concretely, in HQET, the momentum

$$p^\mu = mv^\mu + k^\mu,\tag{2.123}$$

is invariant under a ‘‘reparametrization transformation’’ [66] $\{v, k\} \rightarrow \{v+q/m, k-q\}$, where q^μ has to satisfy $(v+q/m)^2 = 1$ and needs to be of order Λ_{QCD} not to spoil the power counting of the theory. The EFT to correctly reproduce the full theory needs therefore to be reparametrization invariant (RPI). RPI can be seen as a manifestation of the Poincaré symmetry which was broken by the introduction of the reference vectors.

The same concept applies to SCET, where, due to the richer structure of the momenta decomposition, there are three types of reparametrization transformations [67]

$$\text{(I)} \begin{cases} n_-^\mu \rightarrow n_-^\mu + \delta_\perp^\mu, \\ n_+^\mu \rightarrow n_+^\mu, \end{cases} \quad \text{(II)} \begin{cases} n_-^\mu \rightarrow n_-^\mu, \\ n_+^\mu \rightarrow n_+^\mu + \epsilon_\perp^\mu, \end{cases} \quad \text{(III)} \begin{cases} n_-^\mu \rightarrow \alpha n_-^\mu, \\ n_+^\mu \rightarrow \frac{1}{\alpha} n_+^\mu, \end{cases}\tag{2.124}$$

which leave the properties $n_\pm^2 = 0$ and $n_- \cdot n_+ = 2$ intact. The parameters of the transformation are real, and need to scale as $\delta_\perp^\mu \sim \beta$, $\epsilon_\perp^\mu \sim 1$ and $\alpha \sim 1$ when applied to collinear

operators, again to preserve the power counting in the EFT [67]. As bHQET also depends on the choice of light-like vectors n_{\pm}^{μ} , it will inherit the same set of reparametrization transformations (2.124).

The power of RPI is in constraining the structure of operators in the EFT. In particular RPI relations can be used to link different orders in the power expansion [66]. Here we are only scratching the surface of this topic, as we will limit the use of RPI to Section 3.3.2 for building a basis of leading power operators in bHQET.

2.7 Standard Model Effective Field Theory

All the effective theories discussed so far follow a *top-down* philosophy. Namely that we start from a known full theory, and we deliberately integrate out some hard scales to finally get an EFT with its calculable Wilson coefficients. One can follow the opposite approach, so-called *bottom-up*, by specifying the field content and symmetries of the EFT without knowing the full theory. The second step is to build all possible effective operators, at a given power, with unknown Wilson coefficients. In this case one could try to constrain or determine the Wilson coefficients from experimental measurements, potentially obtaining informations on the structure of the full theory (in this contexts also called “UV completion”).

The most important example of a bottom-up EFT is the Standard Model Effective Field Theory (SMEFT). This is the theory arising from the full Standard Model with the addition of higher-dimensional operators.⁸ Explicitly this results in building the Lagrangian with gauge symmetry $SU(3)_c \times SU(2)_L \times U(1)_Y$

$$\mathcal{L}_{\text{SMEFT}} = \mathcal{L}_{\text{SM}} + \frac{1}{\Lambda_{\text{NP}}} \sum_k C_k^{(5)} \mathcal{Q}_k^{(5)} + \frac{1}{\Lambda_{\text{NP}}^2} \sum_k C_k^{(6)} \mathcal{Q}_k^{(6)} + \mathcal{O}\left(\frac{1}{\Lambda_{\text{NP}}^3}\right), \quad (2.125)$$

where \mathcal{L}_{SM} is the renormalizable Standard Model Lagrangian, $\mathcal{Q}_k^{(n)}$ are all the effective operators of mass dimension $n > 4$ labelled by k and $C_k^{(n)}$ are the respective dimensionless unknown Wilson coefficients. The scale Λ_{NP} sets the threshold between the Standard Model physics and the heavy, weakly coupled, new physics which is formally integrated out. Of course this picture cannot be applied to new physics models featuring undiscovered weakly coupled light degrees of freedom. In the SMEFT the power counting parameter is determined by the ratio between the higher scale in the SM, i.e. the Higgs vacuum expectation value (vev) v , and Λ_{NP} .

The Lagrangian is written in terms of the degrees of freedom of the SM before spontaneous symmetry breaking occurs. We denote the left-handed $SU(2)_L$ doublets by Q and L for quarks and leptons, while the right-handed singlets with U , D and E for the up-, down-quark and charged lepton respectively. Every field has a generation label⁹ running

⁸With this in jargon we intend operators with mass dimensions greater than 4, which hence are multiplied by coupling constants with negative mass dimensions. The presence of such operators makes the theory non-renormalizable, which therefore must be intended as an EFT valid only below a certain energy scale.

⁹We will refer to this also as the “flavour space”.

from 1 to 3, and the only non-diagonal SM interaction in flavour space comes from the Yukawa Lagrangian

$$\mathcal{L}_Y = -Y_{pr}^u \bar{Q}_p \varepsilon \phi^* U_r - Y_{pr}^d \bar{Q}_p \phi D_r - Y_{pr}^e \bar{L}_p \phi E_r + \text{h.c.}, \quad (2.126)$$

where ϕ is the $SU(2)_L$ Higgs doublet scalar field, which at the electroweak scale will acquire the vev $\langle \phi \rangle = (0, v/\sqrt{2})$. Here ε stands for the two dimensional Levi-Civita tensor, with $\varepsilon_{12} = 1$. The Yukawa couplings Y^u , Y^d and Y^e are 3×3 matrices in flavour space.

We can choose a specific generation basis for the five fermion fields without loss of generality, by reabsorbing the five unitary rotation matrices for the fields Q , U , D , L and E into the SMEFT Wilson coefficients. This will leave the SM Lagrangian invariant except for the Yukawa interactions in (2.126). We adopt the standard choice where the matrices Y^u and Y^e are diagonal while $Y_{rs}^d \propto V_{rt} [\text{diag}(m_d, m_s, m_b)]_{ts}$ is the only flavour non-diagonal term of the dimension-4 Lagrangian, whose rotation is parametrized by the physical CKM matrix. In this basis the transition from the weak eigenstates basis to the mass basis, after spontaneous symmetry breaking, requires only to perform the rotation $Q_{2p} = V_{pr} d_{Lr}$ of the second component of the $SU(2)_L$ doublet Q in generation space.

The most widely used basis for the dimension-6 operators in the SMEFT is the so-called Warsaw basis [68], with 63 operators (without considering hermitian conjugated and the flavour structure). In this thesis we will use, in Chapter 8, only the four operators which do not conserve baryon number. Explicitly they are given by

$$\begin{aligned} \mathcal{Q}_{dvw} &= \varepsilon^{abc} [\tilde{D}^a U^b] [\tilde{U}^c E], \\ \mathcal{Q}_{duq} &= \varepsilon^{abc} \varepsilon_{jk} [\tilde{D}^a U^b] [\tilde{Q}_j^c L_k], \\ \mathcal{Q}_{qqu} &= \varepsilon^{abc} \varepsilon_{jk} [\tilde{Q}_j^a Q_k^b] [\tilde{U}^c E], \\ \mathcal{Q}_{qqq} &= \varepsilon^{abc} \varepsilon_{jn} \varepsilon_{km} [\tilde{Q}_j^a Q_k^b] [\tilde{Q}_m^c L_n], \end{aligned} \quad (2.127)$$

where spinor indices are contracted within the brackets, a, b, c are colour indices ($\varepsilon^{123} = +1$), j, k, m, n are $SU(2)_L$ doublets indices, and the generation labels on the fermion fields (p, r, s, t) are not shown and can take any value. We use the short-hand notation $\tilde{\psi} \equiv \bar{\psi}^c$ for charged-conjugated fields which obey the following relations [69]

$$\psi^c = \mathcal{C} \bar{\psi}^T, \quad \bar{\psi}^c = -\psi^T \mathcal{C}^{-1}. \quad (2.128)$$

In the Dirac representation the charge conjugation matrix $\mathcal{C} = i\gamma^2\gamma^0$ satisfies

$$\mathcal{C}^\dagger = \mathcal{C}^{-1} = \mathcal{C}^T = -\mathcal{C}, \quad \mathcal{C} \gamma_\mu^T \mathcal{C}^{-1} = -\gamma_\mu. \quad (2.129)$$

Furthermore the operator structure can be simplified with the general relation

$$\tilde{\psi}_a P_{L,R} \psi_b = \tilde{\psi}_b P_{L,R} \psi_a, \quad (2.130)$$

where a and b stand for all the possible indices of the fields (colour, flavour, ...) and we made explicit the chiral projectors (implicitly understood in (2.127)).

2.8 Introduction to QCD Factorization

QCD factorization (QCDF) [70–72] is a theoretical framework where the pivotal ideas of scales separation find application. It provides a systematic way to obtain theoretical predictions for exclusive processes with energetic hadrons in the final state. The non-perturbative nature of hadronization is indeed the main obstacle, preventing us from calculating the scattering amplitudes as a sum over partonic Feynman diagrams. The central idea of QCDF is that hadronization takes place at much larger space-time distances with respect to the partonic scattering characterized by a large energy release $Q \gg \Lambda_{\text{QCD}}$. Exploiting the hierarchy between these scales, one can disentangle the short-distance (hard) scattering from the hadronic long-distance physics which does not know about the details of the partonic interaction. Since the hard-scattering happens at the partonic level with high-energy interactions, it can be treated in perturbation theory, yielding process dependent hard-functions (Wilson coefficients) order by order in the coupling constant. The left-over long-distance physics will be encoded into more universal hadronic matrix elements, which need to be determined from experimental data or with non-perturbative techniques, as lattice QCD or sum-rules.

Obviously the result is in the form of an expansion in Λ_{QCD}/Q , pointing towards a natural description within the EFT paradigm, and in particular SCET. In fact, the power of effective theories allows to prove factorization formulas valid to all orders in the perturbative expansion.

We are going to introduce QCDF for two-body non-leptonic \bar{B} decays, as it will be useful for better understanding similarities and differences with respect to QED factorization for the same process, discussed in Chapter 6.

2.8.1 Factorization Formula for $\bar{B} \rightarrow M_1 M_2$

As anticipated in Section 2.1, the starting point for describing the weakly decaying \bar{B} meson is the weak effective Hamiltonian where all the electroweak degrees of freedom have been integrated out. The \bar{B} meson mass m_B plays the role of the hard scale, as in a two-body decay the final state mesons will have back-to-back momenta of order $\mathcal{O}(m_B/2) \gg \Lambda_{\text{QCD}}$. We have to distinguish between heavy-light and light-light final states.

We start by considering decays with heavy-light final states, namely $\bar{B} \rightarrow D^{(*)}L$ decays, where L is a generic light meson. In this case the standard factorization approach considers $m_c \sim \mathcal{O}(m_b)$ and aims at integrating out the charm and bottom masses simultaneously. In Chapter 5 we will investigate the consequences of adopting a different power counting for m_c , but here we review the classic treatment.

The QCDF result is a factorization formula, up to corrections suppressed by $\mathcal{O}(\Lambda_{\text{QCD}}/m_b)$, for the matrix elements of the effective operators (2.2)

$$\langle D^{(*)}L | Q_i | \bar{B} \rangle = i f_L \sum_j F_j^{\bar{B} \rightarrow D^{(*)}}(m_L^2) \int_0^1 du T_{ij}^I(u) \phi_L(u), \quad (2.131)$$

where f_L is the light meson decay constant. The three main characters of (2.131) are the form factors $F_j^{\bar{B} \rightarrow D^{(*)}}(q^2)$, the hard-scattering kernels $T_{ij}^I(u)$ and the light-cone distribution amplitude (LCDA) $\phi_L(u)$. Each of them has a specific origin, and describes different parts of the process. Notice that this formula applies to decays where the light anti-quark in the \bar{B} meson is absorbed by the heavy $D^{(*)}$ meson. Other channels exist, depending on the specific flavour structure of the initial and final states, where factorization is not applicable. We will come back to this topic in Chapter 5.

Hard-Scattering Kernels

The hard-scattering kernels $T_{ij}^I(u)$ are the non-local Wilson coefficients encoding the physics of the short-distance partonic scattering, capturing the dependence on the hard scales m_b and m_c . They arise from a perturbative matching from QCD to HQET \times SCET_I, and will depend on the factorization scale¹⁰ μ . The non-locality arises from the arguments explained in Section 2.3.4, and is reflected by the u dependence of the hard-scattering kernels, where u is the light-cone momentum fraction of the quark inside the light meson L .

Form Factors

The form factors $F_j^{\bar{B} \rightarrow D^{(*)}}(q^2)$ are given by the matrix element of the $b \rightarrow c$ local current between the \bar{B} and $D^{(*)}$ states with momentum transfer q^μ . They describe the physics of the $\bar{B} \rightarrow D^{(*)}$ transition. The matrix element of the vector current for the transition $\bar{B} \rightarrow P$, with P a generic pseudoscalar meson, is parametrized by two scalar form factors as

$$\langle P(p') | \bar{q} \gamma^\mu b | \bar{B}(p) \rangle = F_+^{\bar{B}P}(q^2)(p^\mu + p'^\mu) + (F_0^{\bar{B}P}(q^2) - F_+^{\bar{B}P}(q^2)) \frac{m_B^2 - m_P^2}{q^2} q^\mu, \quad (2.132)$$

where $q = p - p'$ is the momentum transfer. The form factors in (2.132) do not depend on the renormalization scale since they come from a matrix element of a conserved current in QCD. At zero momentum transfer, $q^2 = 0$, the two scalar form factors are equal $F_+^{\bar{B}P}(0) = F_0^{\bar{B}P}(0)$. For the decay of a pseudoscalar \bar{B} meson to a vector meson M^* the matrix elements of the vector and axial currents are decomposed in four scalar form factors

$$\begin{aligned} \langle M^*(p', \varepsilon) | \bar{q} \gamma^\mu b | \bar{B}(p) \rangle &= - \frac{2iV^{\bar{B}M^*}(q^2)}{m_B + m_{M^*}} \varepsilon^{\mu\nu\rho\sigma} p'_\nu p_\rho \varepsilon_\sigma^*, \\ \langle M^*(p', \varepsilon) | \bar{q} \gamma^\mu \gamma^5 b | \bar{B}(p) \rangle &= (m_B + m_{M^*}) A_1^{\bar{B}M^*}(q^2) \varepsilon^{*\mu} - A_2^{\bar{B}M^*}(q^2) \frac{\varepsilon^* \cdot q}{m_B + m_{M^*}} (p + p')^\mu \\ &\quad - \frac{\varepsilon^* \cdot q}{q^2} q^\mu \left[(m_B + m_{M^*}) A_1^{\bar{B}M^*}(q^2) - (m_B - m_{M^*}) A_2^{\bar{B}M^*}(q^2) \right] \end{aligned}$$

¹⁰The hard-scattering kernels also reproduce the dependence on the UV renormalization scale ν of the weak Hamiltonian operators Q_i . This scale dependence will cancel against the scale dependence of the Wilson coefficients $C_{1,2}$ in (2.1).

$$\left. - 2m_{M^*} A_0^{\bar{B}M^*}(q^2) \right], \quad (2.133)$$

where $\varepsilon^{0123} = +1$ and all scalar form factors are positive. As the form factors include non-perturbative physics, they are usually computed in lattice QCD, or extracted from experimental data. The same form factors contribute to different processes, e.g. the semi-leptonic $\bar{B} \rightarrow D^{(*)} \ell \bar{\nu}_\ell$ decay, enhancing therefore the predictive power of the QCDF approach.

Light-Cone Distribution Amplitude

The LCDA $\phi_L(u)$ captures the soft physics of the boosted light pseudoscalar meson in the final state. It is defined from the matrix element of a non-local bilinear quark current

$$\langle L(p) | \bar{q}_1(x) \not{n}_- \gamma^5 [x, y] q_2(y) | 0 \rangle = -i f_L n_- p \int_0^1 du e^{i(up \cdot x + \bar{u}p \cdot y)} \phi_L(u), \quad (2.134)$$

where q_1 and \bar{q}_2 are the valence quarks of the light meson and $x^\mu - y^\mu \propto n_-^\mu$ is a light-like distance. As stated above, the variable u can be interpreted as the light-cone momentum fraction carried by the quark (q_1 in this case) in the meson, while the anti-quark \bar{q}_2 will carry momentum fraction $\bar{u} \equiv 1 - u$. We will review the important properties of the QCD LCDA in Section 3.1.

Light-Light Final States and the Hard-Collinear Scale

The factorization formula for $\bar{B} \rightarrow M_1 M_2$, where M_i are light mesons of masses m_{M_i} , is more complicated. It receives three contributions

$$\begin{aligned} \langle M_1 M_2 | Q_i | \bar{B} \rangle &= i f_{M_2} \sum_j F_j^{\bar{B} \rightarrow M_1}(m_{M_2}^2) \int_0^1 du T_{ij}^I(u) \phi_{M_2}(u) + (M_1 \leftrightarrow M_2) \\ &+ i f_B f_{M_1} f_{M_2} \int_0^\infty d\omega \varphi_+(\omega) \int_0^1 du dv T_i^{II}(\omega, u, v) \phi_{M_1}(v) \phi_{M_2}(u). \end{aligned} \quad (2.135)$$

The first line is the equivalent of (2.131), where the second term is taking into account the symmetric contributions where the spectator quark in the \bar{B} meson¹¹ goes into the light meson M_2 . In decay channels where only one of the two contributions is possible, M_1 will be the meson formed by the spectator quark, and the second term would be absent. The last term, in the second line, has a different nature and comes from diagrams where the spectator quark interacts with the quarks of the opposite meson M_2 through hard-collinear gluons (see Figure 2.3). This term involves the leading-twist HQET LCDA $\varphi_+(\omega)$ for the \bar{B} meson, where ω is the light-cone momentum component of the spectator quark. We will introduce this object properly in Section 3.2 as it will play a central role in this thesis. The second and third term are absent in the heavy-light final state case as they are power suppressed in that case.

¹¹Usually referred to as ‘‘spectator quark’’ only.

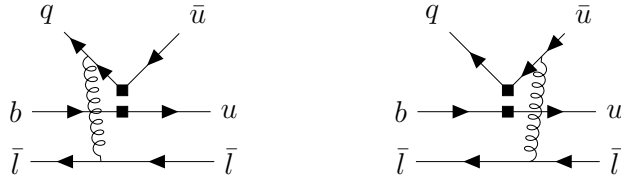


Figure 2.3: Two tree-level diagrams contributing to the spectator scattering term in the factorization formula (2.135) for light-light final states. The two square dots denote an insertion of the weak effective theory operators.

In the spectator scattering term we encounter for the first time the important distinction between the collinear and hard-collinear scale. The light mesons in the final state have highly boosted momenta with virtualities $\mathcal{O}(\Lambda_{\text{QCD}}^2)$ due to their mass. These momenta are what we call collinear and anti-collinear, where the virtuality is the same as for a soft momentum. Introducing the power counting parameter

$$\lambda = \sqrt{\frac{\Lambda_{\text{QCD}}}{m_B}}, \quad (2.136)$$

we would write the following modes

$$\begin{aligned} \text{hard (h):} & \quad k^\mu \sim m_B(1, 1, 1), \\ \text{collinear (c):} & \quad k^\mu \sim m_B(1, \lambda^2, \lambda^4), \\ \text{anti-collinear (\bar{c}):} & \quad k^\mu \sim m_B(\lambda^4, \lambda^2, 1), \\ \text{soft (s):} & \quad k^\mu \sim m_B(\lambda^2, \lambda^2, \lambda^2), \end{aligned} \quad (2.137)$$

where we see the difference with what we have introduced in (2.35). However, if we consider the tree level diagram contributing to the spectator scattering we notice that the gluon will carry the sum of a collinear and a soft momentum. The virtuality of this momentum is $\mathcal{O}(m_B \Lambda_{\text{QCD}})$, which is a new dynamically generated scale: the *hard-collinear* scale. Therefore this induces new virtual modes with homogeneous scaling

$$\begin{aligned} \text{hard-collinear (hc):} & \quad k^\mu \sim m_B(1, \lambda, \lambda^2), \\ \text{anti-hard-collinear (\bar{hc}):} & \quad k^\mu \sim m_B(\lambda^2, \lambda, 1). \end{aligned} \quad (2.138)$$

The hard-collinear scale is still perturbative and can therefore be integrated out, landing on an effective theory where only the non-perturbative degrees of freedom are present. Obviously hard-collinear modes arise in countless physical processes, and are not only relegated to two-body hadronic \bar{B} decays. The theoretical calculation is in general organized as a two step matching $\text{QCD} \rightarrow \text{SCET}_{\text{I}} \rightarrow \text{SCET}_{\text{II}}$, where in the first step only the hard scale m_B is integrated out. The first EFT is therefore a version of SCET with (anti-)hard-collinear and soft modes (the one presented in Section 2.3). The latter is then matched to a version of SCET with only (anti-)collinear and soft modes, by integrating out perturbatively the scale $\sqrt{m_B \Lambda_{\text{QCD}}}$. In this thesis we will always deal with SCET_{I} and hence do not present a complete treatment of the formalism for $\text{SCET}_{\text{I}} \rightarrow \text{SCET}_{\text{II}}$ matchings.

Part II

Mass Effects of Boosted Heavy Mesons

Chapter 3

QCD Light-Cone Distribution Amplitudes for Heavy Mesons

As shown in the example of $\bar{B} \rightarrow M_1 M_2$ decays, LCDAs frequently arise in factorization theorems involving boosted mesons. When the meson is light, the only physical scale on which the matrix element (2.134) depends is Λ_{QCD} , making the LCDA a fully non-perturbative function. On the other hand, for a heavy pseudoscalar meson $H = (h\bar{q})$ of mass $m_H \gg \Lambda_{\text{QCD}}$ moving in the collinear direction, the matrix element¹

$$\langle H(p_H) | \bar{\psi}_h(0) \not{p}_+ \gamma^5 [0, tn_+] q(tn_+) | 0 \rangle = -i f_H n_+ p_H \int_0^1 du e^{iutn_+ p_H} \phi_H(u; \mu), \quad (3.1)$$

will also depend on the perturbative scale m_H . Notice that the LCDA is boost invariant, and therefore cannot depend on the large component of the meson momentum p_H .

In this chapter we will study the LCDA $\phi_H(u; \mu)$ (from now on we will drop the subscript H for simplicity), with the goal of factorizing it, at leading power in λ_h (see (2.81)), into a perturbative mass dependent part, and a universal, mass-independent, fully non-perturbative function. By means of such a factorization formula [28], we will be able to resum the large logarithms of the scale ratio Λ_{QCD}/m_H which threaten the convergence of the perturbative series. In this way we would be able to improve the precision of theoretical predictions on exclusive processes involving boosted heavy mesons. In particular we are going to apply it to the \bar{B} meson QCD LCDA appearing in the process $W^\pm \rightarrow B^\pm \gamma$ in Chapter 4 and to the colour-suppressed amplitudes in $\bar{B} \rightarrow DL$ decays in Chapter 5 where a D meson LCDA is needed.

¹Notice that the definition of the LCDA for a heavy meson is the same one as for a light meson. In this case however we choose u to be the light-cone momentum fraction of the light anti-quark \bar{q} in H .

3.1 The QCD LCDA

We collect in this section some useful properties of the QCD LCDA. First of all, by setting $t = 0$ in (3.1) we have

$$\int_0^1 du \phi(u; \mu) = 1, \quad (3.2)$$

valid at all renormalization scales μ , due to the definition of the decay constant.

The renormalization group evolution equation is written in the form of a convolution [73–75]

$$\mu \frac{d\phi(u; \mu)}{d\mu} = -\frac{\alpha_s C_F}{\pi} \int_0^1 dv V_{\text{ERBL}}(u, v) \phi(v; \mu), \quad (3.3)$$

where $V_{\text{ERBL}}(u, v)$ is the Efremov-Radyushkin-Brodsky-Lepage (ERBL) evolution kernel [73–75], known up to three loops in QCD² [76]. The one-loop evolution kernel in $\overline{\text{MS}}$

$$\begin{aligned} V_{\text{ERBL}}(u, v) &= - \left[\theta(v - u) \frac{u}{v} \left(1 + \frac{1}{v - u} \right) + \theta(u - v) \frac{\bar{u}}{\bar{v}} \left(1 + \frac{1}{u - v} \right) \right]_{u+} \\ &= - \left[\theta(v - u) \frac{u}{v} \left(1 + \frac{1}{v - u} \right) + \theta(u - v) \frac{\bar{u}}{\bar{v}} \left(1 + \frac{1}{u - v} \right) \right]_{v+} \\ &\quad - \frac{1}{2} \delta(v - u) \left(3 + 2\bar{v} \ln v + 2v \ln \bar{v} \right), \end{aligned} \quad (3.4)$$

is expressed in terms of plus-distributions defined as

$$\begin{aligned} \int_0^1 du f(u) [g(u, v)]_{u+} &= \int_0^1 du (f(u) - f(v)) g(u, v), \\ \int_0^1 dv f(v) [g(u, v)]_{v+} &= \int_0^1 dv (f(v) - f(u)) g(u, v), \end{aligned} \quad (3.5)$$

where we indicate with a subscript the variable in which the integration is intended. We use the standard notation $\bar{x} \equiv 1 - x$ for momentum fraction variables.

A useful and common representation of the LCDA is in terms of Gegenbauer polynomials $C_n^{(3/2)}(2u - 1)$ which diagonalize the one-loop ERBL kernel

$$\phi(u; \mu) = 6u(1 - u) \left[1 + \sum_{n=1}^{\infty} a_n(\mu) C_n^{(3/2)}(2u - 1) \right], \quad (3.6)$$

and automatically ensures that the LCDA is normalized to 1. The Gegenbauer moments $a_n(\mu)$, defined through

$$a_n(\mu) = \frac{2(2n + 3)}{3(n + 1)(n + 2)} \int_0^1 du C_n^{(3/2)}(2u - 1) \phi(u; \mu), \quad (3.7)$$

²Technically at three loops the explicit form of the evolution kernel is not known. Only the evolution equation for the first 12 Gegenbauer moments was derived.

encode the scale dependence of the LCDA and are expected to decrease for increasing n such that the series can be truncated. It is useful to define

$$N_n \equiv \frac{2(2n+3)}{3(n+1)(n+2)}, \quad (3.8)$$

which enters the orthogonality condition of the Gegenbauer polynomials

$$6N_n \int_0^1 du u(1-u) C_n^{(3/2)}(2u-1) C_m^{(3/2)}(2u-1) = \delta_{nm}. \quad (3.9)$$

The evolution of the Gegenbauer moments from an initial scale μ_0 to a scale μ takes the simple form

$$\frac{a_n(\mu)}{a_n(\mu_0)} = \left(\frac{\alpha_s(\mu)}{\alpha_s(\mu_0)} \right)^{\frac{\gamma_n}{2\beta_0}}, \quad (3.10)$$

where β_0 is defined in Appendix A and the anomalous dimension is given by

$$\gamma_n = 2C_F \left(4 \sum_{k=1}^{n+1} \frac{1}{k} - \frac{2}{(n+1)(n+2)} - 3 \right). \quad (3.11)$$

As $\gamma_n > 0$ for $n \geq 1$, the Gegenbauer moments decrease when evolved to higher scales, implying an asymptotic form for the QCD LCDA

$$\phi(u; \mu \rightarrow \infty) = 6u(1-u). \quad (3.12)$$

The behaviour of $\phi(u; \mu)$ at the endpoints $u = 0$ and $u = 1$ is linear, allowing well defined convolutions with $1/u$ and $1/\bar{u}$.

The running of $\phi(u; \mu)$ between two scales μ_0 and μ can be also expressed in the form of a convolution of the LCDA at a lower scale with an evolution kernel

$$\phi(x; \mu) = \int_0^1 du f_{\text{ERBL}}(x, u, \mu, \mu_0) \phi(u; \mu_0), \quad (3.13)$$

which will turn out useful in Section 4.2.1. Using (3.6), (3.7), (3.9) and (3.10), we obtain the evolution function $f_{\text{ERBL}}(x, u, \mu, \mu_0)$ as an expansion in Gegenbauer polynomials

$$f_{\text{ERBL}}(x, u, \mu, \mu_0) = 6x\bar{x} \sum_{n=0}^{\infty} N_n \left(\frac{\alpha_s(\mu)}{\alpha_s(\mu_0)} \right)^{\frac{\gamma_n}{2\beta_0}} C_n^{(3/2)}(2x-1) C_n^{(3/2)}(2u-1). \quad (3.14)$$

This evolution function has the following properties

$$f_{\text{ERBL}}(x, u, \mu, \mu_0) \xrightarrow{\mu \rightarrow \infty} 6x\bar{x}, \quad f_{\text{ERBL}}(x, u, \mu_0, \mu_0) = \delta(x-u). \quad (3.15)$$

3.2 The HQET LCDA

The universal mass-independent non-perturbative function on which we want to match the QCD LCDA is naturally the leading twist HQET LCDA $\varphi_+(\omega; \mu)$. This function is defined after having integrated out the heavy quark mass m_h , i.e. in HQET, as

$$\langle H_v | \bar{h}_v(0) \not{v} \gamma^5 [0, tn_+] q_s(tn_+) | 0 \rangle = -i F_{\text{stat}}(\mu) n_+ v \int_0^\infty d\omega e^{i\omega t n_+ v} \varphi_+(\omega; \mu), \quad (3.16)$$

where $|H_v\rangle$ is the m_h -independent heavy meson state and $F_{\text{stat}}(\mu)$ is the static HQET decay constant

$$|H_v\rangle = \frac{1}{\sqrt{m_H}} \left(1 + \mathcal{O}(\lambda_h) \right) |H(p_H)\rangle, \quad F_{\text{stat}}(\mu) = \sqrt{m_H} f_H^{\text{HQET}}(\mu). \quad (3.17)$$

As anticipated in Section 2.8.1, ω is a dimensionful variable playing the role of the light-cone momentum component of the light anti-quark. The integration domain in (3.16) is extended up to infinity since the heavy quark mass in the effective theory is an infinite source of energy, but parametrically $\omega \sim \Lambda_{\text{QCD}} \ll m_h$. An important hadronic parameter, entering many results from QCD factorization, is the first inverse moment [70]

$$\lambda_B^{-1}(\mu) \equiv \int_0^\infty \frac{d\omega}{\omega} \varphi_+(\omega; \mu). \quad (3.18)$$

We now briefly review some important properties of the HQET LCDA which will be of high relevance in the following of this thesis.

3.2.1 Renormalization Group Evolution

The evolution equation for the HQET LCDA is also in the form of a convolution [77]

$$\mu \frac{d\varphi_+(\omega; \mu)}{d\mu} = -\frac{\alpha_s C_F}{\pi} \int_0^\infty d\nu \Gamma_{\text{LN}}(\omega, \nu; \mu) \varphi_+(\nu; \mu), \quad (3.19)$$

with the Lange-Neubert kernel, at one-loop, given by [77]

$$\Gamma_{\text{LN}}(\omega, \nu; \mu) = -\omega \left[\frac{\theta(\nu - \omega)}{\nu(\nu - \omega)} + \frac{\theta(\omega - \nu)}{\omega(\omega - \nu)} \right]_{\nu_+} + \delta(\omega - \nu) \left(\ln \frac{\mu}{\omega} - \frac{1}{2} \right), \quad (3.20)$$

where the plus-distributions are defined in analogy to (3.5) as

$$\begin{aligned} \int_0^\infty d\omega f(\omega) \left[g(\omega, \nu) \right]_{\omega_+} &= \int_0^\infty d\omega (f(\omega) - f(\nu)) g(\omega, \nu), \\ \int_0^\infty d\nu f(\nu) \left[g(\omega, \nu) \right]_{\nu_+} &= \int_0^\infty d\nu (f(\nu) - f(\omega)) g(\omega, \nu). \end{aligned} \quad (3.21)$$

The two-loop evolution kernel is also known [78, 79], as well as the analytical solution to the two-loop RG equation in momentum space [80].

3.2.2 Normalization and Cut-Off Moments

A peculiar property of the HQET LCDA is that, due to its evolution equation (3.19), it has a divergent normalization integral. In particular the singularity arises from the region $\omega \rightarrow \infty$, where a non-integrable tail is radiatively generated. Nevertheless one can define the so-called “cut-off moments”, for integers $N \geq 0$, as [81]

$$M_N(\Lambda_{\text{UV}}; \mu) \equiv \int_0^{\Lambda_{\text{UV}}} d\omega \omega^N \varphi_+(\omega; \mu), \quad (3.22)$$

where $\Lambda_{\text{UV}} \gg \Lambda_{\text{QCD}}$ plays the role of a hard cut-off. It has been shown that the cut-off moments can be computed perturbatively as a power expansion in $\Lambda_{\text{QCD}}/\Lambda_{\text{UV}}$ [81]. Of particular importance for us is the leading power expression for the zeroth moment

$$M_0(\Lambda_{\text{UV}}) = \int_0^{\Lambda_{\text{UV}}} d\omega \varphi_+(\omega) = 1 - \frac{\alpha_s C_F}{4\pi} \left(2 \ln^2 \frac{\mu}{\Lambda_{\text{UV}}} + 2 \ln \frac{\mu}{\Lambda_{\text{UV}}} + \frac{\pi^2}{12} \right) + \mathcal{O}\left(\alpha_s \frac{\Lambda_{\text{QCD}}}{\Lambda_{\text{UV}}}, \alpha_s^2\right), \quad (3.23)$$

where we omitted the μ dependence.

3.2.3 Asymptotic Behaviours

An important consequence of (3.23) is that it can be used to extract, in a model-independent way, the asymptotic behaviour of $\varphi_+(\omega)$ for $\omega \gg \Lambda_{\text{QCD}}$ [81]

$$\varphi_+(\omega) = \frac{dM_0(\Lambda_{\text{UV}})}{d\Lambda_{\text{UV}}} \Big|_{\Lambda_{\text{UV}}=\omega} = \frac{\alpha_s C_F}{2\pi\omega} \left(\ln \frac{\mu^2}{\omega^2} + 1 + \mathcal{O}\left(\frac{\Lambda_{\text{QCD}}}{\omega}\right) \right) + \mathcal{O}(\alpha_s^2), \quad (3.24)$$

which is often referred to as the “radiative tail” of the HQET LCDA. For later convenience we define the asymptotic function

$$\varphi_+^{\text{asy}}(\omega) \equiv \frac{\alpha_s C_F}{2\pi\omega} \left(\ln \frac{\mu^2}{\omega^2} + 1 \right), \quad (3.25)$$

such that we can approximate $\varphi_+(\omega) \rightarrow \varphi_+^{\text{asy}}(\omega)$ when $\omega \gg \Lambda_{\text{QCD}}$. The $1/\omega$ behaviour of the tail is indeed responsible for the logarithmically divergent normalization.

On the opposite end of the spectrum, $\omega \rightarrow 0$, the HQET LCDA behaves linearly

$$\varphi_+(\omega) \sim \omega, \quad (3.26)$$

as emerges from QCD sum rules [82].

3.3 Matching

In order to achieve a factorization formula for the QCD LCDA of the boosted heavy meson H , we will perform a perturbative matching³ from SCET_I \rightarrow bHQET, introduced respectively in Sections 2.3 and 2.4. By means of the gauge invariant building blocks (2.77), we

³Since the LCDAs are boost invariant quantities one can also perform the matching in the rest frame, and we explicitly checked that we would get the same result by matching QCD \rightarrow HQET. However the boosted frame is the more natural one when thinking about a full process with various collinear sectors.

define in momentum space the two-particle operator

$$\mathcal{O}_C(u) = \int \frac{dt}{2\pi} e^{-iutn_+ + p} \bar{\chi}_C^{(h)}(0) \not{n}_+ \gamma^5 \chi_C(tn_+), \quad (3.27)$$

such that

$$\langle H(p_H) | \mathcal{O}_C(u) | 0 \rangle = -i f_H \phi(u; \mu). \quad (3.28)$$

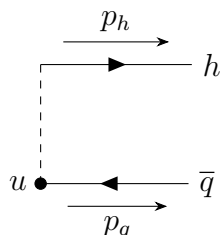
The momentum p assumes the value p_H when taking the matrix element with the meson state, or the sum of the parton momenta in partonic computations. The subscript h in (3.27) denotes the massive SCET field, opposed to the massless χ_C field. To have a physical intuition, the LCDA $\phi(u; \mu)$ can be roughly interpreted as the probability amplitude of producing the meson in a configuration where the light anti-quark carries light-cone momentum fraction u and the heavy quark carries light-cone momentum fraction $\bar{u} = 1 - u$.

The dependence on u of $\mathcal{O}_C(u)$ introduces a new complication with respect to the usual factorization of local operators. In fact, we know that the QCD LCDA $\phi(u; \mu)$ for renormalization scales $\mu \gg m_h$ tends to a symmetric form in the exchange $u \leftrightarrow \bar{u}$. However for scales $\mu \lesssim m_h$ we expect the function to develop an asymmetric peak due to the large mass difference of its constituents quarks. The latter is the situation we want to study, and we set for now the scale $\mu \sim m_h$, dropping it from the arguments of $\phi(u)$ unless otherwise specified. At this matching scale, the light anti-quark in the heavy meson will carry only a fraction $\mathcal{O}(\lambda_h)$ of the total light-cone momentum. For this reason we can expect the LCDA to have a peak in the region $u \sim \mathcal{O}(\lambda_h)$ and to be suppressed in the region $u \sim \mathcal{O}(1)$. This implies that we have to deal with an inhomogeneous function in the power counting parameter, characterized by two regions [71]

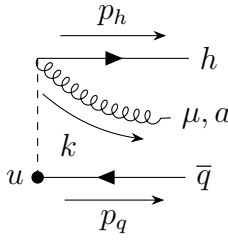
$$\phi(u) \sim \begin{cases} \lambda_h^{-1}, & \text{for } u \sim \lambda_h \quad (\text{“peak”}) \\ 1, & \text{for } u \sim 1 \quad (\text{“tail”}) \end{cases} \quad (3.29)$$

where the scalings are fixed by the normalization condition. In light of these facts, in order to perform a consistent calculation at leading power in λ_h , we will have to perform the matching in the two regions separately. Whether the two results agree in an intermediate region $\lambda_h \ll u \ll 1$, which we will call the “overlap region”, will be a strong consistency check of the matching.

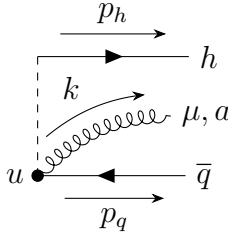
Before diving into the details of the computation, it is helpful to understand the Feynman rules for the insertion of the non-local operator $\mathcal{O}_C(u)$



$$= \not{n}_+ \gamma^5 \delta(n_+ p_q - u n_+ p_H), \quad (3.30)$$



$$= g_s T^a \not{k}_+ \gamma^5 \frac{n_+^\mu}{n_+ k_+ + i\eta} \delta(n_+ p_q - u n_+ p_H), \quad (3.31)$$



$$= -g_s T^a \not{k}_+ \gamma^5 \frac{n_+^\mu}{n_+ k_+ + i\eta} \delta(n_+ p_q + n_+ k - u n_+ p_H). \quad (3.32)$$

The dashed line represents the non-locality of $\mathcal{O}_C(u)$, and the momentum fraction u is injected at the vertex denoted by the dot. The gluons come from the Wilson lines in the definition of the gauge invariant fields $\bar{\chi}_C^{(h)}$ and χ_C . They arise from the first non-trivial term in the expansion in g_s of the exponential in (2.74), while terms $\mathcal{O}(g_s^2)$ from a single Wilson line do not contribute to the on-shell matrix elements computed in the following. The most important elements, which introduce the u dependence in the partonic graphs, are the delta functions. They enforce the large component of the sum of momenta flowing out from the light anti-quark vertex to take the value $u n_+ p_H$.

3.3.1 Peak Region

We start by considering the matching of the QCD LCDA in the peak region, namely for values of $u \sim \lambda_h$. Since in the HQET LCDA $\varphi_+(\omega)$ the variable ω must have values parametrically of order $\mathcal{O}(\Lambda_{\text{QCD}})$, we expect in this region to have a contribution to the matching already at tree level. We define the bHQET non-local operator

$$\mathcal{O}_h(\omega) = \frac{1}{m_H} \int \frac{dt}{2\pi} e^{-i\omega t n_+ v} \sqrt{\frac{n_+ v}{2}} \bar{h}_n(0) W_{sc}(0) \not{k}_+ \gamma^5 \chi_{sc}(t n_+) \sim \frac{\Lambda_{\text{QCD}}^2}{m_H}, \quad (3.33)$$

which is simply the boosted version of the Fourier transform of the operator in (3.16). Notice that the explicit factor $n_+ v$ in the exponential leaves ω to be the light-cone component of the spectator anti-quark momentum in the H rest frame. The Feynman rules for the insertion of $\mathcal{O}_h(\omega)$ are analogous to (3.30)–(3.32) with the replacement $u n_+ p_H \rightarrow \omega n_+ v$.

Due to the relation (2.90), the matrix element of $\mathcal{O}_h(\omega)$ can be expressed in terms of the leading twist HQET LCDA

$$\langle H(p_H) | \mathcal{O}_h(\omega) | 0 \rangle = -i \tilde{f}_H \varphi_+(\omega), \quad (3.34)$$

where \tilde{f}_H is the scale-dependent bHQET decay constant, shown to be equivalent to the HQET one in Section 2.4.4. For the external state we will always use the standard QCD normalization convention. The relation (3.34) holds at leading power in λ_h , but power

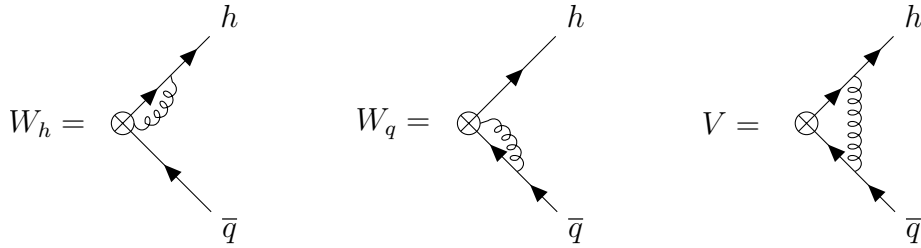


Figure 3.1: Contributions to the on-shell partonic matrix elements: the operator insertions are represented with \otimes . The vertex diagram V represents the gluon exchange between the two constituent quarks. W_h and W_q stand for interactions between the Wilson lines and the heavy and light quark, respectively. External field renormalization diagrams are not shown.

corrections to this relation are not worrying as they could be removed by employing the definition (2.91) for the bHQET field.

The matching equation takes the form of a convolution

$$\mathcal{O}_C(u) = \int_0^\infty d\omega \mathcal{J}_p(u, \omega) \mathcal{O}_h(\omega), \quad (3.35)$$

where $\mathcal{J}_p(u, \omega)$ is the perturbative “jet function” capturing the hard-collinear scale m_h^2 in the peak region. Once the jet function is determined, by taking the hadronic matrix element of the matching equation we can finally establish a relation between the QCD LCDA and the HQET LCDA in the peak region

$$\phi(u) = \frac{\tilde{f}_H}{f_H} \int_0^\infty d\omega \mathcal{J}_p(u, \omega) \varphi_+(\omega). \quad (3.36)$$

Our goal is to compute $\mathcal{J}_p(u, \omega)$ at the one-loop order by taking the on-shell matrix elements of the matching equation (3.35) between partonic states. This is allowed since $\mathcal{J}_p(u, \omega)$ is independent on the low-energy hadronic physics. We start by writing

$$\langle h(p_h) \bar{q}(p_q) | \mathcal{O}_C(u) | 0 \rangle_{\text{SCET}} = \int_0^\infty d\omega \mathcal{J}_p(u, \omega) \langle h(p_h) \bar{q}(p_q) | \mathcal{O}_h(\omega) | 0 \rangle_{\text{bHQET}}, \quad (3.37)$$

where we will use for brevity the notation $p_H \equiv p_h + p_q$.

We begin with the computation of the SCET matrix element on the left-hand side to $\mathcal{O}(\alpha_s)$. This involves the three diagrams shown in Figure 3.1, where \otimes denotes the operator insertion, summing up the two Wilson lines contributions from (3.31) and (3.32) in the first two diagrams. We define the external momentum fraction variable $s \equiv n_+ p_q / n_+ p_H$, which in general satisfies $0 \leq s \leq 1$. As a first step we perform the computation in SCET without any scaling assumption on the variables u and s . This means that the result will contain both the peak and the tail region. Only later we will impose the condition from the matching equation of p_q being soft-collinear, implying always $s \sim \lambda_h$, and either $u \sim \lambda_h$ or $u \sim 1$ for the peak or tail region respectively.

As the tree-level trivially implies $u = s$, we write the matrix element to the one-loop order in the form

$$\begin{aligned} \langle h(p_h)\bar{q}(p_q)|\mathcal{O}_C(u)|0\rangle_{\text{SCET}} &= \frac{1}{n_+p_H}\bar{u}(p_h)\not{n}_+\gamma^5v(p_q)\left\{\delta(u-s)+\frac{\alpha_s C_F}{4\pi}M_+^{(1)}(u,s)\right\} \\ &+ \frac{1}{n_-p_H}\bar{u}(p_h)\not{n}_-\gamma^5v(p_q)\frac{\alpha_s C_F}{4\pi}M_-^{(1)}(u,s), \end{aligned} \quad (3.38)$$

where at order α_s another independent Dirac structure arises from the vertex diagram. The superscripts denote the coefficients of $\alpha_s C_F/(4\pi)$ in the perturbative expansion. We made the notation more compact and transparent by re-expressing the SCET result in terms of full QCD spinors through $\bar{\xi}_{n_-}(p_h) = \bar{u}(p_h)\frac{\not{n}_+\not{n}_-}{4}$ and $\xi_{n_-}(p_q) = \frac{\not{n}_-\not{n}_+}{4}v(p_q)$. Explicitly the substitution reads

$$\begin{aligned} \frac{1}{n_+p_H}\bar{\xi}_{n_-}(p_h)\not{n}_+\gamma^5\xi_{n_-}(p_q) &= \frac{1}{n_+p_H}\bar{u}(p_h)\not{n}_+\gamma^5v(p_q), \\ \frac{1}{m_H}\bar{\xi}_{n_-}(p_h)\not{n}_+\frac{\not{p}_{q\perp}}{n_+p_q}\gamma^5\xi_{n_-}(p_q) &= \frac{1}{m_H}\bar{u}(p_h)\not{n}_+\frac{\not{p}_{q\perp}}{n_+p_q}\gamma^5v(p_q) = \frac{(-1)}{n_-p_H}\bar{u}(p_h)\not{n}_-\gamma^5v(p_q). \end{aligned} \quad (3.39)$$

In the second line we used the equations of motion of both quarks to simplify the Dirac structure

$$\bar{u}(p_h)\not{n}_+\frac{\not{p}_{q\perp}}{n_+p_q}\gamma^5v(p_q) = -\frac{1}{n_-v}\bar{u}(p_h)\not{n}_-\gamma^5v(p_q). \quad (3.40)$$

Notice that in order not to miss the second Dirac structure in SCET one has to keep the power suppressed momentum component $p_{q\perp}$ at the early stage of the computation, and finally set $p_{q\perp} \rightarrow 0$ after the substitution (3.40). This term appears due to the equation of motion of the suppressed η spinor in SCET.

In the peak region, $M_-(u, s)$ is power suppressed, as explicitly checked in Appendix B.3, and we hence focus only on $M_+(u, s)$ for now. We use dimensional regularization with $d = 4 - 2\epsilon$ for both UV and IR divergences. Since in this case the diagram W_q is scaleless, the renormalized one-loop on-shell matrix element is given by

$$M_+^{(1)}(u, s) = V_+(u, s) + W_h(u, s) + \frac{1}{2}Z_\xi^{OS(1)}\delta(u-s) + Z_{\mathcal{O}_C}^{(1)}(u, s), \quad (3.41)$$

with the on-shell field-strength renormalization constant of the heavy quark

$$Z_\xi^{OS(1)} = -\frac{3}{\epsilon} - 3\ln\frac{\mu^2}{m_h^2} - 4, \quad (3.42)$$

and the operator renormalization kernel [73–75] in $\overline{\text{MS}}$

$$Z_{\mathcal{O}_C}^{(1)}(u, s) = -\frac{2}{\epsilon}\left[\theta(s-u)\frac{u}{s}\left(1+\frac{1}{s-u}\right) + \theta(u-s)\frac{\bar{u}}{s}\left(1+\frac{1}{u-s}\right)\right]_{s+}$$

$$-\frac{1}{\epsilon}\delta(s-u)\left(3+2\bar{s}\ln s+2s\ln\bar{s}\right), \quad (3.43)$$

here written as plus-distributions with respect to the second argument s instead of the more conventional first one, u . The renormalization kernel (3.43) is related to the one-loop ERBL evolution kernel by

$$V_{\text{ERBL}}(u,v)=\frac{\epsilon}{2}Z_{\mathcal{O}_C}^{(1)}(u,v). \quad (3.44)$$

The results for the single diagrams, as well as their expansions in regions, are reported in detail in Appendix B.

We find

$$\begin{aligned} M_+^{(1)}(u,s) = & 2\left[\theta(s-u)\frac{u}{s}\left(\left(\frac{1}{s-u}+1\right)\left(\ln\frac{\bar{s}\mu^2}{u(s-u)m_h^2}+i\pi\right)-1\right)\right]_{s+} \\ & +2\left[\theta(u-s)\frac{\bar{u}}{\bar{s}(u-s)}\left(2\ln\frac{\bar{s}\mu}{(u-s)m_h}+\frac{u}{s}\ln\frac{u\bar{s}}{u-s}\right)\right]_{s+} \\ & +\delta(u-s)\left\{-\frac{1}{\epsilon^2}-\frac{1}{\epsilon}\left(2\ln\frac{\bar{s}\mu}{sm_h}+2\pi i+\frac{5}{2}\right)\right. \\ & -2\ln^2\frac{\mu}{sm_h}+2\ln s\ln\frac{\mu^2}{sm_h^2}+\ln\frac{\mu}{m_h}-4\pi i\ln\frac{\mu}{sm_h}+\frac{11}{12}\pi^2+2 \\ & -s\left(\ln^2 s+2\left(1-2\ln\frac{\mu}{sm_h}\right)\ln\frac{\bar{s}}{s}+2\pi i\ln s+\frac{\pi^2}{3}\right) \\ & \left.-2\ln\bar{s}\left(2\ln\frac{\mu}{sm_h}-1\right)+2(2-s)\text{Li}_2(s)\right\} \\ & +2\left[\theta(u-s)\left(\frac{\bar{u}}{\bar{s}}\left(2\ln\frac{\bar{s}\mu}{(u-s)m_h}-1\right)+\frac{u}{s}\ln\frac{u\bar{s}}{u-s}\right)\right]_{s+}, \quad (3.45) \end{aligned}$$

where, by employing a non-dimensional IR regulator, we explicitly checked that only IR divergences are left after UV renormalization.

As previously mentioned, the matching equation (3.35) in the peak region is valid when $s\sim\lambda_h$ and $u\sim\lambda_h$. Expanding (3.45) in this limit at leading power yields to

$$\begin{aligned} M_+^{(1)}(u,s)|_{u,s\ll 1} = & 2\left[\frac{\theta(s-u)u}{s-u}\frac{u}{s}\left(\ln\frac{\mu^2}{u(s-u)m_h^2}+i\pi\right)\right]_{s+} \\ & +2\left[\frac{\theta(u-s)}{u-s}\left(2\ln\frac{\mu}{(u-s)m_h}+\frac{u}{s}\ln\frac{u}{u-s}\right)\right]_{s+} \\ & +\delta(u-s)\left\{-\frac{1}{\epsilon^2}-\frac{1}{\epsilon}\left(2\ln\frac{\mu}{sm_h}+2\pi i+\frac{5}{2}\right)\right\} \end{aligned}$$

$$- 2 \ln^2 \frac{\mu}{sm_h} + 2 \ln s \ln \frac{\mu^2}{sm_h^2} + \ln \frac{\mu}{m_h} - 4\pi i \ln \frac{\mu}{sm_h} + \frac{11}{12} \pi^2 + 2 \left. \right\}. \quad (3.46)$$

The expanded result agrees with the region computation [57] performed in Appendix B.3, as expected. The result consists in the sum of a hard-collinear and a soft-collinear region, where the bHQET matrix element in the matching equation should exactly cancel the soft-collinear region, such that the perturbative jet function reproduces correctly the physics of the hard-collinear scale.

We now proceed to the calculation of the bHQET matrix element, in order to finally be able to extract the jet function $\mathcal{J}_p(u, \omega)$ on the right-hand side of the matching equation (3.35). We write the bHQET matrix element in the form

$$\begin{aligned} & \langle h(p_h) \bar{q}(p_q) | \mathcal{O}_h(\omega) | 0 \rangle_{\text{bHQET}} \\ &= \frac{1}{n_+ p_H} \bar{u}(p_h) \not{h}_+ \gamma^5 v(p_q) \left\{ \delta \left(\frac{n_+ p_q}{n_+ v} - \omega \right) + \frac{\alpha_s C_F}{4\pi} N^{(1)} \left(\omega, \frac{n_+ p_q}{n_+ v} \right) \right\}. \end{aligned} \quad (3.47)$$

The renormalized one-loop on-shell amplitude

$$N^{(1)}(\omega, \nu) = V_{\text{bHQET}}(\omega, \nu) + W_{h\text{bHQET}}(\omega, \nu) + Z_{\mathcal{O}_h}^{(1)}(\omega, \nu), \quad (3.48)$$

is expressed in terms of the equivalent of the diagrams in Figure 3.1 and UV renormalization factors. Since the heavy mass has been integrated out, the one-loop bHQET on-shell field strength renormalization constant is scaleless. The $\overline{\text{MS}}$ operator renormalization kernel

$$Z_{\mathcal{O}_h}^{(1)}(\omega, \nu) = -\frac{2}{\epsilon} \left[\frac{\theta(\omega - \nu)}{\omega - \nu} + \frac{\omega \theta(\nu - \omega)}{\nu \nu - \omega} \right]_{\nu_+} + \delta(\omega - \nu) \left(\frac{1}{\epsilon^2} + \frac{2}{\epsilon} \ln \frac{\mu}{\nu} - \frac{5}{2\epsilon} \right), \quad (3.49)$$

is the usual Lange-Neubert kernel for the HQET leading-twist LCDA $\varphi_+(\omega)$ [77], as expected from boost invariance. Combining the results for the single diagrams provided in Appendix B.2 and expanding in ϵ , we find

$$\begin{aligned} N^{(1)}(\omega, \nu) &= 2 \left[\frac{\theta(\nu - \omega)}{\nu - \omega} \frac{\omega}{\nu} \left(\ln \frac{\mu^2}{\omega(\nu - \omega)} + i\pi \right) \right]_{\nu_+} \\ &+ 2 \left[\frac{\theta(\omega - \nu)}{\omega - \nu} \left(2 \ln \frac{\mu}{\omega - \nu} + \frac{\omega}{\nu} \ln \frac{\omega}{\omega - \nu} \right) \right]_{\nu_+} \\ &- \delta(\omega - \nu) \left(\frac{1}{\epsilon^2} + \frac{1}{\epsilon} \left(2 \ln \frac{\mu}{\nu} + 2\pi i + \frac{5}{2} \right) + 4 \ln^2 \frac{\mu}{\nu} + 4\pi i \ln \frac{\mu}{\nu} - \frac{5\pi^2}{6} \right). \end{aligned} \quad (3.50)$$

By expanding the matching equation (3.35) in α_s we are now able to extract the matching function $\mathcal{J}_p(u, \omega)$ at one loop. At tree level

$$\delta \left(\frac{n_+ p_q}{n_+ p_H} - u \right) = \int_0^\infty d\omega \mathcal{J}_p^{(0)}(u, \omega) \delta \left(\frac{n_+ p_q}{n_+ v} - \omega \right), \quad (3.51)$$

and, up to power corrections, we can identify $p_H = p_h + p_q$ with $m_H v$, such that

$$\mathcal{J}_p^{(0)}(u, \omega) = \delta\left(u - \frac{\omega}{m_H}\right)\theta(m_H - \omega), \quad (3.52)$$

where the theta-function arises from the constraint $u \leq 1$ of the full theory. At order α_s , we obtain the general expression

$$\mathcal{J}_p^{(1)}(u, \omega) = \theta(m_H - \omega) \left\{ M^{(1)}\left(u, \frac{\omega}{m_H}\right) - m_H N^{(1)}(u m_H, \omega) \right\}, \quad (3.53)$$

where we have to insert (3.46) and (3.50). As they should, the IR poles of the full theory and the EFT coincide, giving a well defined short-distance matching coefficient. Due to the simple replacement $[\dots]_{\omega/m_H+} \rightarrow [\dots]_{\omega+}$ on the plus-distributions, the non-local terms drop out in the difference (3.53). The one-loop jet function in the peak region takes therefore a very simple form

$$\mathcal{J}_p(u, \omega) = \theta(m_H - \omega) \delta\left(u - \frac{\omega}{m_H}\right) \left(1 + \frac{\alpha_s C_F}{4\pi} \mathcal{J}_{\text{peak}}^{(1)} + \mathcal{O}(\alpha_s^2) \right), \quad (3.54)$$

with

$$\mathcal{J}_{\text{peak}}^{(1)} \equiv \frac{L^2}{2} + \frac{L}{2} + \frac{\pi^2}{12} + 2. \quad (3.55)$$

and the definition

$$L \equiv \ln \frac{\mu^2}{m_H^2}, \quad (3.56)$$

where, since we are working at leading power in λ_h , we are allowed to substitute the heavy quark mass m_h with the heavy meson mass m_H . As anticipated, only logarithms of the hard-collinear scale m_H^2 appear in the jet function.

The simplicity of the result (3.54) has actually a deep origin, and we argue that holds to all orders in α_s . Thinking about the matching in a diagrammatic approach, we are able to understand that the only hard-collinear gluon exchanges allowed in the peak region ($u \sim \lambda_h$) are those between the heavy quark and its own Wilson line $W_C(0)$. For proving this statement, the role of the delta functions in the Feynman rules (3.30)-(3.32) and the fact that u and s are $\mathcal{O}(\lambda_h)$ in the peak region is crucial. Consider a general diagram relevant for the matching. As soon as the loop momentum enters the delta functions from the Feynman rules, it is forced to assume the same scaling as $u n_+ p_H$ and $n_+ p_q$, resulting in a soft-collinear contribution⁴. Therefore the only contributions to the jet function will come from diagrams where the hard-collinear loop momentum is not in the delta function argument, which happens only in the case of the diagram W_h at one loop. To all orders, the loop momentum does not enter the delta functions only when the light anti-quark, and its Wilson line, are not involved. This results in the class of diagrams shown in the left panel of Figure 3.2.

⁴One could think about it reversing the argument, namely “as soon as a hard-collinear loop momentum enters the delta function, u is forced to be $\mathcal{O}(1)$ and therefore contributing to the tail and not the peak”.

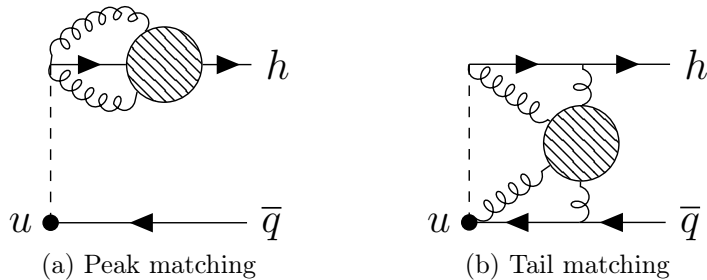


Figure 3.2: Schematic diagrams for the all orders contributions to the jet function (only gluons with hard-collinear momentum), divided into the peak (left) and tail (right) part.

It is hence clear from (3.30)-(3.32) that the structure of the jet function in the peak region, to all orders in α_s , is

$$\mathcal{J}_p(u, \omega) = \mathcal{J}_{\text{peak}} \delta\left(u - \frac{\omega}{m_H}\right) \theta(m_H - \omega), \quad (3.57)$$

where $\mathcal{J}_{\text{peak}}$ is independent of u and ω . In fact, since the light anti-quark is not involved, the injected momentum fraction u is forced to assume the external soft value ω/m_H , which is reflected by the delta function in (3.57). This discussion suggests that $\mathcal{J}_{\text{peak}}$ is actually the m_h dependent matching coefficient when integrating out the heavy-quark mass and hard-collinear modes from the gauge invariant SCET quark field

$$\chi_C^{(h)} = W_C^\dagger \xi_C^{(h)} \rightarrow \mathcal{J}_{\text{peak}}(m_h) \sqrt{\frac{n+v}{2}} W_{sc}^\dagger h_n. \quad (3.58)$$

With this result, the QCD LCDA in the peak region (3.36) takes the all-order form

$$\phi_p(u) = \frac{\tilde{f}_H}{f_H} \mathcal{J}_{\text{peak}} m_H \varphi_+(um_H), \quad \text{for } u \sim \lambda_h, \quad (3.59)$$

where the subscript p means that this expression for $\phi(u)$ holds in the peak region only. The peak of the QCD LCDA is therefore a simple mass-dependent rescaling of the universal HQET LCDA.

3.3.2 Tail Region

The matching in the tail region ($u \sim 1$) is substantially different. First of all the tail of the QCD LCDA is suppressed by one power of λ_h with respect to the peak, and scales like the normalization (see (3.29)). Momentum fractions $u \sim 1$ would correspond to values $\omega \gg \Lambda_{\text{QCD}}$, where the HQET LCDA is determined through an operator product expansion (OPE) [81] depending only on local non-perturbative parameters. In practice this results in a determination of the HQET LCDA as an expansion in $\Lambda_{\text{QCD}}/\omega$, where at leading power the only non-perturbative input is the decay constant. The complication is that, being the tail region power suppressed, we might be sensitive to new operators, as the second

Dirac structure in (3.38) suggests. For this reason we find instructive to first perform a systematic bottom-up analysis of all the possible two-particle operators at this order in the power counting. Notice that the matching of the local version of the SCET operator $\mathcal{O}_C(u)$, performed in 2.4.4, required two bHQET operators at the one-loop level. Finally we will compute in detail the LCDA matching in the tail region.

Bottom-Up Operator Basis

In this section we want to write down a complete basis of local two-particle operators which could contribute at the first non-vanishing order to the matching of the LCDA in the tail region. To find out the power counting of such operators we know from (3.33) that $\mathcal{O}_h(\omega) \sim \Lambda_{\text{QCD}}^2/m_H$. Taking into account $\mathcal{J}_p(u, \omega) \sim 1/\lambda_h$ and $d\omega \sim \Lambda_{\text{QCD}}$ in the matching equation (3.35), and excluding the normalization factor $1/m_H$, we arrive at the conclusion that for the tail region we need operators of order $\mathcal{O}(\Lambda_{\text{QCD}}^3)$.

Here we need to use the reparametrization transformations of (2.124) as the presence of the large parameter $n_{+v} \sim 1/\beta_h$ of bHQET in operators could potentially spoil the power counting. Transformations of type-III correspond to boosts which leave invariant the perpendicular components of Lorentz vectors. Schematically, they imply that every n_{\pm} in a RPI operator is balanced by a n_{\mp} or a $1/n_{\pm}$. For simplicity we are allowed to set $v_{\perp} = 0$, as this condition is not changed by type-III transformations. Hence only one component of v^{μ} is independent, as $v^2 = 1$ implies $n_{-v} = 1/n_{+v}$.

While the ξ_{sc} field is already RPI, the bHQET field transforms as $h_n \rightarrow \sqrt{\alpha} h_n$, and it is therefore natural to start building the operators from the two RPI fields

$$\sqrt{\frac{n_{+v}}{2}} h_n \sim \frac{1}{\sqrt{\beta_h}} \Lambda_{\text{QCD}}^{3/2}, \quad \xi_{sc} \sim \frac{1}{\sqrt{\beta_h}} \Lambda_{\text{QCD}}^{3/2}. \quad (3.60)$$

The two-particle operators can be written, without loss of generality, in the form

$$\hat{\mathcal{O}} = \frac{1}{n_{+v}} \sqrt{\frac{n_{+v}}{2}} \bar{h}_n \not{n}_{+v} f(D^{\mu}, n_{+v}, \Gamma_{\perp}) \gamma^5 \xi_{sc} \sim \Lambda_{\text{QCD}}^3 \times f(D^{\mu}, n_{+v}, \Gamma_{\perp}), \quad (3.61)$$

such that $f(D^{\mu}, n_{+v}, \Gamma_{\perp})$ is a dimensionless, Lorentz scalar function which depends on covariant-derivative components, n_{+v} and a Dirac structure Γ_{\perp} . Due to the projection properties of the spinors, the only possible Dirac structure must contain one \not{n}_{+v} , while the explicit γ^5 ensures a non-zero overlap with the pseudoscalar meson H . It follows that the remaining matrix Γ_{\perp} is independent from \not{n}_{+v} and \not{n}_{-v} . The chosen prefactor ensures that $f(D^{\mu}, n_{+v}, \Gamma_{\perp})$ is type-III reparametrization-invariant and, for leading power operators, scales as $\mathcal{O}(1)$.

We consider only derivatives on the light-quark field due to integration by parts, and we neglect commutators of covariant derivatives as they are proportional to $G_{\mu\nu}$ generating three-particle operators. We can also use the equations of motion

$$\not{n}_{+v} i\not{D}_{\perp} \frac{1}{in_{+v} D} i\not{D}_{\perp} \xi_{sc} = -\not{n}_{+v} in_{-v} D \xi_{sc},$$

$$n_{+v} \bar{h}_n \not{p}_+ i n_- \overleftarrow{D} = -\frac{1}{n_{+v}} \bar{h}_n \not{p}_+ i n_+ \overleftarrow{D}, \quad (3.62)$$

as on-shell matrix elements of operators proportional to the equations of motion vanish. From these considerations, the only two dimensionless and RPI building blocks with $\mathcal{O}(1)$ scaling are

$$n_{+v} \frac{i \not{D}_\perp}{i n_+ D}, \quad (n_{+v})^2 \frac{i n_- D}{i n_+ D}. \quad (3.63)$$

Nevertheless, the second building block in (3.63) is not independent, since it can be shown by using the equation of motion of the light-quark field (3.62) that is related to two insertions of the first building block.

The general $f(D^\mu, n_{+v}, \Gamma_\perp)$ is therefore given by an arbitrary power of the first structure in (3.63), resulting in the infinite tower of order Λ_{QCD}^3 operators

$$\hat{\mathcal{O}}_k = \frac{1}{n_{+v}} \sqrt{\frac{n_{+v}}{2}} \bar{h}_n \not{p}_+ \left(n_{+v} \frac{i \not{D}_\perp}{i n_+ D} \right)^k \gamma^5 \xi_{sc}. \quad (3.64)$$

Now we analyze the operator $\hat{\mathcal{O}}_2$ and we apply the equations of motion (3.62) so that, by using integration by parts, we get

$$\begin{aligned} \hat{\mathcal{O}}_2 &= \sqrt{\frac{n_{+v}}{2}} \bar{h}_n \not{p}_+ \frac{n_{+v}}{i n_+ D} i \not{D}_\perp \frac{1}{i n_+ D} i \not{D}_\perp \gamma^5 \xi_{sc} \\ &= -\sqrt{\frac{n_{+v}}{2}} \bar{h}_n \not{p}_+ \frac{n_{+v}}{i n_+ D} i n_- D \gamma^5 \xi_{sc} = \hat{\mathcal{O}}_0. \end{aligned} \quad (3.65)$$

showing that the operator basis closes on $\hat{\mathcal{O}}_0, \hat{\mathcal{O}}_1$. The two leading-power operators in the rest frame account for the two independent Dirac structures $\bar{h}_v \not{p}_+ q_s$ and $\bar{h}_v \not{p}_- q_s$.

Non-Local Matching

We now turn to the matching of $\mathcal{O}_C(u)$ from SCET to bHQET in the region $u \sim 1$. Lets start by performing a diagrammatic analysis of the structure of the matching equation to all orders in the perturbative expansion. The class of diagrams contributing to the jet function is show in the right panel of Figure 3.2, where the gluons have hard-collinear virtualities. By recalling the Feynman rules (3.30)–(3.32), we see that since the external momentum of the light anti-quark needs to be soft-collinear, for u in order to be $\mathcal{O}(1)$ at the insertion of $\mathcal{O}_C(u)$ there must be a hard-collinear gluon interacting with the massless SCET field $\chi_C(tn_+)$. In this way the large components of the hard-collinear loop momenta will enter the argument of the delta functions, forcing the scaling $u \sim 1$. Moreover, the variable of the HQET LCDA ω in the matching plays the role of the external light-cone component of the soft-collinear momentum, which is therefore a power correction with respect to $un_+ p_H$. For this reason, at leading power, the loop integrals are insensitive to the external suppressed light anti-quark momentum, and hence ω independent.

As anticipated by the local OPE of the HQET LCDA for $\omega \gg \Lambda_{\text{QCD}}$, these considerations translate into a matching equation of the form

$$\mathcal{O}_C(u) = \mathcal{J}_+(u)\mathcal{O}_+^h + \mathcal{J}_-(u)\mathcal{O}_-^h, \quad (3.66)$$

where the basis of local operators in bHQET is the same as for the matching of the decay constant (2.107). The u dependence is fully determined perturbatively, and from the bottom-up analysis of the operator basis we know that no other two-particle operators can arise at this power.

To extract the jet functions $\mathcal{J}_\pm(u)$ we take the on-shell partonic matrix element of the matching equation (3.66). The SCET matrix element from the left-hand side, for $u \sim 1$, starts at the one-loop level

$$\langle h(p_h)\bar{q}(p_q)|\mathcal{O}_C(u)|0\rangle_{\text{SCET}} = \frac{\alpha_s C_F}{4\pi} \sum_{\pm} M_{\pm}^{(1)}(u) \frac{1}{n_{\pm} p_H} \bar{u}(p_h)\not{n}_{\pm}\gamma^5 v(p_q), \quad (3.67)$$

and does not include any soft-collinear physics, as explicitly checked in the region analysis of Appendix B.4. $M_{\pm}^{(1)}(u)$ can be obtained from the full result (3.45) by expanding for $s \sim \lambda_h$ and $u \sim 1$, which at leading power reduces to set $s \rightarrow 0$. One has to take into account that, for u always intended inside the allowed interval $[0, 1]$, the following simplifications apply

$$\theta(u-s) \rightarrow 1, \quad \theta(s-u) \rightarrow 0, \quad \delta(u-s) \rightarrow 0, \quad (3.68)$$

and the plus-distribution in s is not needed anymore. The result of the expansion is⁵

$$M_{+}^{(1)}(u \sim 1, s \sim \lambda_h) = \frac{2\bar{u}}{u} \left(2(1+u) \ln \frac{\mu}{um_h} - 2u + 1 \right). \quad (3.69)$$

This can also be obtained by expanding the matrix element at the integrand level, which coincides with the hard-collinear region of the full result, computed for the separate diagrams in Appendix B.4. In this case we would write

$$\begin{aligned} M_{+}^{(1)}(u) &= V_{+}(u)|_{hc} + W_h(u)|_{hc} + Z_{\mathcal{O}_C}^{(1)}(u)|_{hc}, \\ M_{-}^{(1)}(u) &= V_{-}(u)|_{hc}, \end{aligned} \quad (3.70)$$

where the contribution proportional to the Dirac structure (3.40) is UV and IR finite, and comes only from the vertex diagram.

For determining the $\mathcal{O}(\alpha_s)$ jet functions it is sufficient to compute the bHQET matrix element of the local operators at tree level

$$\langle h(p_h)\bar{q}(p_q)|\mathcal{O}_{\pm}^h|0\rangle_{\text{bHQET}} = \frac{1}{n_{\pm} p_H} \bar{u}(p_h)\not{n}_{\pm}\gamma^5 v(p_q), \quad (3.71)$$

⁵Notice that we are not worried about the singularity in $u = 0$ as we are in the region $u \gg \lambda_h$, which we will enforce with a cut-off.

and taking the partonic matrix element of the matching equation (3.66) we can easily extract

$$\mathcal{J}_{\pm}(u) = \frac{\alpha_s C_F}{4\pi} M_{\pm}^{(1)}(u) + \mathcal{O}(\alpha_s^2), \quad (3.72)$$

with

$$\begin{aligned} \mathcal{J}_+^{(1)}(u) &= \frac{2\bar{u}}{u} \left((1+u)[L - 2\ln u] - 2u + 1 \right), \\ \mathcal{J}_-^{(1)}(u) &= 2\bar{u}. \end{aligned} \quad (3.73)$$

The LCDA in the tail region is obtained by taking the hadronic matrix element of the matching equation (3.66). Due to the presence of a single non-perturbative parameter, $\langle H(p_H) | \mathcal{O}_{\pm}^h | 0 \rangle = -i f_H(\mu)$, the jet functions combine to a single perturbative function

$$\mathcal{J}_{\text{tail}}(u) = \mathcal{J}_+(u) + \mathcal{J}_-(u) = \frac{\alpha_s C_F}{4\pi} \frac{2\bar{u}}{u} \left((1+u)[L - 2\ln u] - u + 1 \right) + \mathcal{O}(\alpha_s^2), \quad (3.74)$$

determining the QCD LCDA in the tail region (hence the subscript t) completely

$$\phi_t(u) = \frac{\tilde{f}_H}{f_H} \mathcal{J}_{\text{tail}}(u), \quad \text{for } u \sim 1. \quad (3.75)$$

Notice that the QCD LCDA tail is radiatively generated, similarly to the well known asymptotic tail of the HQET LCDA [81], reviewed in Section 3.2.3. We will explore this connection in the next section.

3.3.3 Merging of the Peak and Tail

From Sections 3.3.1 and 3.3.2 we obtained two expressions for the QCD LCDA of a heavy meson in the regions $u \sim \lambda_h$ and $u \sim 1$ respectively. In this section we will check the consistency of the matching by studying the continuity of $\phi(u)$ when merging the two regions.

We start by writing the QCD LCDA, at the matching scale, as a piecewise function

$$\phi(u) = \begin{cases} \phi_p(u) = \frac{\tilde{f}_H}{f_H} \mathcal{J}_{\text{peak}} m_H \varphi_+(um_H), & \text{for } u \sim \lambda_h, \\ \phi_t(u) = \frac{\tilde{f}_H}{f_H} \mathcal{J}_{\text{tail}}(u), & \text{for } u \sim 1. \end{cases} \quad (3.76)$$

But, since $\phi(u)$ should be continuous on $u \in [0, 1]$, the two expressions must be equal in the overlap region $\lambda_h \ll u \ll 1$, requiring the consistency condition

$$\mathcal{J}_{\text{peak}} m_H \varphi_+^{\text{asy}}(um_H) \stackrel{!}{=} \mathcal{J}_{\text{tail}}(u) \Big|_{u \ll 1}. \quad (3.77)$$

In (3.77) we have inserted the asymptotic form of the HQET LCDA (3.25). As anticipated at the end of Section 3.3.2, the fact that at this order $\varphi_+^{\text{asy}}(\omega)$ is perturbative and independent

of hadronic parameters is the crucial property for the consistency of the matching, showing a deep connection between the LCDAs in the two theories.

To check that (3.77) is satisfied at order α_s , it is sufficient to use $\mathcal{J}_{\text{peak}} = 1 + \mathcal{O}(\alpha_s)$, giving on the left-hand side

$$m_H \varphi_+^{\text{asy}}(um_H) = \frac{\alpha_s C_F}{2\pi u} (L - 2 \ln u + 1), \quad (3.78)$$

indeed coinciding with $\mathcal{J}_{\text{tail}}(u)|_{u \ll 1}$ from (3.74).

With this we have shown that $\phi(u)$ is parametrically continuous in the overlap region, and therefore in its whole domain. Obviously the function will not be numerically continuous due to unknown power corrections and higher order terms in the perturbative expansion. We are nevertheless allowed to write it in a numerically continuous form by introducing a “merging function” $\vartheta(u; \delta, \sigma)$ satisfying

$$\vartheta(u; \delta, \sigma)|_{u \ll \delta} = 1, \quad \vartheta(u; \delta, \sigma)|_{u \gg \delta} = 0, \quad (3.79)$$

which performs a smooth switching between the two regions of $\phi(u)$

$$\phi(u) = \vartheta(u; \delta, \sigma) \phi_p(u) + (1 - \vartheta(u; \delta, \sigma)) \phi_t(u). \quad (3.80)$$

The parameter δ defines the centre of the overlap region $\lambda_h \ll \delta \ll 1$, while σ its width. We employ the explicit form

$$\vartheta(u; \delta, \sigma) = \frac{1}{1 + e^{\frac{u-\delta}{\sigma}}}, \quad (3.81)$$

which satisfies the properties (3.79) and includes the discontinuous limiting case

$$\vartheta(u; \delta, 0) = \theta(\delta - u), \quad (3.82)$$

useful in analytic computations. Since δ must satisfy $\lambda_h \ll \delta \ll 1$, its appropriate numerical value will depend on the heavy quark mass m_h . On the other hand the parameter σ carries less physical meaning, and will be tuned depending on the magnitude of the numerical discontinuity at $u = \delta$ in order for the resulting function to have a plausible shape.

3.4 Properties of the QCD LCDA

In (3.80) we found an expression for the QCD LCDA of a heavy meson, determined by a combination of m_h -dependent perturbative functions and a universal non-perturbative input, the HQET LCDA. In this section we further analyse the consistency of this result by comparing the properties of (3.80) with the known properties of the QCD LCDA. In particular we study the endpoint behaviours, the normalization and the renormalization group evolution of $\phi(u)$. For simplicity we define here the ratio between the HQET and QCD decay constants, again identifying m_h with m_H

$$d_H(\mu) \equiv \frac{\tilde{f}_H(\mu)}{f_H} = 1 + \frac{\alpha_s C_F}{4\pi} \left(\frac{3}{2} L + 2 \right) + \mathcal{O}(\alpha_s^2), \quad (3.83)$$

entering the expressions for the matched QCD LCDA.

3.4.1 Endpoint Behaviour

At the endpoints $u = 0$ and $u = 1$, the QCD LCDA vanish linearly. For $u \rightarrow 0$ the function $\phi(u)$ from (3.80) inherits the asymptotic limit of the HQET LCDA for small argument (3.26), as $\mathcal{J}_{\text{peak}}$ is independent of u , hence fulfilling the expected endpoint behaviour for $\phi(u)$. On the other hand, for $u \rightarrow 1$, we easily find from (3.74)

$$\phi(u) \xrightarrow{u \rightarrow 1} \frac{\alpha_s C_F}{\pi} \bar{u} L \rightarrow 0, \quad (3.84)$$

showing the correct endpoint behaviour, at order α_s .

3.4.2 Normalization

A strong check of the result (3.80) for $\phi(u)$ is to compute its normalization analytically at order α_s . We use the merging function (3.82), since for analytical calculations the discontinuity in $u = \delta$ is parametrically absent.

To calculate the normalization integral we employ the hierarchy $\lambda_h \ll \delta \ll 1$, allowing us to use the zeroth cut-off moment of the HQET LCDA (3.23)

$$\begin{aligned} \int_0^1 du \phi(u) &= \int_0^\delta du \phi_p(u) + \int_\delta^1 du \phi_t(u) \\ &= d_H \mathcal{J}_{\text{peak}} M_0(m_H \delta) + d_H \int_\delta^1 du \mathcal{J}_{\text{tail}}(u) \\ &= 1 + \frac{\alpha_s C_F}{4\pi} \left[M_0^{(1)}(m_H \delta) + \mathcal{J}_{\text{peak}}^{(1)} + d_H^{(1)} + \int_\delta^1 du \mathcal{J}_{\text{tail}}^{(1)}(u) \right] + \mathcal{O}(\alpha_s^2) \\ &= 1 + \mathcal{O}\left(\delta, \frac{\lambda_h}{\delta}\right) + \mathcal{O}(\alpha_s^2). \end{aligned} \quad (3.85)$$

The LCDA is therefore correctly normalized to 1, at leading power in δ and λ_h/δ . As stated before, this constitutes a non-trivial check of our matching calculation.

3.4.3 Evolution Equation

Another non-trivial check consists in the evolution equation of $\phi(u)$ from (3.80). The full QCD LCDA obeys the evolution equation (3.3), which we rewrite here as

$$\mu \frac{d\phi(u)}{d\mu} = -\frac{\alpha_s C_F}{\pi} \int_0^1 dv V_{\text{ERBL}}(u, v) \phi(v) \equiv \frac{\alpha_s C_F}{\pi} R(u). \quad (3.86)$$

The integral $R(u)$ on the right-hand side is needed only at $\mathcal{O}(\alpha_s^0)$, due to the factored out coupling constant, receiving contribution only from the peak

$$R(u) = -\int_0^\delta dv m_H V_{\text{ERBL}}(u, v) \varphi_+(m_H v), \quad (3.87)$$

as the tail part would be of higher order in α_s . For this reason the variable v scales as $\mathcal{O}(\lambda_h)$, but u has not yet a definite scaling. We therefore split the kernel in u by multiplying it by $1 = \theta(\delta - u) + \theta(u - \delta)$ and expand it accordingly in the two regions

$$V_{\text{ERBL}}(u, v) \approx \theta(\delta - u) \left\{ -u \left[\frac{\theta(v - u)}{v(v - u)} + \frac{\theta(u - v)}{u(u - v)} \right]_{v+} - \delta(u - v) \left(\ln u + \frac{3}{2} \right) \right\} \\ - \theta(u - \delta) \left[\bar{u} \left(1 + \frac{1}{u} \right) \right]_{v+}. \quad (3.88)$$

The convolution of the $u > \delta$ term can be immediately evaluated

$$\theta(u - \delta) \bar{u} \frac{1 + u}{u} \int_0^\delta dv m_H (\varphi_+(vm_H) - \varphi_+(um_H)) \\ \approx \theta(u - \delta) \bar{u} \frac{1 + u}{u} M_0(m_H \delta) \approx \theta(u - \delta) \bar{u} \frac{1 + u}{u}, \quad (3.89)$$

where we used again the hierarchy $\lambda_h \ll \delta \ll 1$, allowing us to employ the tree-level expression for $M_0(m_H \delta) = 1 + \mathcal{O}(\alpha_s)$. We also neglected $\varphi_+(um_H) \ll \varphi_+(vm_H)$ since $u \gg v$.

For the other half of $R(u)$, namely the $u < \delta$ contribution, we need to compare the low- u part of the ERBL kernel in (3.88) with the HQET evolution kernel (3.20). In fact $V_{\text{ERBL}}(u, v)$, for small arguments $u, v \sim \lambda_h$, can be expressed as

$$\theta(\delta - u) V_{\text{ERBL}}(u, v) = \theta(\delta - u) \left[m_H \Gamma_{\text{LN}}(um_H, vm_H) - \delta(u - v) \left(\ln \frac{\mu}{m_H} + 1 \right) \right]. \quad (3.90)$$

Summing the two regions we find

$$R(u) = \theta(\delta - u) m_H \left[- \int_0^{\delta m_H} d\nu \Gamma_{\text{LN}}(um_H, \nu) \varphi_+(\nu) + \varphi_+(um_H) \left(\ln \frac{\mu}{m_H} + 1 \right) \right] \\ + \theta(u - \delta) \bar{u} \frac{1 + u}{u}. \quad (3.91)$$

Now we turn to the left-hand side of (3.86). The derivative of α_s with respect to μ counts as $\mathcal{O}(\alpha_s^2)$, and will hence be neglected. Employing (3.19) we find

$$\frac{\pi}{\alpha_s C_F} \frac{d\phi(u)}{d \ln \mu} = \theta(\delta - u) m_H \left[- \int_0^\infty d\nu \Gamma_{\text{LN}}(um_H, \nu) \varphi_+(\nu) \right. \\ \left. + \frac{\varphi_+(um_H)}{4} \left(\frac{d\mathcal{J}_{\text{peak}}^{(1)}}{d \ln \mu} + \frac{d}{d \ln \mu} d_H^{(1)} \right) \right] + \frac{1}{4} \theta(u - \delta) \frac{d\mathcal{J}_{\text{tail}}^{(1)}(u)}{d \ln \mu} \\ = \theta(\delta - u) m_H \left[- \int_0^\infty d\nu \Gamma_{\text{LN}}(um_H, \nu) \varphi_+(\nu) + \varphi_+(um_H) \left(\ln \frac{\mu}{m_H} + 1 \right) \right]$$

$$+ \theta(u - \delta) \bar{u} \frac{1 + u}{u}. \quad (3.92)$$

agreeing with the right-hand side of (3.86), shown in (3.91), where we are able to extend the upper limit of the ν -integral in (3.91) up to infinity since $m_H \delta \gg \Lambda_{\text{QCD}}$ and including the tail adds only a suppressed contribution.

The relation (3.90) is quite interesting as it shows that in the peak region (i.e. in the soft limit) the evolution of the QCD LCDA is the same as in HQET, except for a local term, as was already noted in [83]. This can be used to derive an RGE for $\mathcal{J}_{\text{peak}}$ from (3.59)

$$\frac{d}{d \ln \mu} \mathcal{J}_{\text{peak}} = \left(\frac{1}{\phi_p(u)} \frac{d\phi_p(u)}{d \ln \mu} - \frac{1}{\varphi_+(um_H)} \frac{d\varphi_+(um_H)}{d \ln \mu} - \frac{1}{d_H(\mu)} \frac{d}{d \ln \mu} d_H(\mu) \right) \mathcal{J}_{\text{peak}}, \quad (3.93)$$

where the u -dependent terms cancel between the first two terms. The final form for the RGE of the peak jet function is given by

$$\mu \frac{d\mathcal{J}_{\text{peak}}}{d\mu} = \frac{\alpha_s C_F}{4\pi} \left[4 \ln \frac{\mu}{m_H} + 1 \right] \mathcal{J}_{\text{peak}} + \mathcal{O}(\alpha_s^2). \quad (3.94)$$

3.4.4 Comparison with Previous Works

Previous works on the relation between the QCD LCDA and the HQET one exist. In particular in Ref. [84] the authors obtained a relation which in spirit should be equivalent to our result presented in Section 3.3.3 but with very different results. Their matching does not take into account the different scaling of the QCD LCDA in the peak and tail regions, finding an expression for the matching function which is non-homogeneous in the expansion parameter Λ_{QCD}/m_h . This is already present at tree-level where the matching function

$$\mathcal{J}^{(0)}(u, \omega) = \delta\left(u - \frac{\omega}{\omega + m_h}\right) \quad (3.95)$$

smoothly maps the interval $u \in [0, 1]$ to $\omega \in [0, \infty]$. In the framework of HQET the combination $\omega + m_h$ in the denominator, which is inhomogeneous in the power counting, poses serious problems as $\omega \ll m_h$ but the support is extended to infinity since the heavy quark mass is integrated out. From the δ function at tree-level one would conclude that the situation where the light-quark carries the totality of the momentum in QCD ($u = 1$) is mapped to values where $\omega \gg m_h$ which are obviously unphysical.

The one-loop matching function $Z^{(1)}$ in (15) of Ref. [84] inherits and enhances such problems. The comparison with our results is quite involved due to the fact that $Z^{(1)}$ is written in terms of distributions in both variables u and ω . This also has the drawback of not allowing a determination of the QCD LCDA from an input HQET LCDA.

Similar considerations can be made for the position space matching of the QCD to HQET LCDA proposed in Ref. [85]. The one-loop matching function $C^{(1)}(\alpha, \beta, t, M, \mu, \tilde{\mu})$ in (18) is also non-homogeneous which can be seen by Fourier transforming to momentum space. Indeed the terms $e^{-i\beta M t}$ combine with exponentials of the form $e^{i\beta t \omega}$, inducing unexpanded combinations of the type $M - \omega$ in the matching coefficient, which have similar consequences as for Ref. [84].

3.5 Numerical Models for \bar{B} and D Meson QCD LCDAs

In this section, starting from non-perturbative models for the HQET LCDA at the soft scale, we want to study the numerical behaviour of the QCD LCDA for \bar{B} and D mesons. The resulting functions will serve as practical inputs, at the hard scale Q , for factorization theorems involving boosted heavy mesons. To properly resum the large logarithms of Λ_{QCD}/m_H and m_H/Q we proceed in three steps. First, we specify the non-perturbative HQET LCDA as an input at the soft scale $\mu_s = 1$ GeV and we evolve it in HQET up to the matching scale $\mu \sim \mathcal{O}(m_H)$. Second, we employ the result of the matching of Section 3.3, where the perturbative functions are free from large logarithms at the matching scale $\mu \sim \mathcal{O}(m_H)$. Third, we finally evolve the LCDA within QCD with the ERBL evolution kernel to a hard scale $\mu_Q \sim \mathcal{O}(Q)$ where it can be used in convolutions with hard-scattering kernels.

3.5.1 Input HQET LCDA and Evolution to the Matching Scale

As the functional form of the HQET LCDA $\varphi_+(\omega)$ is unknown, we need to use some models. Such models are posited at the soft scale $\mu_s = 1$ GeV and need to satisfy the model-independent properties

$$\begin{aligned} \int_0^{\Lambda_{\text{UV}}} d\omega \varphi_+(\omega; \mu_s) &= M_0(\Lambda_{\text{UV}}; \mu), \\ \varphi_+(\omega; \mu_s) &\xrightarrow{\omega \gg \Lambda_{\text{QCD}}} \varphi_+^{\text{asy}}(\omega; \mu_s), \\ \int_0^\infty \frac{d\omega}{\omega} \varphi_+(\omega; \mu_s) &= \lambda_B^{-1}(\mu_s), \end{aligned} \quad (3.96)$$

introduced in Section 3.2, which are essential in our framework. The properties (3.96) can be satisfied by using auxiliary normalized models $\varphi_+^{\text{mod}}(\omega; \mu_s)$ such that

$$\begin{aligned} \int_0^\infty d\omega \varphi_+^{\text{mod}}(\omega; \mu_s) &= 1, \\ \omega \varphi_+^{\text{mod}}(\omega; \mu_s) &\xrightarrow{\omega \rightarrow \infty} 0, \\ \int_0^\infty \frac{d\omega}{\omega} \varphi_+^{\text{mod}}(\omega; \mu_s) &= \frac{1}{\omega_0}, \end{aligned} \quad (3.97)$$

and by gluing continuously on top of them the radiative tail (3.25) [81] as

$$\varphi_+(\omega; \mu_s) = \left(1 + \frac{\alpha_s(\mu_s) C_F}{4\pi} \left[\frac{1}{2} - \frac{\pi^2}{12} \right] \right) \varphi_+^{\text{mod}}(\omega; \mu_s) + \theta(\omega - \sqrt{e} \mu_s) \varphi_+^{\text{asy}}(\omega; \mu_s). \quad (3.98)$$

From (3.98) one can derive an order α_s relation between the parameters ω_0 and λ_B

$$\omega_0 = \lambda_B \left(1 + \frac{\alpha_s(\mu_s) C_F}{4\pi} \left(\frac{1}{2} - \frac{\pi^2}{12} - \frac{4}{\sqrt{e}} \frac{\lambda_B}{\mu_s} \right) \right). \quad (3.99)$$

For the numerical analysis we choose the conservative range $\lambda_B = (350 \pm 150)$ MeV, which translates into $\omega_0 = (329.5 \pm 134.8)$ MeV.

Our benchmark model is for simplicity the exponential model [82]

$$\varphi_+^{\text{exp}}(\omega, \omega_0; \mu_s) = \frac{\omega}{\omega_0^2} e^{-\omega/\omega_0}, \quad (3.100)$$

while to account for the model dependence we choose three two-parameter models [86]

$$\begin{aligned} \varphi_+^{(\text{I})}(\omega; \mu_s) &= \left[1 - \beta + \frac{\beta}{2 - \beta} \frac{\omega}{\omega_0} \right] \varphi_+^{\text{exp}}(\omega, (1 - \beta/2)\omega_0; \mu_s), & \text{for } 0 \leq \beta \leq 1, \\ \varphi_+^{(\text{II})}(\omega; \mu_s) &= \frac{(1 + \beta)^\beta}{\Gamma(2 + \beta)} \left(\frac{\omega}{\omega_0} \right)^\beta \varphi_+^{\text{exp}}\left(\omega, \frac{\omega_0}{1 + \beta}; \mu_s\right), & \text{for } -\frac{1}{2} < \beta < 1, \\ \varphi_+^{(\text{III})}(\omega; \mu_s) &= \frac{\sqrt{\pi}}{2\Gamma(3/2 + \beta)} U\left(-\beta, \frac{3}{2} - \beta, (1 + 2\beta)\frac{\omega}{\omega_0}\right) \\ &\quad \times \varphi_+^{\text{exp}}\left(\omega, \frac{\omega_0}{1 + 2\beta}; \mu_s\right), & \text{for } 0 \leq \beta < \frac{1}{2}, \end{aligned} \quad (3.101)$$

with $U(a, b, z)$ the confluent hypergeometric function of the second kind. All of the three models for $\beta = 0$ reduce to $\varphi_+^{\text{exp}}(\omega, \omega_0; \mu_s)$.

We then proceed to evolve $\varphi_+(\omega; \mu_s)$ to the matching scale μ , which can be done analytically for $\varphi_+^{(\text{I,II,III})}(\omega; \mu)$ [83, 86] for leading-logarithmic (LL) evolution. Technically the fixed order one-loop matching has to be combined with two-loop running, i.e. next-to-leading-logarithmic (NLL) evolution. However, here for simplicity, we restrict to LL evolution as the main uncertainty comes from the model dependence of the HQET LCDA. For this reason we do not evolve the tail $\varphi_+^{\text{asy}}(\omega; \mu_s)$, with the other $\mathcal{O}(\alpha_s)$ term, as it would formally be an NLL effect. This choice is supported from the fact that the evolved $\varphi_+(\omega; \mu)$ develops the correct asymptotic behaviour $\varphi_+^{\text{asy}}(\omega; \mu)$. This can be seen from Figure 3.3, where we show $\varphi_+(\omega; \mu_b)$ at the matching scale $\mu_b = 4.8$ GeV for the limiting values of the parameter β .

The analytic solution for the LL evolved exponential model is [86, 87]

$$\varphi_+^{\text{exp-LL}}(\omega; \mu) = e^{V+2a\gamma_E} \Gamma(2 + a) \left(\frac{\mu_s}{\omega_0} \right)^a \frac{\omega}{\omega_0^2} {}_1F_1\left(2 + a, 2, -\frac{\omega}{\omega_0}\right), \quad (3.102)$$

with [81]

$$\begin{aligned} a \equiv a(\mu, \mu_s) &= - \int_{\alpha_s(\mu_s)}^{\alpha_s(\mu)} \frac{d\alpha}{\beta(\alpha)} \Gamma_{\text{cusp}}(\alpha) = \frac{\Gamma_0}{2\beta_0} \ln r + \mathcal{O}(\alpha_s), \\ V \equiv V(\mu, \mu_s) &= - \int_{\alpha_s(\mu_s)}^{\alpha_s(\mu)} \frac{d\alpha}{\beta(\alpha)} \left[\Gamma_{\text{cusp}}(\alpha) \int_{\alpha_s(\mu_s)}^{\alpha} \frac{d\alpha'}{\beta(\alpha')} + \gamma_+(\alpha) \right] \\ &= \frac{\Gamma_0}{4\beta_0^2} \left[\frac{4\pi}{\alpha_s(\mu_s)} \left(-\ln r + 1 - \frac{1}{r} \right) + \frac{\beta_1}{2\beta_0} \ln^2 r + \frac{2\gamma_0^+}{\Gamma_0} \beta_0 \ln r \right] \end{aligned}$$

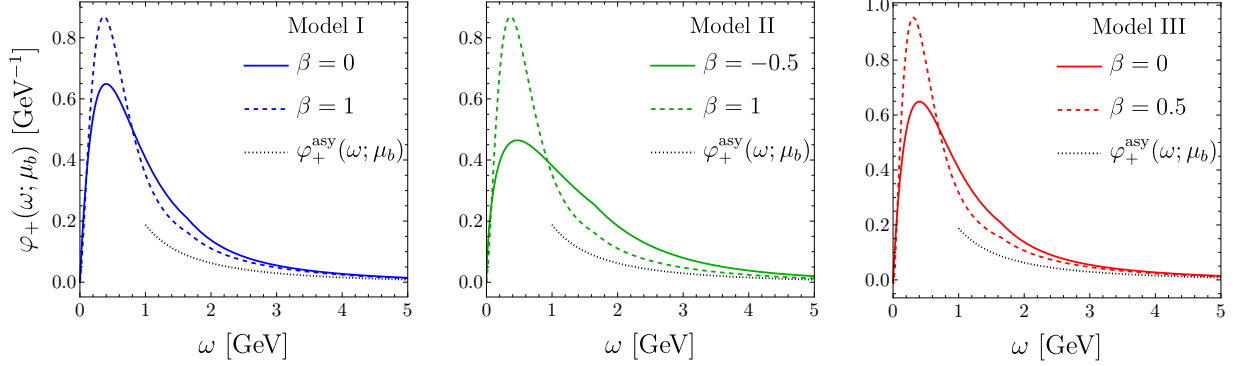


Figure 3.3: The solid (dashed) curves show the three models (3.101) evolved at the matching scale $\mu_b = 4.8$ GeV at the lower (upper) β value. The dotted curve is the asymptotic form of the HQET LCDA (3.25).

$$+ \left(\frac{\Gamma_1}{\Gamma_0} - \frac{\beta_1}{\beta_0} \right) (\ln r - r + 1) \Big] + \mathcal{O}(\alpha_s), \quad (3.103)$$

where $r = \alpha_s(\mu)/\alpha_s(\mu_s)$ and $\gamma_+(\alpha_s) = \gamma_0^+ \alpha_s C_F / (4\pi) + \mathcal{O}(\alpha_s^2)$ with $\gamma_0^+ = -2C_F$. The QCD beta function is defined in Appendix A while the cusp anomalous dimension is defined as

$$\Gamma_{\text{cusp}}(\alpha_s) = \sum_{n=0}^{\infty} \Gamma_n \left(\frac{\alpha_s}{4\pi} \right)^{n+1}, \quad (3.104)$$

with $\Gamma_0 = 4C_F$ and $\Gamma_1 = 4C_F \left(\frac{67}{3} - \pi^2 - \frac{10}{9} n_f \right)$.

The evolution of the HQET LCDA, when focusing in particular on the cut-off moments, comes with a tricky subtlety. The introduction of the hard cut-off Λ_{UV} induces new potentially large logarithms, as explicitly seen in (3.23). If the integral of the initial condition reproduces the OPE result (3.23) for $M_0(\Lambda_{\text{UV}}; \mu_s)$, the integral of the RG evolved function $\varphi_+(\omega; \mu)$ suffers from unresummed large logarithms $\ln \frac{\mu_s}{\Lambda_{\text{UV}}}$. This is due to the fact that the standard evolution equation resums only logarithms of the form $\ln \frac{\mu_s}{\mu}$. Because of this, the zeroth moment at the scale μ computed from the evolved $\varphi_+(\omega; \mu)$ will numerically deviate from $M_0(\Lambda_{\text{UV}}; \mu)$ obtained from the OPE. While this issue conceptually invalidates our treatment of the evolution of the HQET LCDA, for the cases of the physical \bar{B} and D mesons it is not a problem numerically, as power corrections still dominate over the unresummed logarithms. We leave a detailed treatment of the problem to Section 3.6 where we will explain how to consistently perform the large meson mass limit.

3.5.2 QCD LCDA Initial Condition at the Matching Scale

We are now ready to apply the results of Section 3.3 for a \bar{B} and a D meson. We use the meson masses m_B and m_D (numerical values in Appendix A) in place of the quark masses as they are better defined quantities and the difference is formally a power correction.

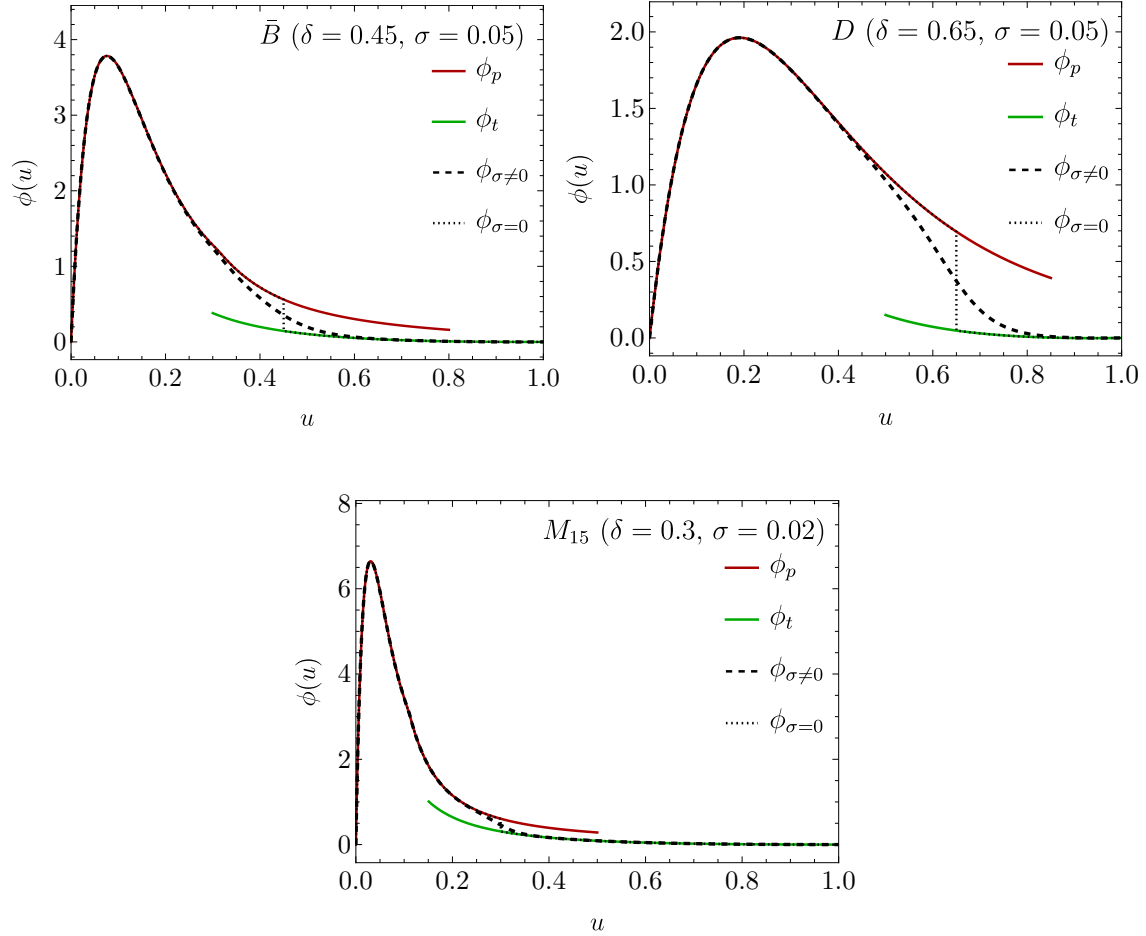


Figure 3.4: The QCD LCDA $\phi(u)$ obtained from (3.80) with $\sigma \neq 0$ (dashed) and $\sigma = 0$ (dotted) for the cases of the \bar{B} , D and 15 GeV meson. The peak (red) and tail (green) functions are shown as a reference.

The matching scales are set to $\mu_b = 4.8$ GeV and $\mu_c = 1.6$ GeV respectively. For the numerical evaluation of α_s and its running we refer to Appendix A. We also display results for a fictitious meson M_{15} with 15 GeV mass in order to show the behaviour of the power corrections. The matching scale for such meson is set to $\mu_{15} = 15$ GeV. The arbitrary parameter δ entering the smoothing function $\vartheta(u; \delta, \sigma)$ defined in (3.81) is set to

$$\delta(\bar{B}) = 0.45, \quad \delta(D) = 0.65, \quad \delta(M_{15}) = 0.30, \quad (3.105)$$

such that it satisfies $\lambda_h \ll \delta \ll 1$, and it will be varied by $\pm 15\%$ to take into account the systematic uncertainty on $\phi(u)$. The default values for the smoothing parameter σ are

$$\sigma(\bar{B}) = 0.05, \quad \sigma(D) = 0.05, \quad \sigma(M_{15}) = 0.02. \quad (3.106)$$

In Figure 3.4 we show the result of the matching in the form of peak and tail functions, in red and green respectively, as well as the merged function (3.80) (dashed black) with

the parameters (3.105) and (3.106). The discontinuity between $\phi_p(u)$ and $\phi_t(u)$ at the threshold $u = \delta$ is shown by the black dotted curve, and gives an idea about the magnitude of the power corrections. As expected, the leading power approximation for the D meson is quite crude as we expect large $\mathcal{O}(\Lambda_{\text{QCD}}/m_c)$ corrections. The situation for the \bar{B} meson is better, and the hypothetical meson M_{15} shows how the discontinuity would decrease for larger heavy quark masses. One has to keep in mind that the discontinuity, due to power corrections and missing higher orders in the perturbative expansion, carries also a model dependence, as can be inferred from the different HQET LCDA models in Figure 3.3.

We proved in Section 3.4.2 that the obtained QCD LCDA is parametrically normalized to 1, as it should. This is not the case numerically, where the normalization is from 10% to 15% less than 1, again due to power corrections. In order to work with a proper QCD LCDA, we rescale $\phi(u)$ such that it is numerically normalized to 1, and use it in the following.

We now compute up to 20 Gegenbauer moments according to (3.7), for the \bar{B} and D meson LCDAs at the matching scale with parameters (3.105)–(3.106). For the \bar{B} meson we observe a good convergence

$$a_n^{\bar{B}}(\mu_b) = \{-1.082, 0.826, -0.513, 0.288, -0.157, 0.078, -0.030, 0.008, \dots\}, \quad (3.107)$$

with $n \geq 1$ and the dots standing for higher moments, which modulus is smaller than 0.005. In the case of the D meson the Gegenbauer series exhibits a faster convergence

$$a_n^D(\mu_c) = \{-0.659, 0.206, -0.057, 0.036, -0.004, -0.007, \dots\}, \quad (3.108)$$

which is expected as $\phi_D(u)$ is in form “closer” to the asymptotic LCDA (3.12) than $\phi_{\bar{B}}(u)$.

In Figure 3.5 we display the results for the \bar{B} (blue) and the D (orange) QCD LCDAs at the matching scale, divided in LO (dashed) and NLO (solid) contributions⁶. The “transverse-dashed” curves come from the Gegenbauer expansion, with the perfect agreement with the full functions (3.80) justifying the truncation of the series. The effect of varying σ between $[0, 0.05]$ is subdominant with respect to the effect of varying δ by $\pm 15\%$, represented by the shaded bands. We notice that the one-loop matching corrections are important in the peak region, while they are entirely responsible for the existence of the tail, as explained in Section 3.3.2.

3.5.3 Evolution to the Hard Scale

Finally, after having determined the Gegenbauer moments at the matching scale (3.107) and (3.108) we can easily evolve them to the high scale using (3.10). We choose as a reference value for the hard scale $m_W = 80.377$ GeV, yielding to

$$\begin{aligned} a_n^{\bar{B}}(m_W) &= \{-0.826, 0.542, -0.302, 0.156, -0.079, 0.037, -0.014, \dots\}, \\ a_n^D(m_W) &= \{-0.416, 0.100, -0.023, 0.013, \dots\}, \end{aligned} \quad (3.109)$$

⁶Notice that the NLO LCDA is normalized to 1, and the same normalization factor is applied to the LO curve in order to have a fair comparison of the one-loop corrections.

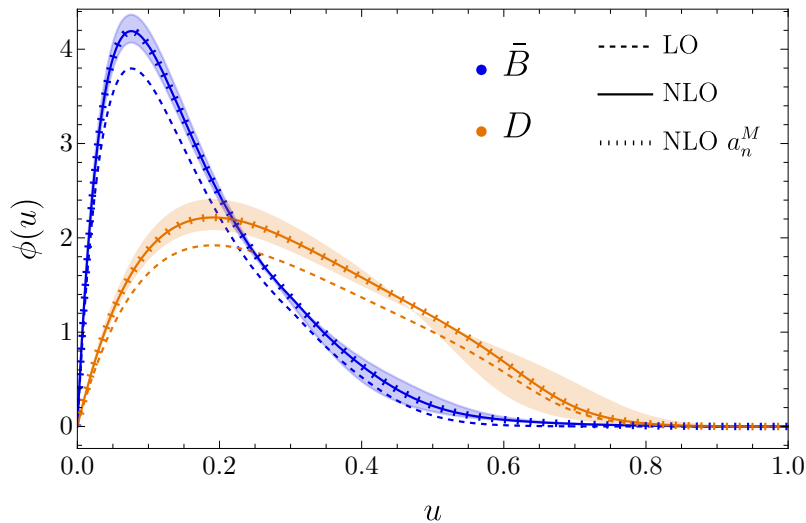


Figure 3.5: QCD LCDA $\phi(u)$ at the heavy quark scale for a \bar{B} (blue) and a D (orange) meson at tree level (dashed) and including NLO corrections (solid). The “transverse-dashed” curves are the results for the Gegenbauer expansion and the shaded areas is the uncertainty obtained by varying δ by $\pm 15\%$.

which gives the LCDAs drawn in blue in Figure 3.6, together with all the functions involved in the three steps described in this section. We also display for the D meson the LCDA at the scale m_B which might be used in exclusive $\bar{B} \rightarrow D$ decays, as we will show in Chapter 5.

3.6 On the Normalization of the QCD LCDA

We devote this last section to the study of the normalization of the QCD LCDA obtained from the matching to HQET. In particular in Section 3.4.2 we explicitly showed to order $\mathcal{O}(\alpha_s)$ that the QCD LCDA (3.80) is normalized to 1 only up to power corrections in the parameters δ and λ/δ . Here we want to investigate the large meson mass limit which should in principle reduce the numerical impact of such corrections. In Section 3.5, for physical masses of the D and \bar{B} mesons the normalization was about $\sim 10 - 15\%$ smaller than 1, which is the order of magnitude expected from power corrections. Nevertheless by increasing the meson mass we unexpectedly observed the opposite behaviour, namely an increasing departure from unity of the normalization. This shows that the procedure described and implemented in Section 3.5 is not consistent with the heavy-quark limit.

In this section we investigate and deal with this conceptual problem. As a result we find confirmation that the modified procedure presented in the following is not needed for the physical cases of the D and \bar{B} mesons.

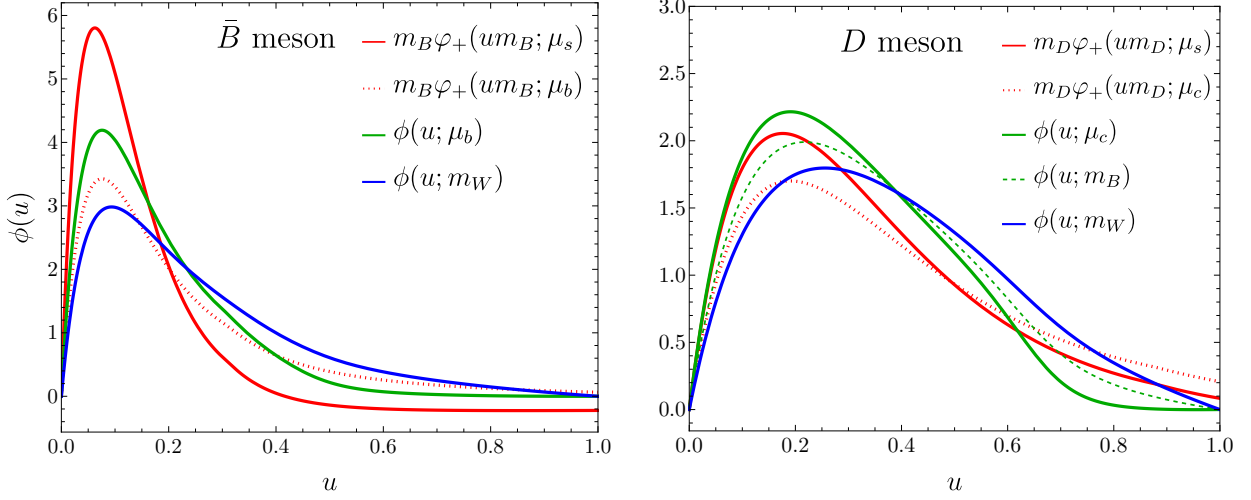


Figure 3.6: Evolution of the LCDA from the initial HQET condition (red) to the hard scale m_W (blue) and the LCDA at the matching scale for the \bar{B} (left) and D meson (right).

3.6.1 Log Analysis of the Cut-Off Moment

Given the difference between the analytical evaluation of the normalization (3.85) and the numerical analysis of Section 3.5 we easily pin down the problem to the HQET LCDA cut-off moment $M_0(\Lambda_{UV}, \mu)$, which is the only quantity computed differently between the two approaches. As already shown in (3.85), the OPE prediction for M_0

$$M_0^{\text{OPE}}(\Lambda_{UV}, \mu) = 1 - \frac{\alpha_s(\mu)C_F}{4\pi} \left(2 \ln^2 \frac{\mu}{\Lambda_{UV}} + 2 \ln \frac{\mu}{\Lambda_{UV}} + \frac{\pi^2}{12} \right), \quad (3.110)$$

implies that the corrections to the normalization of the QCD LCDA are of order $\delta = \Lambda_{UV}/m_H$ and λ_h/δ , which should decrease for increasing meson mass. Hence the problem in the heavy-quark limit must arise from

$$\int_0^{\Lambda_{UV}} d\omega \varphi_+(\omega; \mu) \neq M_0^{\text{OPE}}(\Lambda_{UV}, \mu), \quad (3.111)$$

namely that the integral of the HQET LCDA evolved from μ_s to the matching scale $\mu \sim \mathcal{O}(m_h)$ is not in good agreement with the OPE prediction.

We now take a closer look at the case of the model employed in Section 3.5. In this case the HQET LCDA after LL evolution has a closed form

$$\varphi_+(\omega; \mu) = \varphi_+^{\text{exp-LL}}(\omega; \mu) + \frac{\alpha_s(\mu_s)C_F}{4\pi} \left[\frac{1}{2} - \frac{\pi^2}{12} \right] \varphi_+^{\text{exp}}(\omega; \mu_s) + \theta(\omega - \sqrt{e}\mu_s) \varphi_+^{\text{asy}}(\omega; \mu_s), \quad (3.112)$$

with $\varphi_+^{\text{exp-LL}}(\omega; \mu)$ given in (3.102). This allows us to compute the left-hand side of (3.111) analytically, giving

$$N_f(\Lambda_{UV}, \mu) \equiv \int_0^{\Lambda_{UV}} d\omega \varphi_+(\omega; \mu) = N_f^{\text{exp-LL}}(\Lambda_{UV}, \omega_0, \mu, \mu_s)$$

$$- \frac{\alpha_s(\mu_s)C_F}{4\pi} \left(2 \ln^2 \frac{\mu_s}{\Lambda_{\text{UV}}} + 2 \ln \frac{\mu_s}{\Lambda_{\text{UV}}} + \frac{\pi^2}{12} + \mathcal{O}(e^{-\frac{\Lambda_{\text{UV}}}{\omega_0}}) \right), \quad (3.113)$$

where we checked that the exponentially small corrections $\mathcal{O}(\alpha_s e^{-\Lambda_{\text{UV}}/\omega_0})$ can be safely neglected. The terms in the second line come from the $\mathcal{O}(\alpha_s)$ terms in (3.112). We have denoted the analytical integral of the evolved exponential model as $N_f^{\text{exp-LL}}$, which is a function of the cut-off Λ_{UV} , the scales μ , μ_s and the model hadronic parameter ω_0 . The analytic expression, in terms of the RGE parameter a defined in (3.103), is

$$\begin{aligned} N_f^{\text{exp-LL}}(\Lambda_{\text{UV}}, \omega_0, \mu, \mu_s) &= e^{V+2\gamma_E a} \Gamma(a+2) \left(\frac{\mu_s}{\Lambda_{\text{UV}}} \right)^a \frac{1}{2x^{2+a}} {}_1F_1\left(2+a, 3, -\frac{1}{x}\right) \\ &= e^{V+2\gamma_E a} \frac{\Gamma(a+2)}{\Gamma(1-a)} \left(\frac{\mu_s}{\Lambda_{\text{UV}}} \right)^a + \mathcal{O}(x), \end{aligned} \quad (3.114)$$

where in the second line we have expanded at leading power in $x \equiv \omega_0/\Lambda_{\text{UV}} \sim \lambda/\delta$.

The fact that the leading power expansion of (3.113) in x is independent on ω_0 means that it is model independent, and free of power corrections by construction. We therefore define⁷

$$\begin{aligned} M_0^{\text{LL}-\mu_s}(\Lambda_{\text{UV}}, \mu) &= \frac{e^{V+2\gamma_E a} \Gamma(a+2)}{\Gamma(1-a)} \left(\frac{\mu_s}{\Lambda_{\text{UV}}} \right)^a - \frac{\alpha_s(\mu_s)C_F}{4\pi} \left[2 \ln^2 \frac{\mu_s}{\Lambda_{\text{UV}}} + 2 \ln \frac{\mu_s}{\Lambda_{\text{UV}}} + \frac{\pi^2}{12} \right] \\ &= M_0^{\text{OPE}}(\Lambda_{\text{UV}}, \mu) + \mathcal{O}\left(\alpha_s^2 \ln^2 \frac{\mu_s}{\Lambda_{\text{UV}}} \ln^2 \frac{\mu_s}{\mu}\right), \end{aligned} \quad (3.115)$$

to be compared with the OPE prediction M_0^{OPE} . We observe that the one-loop fixed-order result (3.110) is reproduced by re-expanding this result in α_s , and that the μ_s -dependence drops out as required. However the expansion is not fully justified as $M_0^{\text{LL}-\mu_s}$ suffers from higher-order corrections plagued by large logarithms $\ln \mu_s/\Lambda_{\text{UV}}$ which are not resummed by evolving φ_+ from μ_s to μ .

To show the numerical importance of such corrections we plot both M_0^{OPE} and $M_0^{\text{LL}-\mu_s}$ for different values of the soft scale μ_s and the matching scale μ in Figure 3.7. Notice that the matching scale plays the role of the heavy-quark mass. In the heavy-quark limit we would like to increase Λ_{UV} as much as possible, to reduce the power corrections in $\omega_0/\Lambda_{\text{UV}}$, but we also require the hierarchy $\mu_s \sim \Lambda_{\text{QCD}} \ll \Lambda_{\text{UV}} \ll \mu \sim m_h$. We make the choice⁸

$$\Lambda_{\text{UV}} = \sqrt{0.01\mu^2 + \mu \cdot 1 \text{ GeV}} \equiv \Lambda_\mu, \quad (3.116)$$

such that Λ_{UV} approaches $\mu/10$ for large values of μ . In the left panel of Figure 3.7 we fixed the matching scale $\mu = \mu_b = 4.8 \text{ GeV}$, and we show the residual μ_s -dependence of $M_0^{\text{LL}-\mu_s}$

⁷The superscript LL- μ_s on the left-hand side indicates that the cut-off moment has been computed from the HQET LCDA evolved from the low scale μ_s .

⁸With this choice the QCD LCDA normalization (3.85) would suffer from constant corrections $\mathcal{O}(\alpha_s \delta/(4\pi)) \lesssim 1\%$ in the heavy-quark limit. One could eliminate them by choosing $\Lambda_{\text{UV}} = \sqrt{\mu \cdot 1 \text{ GeV}}$, generating however power corrections to M_0 decreasing with the inverse square root of the heavy meson mass (once setting $\mu = m_H$). Since the focus of this section is on M_0 (while δ is an artificial parameter) we defined Λ_μ such that the power corrections in HQET are still linear.

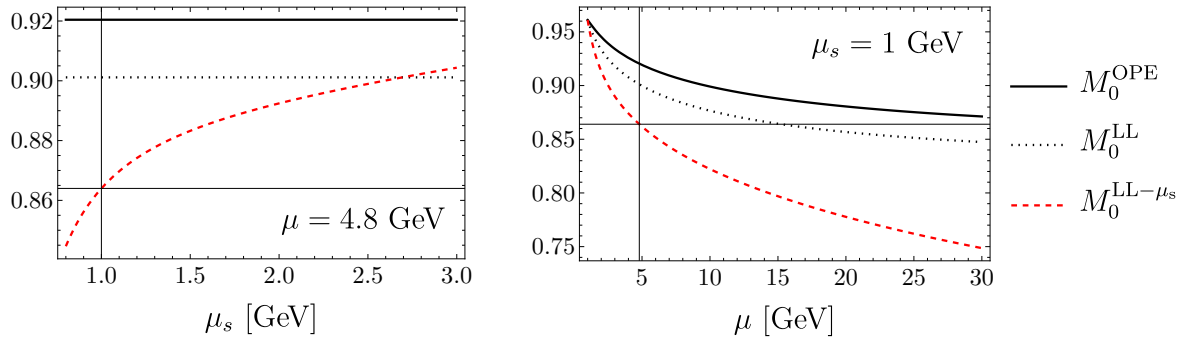


Figure 3.7: Numerical comparison of M_0^{OPE} , $M_0^{\text{LL}-\mu_s}$ and M_0^{LL} , as functions of the low scale μ_s (left) and the matching scale μ (right). The cut-off Λ_{UV} is set to Λ_μ . The solid lines correspond to the default values for the \bar{B} meson.

(dashed red), indicating the effects of the higher-order corrections. The OPE result M_0^{OPE} (solid black) on the other hand is obviously μ_s -independent. The opposite situation is shown in the right panel, where for the default value $\mu_s = 1$ GeV, the μ -dependence of the different evaluations of M_0 is displayed. As anticipated, the heavy-quark limit corresponds to large values of μ , as $\mu \sim m_h$. From these two plots it is evident that the evaluation of the zeroth moment from the evolved HQET LCDA $M_0^{\text{LL}-\mu_s}$ strongly deviates from the OPE prediction, carrying a sizeable residual μ_s dependence. Furthermore, as the difference with respect to M_0^{OPE} increases with μ , the behaviour for large μ is opposite with respect to the expectations in the heavy-quark limit.

Before moving on and identifying the source of this problem, we want to make sure that the accuracy of the model-independent OPE evaluation (3.110) is not spoiled by large logarithms of μ/Λ_{UV} . For this reason we consider a third determination of M_0 , by resumming the logarithms $\ln \mu/\Lambda_{\text{UV}}$ in (3.110) to LL accuracy. The RGE of M_0 is easily derived from

$$\frac{dM_0}{d \ln \mu} = \int_0^{\Lambda_{\text{UV}}} d\omega \frac{d\varphi_+(\omega; \mu)}{d \ln \mu} = - \left[\Gamma_{\text{cusp}} \ln \frac{\mu}{\Lambda_{\text{UV}}} + \frac{\alpha_s}{4\pi} (\Gamma_0 + \gamma_0^+) + \mathcal{O}(\alpha_s^2) \right] M_0(\Lambda_{\text{UV}}, \mu), \quad (3.117)$$

where we employed the RGE for φ_+ (3.19) and the knowledge of its asymptotic form. The solution to (3.117) is

$$M_0^{\text{LL}}(\Lambda_{\text{UV}}, \mu) = e^{V_M(\mu, \Lambda_{\text{UV}})} M_0^{\text{OPE}}(\Lambda_{\text{UV}}, \Lambda_{\text{UV}}), \quad (3.118)$$

with

$$V_M(\mu, \Lambda_{\text{UV}}) = - \int_{\alpha_s(\Lambda_{\text{UV}})}^{\alpha_s(\mu)} \frac{d\alpha}{\beta(\alpha)} \left[\Gamma_{\text{cusp}}(\alpha) \int_{\alpha_s(\Lambda_{\text{UV}})}^{\alpha} \frac{d\alpha'}{\beta(\alpha')} + \frac{\alpha}{4\pi} (\gamma_0^+ + \Gamma_0) + \mathcal{O}(\alpha^2) \right]. \quad (3.119)$$

In Figure 3.7 M_0^{LL} is the black-dotted curve, showing that the higher-order logarithms are numerically not relevant. This check strengthens the hypothesis that the problem with $M_0^{\text{LL}-\mu_s}$ arises from the uncanceled logarithms of $\mu_s/\Lambda_{\text{UV}}$ in higher-orders, as hinted by the μ_s dependence of $M_0^{\text{LL}-\mu_s}$.

3.6.2 Improved Evolution

The previous section highlighted an issue with the evolution of the HQET LCDA when computing cut-off moments. We pinned down the numerical differences between a direct computation of the integral and the OPE prediction to be given by large unresummed logarithms of $\mu_s/\Lambda_{\text{UV}}$. The origin for such large corrections is to be attributed to the fact that the HQET LCDA is non-trivially a two-scale object, containing logarithms of the form

$$\ln \frac{\mu}{\Lambda_{\text{QCD}}}, \quad \ln \frac{\mu}{\omega}, \quad (3.120)$$

where the role of Λ_{QCD} is taken by the initial condition low scale μ_s , while ω can vary between zero and values much larger than Λ_{QCD} in the perturbative asymptotic region. The two-scale nature of $\varphi_+(\omega)$ is not manifest when computing the convergent inverse moments. This can be understood as the integration path in ω goes from 0 to ∞ effectively making the $\ln(\mu/\omega)$ scaleless. On the other hand, when imposing an UV cut-off $\Lambda_{\text{UV}} \gg \Lambda_{\text{QCD}}$, necessary for the divergent moments, new logarithms $\ln \mu/\Lambda_{\text{UV}}$ develop from the $\ln \mu/\omega$ term. The latter are not summed by the standard RGE, employed in Section 3.5, that deals with the collinear logarithms $\ln \mu/\mu_s$.

This problem has been already noted in the literature, and in Ref. [88] an ‘‘improved evolution’’ was developed. The key idea is to set the initial scale of the LCDA to an ω dependent scale which should capture the different logarithms in different regions of ω . However this idea finds a simpler implementation in the so-called ‘‘dual space’’ [89], where the one-loop evolution is diagonal in the dual space variable. Before covering the implementation of the improved evolution, we briefly report here the essential dual space definitions and relations needed in the following.

We define the dual function $\rho_+(\eta; \mu)$ as a Bessel-function transformation of φ_+ [89] Bessel-function transformation

$$\rho_+(\eta; \mu) = \int_0^\infty \frac{d\omega}{\omega} \sqrt{\frac{\omega}{\eta}} J_1\left(2\sqrt{\frac{\omega}{\eta}}\right) \varphi_+(\omega; \mu), \quad (3.121)$$

such that it diagonalizes the one-loop evolution kernel

$$\frac{d\rho_+(\eta; \mu)}{d \ln \mu} = - \left[\Gamma_{\text{cusp}} \ln \frac{\mu}{\hat{\eta}} + \gamma_+ \right] \rho_+(\eta; \mu), \quad (3.122)$$

with $\hat{\eta} = e^{-2\gamma_E} \eta$, while the explicit form of the anomalous dimensions is given below (3.103) and in (3.104). The diagonalized evolution equation is solved by

$$\rho_+(\eta; \mu) = e^{V(\mu, \mu_s)} \left(\frac{\mu_s}{\hat{\eta}} \right)^{a(\mu, \mu_s)} \rho_+(\eta; \mu_s). \quad (3.123)$$

In this formalism, the zeroth cut-off moment is expressed as an integral over η [88] from 0 to ∞

$$M_0(\Lambda_{\text{UV}}, \mu) = \int_0^\infty d\eta \frac{\Lambda_{\text{UV}}}{\eta} J_2\left(2\sqrt{\frac{\Lambda_{\text{UV}}}{\eta}}\right) \rho_+(\eta; \mu). \quad (3.124)$$

The dual function $\rho_+(\eta; \mu)$ also presents a perturbative-partonic determination [88], in analogy to the perturbative asymptotic form of the HQET LCDA in momentum space

$$\rho_+(\eta; \mu)_{\text{pert}} = \frac{C_0(\eta, \mu)}{\omega_0} J_2 \left(2\sqrt{\frac{2\omega_0}{\eta}} \right),$$

$$C_0(\eta, \mu) = 1 + \frac{\alpha_s(\mu)C_F}{4\pi} \left(-2\ln^2 \frac{\mu}{\hat{\eta}} + 2\ln \frac{\mu}{\hat{\eta}} - \frac{\pi^2}{12} - 2 \right) + \mathcal{O}(\alpha_s^2), \quad (3.125)$$

which can be used to reproduce the fixed-order result $M_0^{\text{OPE}}(\Lambda_{\text{UV}}, \mu)$ [88] by expanding in $x = \omega_0/\Lambda_{\text{UV}}$, making the final result ω_0 independent, and hence model-independent. With this formula we see the explicit appearance of logarithms of $\mu/\hat{\eta}$.

We can finally come back to the idea behind the ‘‘improved running’’, but in dual space. The initial scale of the LCDA evolution is set to an η dependent scale

$$\mu_{s\eta} = \sqrt{\mu_s^2 + \hat{\eta}^2}, \quad (3.126)$$

giving the evolved

$$\rho_+^{\text{FLW}}(\eta; \mu) = e^{V(\mu, \mu_{s\eta})} \left(\frac{\mu_{s\eta}}{\hat{\eta}} \right)^{\alpha(\mu, \mu_{s\eta})} \rho_+(\eta; \mu_{s\eta}), \quad (3.127)$$

with the initial condition

$$\rho_+(\eta, \mu_{s\eta}) = \frac{1}{\eta} e^{-\frac{\omega_0}{\eta}} \left(1 + \frac{\alpha_s(\mu_{s\eta})C_F}{4\pi} \left(\frac{1}{2} - \frac{\pi^2}{12} \right) \right) - \frac{\alpha_s(\mu_{s\eta})C_F}{4\pi\eta} \left(2\ln^2 \frac{\mu_{s\eta}}{\hat{\eta}} - 2\ln \frac{\mu_{s\eta}}{\hat{\eta}} - 2\sqrt{e} \frac{\mu_{s\eta}}{\eta} {}_3F_4 \left(1, 1, 1; 2, 2, 2, 3; -\sqrt{e} \frac{\mu_{s\eta}}{\eta} \right) + \frac{5}{2} \right), \quad (3.128)$$

derived from the model (3.98) after the transformation (3.121).

The crucial novelty of the improved evolution is that for $\hat{\eta} \gg \mu_s \sim \Lambda_{\text{QCD}}$, the evolution starts already at the scale $\hat{\eta}$ instead of the low scale μ_s . The zeroth moment associated to the evolved $\rho_+^{\text{FLW}}(\eta; \mu)$ is then computed numerically through (3.124)

$$N_f^{\text{FLW}}(\Lambda_{\text{UV}}, \mu) \equiv \int_0^\infty d\eta \frac{\Lambda_{\text{UV}}}{\eta} J_2 \left(2\sqrt{\frac{\Lambda_{\text{UV}}}{\eta}} \right) \rho_+^{\text{FLW}}(\eta; \mu). \quad (3.129)$$

3.6.3 Numerical Comparisons of M_0

In this section we finally compare the model-independent predictions of Section 3.6.1 (M_0^{OPE} , $M_0^{\mu_s\text{-LL}}$ and M_0^{LL}) with the two model-dependent numerical evaluations of M_0 ($N_f(\Lambda_{\text{UV}}, \mu)$ and $N_f^{\text{FLW}}(\Lambda_{\text{UV}}, \mu)$) which differ only in the HQET LCDA evolution employed. We should not forget that the model-independent predictions are only valid in the limit $\Lambda_{\text{UV}} \gg \Lambda_{\text{QCD}}$, meaning that the comparison is affected by power corrections in $x = \omega_0/\Lambda_{\text{UV}}$.

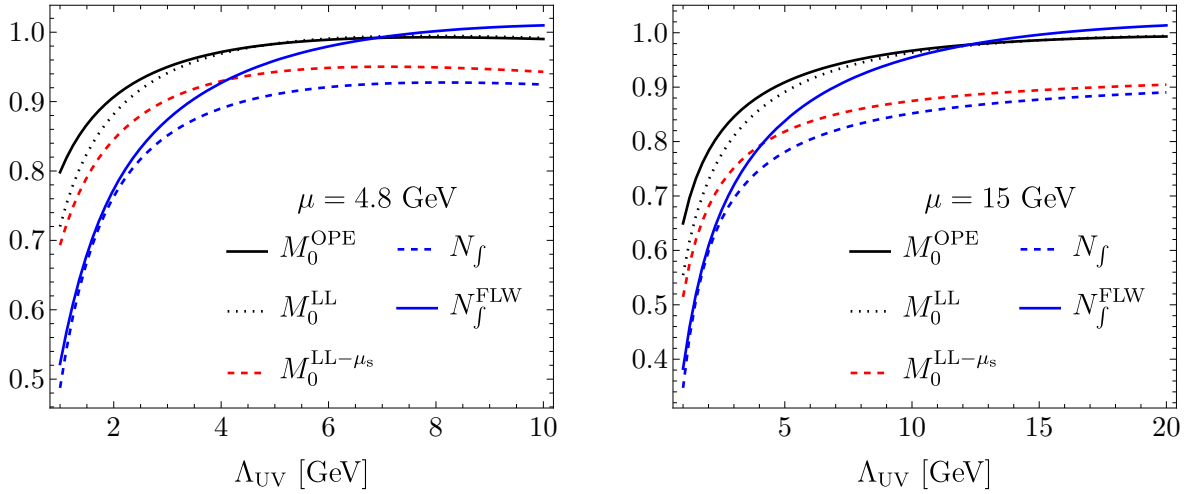


Figure 3.8: Comparison of the five different determinations of M_0 at two values of the renormalization scale, μ_b and μ_{15} .

Notice that the model (3.98) at the low scale μ_s is specifically constructed in order to have the correct asymptotic behaviour and to reproduce the fixed order $M_0^{\text{OPE}}(\Lambda_{\text{UV}}, \mu_s)$, up to negligible corrections of order $\mathcal{O}(e^{-\Lambda_{\text{UV}}/\omega_0})$ for sufficiently large $\Lambda_{\text{UV}} \geq 3$ GeV. Nevertheless, as emerges from (3.114), much more important linear power corrections arise after evolution. To quantify the impact of power corrections we expand (3.114) to order $\mathcal{O}(x)$ and we examine the following difference

$$N_f(\Lambda_{\text{UV}}, \mu) - M_0^{\text{LL}-\mu_s} \approx e^{V+2\gamma_E a} \frac{a\Gamma(a+3)}{\Gamma(1-a)} \left(\frac{\mu_s}{\Lambda_{\text{UV}}}\right)^a \frac{\omega_0}{\Lambda_{\text{UV}}} + \mathcal{O}(x^2), \quad (3.130)$$

whose numerical evaluation gives -0.06 for $\Lambda_{\text{UV}} = 2$ GeV and $\mu = 4.8$ GeV. As a reference value we recall that in Section 3.5 for the \bar{B} meson we used $\Lambda_{\text{UV}} = \delta m_B = 2.38$ GeV. From (3.130) we can see that the power correction is negative and depends mildly on μ through a .

Finally we are ready to compare the five evaluations of M_0 previously defined. Our main goal is to show that the improved evolution [88], implemented in N_f^{FLW} , solves, for sufficiently high Λ_{UV} , the issue of the disagreement between the OPE prediction and the numerical evaluation of the zeroth moment starting from the model at the low scale. The comparison is shown in Figure 3.8 for two values of the matching scale, which in practice stands for the heavy quark mass. We recapitulate the meaning and purpose of the several curves:

1. M_0^{OPE} (solid black) is the fixed-order OPE result, serving as the reference prediction.
2. M_0^{LL} (dotted black) has the logarithms $\ln \mu/\Lambda_{\text{UV}}$ correctly resummed to LL, improving the convergence of the perturbative series of M_0^{OPE} .
3. $M_0^{\text{LL}-\mu_s}$ (dashed red) is the model-independent prediction, free from power corrections, obtained from integrating the HQET LCDA evolved from μ_s .

4. N_f (dashed blue) is the integration of the model $\varphi_+(\omega; \mu)$ evolved from μ_s including the power corrections.
5. N_f^{FLW} (solid blue) is the integration of $\varphi_+(\omega; \mu)$ (in dual space) evolved from $\mu_{s\eta}$, namely following the “improved evolution”.

The first thing to notice is that, due to (3.130), the dashed blue and dashed red curves differ only by power corrections. Furthermore, as shown in the beginning of this section, the dashed red curve differs from the solid black one by higher-order $\ln \mu_s/\Lambda_{\text{UV}}$ terms. The key of the plot is the solid blue curve, where the improved evolution is employed, in which these corrections should be resummed. In fact, for sufficiently large values of Λ_{UV} where power corrections are less pronounced, the solid blue curve gets closer to the solid and dotted black curves. This happens for the two values of μ shown in the two panels of Figure 3.8. As mentioned before the resummation of the logarithms of μ/Λ_{UV} in the OPE prediction is not extremely important⁹, as can be seen by the small difference in the solid and dotted black curves. The dashed blue curve, which would be the one used in Section 3.5, inherits the problem of higher order corrections of the dashed red curve on top of the linear power corrections generated by the standard evolution of the HQET LCDA. It is therefore evident the advantage of the improved evolution in N_f^{FLW} which makes it much closer to the OPE result for $\mu_s \ll \Lambda_{\text{UV}} \lesssim \mu$. As an additional check we show in Figure 3.9 that the residual μ_s -dependence is almost totally eliminated by using the improved evolution. This corroborates the fact that the improved evolution solves the main issues with the standard running, when dealing with cut-off moments.

Having said this however, we can finally look back at what would be the difference induced by the improved evolution in the case of the physical \bar{B} and D mesons. The cut-off Λ_{UV} was set to 2.38 GeV and 1.22 GeV, for the \bar{B} and D respectively. One can notice, in the case of the \bar{B} displayed in the left panel of Figure 3.8, that the difference between N_f and N_f^{FLW} is very small, justifying the usage of the simpler standard running over the more involved improved running.

3.6.4 Large Meson Mass Limit

Now that we have understood the advantage of the improved evolution, we are ready to investigate the heavy-quark limit. Obviously the HQET LCDA cannot depend directly on the heavy quark mass, nevertheless it depends on the matching scale which we set to $\mu = m_H$. For this reason the large-meson mass limit corresponds to evolution to very high scales. Together with the scale, we vary the cut-off by setting it to $\Lambda_{\text{UV}} = \Lambda_\mu$ such that power corrections in the cut-off moments decrease with increasing scale. In Figure (3.10) (upper panel) we show the five evaluations of M_0 as functions of the matching scale, up to very large values (100 GeV). Again the improved resummation tends to the OPE prediction, in particular closer to the LL resummed one M_0^{LL} . On the other hand we see how the

⁹The only region where it is appreciable it's when Λ_{UV} is very small, which is anyway a region where the OPE prediction cannot be trusted.

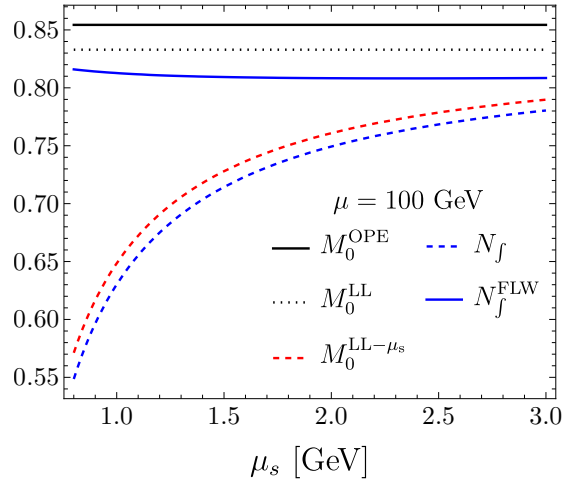


Figure 3.9: As left panel of Figure 3.7 with N_f (dashed blue) and N_f^{FLW} (blue) added. The scale μ has been set to 100 GeV in order to reduce the effect of power corrections ($\Lambda_{\text{UV}} = \Lambda_\mu = 14.1$ GeV).

standard evolution dramatically fails and departs from the OPE predictions for increasing μ . This proves that the prescription first introduced in Ref. [88] is crucial to ensure a consistent heavy-quark limit, and is therefore of great conceptual importance.

We can now finally focus on the quantity for which this whole section was written: the QCD LCDA normalization, obtained from the matching to the HQET LCDA. The matching scale is set to $\mu = m_H$ while the arbitrary parameter δ to Λ_μ/m_H , so that in the large-meson mass limit it will tend to the constant 0.1. In the lower panel of Figure 3.10 we plot the QCD LCDA normalization as a function of the heavy meson mass. When the improved RGE is employed (solid blue) the normalization correctly tends to 1 for increasing meson mass, while the standard evolution (dashed blue) drastically fails. This is an important conceptual check of our result, without which the whole framework could be questioned. The vertical grey lines stand for the D and \bar{B} meson masses. As mentioned above, the difference between the two methods at those meson masses values is still small, justifying the simplified treatment adopted in the numerical analysis of Section 3.5.

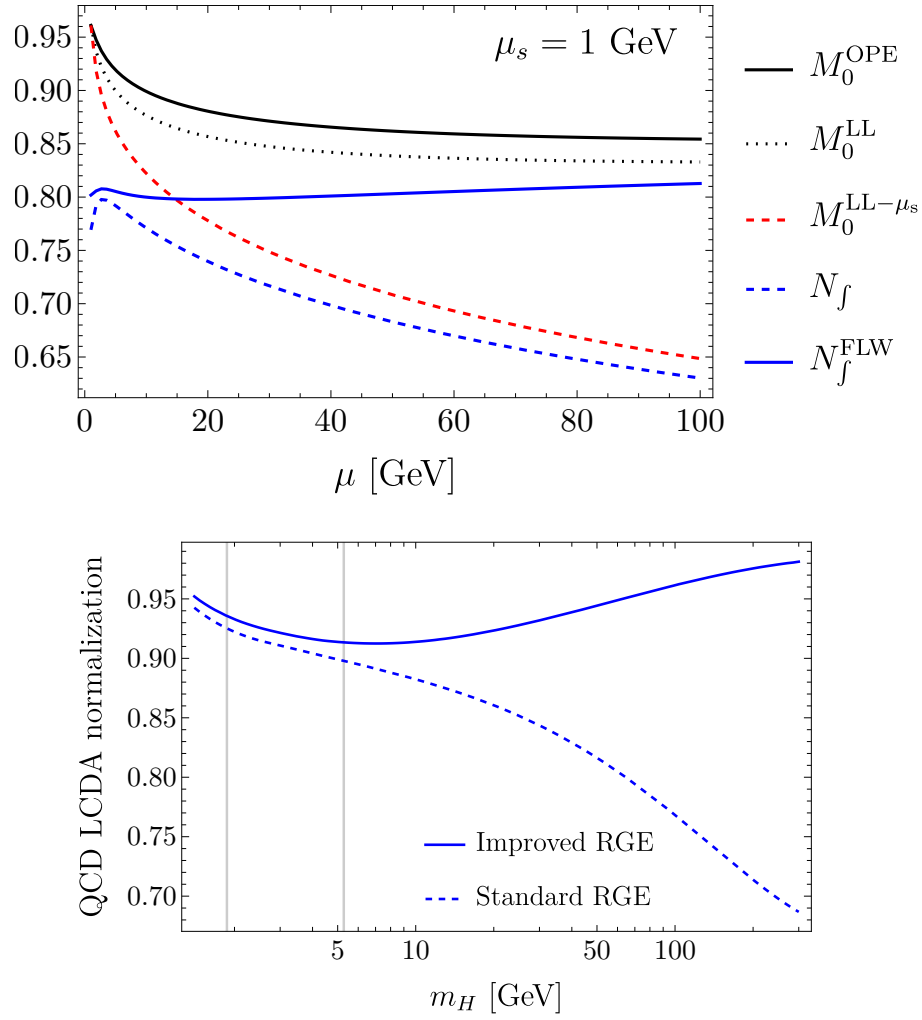


Figure 3.10: Upper panel: μ -dependence of the five evaluations of the cut-off moment discussed in the text. Lower panel: QCD LCDA normalization as a function of the meson mass.

Chapter 4

Branching Fraction of $W^\pm \rightarrow B^\pm \gamma$ Decays

In this chapter we apply the results of Chapter 3 on the factorization of the QCD LCDA. A natural example where the QCD LCDA of a heavy meson enters the factorization theorem is the decay $W^- \rightarrow B^- \gamma$. In this process a boosted B^- meson is produced with energies of order $\mathcal{O}(m_W) \gg m_b$. The amplitude will then depend on three largely separated scales $\Lambda_{\text{QCD}} \ll m_b \ll m_W$, requiring a two-step matching which allows to resum the potentially large logarithms, as explained in Chapter 1. Due to the large hierarchy of scales the amplitude obeys a leading power factorization theorem (in the expansion parameter m_b/m_W), where the QCD LCDA is convoluted with perturbative hard-scattering kernels. Such a factorization theorem has been derived in Ref. [90], together with the computation of the one-loop hard-scattering kernels. With our result we can further separate the scales Λ_{QCD} and m_b present in the QCD LCDA achieving the resummation of all the relevant large logarithms: $\ln(\Lambda_{\text{QCD}}/m_b)$ and $\ln(m_b/m_W)$. In this way the only non-perturbative inputs will be the B^- meson decay constant and the universal leading-twist HQET LCDA $\varphi_+(\omega)$.

We first review the QCD factorization for the amplitude $\mathcal{A}(W^- \rightarrow B^- \gamma)$, which is parametrized in terms of two form factors F_1^B and F_2^B as [90]

$$i\mathcal{A}(W^- \rightarrow B^-(p_B)\gamma(q)) = \frac{eg_2 f_B}{4\sqrt{2}} V_{ub}^* \left(i\varepsilon_{\mu\nu\alpha\beta} \frac{p_B^\mu q^\nu \varepsilon_W^\alpha \varepsilon_\gamma^{*\beta}}{p_B \cdot q} F_1^B - \varepsilon_W^\perp \cdot \varepsilon_\gamma^{\perp*} F_2^B \right), \quad (4.1)$$

where ε_W and ε_γ are the polarization vectors of the W boson and the photon respectively, while e is the positron charge. We used the short hand notation

$$\varepsilon_W^\perp \cdot \varepsilon_\gamma^{\perp*} = \varepsilon_W \cdot \varepsilon_\gamma^* - \frac{q \cdot \varepsilon_W p_B \cdot \varepsilon_\gamma^*}{p_B \cdot q}. \quad (4.2)$$

The tree level diagrams contributing to the amplitude are shown in Figure 4.1, where x stands for the light-cone momentum fraction of the \bar{u} anti-quark, while \bar{x} for the one of the b quark. Except for the electric charges, the first two diagrams are symmetric under the exchange $x \leftrightarrow \bar{x}$ at leading power in m_b/m_W . The third diagram stands for a constant

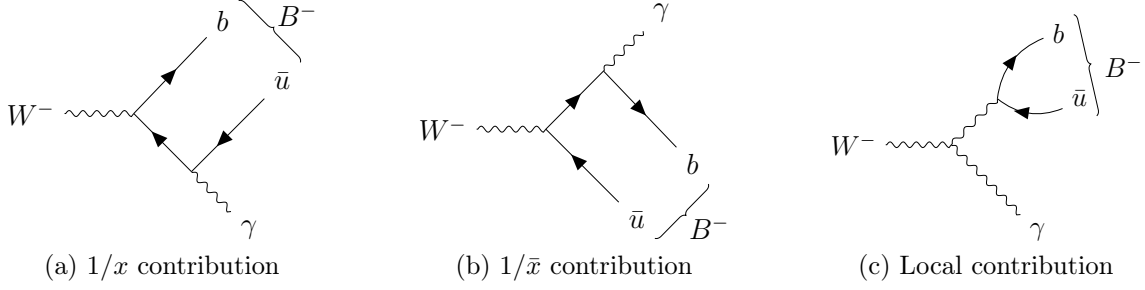


Figure 4.1: Tree-level diagrams contributing to the process $W^- \rightarrow B^- \gamma$.

local contribution, as the hadronic matrix element is simply the decay constant. The form factors $F_{1,2}^B$ in (4.1) are given by

$$\begin{aligned} F_1^B &= Q_u I_+^B + Q_d \bar{I}_+^B, \\ F_2^B &= 2(Q_u - Q_d) - Q_u I_-^B + Q_d \bar{I}_-^B, \end{aligned} \quad (4.3)$$

where the constant term $2(Q_u - Q_d) = 2$ in F_2^B comes from the local contribution of Figure 4.1c, while the convolution integrals are defined as

$$I_{\pm}^B \equiv \int_0^1 dx H_{\pm}(x; \mu_W) \phi_B(x; \mu_W), \quad \bar{I}_{\pm}^B \equiv \int_0^1 dx H_{\pm}(\bar{x}; \mu_W) \phi_B(x; \mu_W), \quad (4.4)$$

where the factorization scale μ_W is of the order of the hard scale m_W . The quark electric charges in units of e are $Q_u = 2/3$ and $Q_d = -1/3$. The two one-loop hard-scattering kernels can be written as

$$H_{\pm}(x; \mu_W) = \frac{1}{x} \left(1 + \frac{\alpha_s(\mu_W) C_F}{4\pi} h_{\pm}(x, m_W; \mu_W) + \mathcal{O}(\alpha_s^2) \right), \quad (4.5)$$

with the perturbative functions [90]

$$h_{\pm}(x, m_W; \mu_W) = -(2 \ln x + 3) \left(\ln \frac{\mu_W^2}{m_W^2} + i\pi \right) + \ln^2 x - 9 + (\pm 1 - 2) \frac{x \ln x}{1 - x}. \quad (4.6)$$

The form factors are thus perturbative series in α_s , and can be written as functions of the Gegenbauer moments of the \bar{B} meson LCDA.

The branching ratio is obtained by squaring the amplitude (4.1) and dividing by the W total decay width Γ_W

$$\text{Br}(W^{\pm} \rightarrow B^{\pm} \gamma) = \frac{\Gamma(W^{\pm} \rightarrow B^{\pm} \gamma)}{\Gamma_W} = \frac{\alpha_{\text{em}} m_W f_B^2}{48 v^2 \Gamma_W} |V_{ub}|^2 \left(|F_1^B|^2 + |F_2^B|^2 \right), \quad (4.7)$$

which holds also for the CP-conjugated decay $W^+ \rightarrow B^+ \gamma$. At this stage, in order to resum correctly the logarithms between Λ_{QCD} and m_b , we employ the QCD LCDA obtained from the matching to HQET in Section 3.3 at the matching scale $\mu_b = 4.8$ GeV, subsequently

evolved to the hard scale $\mu_W = m_W$ resumming the logarithms of m_b/m_W . Therefore using the first 20 Gegenbauer moments at m_W from (3.109) we get the following branching ratio

$$\text{Br}(W^\pm \rightarrow B^\pm \gamma) = (2.58 \pm 0.21_{\text{in } -0.08}^{+0.05} \mu_W \text{ }_{-0.08}^{+0.05} \mu_b \text{ }_{-0.13}^{+0.18} \delta \text{ }_{-0.34}^{+0.61} \beta \text{ }_{-0.98}^{+2.95} \lambda_B) \cdot 10^{-12}, \quad (4.8)$$

where the uncertainty budget is divided into the different sources:

1. input uncertainties (f_B , Γ_W , m_W , mainly $|V_{ub}|$),
2. hard-scale variation in the range $\mu_W \in [m_W/2, 2m_W]$,
3. matching scale variation in the range $\mu \in [\mu_b/2, 2\mu_b]$,
4. variation of the peak-tail merging point δ by $\pm 15\%$,
5. HQET LCDA model-shape dependence by varying β for the three models within its respective domain,
6. varying $\lambda_B = (350 \pm 150)$ MeV within its uncertainty.

We have to mention that since the factorization formula (4.1) holds at the level of the amplitude, we kept the $\mathcal{O}(\alpha_s^2)$ terms from the square of the form factors to obtain the above numbers. One also has the option of truncating the expansion of the square to first order, in which case the central value would be $\text{Br}^{\text{trunc}} = 2.54 \cdot 10^{-12}$ with similar uncertainties.

From the result (4.8) it is evident that the precision is limited by the poor knowledge of the input HQET LCDA, as the largest source of uncertainties are indeed the model dependence reflected by β and the uncertainty on the inverse moment λ_B . For this reason we plot in Figure 4.2 the branching ratio as a function of the parameters ω_0 and β of (3.101). The axis origin denotes the default value, and the plot in the left panel is performed with $\beta = 0$, namely the exponential model. Quite naturally the branching ratio is highly sensitive to the low bound on λ_B , which is because at tree level the amplitude is essentially proportional to λ_B^{-1} .

4.1 Comparison with QCD Factorization

In Ref. [90] the numerical predictions were obtained by assuming a model for the QCD LCDA of the heavy meson at the low scale 1 GeV

$$\phi_B(x; 1 \text{ GeV}) = N_\phi \frac{m_b^2}{\lambda_B^2} x(1-x) e^{-\frac{xm_b}{\lambda_B}}, \quad (4.9)$$

where N_ϕ is a calculable constant assuring the correct normalization of $\phi_B(x; 1 \text{ GeV})$. The HQET inspired model was then evolved up to the hard scale with the ERBL evolution kernel. We now will use the same approach, with our numerical inputs, in order to quantify

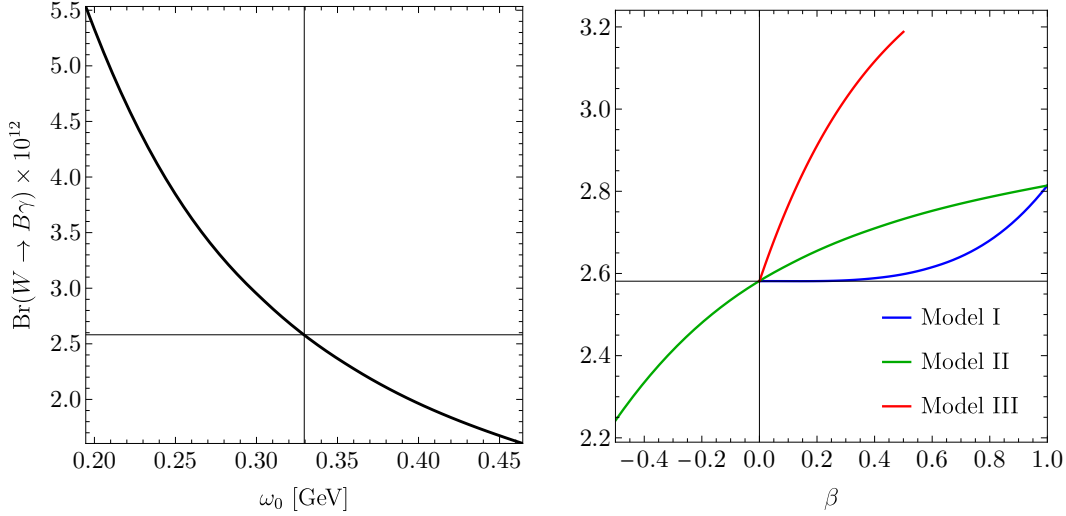


Figure 4.2: Branching ratio as a function of the parameters in the HQET LCDA models (3.101).

the numerical impact of properly matching the QCD LCDA to HQET at the intermediate scale of order of the heavy quark mass. The branching ratio is

$$\text{Br}(W^\pm \rightarrow B^\pm \gamma) \Big|_{\text{exp. model}} = (1.99 \pm 0.17)_{\text{in } -0.06}^{+0.03} \mu_W \cdot \lambda_B \cdot 10^{-12}, \quad (4.10)$$

close to its truncated expansion $\text{Br}^{\text{trunc}}|_{\text{exp. model}} = 1.96 \cdot 10^{-12}$. The central value of our result (4.8) is roughly bigger by 30% with respect to (4.10), while the uncertainties are similar. This shows that the effect of resumming the logarithms between Λ_{QCD} and m_b within HQET has a non-negligible impact.

4.2 Comparison with HQET Factorization

While the QCD factorization essentially assumes the scalings $\Lambda_{\text{QCD}} \sim m_b \ll m_W$, there is another possible approach which consists in considering $\Lambda_{\text{QCD}} \ll m_b \sim m_W$ [91]. In this way the hard-scattering kernels of the factorization formula are obtained by directly matching onto HQET, integrating out the hard scales m_b and m_W simultaneously. This results in a factorization formula given by the convolution of the HQET LCDA with hard-scattering kernels at the scale μ_b , which leaves the large logarithms $\ln m_b/m_W$ unresummed, but properly deals with the ones between Λ_{QCD} and m_b . In this framework, at leading power in Λ_{QCD}/m_b , only the first class of diagrams of Figure 4.1 contributes as the convolutions $I_+^B \simeq I_-^B \sim m_b/\Lambda_{\text{QCD}}$ are the dominant ones. For this reason the form factors (4.3) at leading power in λ_b have the same absolute value

$$F_{1,2}^B \Big|_{\text{HQET}} = \pm Q_u \frac{\tilde{f}_B(\mu_b)}{f_B} \int_0^\infty d\omega T(\omega, m_b, m_W; \mu_b) \varphi_+(\omega; \mu_b), \quad (4.11)$$

where $T(\omega, m_b, m_W; \mu_b)$ is the HQET hard-scattering kernel, and the upper (lower) sign refers to F_1^B (F_2^B). Computing the form factors with the HQET factorization formula and

inserting them in the expression for the branching ratio (4.7) gives

$$\text{Br}(W^\pm \rightarrow B^\pm \gamma) \Big|_{\text{HQET}} = (2.61 \pm 0.22)_{\text{in}} \begin{matrix} +0.19 \\ -0.71 \end{matrix} \mu_b \begin{matrix} +0.50 \\ -0.42 \end{matrix} \beta \begin{matrix} +3.09 \\ -1.03 \end{matrix} \lambda_B \cdot 10^{-12}. \quad (4.12)$$

The difference in the central value with respect to (4.8) is surprisingly small, however the large uncertainty deriving from varying the matching scale between $\mu_b/2$ and $2\mu_b$ reflects the unreliability of the perturbative expansion. Truncating the expansion of the form factors squared after the $\mathcal{O}(\alpha_s)$ term one would get $\text{Br}^{\text{trunc}}|_{\text{HQET}} = 2.11 \cdot 10^{-12}$ where the uncertainty from the scale variation would break into negative values for the branching ratio. This is because the one-loop correction is negative and about 50% the size of the tree-level result. These considerations highlight the importance of resumming the collinear logarithms of m_b/m_W .

4.2.1 Cross-Check with HQET Factorization

We now want to further check our result of Chapter 3 by comparing the HQET hard-scattering kernel, expanded to leading power in m_b/m_W , and the combination of the QCD hard-scattering kernel with the LCDA jet function re-expanded to one-loop fixed order after the evolution of the LCDA. In other words, we expect

$$T(\omega, m_b, m_W; \mu_b) \Big|_{m_b \ll m_W} = H(x, m_W; \mu_W) \otimes_x f_{\text{ERBL}}(x, u, \mu_W, \mu_b) \otimes_u \mathcal{J}_p(u, \omega, m_b; \mu_b), \quad (4.13)$$

to be satisfied, with $f_{\text{ERBL}}(x, u, \mu_W, \mu_b)$ being the function encoding the evolution of the QCD LCDA between μ_b and μ_W introduced in (3.13). To explicitly get the logarithms of the two scales $\ln \mu_b/\mu_W$ at fixed order $\mathcal{O}(\alpha_s)$ we have to re-expand the evolution function. This can be done by using

$$\left(\frac{\alpha_s(\mu_W)}{\alpha_s(\mu_b)} \right)^{\frac{\gamma_n}{2\beta_0}} = 1 + \gamma_n \frac{\alpha_s(\mu_b)}{8\pi} \ln \frac{\mu_b^2}{\mu_W^2} + \mathcal{O}(\alpha_s(\mu_b)^2), \quad (4.14)$$

which, inserted in (3.14), gives

$$f_{\text{ERBL}}(x, u, \mu_W, \mu_b) = \delta(x - u) + \frac{\alpha_s(\mu_b)}{8\pi} \ln \frac{\mu_b^2}{\mu_W^2} 6x\bar{x} \sum_{n=0}^{\infty} \gamma_n N_n C_n^{(3/2)}(2x-1) C_n^{(3/2)}(2u-1). \quad (4.15)$$

With this we can express the evolved LCDA in terms of the LCDA at the scale μ_b as

$$\phi(x; \mu_W) = \phi(x; \mu_b) + \frac{\alpha_s(\mu_b)}{8\pi} \ln \frac{\mu_b^2}{\mu_W^2} 6x\bar{x} \sum_{n=0}^{\infty} \gamma_n N_n C_n^{(3/2)}(2x-1) \int_0^1 du C_n^{(3/2)}(2u-1) \phi(u; \mu_b). \quad (4.16)$$

We can finally expand at fixed-order in α_s the convolutions (4.4) to recover the HQET factorization result [91]. In practice this means inserting the LCDA (4.16) into the integrals of (4.4). We know that the convolution of $H_\pm(\bar{x}, \mu_W)$ with the LCDA of a heavy meson

gives a subleading contribution, as well as the $\mathcal{O}(x)$ terms in h_{\pm} , since the LCDA is forcing the scaling $x \sim \lambda_b$. Therefore at leading power in λ_b the two hard-scattering kernels are equal, $H_+(x; \mu_W) = H_-(x; \mu_W) \equiv H(x; \mu_W)$, with analogous definition for $h(x, m_W; \mu_W)$.

To extract the HQET hard-scattering kernel $T(\omega; \mu_b)$ it is sufficient to require that the QCD and HQET factorization formulas give the same amplitude. Explicitly, when expanding to fixed order, the following relation holds

$$\tilde{f}_B(\mu_b) \int_0^{\infty} d\omega T(\omega; \mu_b) \varphi_+(\omega; \mu_b) = f_B \int_0^1 dx H(x; \mu_W) \phi_B(x; \mu_W). \quad (4.17)$$

We then take the convolution of the hard-scattering kernel (4.5) at the scale μ_W with the LCDA (4.16), and apply our result (3.80) to $\phi_B(u; \mu_b)$ with $\sigma = 0$:

$$\begin{aligned} \int_0^{\infty} d\omega T(\omega; \mu_b) \varphi_+(\omega; \mu_b) &= \frac{f_B}{\tilde{f}_B(\mu_b)} \int_0^1 dx H(x; \mu_W) \phi_B(x; \mu_W) \\ &= \int_0^{\delta m_b} d\omega \frac{m_b}{\omega} \varphi_+(\omega; \mu_b) \left[1 + \frac{\alpha_s C_F}{4\pi} \left(h\left(\frac{\omega}{m_b}, m_W, \mu_W\right) + \mathcal{J}_{\text{peak}}^{(1)}(m_b; \mu_b) \right) \right] \\ &\quad + \frac{\alpha_s}{8\pi} \ln \frac{\mu_b^2}{\mu_W^2} \int_0^{\delta m_b} d\omega \varphi_+(\omega; \mu_b) \sum_{n=0}^{\infty} \left[\gamma_n N_n \int_0^1 dx 6\bar{x} C_n^{(3/2)}(2x-1) \right] C_n^{(3/2)}\left(2\frac{\omega}{m_b} - 1\right), \end{aligned} \quad (4.18)$$

where the contribution from the tail

$$\frac{\alpha_s C_F}{4\pi} \int_{\delta}^1 dx \frac{1}{x} \mathcal{J}_{\text{tail}}^{(1)}(x) \propto \frac{1}{\delta} \ll \frac{m_b}{\Lambda_{\text{QCD}}}, \quad (4.19)$$

is subleading and has been neglected.

The last line of (4.18) looks rather complicated, but it is possible to express the sum in closed form. First of all, by recalling the relation between Gegenbauer polynomials and Legendre polynomials $P_n(x)$

$$C_n^{(3/2)}(z) = \frac{d}{dz} P_{n+1}(z), \quad (4.20)$$

we can evaluate the integral

$$\int_0^1 dx 6\bar{x} C_n^{(3/2)}(2x-1) = 3(-1)^n. \quad (4.21)$$

The Gegenbauer series is then summed giving

$$\sum_{n=0}^{\infty} (-1)^n \frac{3\gamma_n}{2C_F} N_n C_n^{(3/2)}\left(2\frac{\omega}{m_b} - 1\right) = -\frac{m_b}{\omega} \left(2 \ln \frac{\omega}{m_b} + 3\right) \equiv G_C(\omega/m_b), \quad (4.22)$$

which can be proven to hold by expanding the right-hand side in Gegenbauer moments

$$G_C(y) = \sum_{n=0}^{\infty} g_n C_n^{(3/2)}(2y-1), \quad \text{with} \quad g_n = 6N_n \int_0^1 dy y(1-y) G_C(y) C_n^{(3/2)}(2y-1), \quad (4.23)$$

and showing

$$g_n = (-1)^n \frac{3\gamma_n}{2C_F} N_n, \quad (4.24)$$

for every n . The technique to compute g_n to all orders is to employ the generating function of the Gegenbauer polynomials

$$\frac{1}{(1-2zt+t^2)^{\frac{3}{2}}} = \sum_{n=0}^{\infty} C_n^{(3/2)}(z)t^n, \quad (4.25)$$

as

$$G_F(t) \equiv 6 \int_0^1 dy y(1-y) \frac{G_C(y)}{[1+2(1-2y)t+t^2]^{\frac{3}{2}}} = \sum_{n=0}^{\infty} \frac{g_n}{N_n} t^n, \quad (4.26)$$

such that from the Taylor expansion of $G_F(t)$ around $t=0$ one can extract the g_n coefficients. A straightforward calculation yields

$$G_F(t) = -3 \frac{2(t^2+1)\ln(t+1) + (t-2)t}{t^2(t+1)}, \quad (4.27)$$

which when expanded proves the relation (4.24) and therefore (4.22).

Putting these results into (4.18), we can write

$$\begin{aligned} \int_0^{\infty} d\omega T(\omega; \mu_b) \varphi_+(\omega; \mu_b) &= \int_0^{\delta m_b} d\omega \frac{m_b}{\omega} \varphi_+(\omega; \mu_b) \\ &\times \left[1 + \frac{\alpha_s C_F}{4\pi} \left(h\left(\frac{\omega}{m_b}, m_W; \mu_W\right) + \mathcal{J}_{\text{peak}}^{(1)}(m_b; \mu_b) - \ln \frac{\mu_b^2}{\mu_W^2} \left(2 \ln \frac{\omega}{m_b} + 3 \right) \right) \right], \end{aligned} \quad (4.28)$$

finally identifying the HQET hard-scattering kernel with

$$\begin{aligned} T^{(0)}(\omega) &= \frac{m_b}{\omega}, \\ T^{(1)}(\omega, m_b; \mu_b) &= \left(h\left(\frac{\omega}{m_b}, m_W; \mu_W\right) + \mathcal{J}_{\text{peak}}^{(1)}(m_b; \mu_b) - \ln \frac{\mu_b^2}{\mu_W^2} \left(2 \ln \frac{\omega}{m_b} + 3 \right) \right) T^{(0)}(\omega), \end{aligned} \quad (4.29)$$

where, as expected, the μ_W dependence of the perturbative hard function h cancels with the last term from the LCDA evolution. The final result

$$\begin{aligned} T^{(1)}(\omega, m_b; \mu_b) &= \left[\frac{1}{2} \ln^2 \frac{\mu_b^2}{m_b^2} - 2 \ln \frac{\mu_b^2}{m_b^2} \ln \frac{\omega}{m_b} + \ln^2 \frac{\omega}{m_b} - \frac{5}{2} \ln \frac{\mu_b^2}{m_b^2} \right. \\ &\quad \left. - \left(\ln \frac{m_b^2}{m_W^2} + i\pi \right) \left(2 \ln \frac{\omega}{m_b} + 3 \right) + \frac{\pi^2}{12} - 7 \right] T^{(0)}(\omega), \end{aligned} \quad (4.30)$$

is in agreement with (39) of Ref. [91], which is another strong check of our results from Chapter 3.

Chapter 5

Colour-Suppressed $\bar{B} \rightarrow DL$ Decays

At the end of Chapter 2 we gave a very brief introduction to QCD factorization in non-leptonic two-body exclusive \bar{B} decays. In this chapter we focus on the case of heavy-light final state, $\bar{B} \rightarrow DL$ with L being the light pseudoscalar meson. These processes are mediated by three decay topologies showed in Figure 5.1, where the two square dots denote the insertion of a four-fermion operator from the weak effective Hamiltonian presented in Section 2.1. An important feature of such decays is that penguin amplitudes do not contribute, since we require a single charm quark in the final state. In QCDF the only calculable amplitude is the colour-allowed one (T), satisfying a well established factorization formula [71]. The colour-suppressed (C) and the W -exchange (E) amplitudes are both power suppressed in the heavy mass limit $m_c \sim m_b \gg \Lambda_{\text{QCD}}$.

The focus of this chapter is on the colour-suppressed tree topology. Intuitively, when considering $m_c \sim \mathcal{O}(m_b)$, the D^0 meson is produced almost at rest, hence overlapping with the $\bar{B} \rightarrow L$ transition. This causes the breakdown of factorization as soft-gluon exchanges between the meson constituents are not suppressed. On the other hand, if the charm quark is replaced with a light quark (and hence the D^0 substituted with a light meson) the C amplitude is now of the same order as the T one, and obeys the factorization formula (2.135), which takes into account $T + C$. This is also intuitive as the emitted light meson will now be energetic, and will appear as a colour neutral object to soft gluons not able to probe its inner structure. In this chapter we want to adopt the power counting where the charm mass is an intermediate scale between the hard scale m_b and the soft scale Λ_{QCD}

$$m_b \gg m_c \gg \Lambda_{\text{QCD}}, \quad (5.1)$$

and investigate whether under this assumption the C amplitude obeys a factorization formula. More specifically we will consider the charm mass to be a hard-collinear scale, employing the power counting

$$m_c \sim \mathcal{O}(\Lambda_{\text{QCD}} m_b), \quad (5.2)$$

such that we can write the expansion in terms of a single power counting parameter

$$\lambda_c = \frac{\Lambda_{\text{QCD}}}{m_c} \sim \sqrt{\frac{\Lambda_{\text{QCD}}}{m_b}} \ll 1. \quad (5.3)$$

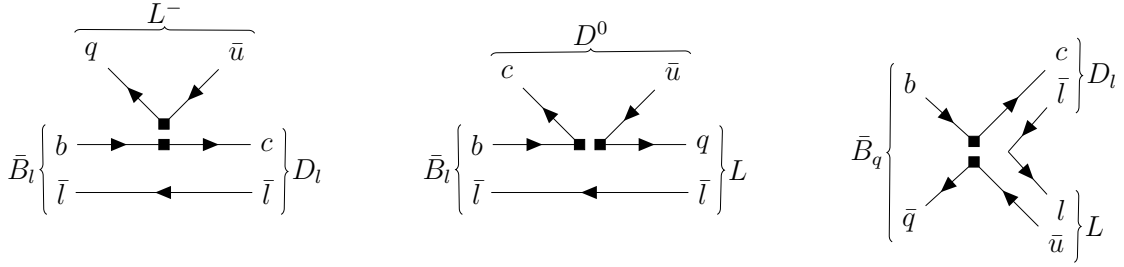


Figure 5.1: Three relevant decay topologies for $\bar{B} \rightarrow DL$ decays. On the left the colour-allowed tree amplitude (T), in the center the colour-suppressed tree amplitude (C), while on the right the W -exchange amplitude (E) where the pair \bar{l} is generated from a gluon (not displayed). In this picture $l = u, d, s$ stands for a generic light quark, while $q = d, s$ for a down-type light quark.

Decay	Amplitude	Exp. branching ratio (10^{-4})
$\bar{B} \rightarrow D^+ K^-$	T	2.05 ± 0.08
$\bar{B}_s \rightarrow D_s^+ \pi^-$	T	29.8 ± 1.4
$\bar{B} \rightarrow D^0 \bar{K}^0$	C	0.55 ± 0.04
$\bar{B}_s \rightarrow D^0 K^0$	C	4.3 ± 0.9
$B^- \rightarrow D^0 \pi^-$	$T + C$	46.1 ± 1.0
$B^- \rightarrow D^0 K^-$	$T + C$	3.64 ± 0.15
$\bar{B} \rightarrow D^+ \pi^-$	$T + E$	25.1 ± 0.8
$\bar{B}_s \rightarrow D_s^+ K^-$	$T + E$	2.25 ± 0.12
$\bar{B} \rightarrow D^0 \pi^0$	$\frac{1}{\sqrt{2}}(-C + E)$	2.67 ± 0.09

Table 5.1: The $\bar{B}_{(s)} \rightarrow DL$ decays with their amplitudes and the CP-averaged branching ratios from PDG [24]. The pure colour-suppressed modes are $\bar{B}_s \rightarrow D^0 K^0$ and $\bar{B} \rightarrow D^0 \bar{K}^0$ with the latter being Cabibbo suppressed due to the CKM matrix element V_{us} .

The potential interest behind this study relies on the decay modes summarized in Table 5.1. It is noticeable that some of the processes are purely mediated by the T amplitude, while others purely by the C one. In this sense they are viewed as clean tests of factorization, and at present puzzling tensions [16, 23] animate the discussion on the factorizable T mediated decays.

5.1 Power Counting of the Amplitudes

Before analyzing in depth the C amplitudes, we would like to understand how the power counting (5.2) affects the scaling of the contributions to different amplitudes. It is therefore instructive to compare this to the standard approach which assumes $m_c \sim m_b$. From

QCDF [71] we have

$$\begin{aligned}
T &\sim m_b^2 F_0^{\bar{B}D}(m_L^2) f_L, \\
C &\sim m_b^2 F_0^{\bar{B}L}(m_D^2) f_D, \\
E &\sim f_B f_D f_L \int_0^1 dv \frac{\phi_D(v)}{\bar{v}^2} \int_0^1 du \frac{\phi_L(u)}{u}, \\
S &\sim f_B f_D f_L \frac{m_b}{\lambda_B} \int_0^1 dv \frac{\phi_D(v)}{\bar{v}} \int_0^1 du \frac{\phi_L(u)}{\bar{u}},
\end{aligned} \tag{5.4}$$

where S stands for the spectator scattering contribution (tree-level α_s correction present in the T and C amplitudes, see Figure 2.3), which depends on the inverse moment of the HQET LCDA $\lambda_B \sim \Lambda_{\text{QCD}}$. The scalings are obtained by using $f_M \sim \Lambda_{\text{QCD}} \sqrt{\Lambda_{\text{QCD}}/m_M}$ for the decay constants, while the LCDAs are considered to be peaked at values $\bar{v} \sim \Lambda_{\text{QCD}}/m_c$ for $\phi_D(v)$ and $u \sim 1$ for $\phi_L(u)$, with the normalization conditions $dx \phi_M(x) \sim 1$. The $\bar{B} \rightarrow D$ form factor power counting can be estimated from the overlap of the mesons wave functions [71]

$$F_0^{\bar{B}D}(0) \sim \int d^2 k_\perp d\xi \Psi_B(\xi, k_\perp) \Psi_D(\xi'(\xi), k_\perp), \tag{5.5}$$

with $k_\perp \sim \Lambda_{\text{QCD}}$. The scaling of the wave functions is derived from the normalization condition, resulting respectively in $\Psi_{B,D}(\xi_{b,c}, k_\perp) \sim \frac{1}{\Lambda_{\text{QCD}}} \sqrt{\frac{m_{b,c}}{\Lambda_{\text{QCD}}}}$ for values $\xi_{b,c} \sim \Lambda_{\text{QCD}}/m_{b,c}$ corresponding to the peak. However, in the convolution (5.5) the longitudinal momentum fraction $\xi' \approx \xi$ is fixed by the kinematics. This means that the D wave function is in the endpoint configuration where momentum fraction $\xi' \sim \xi_b \ll \xi_c$ is small. From the HQET and QCD LCDAs we know that for $\xi \rightarrow 0$ the wave function is linear in ξ . Therefore

$$\Psi_D(\xi, k_\perp) \sim \frac{\xi}{\xi_c} \Psi_D(\xi_c, k_\perp) \sim \frac{m_c}{m_b} \frac{1}{\Lambda_{\text{QCD}}} \sqrt{\frac{m_c}{\Lambda_{\text{QCD}}}}. \tag{5.6}$$

Hence the form factor scales as

$$F_0^{\bar{B}D}(0) \sim \int d^2 k_\perp d\xi \frac{\xi}{\xi_c} \Psi_B(\xi, k_\perp) \Psi_D(\xi_c, k_\perp) \sim (m_c/m_b)^{3/2}. \tag{5.7}$$

Notice that the same result can also be obtained in a simpler way by requiring a smooth transition between the heavy-to-heavy and the heavy-to-light case. In practice we assign a general scaling to the form factor as

$$F_0^{\bar{B}D}(q^2) \sim \left(\frac{\Lambda_{\text{QCD}}}{m_b}\right)^x \left(\frac{m_c}{m_b}\right)^y, \tag{5.8}$$

where when $q^2 \ll m_b^2$ the q^2 dependence is not pronounced. We then apply the two known conditions

$$F_0^{\bar{B}D}(q^2)|_{m_c \sim m_b} \sim 1,$$

$m_c \sim m_b$	$m_c \sim \sqrt{\Lambda_{\text{QCD}} m_b}$
$T \sim \lambda_b$	$T \sim \lambda_b^{7/4}$
$C \sim \lambda_b^3$	$C \sim \lambda_b^{11/4}$
$E \sim \lambda_b^2$	$E \sim \lambda_b^{11/4}$
$S \sim \lambda_b^2$	$S \sim \lambda_b^{9/4}$

Table 5.2: Scalings of the topological amplitudes in the standard QCDF case $m_c \sim m_b$ [71] and in our choice $m_c \sim \sqrt{\Lambda_{\text{QCD}} m_b}$, in units of m_b^3 . We expressed the scalings in terms of λ_b such that they can be compared between the two columns.

$$F_0^{\bar{B}D}(q^2)|_{m_c \sim \Lambda_{\text{QCD}}} \sim (\Lambda_{\text{QCD}}/m_b)^{3/2}, \quad (5.9)$$

and after solving for x and y we find again the result (5.7).

Applying this result to the topological amplitudes we get the two sets of scalings in Table 5.2. Nevertheless these scalings need to be considered with a grain of salt, since they are numerically spoiled by the decay constants where

$$\begin{aligned}
f_B &\simeq 190 \text{ MeV} \sim \Lambda_{\text{QCD}} \sqrt{\frac{\Lambda_{\text{QCD}}}{m_b}}, \\
f_D &\simeq 220 \text{ MeV} \sim \Lambda_{\text{QCD}} \sqrt{\frac{\Lambda_{\text{QCD}}}{m_c}}, \\
f_\pi, f_K &\simeq 130, 150 \text{ MeV} \sim \Lambda_{\text{QCD}}.
\end{aligned} \quad (5.10)$$

For this reason we will take into account the different contributions as separate physics effects, not worrying about the relative power counting. The power expansion will be used to identify in each quantity the leading term, neglecting the subleading ones.

5.2 Region Analysis

We now perform a region analysis of the colour-suppressed amplitude for the process $\bar{B} \rightarrow D^0 L$, which will be useful in checking that, at leading power in λ_c , no non-perturbative modes can connect the emitted D^0 meson from the $\bar{B} \rightarrow L$ transition. If this is the case, we will be able to state a factorization formula for the C amplitude at leading power in λ_c .

We now consider the full process with the emission of a light pseudoscalar meson, including the diagrams with the spectator scattering. The pseudoscalar meson is interpolated with the local current $i\bar{l}\gamma^5 q$. The light meson external momentum is collinear and scales as $p_L \sim (1, \lambda_c^2, \lambda_c^4)m_B$. We denote with p_l the momentum of the on-shell soft spectator anti-quark. Notice that in this way the meson would be formed by a soft anti-quark and a hard-collinear quark, which is not the actual physical situation. To justify this we have to implicitly consider that the form factor will encode a hard-collinear gluon exchange between

the constituents of L which makes both the quark and anti-quark in the light meson to be collinear.¹ The six non-factorizable diagrams are

$$\begin{aligned}
\mathcal{I}_{cq} = & \quad \mathcal{I}_{uq} = \\
\mathcal{I}_{cl} = & \quad \mathcal{I}_{ul} = \\
\mathcal{I}_{bc} = & \quad \mathcal{I}_{bu} =
\end{aligned}
\tag{5.11}$$

We find in total five different regions

hard:	$(1, 1, 1)m_B,$	
hard-collinear (hc):	$(1, \lambda_c, \lambda_c^2)m_B,$	
anti-hard-collinear ($\overline{\text{hc}}$):	$(\lambda_c^2, \lambda_c, 1)m_B,$	
soft:	$(\lambda_c^2, \lambda_c^2, \lambda_c^2)m_B,$	
anti-ultrasoft-collinear ($\overline{\text{usc}}$):	$(\lambda_c^4, \lambda_c^3, \lambda_c^2)m_B,$	(5.12)

also confirmed by the Mathematica package `asy2.1` [92, 93]. Schematically we write the leading power regions contributing to each diagram, where the coloured ones cancel between the different diagrams

$$\begin{aligned}
\mathcal{I}_{cq} = & \text{hard, hc, } \overline{\text{hc}}, \overline{\text{usc}}, & \mathcal{I}_{uq} = & \text{hard, hc,} \\
\mathcal{I}_{cl} = & \text{soft, } \overline{\text{usc}}, & \mathcal{I}_{ul} = & \text{soft,} \\
\mathcal{I}_{bc} = & \text{hard, } \overline{\text{hc}}, & \mathcal{I}_{bu} = & \text{hard,}
\end{aligned}
\tag{5.13}$$

leaving out only the hard region in the non-factorizable diagrams at leading power in λ_c . All the six diagrams have the same colour factor c_{fi} which depends on which weak effective

¹We also considered the situation where the spectator anti-quark in the \bar{B} meson is soft-collinear, such that the quark coming out of the weak effective vertex can be collinear. The region analysis gives the same results, with obvious rescalings of the different regions.

operator Q_i is inserted

$$c_{f1} = -\frac{C_F}{2N_c^2}, \quad c_{f2} = \frac{C_F}{N_c}. \quad (5.14)$$

5.2.1 Hard-Collinear Region

We start with the computation of the hard-collinear region. The cancellation can be seen already at the integrand level

$$\begin{aligned} \mathcal{I}_{cq}^{\text{hc}} &= \frac{\alpha_s c_{fi}}{4\pi} \left(\frac{\mu^2}{2p_L \cdot p_l} \right)^\epsilon \frac{\langle \mathcal{O}_{\text{EFT}} \rangle^{(0)}}{n_{-p_l}} \int \frac{d^d k}{(2\pi)^d} \left(\frac{n_{+p_L} - n_{+k}}{n_{+k} + i\eta} \right) \\ &\times \frac{i(4\pi)^{2-\epsilon} e^{\epsilon\gamma_E} (2p_L \cdot p_l)^\epsilon}{(k^2 + i\eta)(k^2 + n_{+k}n_{-p_l} - n_{+p_L}n_{-k} - n_{+p_L}n_{-p_l} + i\eta)} = -\mathcal{I}_{uq}^{\text{hc}}, \end{aligned} \quad (5.15)$$

where we wrote the result in terms of the tree level matrix element of the following EFT operator

$$\mathcal{O}_{\text{EFT}} = [\bar{\chi}_C^{(m_c)} \gamma_\perp^\mu (1 - \gamma^5) h_v] [\bar{l}_s \not{p}_- \gamma_{\perp\mu} (1 - \gamma^5) \chi_{\bar{C}}]. \quad (5.16)$$

The explicit result for the hard-collinear region is

$$\mathcal{I}_{cq}^{\text{hc}} = \frac{\alpha_s c_{fi}}{4\pi} \left(\frac{\mu^2}{2p_L \cdot p_l} \right)^\epsilon \frac{\langle \mathcal{O}_{\text{EFT}} \rangle^{(0)}}{n_{-p_l}} \left(\frac{1}{\epsilon^2} + \frac{1}{\epsilon} - \frac{\pi^2}{12} + 2 \right). \quad (5.17)$$

5.2.2 Anti-Hard-Collinear Region

The same occurs in the anti-hard-collinear region between the diagrams \mathcal{I}_{cq} and \mathcal{I}_{bc}

$$\begin{aligned} \mathcal{I}_{cq}^{\text{hc}} &= -\frac{\alpha_s c_{fi}}{4\pi} \left(\frac{\mu^2}{m_c^2} \right)^\epsilon \frac{\langle \mathcal{O}_{\text{EFT}} \rangle^{(0)}}{n_{-p_l}} \int \frac{d^d k}{(2\pi)^d} \left(\frac{n_{-p_c} + n_{-k}}{n_{-k}} \right) \\ &\times \frac{i(4\pi)^{2-\epsilon} e^{\epsilon\gamma_E} m_c^{2\epsilon}}{(k^2 + i\eta)(k^2 + 2p_c \cdot k + i\eta)} = -\mathcal{I}_{bc}^{\text{hc}}, \end{aligned} \quad (5.18)$$

with explicit result

$$\mathcal{I}_{cq}^{\text{hc}} = \frac{\alpha_s c_{fi}}{4\pi} \left(\frac{\mu^2}{m_c^2} \right)^\epsilon \frac{\langle \mathcal{O}_{\text{EFT}} \rangle^{(0)}}{n_{-p_l}} \left(\frac{1}{2\epsilon^2} + \frac{1}{\epsilon} + \frac{\pi^2}{24} + 2 \right). \quad (5.19)$$

5.2.3 Soft Region

Now we turn to the soft region present in \mathcal{I}_{cl} and \mathcal{I}_{ul} , where also in this case the cancellation happens at the integrand level

$$\mathcal{I}_{cl}^{\text{soft}} = -\frac{\alpha_s c_{fi}}{4\pi} \left(\frac{\mu^2}{n_{+p_l} n_{-p_l}} \right)^\epsilon \frac{\langle \mathcal{O}_{\text{EFT}} \rangle^{(0)}}{n_{-p_l}} \int \frac{d^d k}{(2\pi)^d} \left(1 + \frac{k_\perp}{p_{l\perp}} \right)$$

$$\frac{i(4\pi)^{2-\epsilon} e^{\epsilon\gamma_E} (n_+ p_l n_- p_l)^\epsilon}{(k^2 + i\eta)(k^2 + 2p_l \cdot k + i\eta)(n_+ k + i\eta)(n_- k + n_- p_l - i\eta)} = -\mathcal{I}_{ul}^{\text{soft}}, \quad (5.20)$$

where we used the equation of motion of the light massless anti-quark

$$\bar{v}(p_l) \not{p}_l = -\bar{v}(p_l) \left(n_+ p_l \frac{\not{p}_-}{2} + n_- p_l \frac{\not{p}_+}{2} \right), \quad (5.21)$$

to get $\langle \mathcal{O}_{\text{EFT}} \rangle^{(0)}$, and the notation $k_\perp/p_{l\perp}$ takes into account that the result of the loop integral with k'_\perp in the numerator will be proportional to $p'_{l\perp}$, and therefore it has been factored out and will cancel in the ratio. The result for the soft region reads

$$\mathcal{I}_{cl}^{\text{soft}} = -\frac{\alpha_s c_{fi}}{4\pi} \left(\frac{\mu^2}{n_+ p_l n_- p_l} \right)^\epsilon \frac{\langle \mathcal{O}_{\text{EFT}} \rangle^{(0)}}{n_- p_l} \left(\frac{1}{\epsilon^2} - \frac{5\pi^2}{12} \right). \quad (5.22)$$

5.2.4 Anti-Ultrasoft-Collinear Region

We are left with the computation of the anti-ultrasoft-collinear region. This is the only case where the cancellation does not happen so clearly at the integrand level, we get

$$\begin{aligned} \mathcal{I}_{cl}^{\text{usc}} &= -\frac{\alpha_s c_{fi}}{4\pi} \mu^{2\epsilon} \frac{\langle \mathcal{O}_{\text{EFT}} \rangle^{(0)}}{n_- p_l} \int \frac{d^d k}{(2\pi)^d} \frac{i(4\pi)^{2-\epsilon} e^{\epsilon\gamma_E} n_- p_c n_- p_l}{(k^2 + i\eta)(2k \cdot p_c + i\eta)(n_- k + n_- p_l - i\eta)(n_- k + i\eta)}, \\ \mathcal{I}_{cq}^{\text{usc}} &= -\frac{\alpha_s c_{fi}}{4\pi} \mu^{2\epsilon} \frac{\langle \mathcal{O}_{\text{EFT}} \rangle^{(0)}}{n_- p_l} \int \frac{d^d k}{(2\pi)^d} \frac{i(4\pi)^{2-\epsilon} e^{\epsilon\gamma_E} n_- p_c}{(k^2 + i\eta)(2k \cdot p_c + i\eta)(n_- k + n_- p_l - i\eta)}, \end{aligned} \quad (5.23)$$

however when summing the two integrals the denominator $n_- k + n_- p_l$ cancels with the numerator and we are left with a scaleless integral. Hence we find the explicit result

$$\mathcal{I}_{cl}^{\text{usc}} = \frac{\alpha_s c_{fi}}{4\pi} \left(\frac{\mu n_- p_c}{m_c (-n_- p_l + i\eta)} \right)^{2\epsilon} \frac{\langle \mathcal{O}_{\text{EFT}} \rangle^{(0)}}{n_- p_l} \left(\frac{1}{2\epsilon^2} + \frac{3\pi^2}{8} \right) = -\mathcal{I}_{cq}^{\text{usc}}. \quad (5.24)$$

To conclude, from the summary of the region analysis anticipated in (5.13) we can clearly see that after the hard matching the process is factorized as no non-perturbative modes connect the constituents of the D meson to the rest of the transition.

5.3 Factorization Formula for T and C Amplitudes

In view of the results of Section 5.2 we state the following parametrization of the T and C amplitudes, including the spectator scattering term encoded in S_{DL} , for $\bar{B} \rightarrow DL$ decays

$$\begin{aligned} \mathcal{A}(\bar{B} \rightarrow DL)|_T &= i \frac{G_F}{\sqrt{2}} V_{uq}^* V_{cb} f_L (m_B^2 - m_D^2) \left[F_0^{\bar{B}D}(m_L^2) a_1(DL) + \frac{f_B f_D}{m_B^2 - m_D^2} C_1 S_{DL} \right], \\ \mathcal{A}(\bar{B} \rightarrow DL)|_C &= i \frac{G_F}{\sqrt{2}} V_{uq}^* V_{cb} f_D (m_B^2 - m_L^2) \left[F_0^{\bar{B}L}(m_D^2) a_2(LD) + \frac{f_B f_L}{m_B^2 - m_L^2} \left(2C_2 - \frac{C_1}{N_c} \right) S_{DL} \right], \end{aligned} \quad (5.25)$$

where q depends on the quark decomposition of the light meson L and the $a_1(DL)$ and $a_2(LD)$ coefficients encode the process dependent QCD vertex corrections at the hard scale $\mu_b \sim \mathcal{O}(m_b)$. The form factor $F_0^{\bar{B}P}$ is defined in (2.132).

The factorization of the amplitudes, at leading power in λ_c , allows us to compute the a_i coefficients in terms of convolutions of perturbatively calculable hard-scattering kernels with QCD LCDAs. In particular we write

$$a_1(DL) = C_1 V_1 + C_2 V_2, \quad a_2(LD) = C_1 \tilde{V}_1 + C_2 \tilde{V}_2, \quad (5.26)$$

where V_i are vertex corrections explicitly defined as the convolution of the hard-scattering kernels T_i and \tilde{T}_i with the LCDA

$$V_i = \int_0^1 du T_i(u) \phi_L(u), \quad \tilde{V}_i = \int_0^1 du \tilde{T}_i(u) \phi_D(u). \quad (5.27)$$

The hard-scattering kernels arise from a matching where the scale m_b is integrated out, and therefore, at leading power, they do not depend on the charm mass in our power counting scheme. The results are hence the same as for the process $\bar{B} \rightarrow \pi\pi$, known at NNLO in QCD [94], where the colour-suppressed amplitude obeys indeed a factorization formula. The leading power charm mass effects in the C amplitude are then included in the D meson LCDA, and are perturbatively taken into account with a second matching, at the hard-collinear scale which is in fact exactly what we have treated in great detail in Chapter 3. In light of this, the leading charm mass corrections will be taken into account by simply employing for $\phi_D(u)$ the function described in Section 3.5.

The function S_{DL} denotes the formally power suppressed spectator scattering term. By computing the two relevant tree-level diagrams we obtain the known result [70]

$$S_{DL} = \pi \alpha_s(\mu_{\text{hc}}) \frac{C_F}{2N_c^2} \frac{m_B}{\lambda_B(\mu_{\text{hc}})} \int_0^1 du \frac{\phi_D(u)}{\bar{u}} \int_0^1 dv \frac{\phi_L(v)}{\bar{v}}. \quad (5.28)$$

The coupling constant in the spectator scattering corrections is evaluated at the hard-collinear scale μ_{hc} , while in the hard scattering kernels at the hard scale μ_b . For the HQET LCDA inverse moment $\lambda_B(\mu)$ we use LL evolution reported in Appendix A. The hard functions, at the one-loop order, for the full process are [94]

$$\begin{aligned} T_1(u) &= \frac{\alpha_s}{4\pi} T(u), & T_2(u) &= 1, \\ \tilde{T}_1(u) &= \frac{C_F}{N_c} + \frac{\alpha_s}{4\pi} \left(-\frac{T(u)}{N_c} - \frac{3C_F}{N_c} \right), & \tilde{T}_2(u) &= \frac{1}{N_c} + \frac{\alpha_s}{4\pi} 2T(u), \end{aligned} \quad (5.29)$$

with

$$\begin{aligned} T(u) &= \frac{C_F}{2N_c} \left\{ -6 \ln \frac{\mu^2}{m_b^2} + \ln^2 \bar{u} + 2 \ln u \ln \bar{u} - \ln^2 u + \left(3 - \frac{1}{\bar{u}} \right) \ln u \right. \\ &\quad \left. + \left(3 - \frac{2}{u} \right) \ln \bar{u} + 4\text{Li}_2(u) - \frac{\pi^2}{3} - 22 + i\pi [2 \ln \bar{u} - 2 \ln u - 3] \right\}. \end{aligned} \quad (5.30)$$

We also include the two loop contributions [94], for massless charm quark, but we do not report the lengthy expressions here.

Obviously, given the relatively large numerical value of our expansion parameter λ_c , it would be interesting to investigate the effect of higher order charm mass corrections. However a formal treatment of power corrections would bring up several technical problems, like endpoint divergences and large amount of new unknown non-perturbative inputs, which would bring us away from phenomenological applications. For this reason we leave to future studies a non-rigorous treatment of such corrections which could however give a hint on the numerical importance of such effects.

5.4 Phenomenology

In this section we finally compare our theoretical predictions to the experimental measurements from Table 5.1. Since the goal here is not to present a complete update on non-leptonic two-body \bar{B} decays, we only focus on processes mediated by the T and C amplitudes. We do not include in our phenomenological study the processes which receive contribution from the weak exchange topology as no factorization formula is known for them, and we would have to postulate a model to estimate such contributions, with rather conservative uncertainties [71]. Furthermore we also leave the extension of the analysis to \bar{B}_s decays to future studies.

We start by evaluating the $a_1(DL)$ and $a_2(LD)$ factorization coefficients from (5.26). The vertex corrections are

$$\begin{aligned}
a_1(D\pi) &= 1.008 + (0.022 + 0.009i)_{\alpha_s} + (0.024 + 0.027i)_{\alpha_s^2} = 1.055_{-0.011}^{+0.012} + i0.036_{-0.011}^{+0.021}, \\
a_1(D\bar{K}) &= 1.008 + (0.022 + 0.010i)_{\alpha_s} + (0.023 + 0.027i)_{\alpha_s^2} = 1.053_{-0.010}^{+0.010} + i0.037_{-0.012}^{+0.022}, \\
a_2(LD) &= 0.222 - (0.151 + 0.116i)_{\alpha_s} + (0.019 - 0.056i)_{\alpha_s^2} = 0.089_{-0.004}^{+0.024} - i(0.172_{-0.026}^{+0.040}),
\end{aligned} \tag{5.31}$$

where the $a_2(LD)$ coefficient for the C amplitude is independent on the light meson. The uncertainties are obtained by varying the scale between $\mu_b/2$ and $2\mu_b$, which dominate with respect to the uncertainty on $\alpha_s^{(5)}(m_Z)$ and on the Gegenbauer moments. We include up to two Gegenbauer moments for the light meson LCDAs and up to four for the D LCDA, with the values reported in Appendix A. In computing (5.31) we used the NNLO hard-scattering kernels for $m_c = 0$ [94]. However for the coefficient related to the colour-allowed topology, $a_1(DL)$, we can also evaluate the convolutions with the two-loop kernels including the available full charm mass dependence [95], resulting in

$$a_1(D\pi) = 1.062_{-0.014}^{+0.017} + i0.036_{-0.012}^{+0.022}, \quad a_1(D\bar{K}) = 1.061_{-0.013}^{+0.015} + i0.037_{-0.012}^{+0.023}, \tag{5.32}$$

showing that the impact of our approximation by considering $m_c \ll m_b$ is at the subpercent level. It is worth noticing that the real part of the one-loop corrections to $a_2(LD)$ largely cancel the tree level term in (5.31), predicting a much smaller amplitude with respect to the colour-allowed one. Also it is interesting to notice the large imaginary part in $a_2(LD)$.

Fixing the hard-collinear scale at $\mu_{\text{hc}} = 1.6 \text{ GeV}$, the spectator scattering function evaluates to

$$S_{D\pi} = 27_{-12}^{+25}, \quad S_{D\bar{K}} = 28_{-12}^{+26}, \quad S_{DK} = 26_{-11}^{+23}, \quad (5.33)$$

where the large uncertainty is given by the scale variation in α_s , λ_B and the LCDAs between 1 and 2 GeV, combined with the large uncertainty from $\lambda_B(1 \text{ GeV}) = 350 \pm 150 \text{ MeV}$. Notice in (5.33) the difference between a \bar{K} and a K in the final state, given by the opposite sign in the first Gegenbauer moment. The processes we consider involve however only \bar{K} mesons.

For later comparison with data we define the following dimensionless effective amplitudes

$$\begin{aligned} a_1^{\text{eff}}(\bar{B} \rightarrow D^+ K^-) &= \frac{\sqrt{2}}{iG_F V_{us}^* V_{cb}} \frac{\mathcal{A}(\bar{B} \rightarrow D^+ K^-)}{f_K(m_B^2 - m_D^2) F_0^{\bar{B}D}(m_K^2)}, \\ a_2^{\text{eff}}(\bar{B} \rightarrow D^0 \bar{K}^0) &= \frac{\sqrt{2}}{iG_F V_{us}^* V_{cb}} \frac{\mathcal{A}(\bar{B} \rightarrow D^0 \bar{K}^0)}{f_D(m_B^2 - m_K^2) F_0^{\bar{B}K}(m_D^2)}, \\ a^{\text{eff}}(B^- \rightarrow D^0 K^-) &= \frac{\sqrt{2}}{iG_F V_{us}^* V_{cb}} \frac{\mathcal{A}(B^- \rightarrow D^0 K^-)}{f_K(m_B^2 - m_D^2) F_0^{\bar{B}D}(m_K^2)}, \\ a^{\text{eff}}(B^- \rightarrow D^0 \pi^-) &= \frac{\sqrt{2}}{iG_F V_{ud}^* V_{cb}} \frac{\mathcal{A}(B^- \rightarrow D^0 \pi^-)}{f_\pi(m_B^2 - m_D^2) F_0^{\bar{B}D}(m_\pi^2)}, \end{aligned} \quad (5.34)$$

where a^{eff} depends on the sum of the T and C amplitudes, and we choose to normalize it by the prefactor of the T amplitude as it is the dominant one. The theoretical expressions predicted by the factorization approach for such amplitudes can be inferred from (5.25)

$$\begin{aligned} a_1^{\text{eff}}(\bar{B} \rightarrow D^+ K^-) &= a_1(DK) + s_1(DK), \\ a_2^{\text{eff}}(\bar{B} \rightarrow D^0 \bar{K}^0) &= a_2(KD) + s_2(KD), \\ a^{\text{eff}}(B^- \rightarrow D^0 L^-) &= a_1(DL) + s_1(DL) + r_L \left(a_2(LD) + s_2(LD) \right), \end{aligned} \quad (5.35)$$

with the spectator scattering functions

$$s_1(DL) = C_1 \frac{f_B f_D S_{DL}}{(m_B^2 - m_D^2) F_0^{\bar{B}D}(m_L^2)}, \quad s_2(LD) = \left(2C_2 - \frac{C_1}{N_c} \right) \frac{f_B f_L S_{DL}}{(m_B^2 - m_L^2) F_0^{\bar{B}L}(m_D^2)}, \quad (5.36)$$

and the ratio

$$r_L = \frac{f_D(m_B^2 - m_L^2) F_0^{\bar{B}L}(m_D^2)}{f_L(m_B^2 - m_D^2) F_0^{\bar{B}D}(m_L^2)}. \quad (5.37)$$

Using the values of the form factors reported in Appendix A [96] we get

$$a_1^{\text{eff}}(\bar{B} \rightarrow D^+ K^-) = (1.053_{-0.010}^{+0.010} + i0.037_{-0.012}^{+0.022})_a - (0.018_{-0.008}^{+0.016})_s,$$

$$a_2^{\text{eff}}(\bar{B} \rightarrow D^0 \bar{K}^0) = (0.089_{-0.004}^{+0.024} - i(0.172_{-0.026}^{+0.040}))_a + (0.18_{-0.08}^{+0.16})_s, \quad (5.38)$$

where the subscripts a and s stand for the vertex and spectator terms respectively. Interestingly the spectator scattering term is only a 2% correction to the vertex term in the T amplitude, while in the C amplitude it is more than two times larger than the real part of the vertex term itself. This is of course due to the difference in $a_1(DL)$ and $a_2(LD)$, the different values of the form factors, as well as the different coefficients in front of S_{DL} , which all point in the same direction. For the mixed amplitudes a^{eff} we notice that the ratios multiplying the terms from the C amplitudes take the values

$$r_K = 0.82 \pm 0.07, \quad r_\pi = 0.60 \pm 0.06, \quad (5.39)$$

while the spectator terms for the final state with the pion give

$$s_1(D\pi) = -(0.017_{-0.007}^{+0.015}), \quad s_2(\pi D) = 0.23_{-0.10}^{+0.21}. \quad (5.40)$$

5.4.1 D Meson LCDA Model Dependence

So far we have treated the Gegenbauer moments of the D meson LCDA at the input scale $\mu_c = \mu_{\text{hc}}$ as fixed inputs. As seen from the analyses in Chapter 3 and 4, the model dependence of the D LCDA will likely be the biggest source of uncertainty and we hence decided to treat it separately from the other sources. We compute the first 10 Gegenbauer moments of the QCD LCDA for a D meson obtained from the matching to HQET described in Chapter 3 by simultaneously varying the following parameters

$$\begin{aligned} \text{HQET model} &= \{\text{I, II, III}\}, \\ \beta &= \{\beta_{\text{low}}, (\beta_{\text{low}} + \beta_{\text{high}})/2, \beta_{\text{high}}\}, \\ \lambda_B(\mu_s) &= \{200 \text{ MeV}, 350 \text{ MeV}, 500 \text{ MeV}\}, \\ \delta(D) &= \{0.5525, 0.65, 0.7475\}, \\ \sigma(D) &= \{0.025, 0.05, 0.1\}, \end{aligned} \quad (5.41)$$

where $\beta_{\text{low}}, \beta_{\text{high}}$ are respectively the lower and higher values that the parameter β can assume in a given model for the HQET LCDA. The larger impact on the peak is due obviously to the variation of λ_B , but also to the variation of the model parameter β as one can see from Figure 3.3. As a result, after evolving to the hard scale μ_b , we get 243 D meson LCDA models which we display in Figure 5.2. The curves are coloured according to the value of their first Gegenbauer moment $a_1^D(\mu_b)$.

5.4.2 Comparison with Data

We can finally compare our theoretical predictions with the effective amplitudes extracted from data. Neglecting CP violation, the CP-averaged branching ratios are obtained from

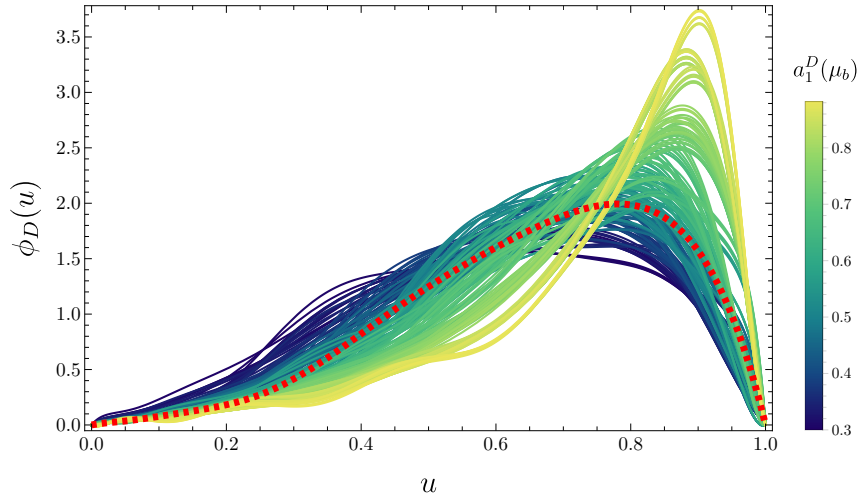


Figure 5.2: Plot of the 243 models for the D LCDA at the hard scale μ_b , coloured according to the value of their first Gegenbauer moment. In dashed red we display our default model.

the amplitude squared as

$$\mathcal{B}(\bar{B} \rightarrow DL) = \frac{\tau_B}{16\pi m_B} \sqrt{1 - \frac{(m_D - m_L)^2}{m_B^2}} \sqrt{1 - \frac{(m_D + m_L)^2}{m_B^2}} |\mathcal{A}(\bar{B} \rightarrow DL)|^2, \quad (5.42)$$

therefore, including the rest of the inputs (see Appendix A), we are able to give a theoretical prediction for the absolute values of the effective amplitudes defined in (5.34)

$$\begin{aligned} |a_1^{\text{eff}}(\bar{B} \rightarrow D^+ K^-)|_{\text{exp}} &= 0.82 \pm 0.04, \\ |a_2^{\text{eff}}(\bar{B} \rightarrow D^0 \bar{K}^0)|_{\text{exp}} &= 0.52 \pm 0.05, \\ |a^{\text{eff}}(B^- \rightarrow D^0 K^-)|_{\text{exp}} &= 1.09 \pm 0.05, \\ |a^{\text{eff}}(B^- \rightarrow D^0 \pi^-)|_{\text{exp}} &= 1.07 \pm 0.05. \end{aligned} \quad (5.43)$$

We display the comparison of the theoretical predictions with the experimental values (5.43) in Figure 5.3. These results confirm the tension in the purely T channel, as to be expected from recent years anomalies in non-leptonic two-body B decays [16]. However keeping in mind that power corrections are unknown, and not included in the theory uncertainty budget, a negative shift of order $\mathcal{O}(15\%)$ in the real part of a_1 does not seem unreasonable. On the other hand the prediction for a_2^{eff} seems more consistent with the data, and within the big theoretical uncertainties does not present any new puzzle. By looking at the lower panels, in which the mixed amplitudes a^{eff} are displayed, we see that the inclusion of the C amplitude decreases the tension with the data. However they show a consistent picture as a negative shift in a_1 would improve the agreement between measurements and predictions.

This analysis is far from being enough to draw any conclusion, and we postpone a more detailed treatment to a future work. Nevertheless we were able to show that a theoretical prediction for the colour-suppressed amplitudes is in principle possible, and that the spectator scattering term (formally a power correction) plays a crucial role. This simple analysis hence shows once again that a precise determination of the HQET LCDA inverse moment is mandatory, and that a lattice determination of the D meson QCD LCDA Gegenbauer moments would be of great interest.

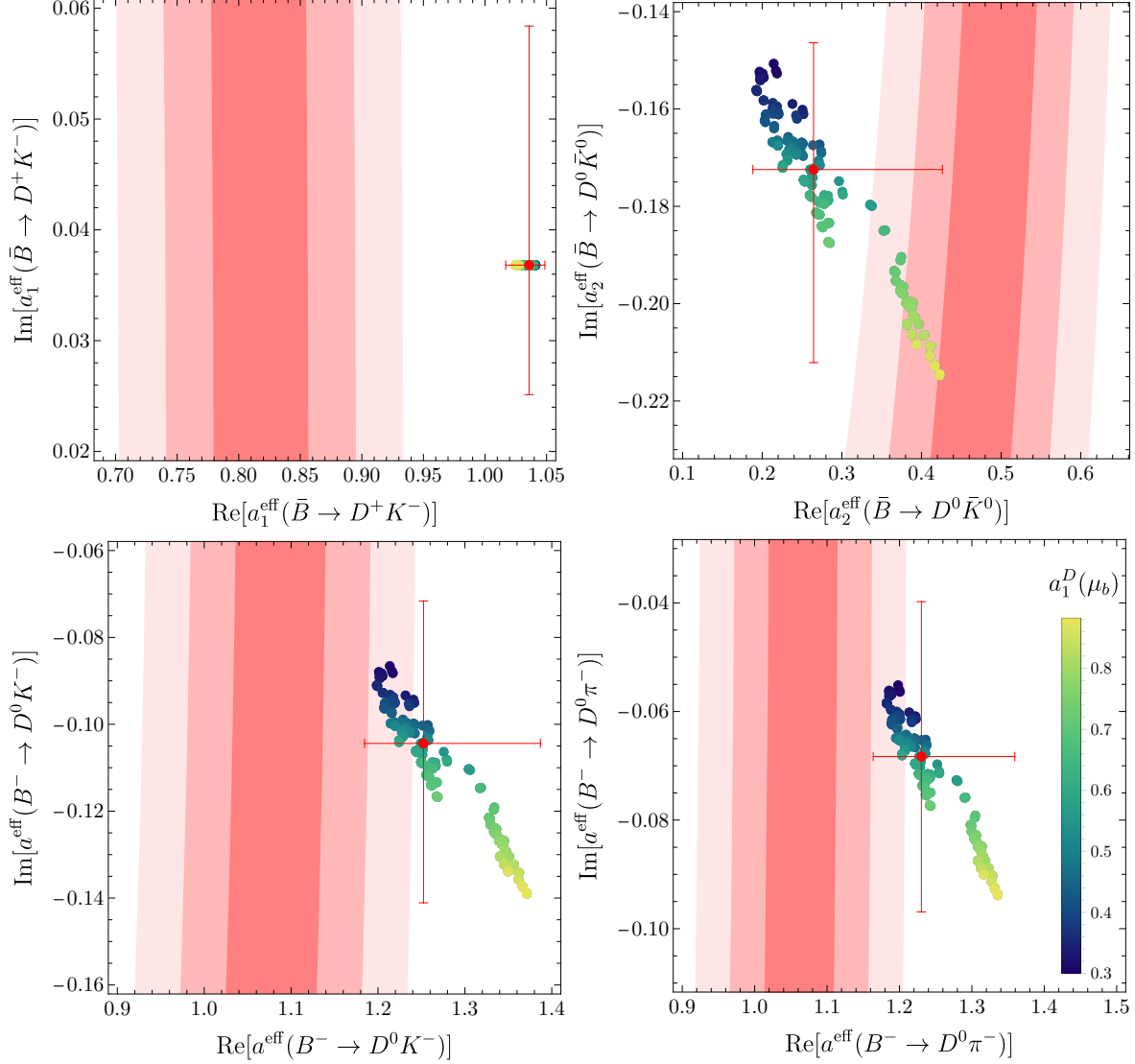


Figure 5.3: Comparison of effective amplitudes in the complex plane with the experimental bounds obtained from the absolute values (5.43). The three red bands with decreasing intensity stand for the 1σ , 2σ and 3σ regions of the experimental results respectively. The red dots with the uncertainty lines stand for the factorization predictions with the default model of the D LCDA. The coloured dots from blue to yellow stand for the factorization predictions with the D LCDA models ordered for increasing $a_1^D(\mu_b)$.

Part III

QED Corrections in B Decays

Chapter 6

QED \times QCD Factorization in $\bar{B} \rightarrow D^{(*)}L$

As the experimental measurements at LHCb and B -factories get more and more precise, it is natural, from the theoretical point of view, to start studying in more detail QED corrections to the well established QCD factorization approach in exclusive B decays. In this chapter we extend the factorization formula (2.131) for $\bar{B} \rightarrow D^{(*)}L$ decays to include QED effects, also motivated by the persisting anomalies in these channels [16, 23].

This work is part of an increasing series of papers on “structure-dependent” QED corrections to exclusive \bar{B} decays [29, 83, 87, 97–100] (for a recent review see Ref. [101]). By structure-dependent corrections we refer to virtual photon exchanges with energies of order $\mathcal{O}(m_B)$ which are able to resolve the parton structure of the hadrons. These QED corrections give rise to qualitatively new effects with respect to QCD as hadrons are neutral under the strong interaction, but can be in general electrically charged. Moreover isospin symmetry is broken in QED due to the quarks different electric charges. In particular for purely leptonic decays, while the QCD effects are all encoded in B meson LCDAs, the QED corrections present a very rich hierarchy of scales [100], and in the case of $B_{s,d} \rightarrow \mu^+\mu^-$ even generate power-enhanced one-loop corrections [97, 98].

Even though two-body non-leptonic decays in QCD are much more complicated than the purely leptonic ones, the hard-scattering kernels in QCDF are known up to $\mathcal{O}(\alpha_s^2)$ [94, 95]. One might hence wonder if one-loop QED corrections could numerically compete with the known two-loop QCD ones, motivating the study of QED \times QCD factorization formulae.

When QED is considered, the amplitudes and the branching ratios become infrared divergent, destroying the concept of purely exclusive processes. Instead one has to consider the infrared-finite soft-photon-inclusive decay $\bar{B} \rightarrow D^{(*)}L + X_s$, where X_s is an arbitrary number of undetected photons and electron-positron pairs. In order to state a factorization theorem we set the threshold $\Delta E \ll \Lambda_{\text{QCD}}$ on the total energy of photons in the final state, such that QED corrections at scales above ΔE are purely virtual. In this chapter we focus on the so-called “non-radiative” amplitude, while in Chapter 7 we will deal with “ultrasoft”¹ real radiations of energies $\mathcal{O}(\Delta E)$.

¹We call as ultrasoft the momenta with virtualities equal or smaller than ΔE^2 , opposed to soft modes whose virtuality is $\Lambda_{\text{QCD}}^2 \gg \Delta E^2$.

6.1 Factorization Formula

We focus on the decays $\bar{B}_{(s)} \rightarrow D_{(s)}^{(*)+} L^-$, with $L^- = \{\pi^-, K^-\}$, as they are mostly mediated by colour-allowed tree topologies, as explained at the beginning of Chapter 5. At the parton level, the decay is mediated by the effective Hamiltonian introduced in (2.1), describing the weak transition $b \rightarrow c\bar{u}q$. The QED \times QCD factorization formula for the matrix elements of the effective operators (2.2) retain the same form as in QCD

$$\langle D^+ L^- | Q_i | \bar{B} \rangle = i f_L 4 E_D E_L \zeta_{Q_L}^{BD}(m_L^2) \int_0^1 du H_{i,Q_L}(u, z) \Phi_L(u), \quad (6.1)$$

where we choose the normalization with the kinematic factors

$$E_D = \frac{m_B^2 + m_D^2 - m_L^2}{2m_B}, \quad E_L = \frac{m_B^2 + m_L^2 - m_D^2}{2m_B}, \quad (6.2)$$

which are the D and L meson energies in the \bar{B} rest frame respectively. The form of the factorization formula (6.1) is the same as (2.131), but now the heavy-to-heavy form factor $\zeta_{Q_L}^{BD}$, the light meson LCDA Φ_L and the hard-scattering kernels H_{i,Q_L} are generalized to include long- and short-distance virtual photon corrections. They now depend on the electric charge $Q_L = -1$ of the light meson, but as we consider only the negatively charged light meson case, we will omit the subscript from now on. We have therefore divided the virtual QED corrections to the non-radiative amplitude in three sources. By construction and convention, we included the QED corrections to the QCD decay constant f_L in the light meson LCDA. The properties of the QED generalized LCDA Φ_L have been studied in detail in Ref. [83]. Hard-photon exchanges are encoded in $H_i(u, z)$, where $z \equiv m_c^2/m_b^2 \sim \mathcal{O}(1)$ will capture the dependence on the charm mass. Terms of order $\mathcal{O}(\alpha_{em})$ in H_i can be perturbatively computed through a matching computation and will be the topic of Section 6.1.3. The form factor ζ^{BD} for the $\bar{B} \rightarrow D$ transition is the trickiest term, as it now knows about the electric charge of the light meson flying away, as opposed to the universal QCD form factors. It is defined in HQET so that it is a single-scale purely non-perturbative object. In QCD factorization it is often replaced by the physical QCD form factor, which includes some of the so-called ‘‘factorizable’’ hard contributions, but allows for an easier determination from data or lattice QCD. With a similar intention we will replace the unknown object ζ^{BD} with a physical form factor extracted from the semi-leptonic decay $\bar{B} \rightarrow D^+ \ell^- \bar{\nu}_\ell$. We postpone this discussion to Section 6.2.2. With appropriate modifications, the factorization formula (6.1) also holds for $\bar{B} \rightarrow D^* L$ and $\Lambda_b \rightarrow \Lambda_c^+ L^-$, as in pure QCD.

6.1.1 Matching Equation

The goal of this section is to compute the one-loop hard-scattering kernels $H_i(u, z)$ in QED, for the factorization formula (6.1). We will perform a one-loop matching QED \times QCD \rightarrow HQET \times SCET_I by integrating out simultaneously the bottom and charm masses. This

means that, recalling the definition (2.81) for λ_h , throughout this section we will use the power counting $\lambda_b \sim \lambda_c \ll 1$.

As we are considering pure QED, i.e. neglecting $\mathcal{O}(\alpha_s \alpha_{\text{em}})$ terms, the colour-octet operator Q_1 is not relevant since [71]

$$\langle D^{(*)+} L^- | Q_1 | \bar{B} \rangle = \mathcal{O}(\alpha_s), \quad (6.3)$$

to all orders in QED, because the L^- meson is a colour singlet. At one-loop in QED the local WET operator Q_2 matches into the colour-singlet HQET \times SCET_I non-local operator basis

$$\tilde{\mathcal{O}}_{\mp}(t) = [\bar{\chi}^{(q)}(tn_-) \frac{\not{n}_-}{2} (1 - \gamma^5) \chi^{(u)}(0)] [\bar{h}_{v'}(0) \not{n}_+ (1 \mp \gamma^5) S_{n_+}^{\dagger(Q_L)}(0) h_v(0)], \quad (6.4)$$

where the flavour superscript on the SCET anti-hard-collinear fields² $\chi^{(q)}$ and $\chi^{(u)}$ is important as they carry different electric charges, $Q_d = -1/3$ and $Q_u = 2/3$, respectively. The anti-collinear direction is denoted with n_+ , as usual. The HQET fields for the charm and bottom quarks have velocities v' and v , and also carry different electric charges, Q_u and Q_d . The soft QED Wilson line in the n_+ direction comes from the soft-decoupling of the constituent quarks of the light meson (see Section 2.5). While the QCD part of the Wilson lines from the redefinition (2.119) cancels out, the QED part remains as

$$S_{n_+}^{(Q_L)}(x) = \exp \left\{ -i Q_L e \int_0^\infty ds n_+ A_s(x + sn_+) \right\}. \quad (6.5)$$

due to the charge difference of the quarks, which gives an overall non-neutral meson. Notice that the two currents in the operator are completely factorized as the anti-hard-collinear fields are decoupled from soft photons.

At one loop, when using dimensional regularization, one also needs to consider evanescent operators, namely operators which vanish only in four dimensions [102]. The tree level matrix elements of such operators are therefore $\mathcal{O}(\epsilon)$ corrections, but if multiplied by $1/\epsilon$ poles from the one-loop bare amplitude they contribute to finite constant terms in the matching (see e.g. Ref. [102]). At the one-loop level in the WET there are two evanescent operators

$$\begin{aligned} E_1 &= [\bar{c} \gamma^\mu \gamma^\nu \gamma^\rho (1 - \gamma^5) T^{ab}] [\bar{q} \gamma_\mu \gamma_\nu \gamma_\rho (1 - \gamma^5) T^{ab} u] - 16 Q_1, \\ E_2 &= [\bar{c} \gamma^\mu \gamma^\nu \gamma^\rho (1 - \gamma^5) b] [\bar{q} \gamma_\mu \gamma_\nu \gamma_\rho (1 - \gamma^5) u] - 16 Q_2, \end{aligned} \quad (6.6)$$

to be added to the physical basis (2.2). In the EFT there are also two evanescent operators

$$\begin{aligned} \tilde{\mathcal{O}}_{E-}(t) &= [\bar{\chi}^{(q)}(tn_-) \frac{\not{n}_-}{2} (1 - \gamma^5) \gamma_\perp^\mu \gamma_\perp^\nu \chi^{(u)}(0)] [\bar{h}_{v'}(0) \not{n}_+ (1 - \gamma^5) \gamma_{\perp\nu} \gamma_{\perp\mu} S_{n_+}^{\dagger(Q_L)}(0) h_v(0)], \\ \tilde{\mathcal{O}}_{E+}(t) &= [\bar{\chi}^{(q)}(tn_-) \frac{\not{n}_-}{2} (1 - \gamma^5) \gamma_\perp^\mu \gamma_\perp^\nu \chi^{(u)}(0)] [\bar{h}_{v'}(0) \not{n}_+ (1 + \gamma^5) \gamma_{\perp\mu} \gamma_{\perp\nu} S_{n_+}^{\dagger(Q_L)}(0) h_v(0)], \end{aligned} \quad (6.7)$$

²We are omitting the subscript \bar{C} on the anti-hard-collinear fields as there are no hard-collinear fields in this chapter.

where the ordering of the γ_\perp is subtle but crucial. One way of dealing with evanescent operators is to renormalize them such that their on-shell matrix elements vanish. In this way the evanescent operators do not enter directly the matching equation, but only contribute through the mixing to constant terms in the hard-scattering kernels of physical operators. The procedure is equivalent to a specific renormalization scheme choice, and should become clearer in the following with the explicit calculation.

The matching equation, in momentum space, takes the form

$$Q_2 = \int_0^1 du H_a(u) \mathcal{O}_a(u), \quad (6.8)$$

where we introduced the EFT operators in momentum space, similarly to (3.27)

$$\mathcal{O}_a(u) = \int \frac{d\hat{t}}{2\pi} e^{-i u \hat{t}} \tilde{\mathcal{O}}_a(t), \quad (6.9)$$

with the dimensionless variable³ $\hat{t} = n_- p_L t$. The index a runs in principle over all the operators in the effective theory $\{\mathcal{O}_-, \mathcal{O}_+, \mathcal{O}_{E-}, \mathcal{O}_{E+}\}$ and H_a are the respective momentum-space matching functions. As previously stated, the evanescent operators are renormalized such that they don't enter the matching equation directly, which means that their matching functions will vanish, effectively restricting the sum over physical operators only.

The renormalization of Q_2 in QED, including mixing, reads⁴

$$Q_2 = Z_{2j} Q_j^{\text{bare}} = \left(\delta_{2j} + \frac{\alpha_{\text{em}}}{4\pi} Z_{2j}^{(1)} + \mathcal{O}(\alpha_{\text{em}}^2) \right) Q_j^{\text{bare}}, \quad (6.10)$$

with the index j labelling the operators $\{Q_1, Q_2, E_1, E_2\}$, and [99]

$$Z_{ij}^{(1)} = \frac{1}{\epsilon} \begin{pmatrix} 6Q_u Q_d & 0 & \frac{1}{4}(Q_u + Q_d)^2 & 0 \\ 0 & 6Q_u Q_d & 0 & \frac{1}{4}(Q_u + Q_d)^2 \end{pmatrix}_{ij}. \quad (6.11)$$

The renormalization of the EFT non-local operators takes the form of a convolution

$$\mathcal{O}_a(u) = \int_0^1 du' Y_{ab}(u, u') \mathcal{O}_b^{\text{bare}}(u'), \quad (6.12)$$

with $Y_{ab}(u, u')$ being the momentum-space renormalization kernels in the EFT, whose perturbative expansion reads

$$Y_{ab}(u, u') = \delta_{ab} \delta(u - u') + \frac{\alpha_{\text{em}}}{4\pi} Y_{ab}^{(1)}(u, u') + \mathcal{O}(\alpha_{\text{em}}^2). \quad (6.13)$$

To extract the hard-scattering kernels, i.e. the matching functions, we can take the partonic renormalized on-shell matrix element of the matching equation (6.8). To this end

³Again p_L here stands for the L^- meson momentum once the hadronic matrix element is taken, or the sum of the momenta of the constituent quarks of L^- in the partonic matching.

⁴Throughout this chapter we indicate with the superscript (i) the coefficients of perturbative expansions in powers of $\alpha_{\text{em}}/(4\pi)$.

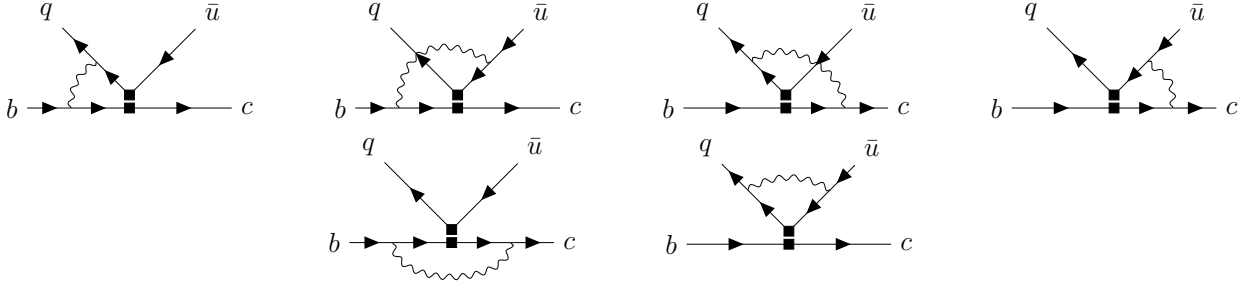


Figure 6.1: One loop diagrams in QED contributing to the matching of the local operator Q_2 , denoted with two square dots.

we define the short-hand notation $\langle c(p_c)\bar{u}(p_{\bar{u}})q(p_q)|\bullet|b(p_b)\rangle \equiv \langle \bullet \rangle$, with $p_q^2 = p_{\bar{u}}^2 = p_q \cdot p_{\bar{u}} = 0$, $p_c^2 = m_c^2$ and $p_b^2 = m_b^2$. At the parton level there are four independent spinor structures contributing at one loop

$$\begin{aligned}
\mathcal{S}_- &= [\bar{u}_q(p_q)\frac{\not{h}_-}{2}(1-\gamma^5)v_{\bar{u}}(p_{\bar{u}})][\bar{u}_c(p_c)\not{h}_+(1-\gamma^5)u_b(p_b)], \\
\mathcal{S}_+ &= [\bar{u}_q(p_q)\frac{\not{h}_-}{2}(1-\gamma^5)v_{\bar{u}}(p_{\bar{u}})][\bar{u}_c(p_c)\not{h}_+(1+\gamma^5)u_b(p_b)], \\
\mathcal{S}_{E-} &= [\bar{u}_q(p_q)\frac{\not{h}_-}{2}(1-\gamma^5)\gamma_{\perp}^{\mu}\gamma_{\perp}^{\nu}v_{\bar{u}}(p_{\bar{u}})][\bar{u}_c(p_c)\not{h}_+(1-\gamma^5)\gamma_{\perp\nu}\gamma_{\perp\mu}u_b(p_b)], \\
\mathcal{S}_{E+} &= [\bar{u}_q(p_q)\frac{\not{h}_-}{2}(1-\gamma^5)\gamma_{\perp}^{\mu}\gamma_{\perp}^{\nu}v_{\bar{u}}(p_{\bar{u}})][\bar{u}_c(p_c)\not{h}_+(1+\gamma^5)\gamma_{\perp\nu}\gamma_{\perp\mu}u_b(p_b)].
\end{aligned} \tag{6.14}$$

The on-shell renormalized partonic matrix element of Q_2 can be expressed as

$$\langle Q_2 \rangle = Z_{\text{ext}} Z_{2j} M_{jb} \mathcal{S}_b, \tag{6.15}$$

where M_{jb} are the bare amplitudes multiplying the structures (6.14), and Z_{ext} accounts for the QED on-shell external field renormalization constants

$$Z_{\text{ext}} \equiv \sqrt{Z_b^{OS} Z_c^{OS}} = 1 - \frac{\alpha_{\text{em}}}{4\pi} \left[Q_d^2 \left(\frac{3}{2\epsilon} + \frac{3}{2} \ln \frac{\mu^2}{m_b^2} + 2 \right) + Q_u^2 \left(\frac{3}{2\epsilon} + \frac{3}{2} \ln \frac{\mu^2}{m_c^2} + 2 \right) \right] + \mathcal{O}(\alpha_{\text{em}}^2). \tag{6.16}$$

The matrix elements in the EFT instead can be written as

$$\langle \mathcal{O}_a(u) \rangle = \int_0^1 du' Y_{ab}(u, u') N_{bc}(u') \mathcal{S}_c, \tag{6.17}$$

where $N_{bc}(u')$ parametrizes the coefficients of the structures (6.14) in the bare amplitudes in the EFT. The external field on-shell renormalization constants are unity as all the fields are massless, and therefore not included in (6.17). Moreover, as the two currents in the EFT operators are decoupled, the bare amplitudes are scaleless in dimensional regularization, therefore only the tree level survives

$$N_{bc}(u') = \delta_{bc} \delta\left(u' - \frac{n-p_q}{n-p_L}\right). \tag{6.18}$$

Using the perturbative expansions of the matrix elements (6.15) and (6.17), together with (6.13) and (6.18), we get from solving iteratively the matching equation (6.8) the following master formula

$$\begin{aligned}
H_a^{(0)}\left(\frac{n-p_q}{n-p_L}\right) &= M_{2a}^{(0)}, \\
H_a^{(1)}\left(\frac{n-p_q}{n-p_L}\right) &= M_{2a}^{(1)} + Z_{\text{ext}}^{(1)}M_{2a}^{(0)} + Z_{2j}^{(1)}M_{ja}^{(0)} - \int_0^1 du M_{2b}^{(0)}Y_{ba}^{(1)}\left(u, \frac{n-p_q}{n-p_L}\right), \quad (6.19)
\end{aligned}$$

where the one-loop amplitude $M_{2a}^{(1)}$ depends on the external momenta of the partons, while the tree level amplitudes are constant and can be written in matricial form

$$M_{ja}^{(0)} = \begin{pmatrix} 0 & 0 & 0 & 0 \\ 1 & 0 & 0 & 0 \\ 0 & 0 & 0 & 0 \\ -12\epsilon & 0 & -3 & 0 \end{pmatrix}_{ja}, \quad (6.20)$$

from which we can already extract the tree-level matching coefficients

$$H_-^{(0)} = 1, \quad H_+^{(0)} = 0, \quad H_{E-}^{(0)} = 0, \quad H_{E+}^{(0)} = 0. \quad (6.21)$$

The one-loop bare amplitude is obtained from the sum of the six diagrams of Figure 6.1, of which individual results are reported in Appendix C.1. In the next section we study the EFT renormalization kernels which are the last ingredient for the determination of the hard-scattering kernels.

6.1.2 SCET×HQET Renormalization Kernels

From (6.19) and (6.20) we notice that we only need to determine the EFT renormalization functions $Y_{-a}^{(1)}(u, w)$. The variable w represents the external light-cone momentum fraction

$$n_{-p_q} = wn_{-p_L} = wm_b(1-z), \quad n_{-p_{\bar{u}}} = \bar{w}n_{-p_L} = \bar{w}m_b(1-z). \quad (6.22)$$

The EFT operator \mathcal{O}_- is factorized into two independent currents, therefore the renormalization kernels are also factorized, which in the perturbative expansion at NLO translates into the sum

$$Y_{-a}^{(1)}(u, w) = \delta_{-a}\delta(u-w)Z_{hh}^{(1)} + \delta_{-a}Z_{\bar{c}}^{(1)}(u, w). \quad (6.23)$$

We furthermore observed that the renormalization of \mathcal{O}_- is diagonal in the operator basis, because the HQET interaction vertex Feynman rule does not contain γ matrices. The renormalization of the non-local anti-collinear current is given by [83, 99]

$$Z_{\bar{c}}^{(1)}(u, w) = -\frac{2Q_L}{\epsilon}\delta(u-w)\left(\frac{Q_L}{\epsilon} + \frac{3}{4}Q_L + Q_d \ln \frac{\mu^2}{-k_q^2} - Q_u \ln \frac{\mu^2}{-k_{\bar{u}}^2}\right)$$

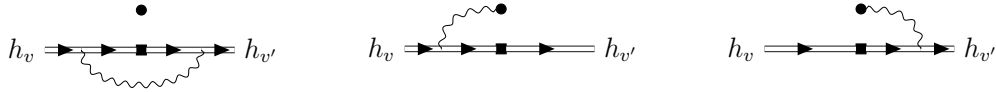


Figure 6.2: Diagrams for the one-loop QED renormalization of the heavy-to-heavy current. The round dot represents the soft Wilson line $S_{n_+}^{\dagger(Q_L)}$.

$$- \frac{2Q_d Q_u}{\epsilon} \left[\theta(w-u) \frac{u}{w} \left(1 + \frac{1}{w-u} \right) + \theta(u-w) \frac{\bar{u}}{\bar{w}} \left(1 + \frac{1}{u-w} \right) \right]_{u_+}, \quad (6.24)$$

where $Q_L = Q_d - Q_u$, and $k_q^2, k_{\bar{u}}^2$ are the off-shellnesses of the quarks regulating the IR divergences. The IR regulators will cancel with similar factors in $Z_{hh}^{(1)}$ as we will explicitly check later. This indicates that the full operator is well defined, but the two currents alone are ill-defined when QED is considered. We will come back to this point later in Section 6.1.4. We notice that by setting $Q_d = Q_u = 1$ one recovers the standard QCD ERLB renormalization kernel (B.11), as expected.

For the renormalization of the local heavy-to-heavy current $\bar{h}_{v'}(0) \not{h}_+(1-\gamma^5) S_{n_+}^{\dagger(Q_L)}(0) h_v(0)$, we need to extract the UV poles of the diagrams in Figure 6.2. We hence regulate the IR divergences by modifying the propagator of the Wilson line according to the prescription described in Appendix A of Ref. [98]

$$\frac{1}{n_+ k - i\eta} \rightarrow \frac{1}{n_+ k - \delta_{\bar{c}} - i\eta}, \quad (6.25)$$

with the condition $\delta_{\bar{c}} = k_q^2/n_- p_q = k_{\bar{u}}^2/n_- p_{\bar{u}}$, which imposes a relation between the IR regulators. This condition is necessary for the relation between regularized Wilson lines $S_{n_+}^{\dagger(q)} S_{n_+}^{(u)} = S_{n_+}^{\dagger(Q_L)}$ to hold. Results for the individual diagrams are reported in Appendix C.1 and, including the $\overline{\text{MS}}$ field renormalization constants from the HQET fields, we get

$$Z_{hh}^{(1)} = \frac{1}{\epsilon} \left\{ -Q_d^2 \left(\frac{1+z}{1-z} \ln z + 2 \right) + 2Q_L Q_d \left(\frac{\ln z}{1-z} + i\pi + 1 \right) + Q_L^2 \left(\frac{1}{\epsilon} + \ln \frac{\mu^2}{z \delta_{\bar{c}}^2} - 1 \right) \right\}. \quad (6.26)$$

As required, when setting the charges to unity in (6.26) we recover the QCD result (up to a factor C_F), see for example (39) in Ref. [95]. As anticipated, adding (6.24) and (6.26) according to (6.23) the IR regulators drop, yielding a well defined renormalization kernel for the EFT operator \mathcal{O}_- . Moreover, the master formula (6.19) at one loop only contains the integrated renormalization kernel $\int_0^1 du Y_{--}^{(1)}(u, w)$, therefore the plus-distribution term in (6.24) simply vanish. We get

$$\int_0^1 du Y_{--}^{(1)}(u, w) = - \frac{Q_d^2}{\epsilon} \left(\frac{1+z}{1-z} \ln z + 2 \right) + \frac{2Q_d Q_L}{\epsilon} \left(\ln \frac{w}{\bar{w}} + \frac{\ln z}{1-z} + i\pi + 1 \right) - \frac{Q_L^2}{\epsilon} \left(\frac{1}{\epsilon} + \ln \frac{\mu^2}{m_b^2} - 2 \ln \bar{w} - 2 \ln(1-z) + \ln z + 2\pi i + \frac{5}{2} \right). \quad (6.27)$$

6.1.3 Hard-Scattering Kernels

We finally have all the ingredients for extracting the one-loop hard-scattering kernels from (6.19). To start we check that the matching functions relative to evanescent operators vanish, that is

$$H_{E\mp}^{(1)}(w) = M_{2E\mp}^{(1)} + Z_{24}^{(1)} M_{4E\mp}^{(0)} = \begin{cases} \frac{3}{4\epsilon}(Q_u + Q_d)^2 + \frac{1}{4\epsilon}(Q_u + Q_d)^2(-3) = 0, \\ 0 + 0 = 0, \end{cases} \quad (6.28)$$

as we expected.

For the physical hard-scattering kernels we can see analytically the cancellation of the poles, leaving IR and UV finite matching functions

$$\begin{aligned} H_-^{(1)}(u) = & -Q_d^2 \left\{ \frac{L_b^2}{2} + L_b \left(\frac{5}{2} - 2 \ln(u(1-z)) \right) + h_-(u(1-z)) + \frac{\pi^2}{12} + 7 \right\} \\ & - Q_u^2 \left\{ \frac{L_c^2}{2} + L_c \left(\frac{5}{2} + 2\pi i - 2 \ln\left(\bar{u} \frac{1-z}{z}\right) \right) + h_-\left(\bar{u} \left(1 - \frac{1}{z}\right)\right) + \frac{\pi^2}{12} + 7 \right\} \\ & + Q_d Q_u \left\{ \frac{L_b^2}{2} + \frac{L_c^2}{2} - 6L_\nu + 2L_b \left(2 - \ln(\bar{u}(1-z)) \right) \right. \\ & \left. - 2L_c \left(1 - i\pi + \ln\left(u \frac{1-z}{z}\right) \right) + g(\bar{u}(1-z)) + g\left(u \left(1 - \frac{1}{z}\right)\right) + \frac{\pi^2}{6} - 12 \right\} \\ & + Q_d Q_u f(z), \\ H_+^{(1)}(u) = & -Q_d^2 \sqrt{z} h_+(u(1-z)) - Q_u^2 \frac{1}{\sqrt{z}} h_+\left(\bar{u} \left(1 - \frac{1}{z}\right)\right) - Q_d Q_u \sqrt{z} \frac{\ln z}{1-z}, \end{aligned} \quad (6.29)$$

containing the logarithms

$$L_b = \ln \frac{\mu^2}{m_b^2}, \quad L_c = \ln \frac{\mu^2}{m_c^2} = L_b - \ln z, \quad L_\nu = \ln \frac{\nu^2}{m_b^2}, \quad (6.30)$$

where ν refers to the UV scale of the WET Wilson coefficient $C_2(\nu)$, while μ is the factorization scale. In addition, we defined the functions

$$\begin{aligned} h_-(x) &\equiv \ln^2 x - 2 \ln x + \frac{x \ln x}{1-x} - 2\text{Li}_2\left(\frac{x-1}{x}\right), \\ g(x) &\equiv h_-(x) - \frac{3x \ln x}{1-x}, \\ f(z) &\equiv \left(1 - \frac{1+z}{1-z} \ln z\right) L_b + \frac{\ln z}{1-z} \left(\frac{1}{2}(1+z) \ln z - 2 - z\right), \\ h_+(x) &\equiv \frac{1-x+x \ln x}{(1-x)^2}. \end{aligned} \quad (6.31)$$

The variable z is understood as $z - i\eta$, such that the imaginary part of (6.29) are non-ambiguous. The contribution from the factorizable diagram where the photon is exchanged between the two heavy quarks is entirely encoded in $f(z)$. For the non-factorizable diagrams contributing to $H_-^{(1)}(u)$, we note the symmetry when exchanging the charm and bottom quarks, as they are both treated as heavy quarks. Practically this reflects in the first four lines of (6.29) being symmetric in the exchanges $\{m_b, Q_d, u\} \leftrightarrow \{m_c, Q_u, \bar{u}\}$.

The hard-scattering kernel $H_-^{(1)}$ in (6.29) diverges when taking the massless charm limit

$$H_-^{(1)}(z \rightarrow 0) = \frac{Q_u^2}{2} \left(\ln^2 z - (2L_b + 1) \ln z \right) + \text{finite terms}, \quad (6.32)$$

while $H_+^{(1)}$ vanish, as we expect since the chirally flipped operator arises from the presence of the charm mass. These collinear divergences will cancel when normalizing to the semi-leptonic decay as discussed in Section 6.2.2 (see also Ref. [99]).

6.1.4 Hadronic Matrix Elements

Now that we have a result for the hard-scattering kernels, we can finally take the hadronic matrix element of the matching equation (6.8) to obtain a factorization formula, previously stated in (6.1). This requires the introduction of the QED generalized LCDA for a light-meson [83, 99]

$$\langle L^-(p_L) | R_{\bar{c}}^{(Q_L)} \bar{\chi}^{(q)}(tn_-) \frac{\not{t}_-}{2} (1 - \gamma^5) \chi^{(u)}(0) | 0 \rangle = i f_L \frac{n_- p_L}{2} \int_0^1 du e^{iutn_- p_L} \Phi_L(u), \quad (6.33)$$

and the QED generalized HQET form factors

$$\begin{aligned} \langle D | \frac{1}{R_{\bar{c}}^{(Q_L)}} \bar{h}_{v'}(0) \not{t}_+ S_{n_+}^{\dagger(Q_L)}(0) h_v(0) | \bar{B} \rangle &= 4E_D \zeta_{Q_L}^{BD}, \\ -\langle D^* | \frac{1}{R_{\bar{c}}^{(Q_L)}} \bar{h}_{v'}(0) \not{t}_+ \gamma^5 S_{n_+}^{\dagger(Q_L)}(0) h_v(0) | \bar{B} \rangle &= 4E_{D^*} \varepsilon^* \cdot v \zeta_{Q_L}^{BD^*}, \end{aligned} \quad (6.34)$$

where we multiplied and divided by the soft-rearrangement factor [98, 99]

$$R_{\bar{c}}^{(Q_L)} = 1 - \frac{\alpha_{\text{em}}}{4\pi} Q_L^2 \left[\frac{1}{\epsilon^2} + \frac{2}{\epsilon} \ln \frac{\mu}{-\delta_{\bar{c}}} + \mathcal{O}(1) \right], \quad (6.35)$$

which ensures that the QED LCDA and form factors are well defined by removing the IR divergences in their renormalization functions (see Section 4.1 in Ref. [99]). We normalized by the energy $E_{D^{(*)}} = (m_B^2 + m_{D^{(*)}}^2 - m_L^2)/(2m_B)$, while ε^* is the D^* polarization vector. As anticipated in Section 6.1 the generalized form factor now depends on the charge of the light meson, and, as we study only the case of a negatively charged L^- , we will drop the subscript in the following. Parity invariance implies

$$\langle D | \bar{h}_{v'}(0) \not{t}_+ \gamma^5 S_{n_+}^{\dagger(Q_L)}(0) h_v(0) | \bar{B} \rangle = 0, \quad \langle D^* | \bar{h}_{v'}(0) \not{t}_+ S_{n_+}^{\dagger(Q_L)}(0) h_v(0) | \bar{B} \rangle = 0, \quad (6.36)$$

requiring a single form factor (one for $\bar{B} \rightarrow D$ and one for $\bar{B} \rightarrow D^*$) despite the presence of two operators \mathcal{O}_- and \mathcal{O}_+ . We can therefore write the factorization formula in a compact way by defining the total hard-scattering kernels $H \equiv H_- + H_+$ and $H^* \equiv H_- - H_+$. We get

$$\begin{aligned}\langle D^+ L^- | Q_2 | \bar{B} \rangle &= i f_L 4 E_L E_D \zeta^{BD} \int_0^1 du H(u, z) \Phi_L(u), \\ \langle D^{*+} L^- | Q_2 | \bar{B} \rangle &= i f_L 4 E_L E_{D^*} (\varepsilon^* \cdot v) \zeta^{BD^*} \int_0^1 du H^*(u, z) \Phi_L(u),\end{aligned}\quad (6.37)$$

where we identified $n_- p_L/2$ with $E_L = (m_B^2 + m_L^2 - m_{D^{(*)}}^2)/(2m_B)$, which is true up to $\mathcal{O}(m_L^2/m_B^2)$ corrections. The formula (6.37) also holds for longitudinally polarized light vector mesons ($L = \rho, K^*$), while decays to transversely polarized mesons are power suppressed.

6.2 Semi-Leptonic $\bar{B} \rightarrow D^{(*)+} \ell^- \bar{\nu}_\ell$ Decay

The factorization formulas (6.37) could be used to predict the amplitude of $\bar{B} \rightarrow D^{(*)+} L^-$ decays at order α_{em} up to power corrections $\mathcal{O}(\Lambda_{\text{QCD}}/m_b)$. However this would require to determine, with non-perturbative methods, the HQET generalized form factors. In QCD usually the EFT form factor is replaced with the better known full QCD one, which already contains part of the perturbative contributions, in particular those related to the factorizable diagram where the b and the c interact through a gluon. Since when including QED this is not possible anymore, we use the fact that an analogous factorization formula can be stated for the semi-leptonic $\bar{B} \rightarrow D^{(*)+} \ell^- \bar{\nu}_\ell$ decay, which contains the same HQET form factors $\zeta^{BD^{(*)}}$. The idea is therefore to eliminate $\zeta^{BD^{(*)}}$ in (6.37) in favour of the physical amplitude for the semi-leptonic decay [29, 99].

6.2.1 Factorization Formula for Semi-Leptonic Decay

The non-radiative amplitude for the semi-leptonic decay $\bar{B} \rightarrow D^{(*)+} \ell^- \bar{\nu}_\ell$ is

$$\mathcal{A}_{\text{non-rad}}^{\text{sl}, D^{(*)}} = \frac{G_F}{\sqrt{2}} V_{cb} C_{\text{sl}} \langle D^{(*)+} \ell^- \bar{\nu}_\ell | Q_{\text{sl}} | \bar{B} \rangle, \quad (6.38)$$

with the semi-leptonic operator

$$Q_{\text{sl}} = [\bar{c} \gamma^\mu (1 - \gamma^5) b] [\bar{\ell} \gamma_\mu (1 - \gamma^5) \nu], \quad (6.39)$$

and the Wilson coefficient $C_{\text{sl}} = 1 + \mathcal{O}(\alpha_{\text{em}})$. Through a QED \times QCD \rightarrow HQET \times SCET matching one gets

$$\begin{aligned}\langle D^+ \ell^- \bar{\nu}_\ell | Q_{\text{sl}} | \bar{B} \rangle &= i 4 E_D E_{\text{sl}} Z_\ell \zeta^{BD} (E_\ell, q^2) H_{\text{sl}}(E_\ell, q^2, z), \\ \langle D^{*+} \ell^- \bar{\nu}_\ell | Q_{\text{sl}} | \bar{B} \rangle &= i 4 E_{D^*} E_{\text{sl}} Z_\ell (\varepsilon^* \cdot v) \zeta^{BD^*} (E_\ell, q^2) H_{\text{sl}}^*(E_\ell, q^2, z),\end{aligned}\quad (6.40)$$

with $q^2 = (p_\ell + p_{\nu_\ell})^2$ being the dilepton invariant mass, E_ℓ the charged lepton energy, and the spinor product

$$iE_{\text{sl}} \equiv \bar{u}_\ell(p_\ell) \frac{\not{h}_-}{2} (1 - \gamma^5) v_{\nu_\ell}(p_{\nu_\ell}). \quad (6.41)$$

With respect to the purely hadronic decay the factorization formula is simpler, as the light meson in the final state is replaced by the point-like lepton and a neutrino which is non-interacting in QED. For this reason the convolution is now changed into a simple product, and the LCDA replaced by a constant factor Z_ℓ . In (6.40) Z_ℓ stands for the semi-leptonic renormalized matrix element

$$\langle \ell^-(p_\ell) | R_{\bar{c}}^{(Q_\ell)} \bar{\chi}^{(\ell)}(0) | 0 \rangle \equiv Z_\ell \bar{u}_\ell(p_\ell) \frac{\not{h}_- \not{h}_+}{4}, \quad (6.42)$$

with the inclusion of the soft-rearrangement factor in analogy to (6.33). The expression reads [99]

$$Z_\ell^{(1)} = -\frac{1}{\epsilon_{\text{IR}}} \left(1 + \ln \frac{m_\ell^2}{(n_- p_\ell)^2} \right) + \frac{1}{2} \ln^2 \frac{\mu^2}{m_\ell^2} + \frac{1}{2} \ln \frac{\mu^2}{m_\ell^2} + \frac{\pi^2}{12} + 2, \quad (6.43)$$

where the leftover IR divergence will be cancelled by the ultrasoft real emission contributions. Interestingly, the finite part is exactly given by the one-loop matching function $\mathcal{J}_{\text{peak}}$ computed in QCD in Section 3.3.1. Indeed the matching of the massive SCET field (3.58) involves precisely the computation of a matrix element analogue to (6.42), in QCD, which at the one-loop level is related to QED by the simple replacement $\alpha_s C_F \rightarrow \alpha_{\text{em}} Q_\ell^2$.

The semi-leptonic decay is a three-body decay, as opposed to the two-body non-leptonic one. Hence the form factor now depends not only on the momentum transfer q^2 but also on the lepton energy. For this reason, we can identify the form factors of the factorization formulas (6.37) and (6.40) only in the specific kinematic limit where the lepton has the same momentum of the light-meson in the $\bar{B} \rightarrow D^{(*)+} L^-$ decay. This occurs when $q^2 = m_L^2$, and the lepton carries maximal energy $E_\ell^{\text{max}} = (E_L + \sqrt{E_L^2 - m_L^2})/2$. In this kinematical configuration we compute the hard-scattering kernels analogously as for the non-leptonic decay. With analogous definitions $H_{\text{sl}} = H_{\text{sl},-} + H_{\text{sl},+}$ and $H_{\text{sl}}^* = H_{\text{sl},-} - H_{\text{sl},+}$, we get

$$\begin{aligned} H_{\text{sl},-}^{(1)}(z) &= Q_u Q_\ell \left\{ \frac{L_c^2}{2} - 3L_\nu + 3L_b - 2L_c \left(1 - i\pi + \ln \left(\frac{1-z}{z} \right) \right) + g \left(1 - \frac{1}{z} \right) + \frac{\pi^2}{12} - 6 \right\} \\ &\quad - Q_d Q_\ell \left\{ \frac{L_b^2}{2} + L_b \left(1 - 2 \ln(1-z) \right) + h_-(1-z) + \frac{\pi^2}{12} + 5 \right\} \\ &\quad + Q_u Q_d f(z) - Q_d^2 \left(\frac{3}{2} L_b + 2 \right) - Q_u^2 \left(\frac{3}{2} L_c + 2 \right), \end{aligned} \quad (6.44)$$

$$H_{\text{sl},+}^{(1)}(z) = -Q_d Q_\ell \sqrt{z} h_+(1-z) - Q_u Q_d \sqrt{z} \frac{\ln z}{1-z}, \quad (6.45)$$

where we fixed $q^2 = 0$ and $E_\ell^{\text{max}} = m_b(1-z)/2$, which is consistent at leading power, and removed them from the arguments.

6.2.2 Physical Form Factor

We can finally write down a physical form factor to replace the unknown HQET form factor $\zeta^{BD(*)}$ in the non-leptonic decay. We define

$$\begin{aligned}\mathcal{F}^{BD} &= \lim_{E_\ell \rightarrow E_\ell^{\max}} \frac{\sqrt{2}\mathcal{A}_{\text{non-rad}}^{\text{sl},D}}{i4G_F V_{cb} E_D E_{\text{sl}}}, \\ \mathcal{F}^{BD*} &= \lim_{E_\ell \rightarrow E_\ell^{\max}} \frac{\sqrt{2}\mathcal{A}_{\text{non-rad}}^{\text{sl},D*}}{i4G_F V_{cb}(\varepsilon^* \cdot v) E_{D*} E_{\text{sl}}}.\end{aligned}\quad (6.46)$$

At $q^2 = m_L^2$ the spinor product for massless leptons reduces to

$$E_{\text{sl}}|_{q^2=m_L^2} = \sqrt{E_\ell^{\max} - E_\ell} \frac{8E_\ell^{\max} \sqrt{E_\ell^{\max}(4E_\ell E_\ell^{\max} - m_L^2)}}{4(E_\ell^{\max})^2 - m_L^2}, \quad (6.47)$$

which vanish for $E_\ell \rightarrow E_\ell^{\max}$, accounting for the behaviour of the non-radiative amplitude at the kinematic endpoint. The physical form factor $\mathcal{F}^{BD(*)}$ remains finite in this limit. Using the factorization formula (6.40), from the definition (6.46) we get

$$\mathcal{F}^{BD(*)}(m_L^2) = C_{\text{sl}} Z_\ell \zeta^{BD(*)}(E_\ell^{\max}, m_L^2) H_{\text{sl}}^{(*)}(z), \quad (6.48)$$

which can be solved for $\zeta^{BD(*)}$ and inserted into the non-leptonic non-radiative amplitudes as

$$\begin{aligned}C_2 \langle D^+ L^- | Q_2 | \bar{B} \rangle &= i f_L 4E_L E_D \frac{C_2}{C_{\text{sl}}} \mathcal{F}^{BD}(m_L^2) \int_0^1 du T(u, z) \frac{\Phi_L(u)}{Z_\ell}, \\ C_2 \langle D^{*+} L^- | Q_2 | \bar{B} \rangle &= i f_L 4E_L E_{D*}(\varepsilon^* \cdot v) \frac{C_2}{C_{\text{sl}}} \mathcal{F}^{BD*}(m_L^2) \int_0^1 du T^*(u, z) \frac{\Phi_L(u)}{Z_\ell},\end{aligned}\quad (6.49)$$

where we defined the new hard-scattering kernels as

$$T^{(*)}(u, z) = \frac{H^{(*)}(u, z)}{H_{\text{sl}}^{(*)}(z)}, \quad (6.50)$$

which are unity at tree level and at $\mathcal{O}(\alpha_{\text{em}})$ are given by

$$\begin{aligned}T^{(1)}(u, z) &= Q_d^2 \left\{ 2L_b \ln u - h_-(u(1-z)) + h_-(1-z) \right\} \\ &\quad + Q_u^2 \left\{ -3L_\nu + 3L_b - L_c(3 - 2 \ln \bar{u}) - h_-\left(\bar{u}\left(1 - \frac{1}{z}\right)\right) + g\left(1 - \frac{1}{z}\right) - 11 \right\} \\ &\quad + Q_d Q_u \left\{ -3L_\nu - 2L_b \ln \bar{u} - 2L_c \ln u + g(\bar{u}(1-z)) + g\left(u\left(1 - \frac{1}{z}\right)\right) \right. \\ &\quad \left. - h_-(1-z) - g\left(1 - \frac{1}{z}\right) - 11 \right\}\end{aligned}$$

$$-\sqrt{z} \left[Q_d^2 \left(h_+(u(1-z)) - h_+(1-z) \right) + Q_u^2 \frac{1}{z} h_+ \left(\bar{u} \left(1 - \frac{1}{z} \right) \right) + Q_d Q_u h_+(1-z) \right]. \quad (6.51)$$

The corresponding $T^*(u, z)$ is obtained by setting $\sqrt{z} \rightarrow -\sqrt{z}$. As anticipated in Section 6.1.3, the hard-scattering kernel $T^{(*)}$ in (6.51) is free from collinear divergences when taking the limit $z \rightarrow 0$. In this limit, we checked that (6.51) reduces to the massless case (73) in Ref. [99].

The physical form factor (6.48) is not anymore a single scale object, and contains physics up to the electroweak scale as well. However it has the appealing advantage of having an explicit prescription (6.46) to extract it from experimental data. In spirit this is similar to QCD factorization where the HQET form factors are replaced by the full QCD ones. Indeed when turning off QED, $\mathcal{F}^{BD^{(*)}}$ becomes proportional to the standard QCD form factors [71] (see (2.132) and (2.133))

$$\begin{aligned} \hat{\mathcal{F}}^{BD} &\equiv \frac{4E_D E_L}{m_B^2 - m_D^2} \mathcal{F}^{BD} \xrightarrow{\alpha_{\text{em}} \rightarrow 0} F_0^{\bar{B}D}, \\ \hat{\mathcal{F}}^{BD^*} &\equiv -\frac{2E_{D^*} E_L}{m_{D^*} m_B} \mathcal{F}^{BD^*} \xrightarrow{\alpha_{\text{em}} \rightarrow 0} A_0^{\bar{B}D^*}. \end{aligned} \quad (6.52)$$

The QED corrections in $\mathcal{F}^{BD^{(*)}}$ are hence so far unknown but might be addressed in the future by means of experimental data. In the meanwhile we have the tempting option of studying ratios between non-leptonic and semi-leptonic decay rates in which such corrections largely cancel. We investigate such quantities in the numerical analysis of Section 7.2.2.

Chapter 7

Radiative Amplitude and Numerical Analysis

In this chapter we will first deal with the ultrasoft-photon inclusive decay rate $\Gamma[\bar{B} \rightarrow D^{(*)+}L^- + X_s](\Delta E)$ with X_s being an arbitrary number of unresolved photons (and electron-positron pairs) with total energy smaller than ΔE in the \bar{B} meson rest frame. We then proceed to perform a numerical analysis of virtual QED corrections to the non-radiative amplitude. We end the chapter with a phenomenological study on ratios of non-leptonic to semi-leptonic decay rates.

7.1 Ultrasoft Effects

To render the decay rate IR finite we need to include real radiation. If we restrict the energy of the final state radiation with a cutoff $\Delta E \ll \Lambda_{\text{QCD}}$, the radiative amplitude factorizes as

$$\mathcal{A}(\bar{B} \rightarrow D^{(*)}L + X_s) = \mathcal{A}(\bar{B} \rightarrow D^{(*)}L) \langle X_s | \bar{S}_v^{(Q_B)}(0) S_{v'}^{\dagger(Q_D)}(0) S_{v_L}^{\dagger(Q_L)}(0) | 0 \rangle, \quad (7.1)$$

up to corrections $\mathcal{O}(\Delta E/\Lambda_{\text{QCD}})$. The time-like ultrasoft Wilson lines for outgoing mesons are defined as (6.5), with $A_s \rightarrow A_{us}$, $n_+ \rightarrow v_i$ and $v_i^2 = 1$, while the one for the incoming \bar{B} meson with velocity v is [98]

$$\bar{S}_v^{(Q_B)}(x) = \exp \left\{ ieQ_B \int_{-\infty}^0 ds v \cdot A_{us}(x + sv) \right\}. \quad (7.2)$$

Charge conservation implies $Q_B = Q_D + Q_L$ which also ensures gauge invariance of the Wilson line product. At the level of the decay rate, for general charges of the final state $D^{(*)}L$, one can therefore write

$$\Gamma[\bar{B} \rightarrow D^{(*)}L + X_s](\Delta E) = |\mathcal{A}(\bar{B} \rightarrow D^{(*)}L)|^2 \mathcal{S}_{\otimes}(\Delta E), \quad (7.3)$$

with $\otimes = \{Q_D, Q_L\}$ and

$$\mathcal{S}_{\otimes}(\Delta E) = \sum_{X_s} |\langle X_s | \bar{S}_v^{(Q_B)}(0) S_{v'}^{\dagger(Q_D)}(0) S_{v_L}^{\dagger(Q_L)}(0) | 0 \rangle|^2 \theta(\Delta E - E_{X_s}). \quad (7.4)$$

At order α_{em} we get

$$\mathcal{S}_{\otimes}(\Delta E) = 1 + \frac{\alpha_{\text{em}}}{4\pi} \left[8b_{\otimes} \ln\left(\frac{\mu_{\text{IR}}}{2\Delta E}\right) + 4F_{\otimes} \right] + \mathcal{O}(\alpha_{\text{em}}^2), \quad (7.5)$$

where for $\bar{B} \rightarrow D^{(*)+}L^-$, the functions $b_{(+,-)}$ and $F_{(+,-)}$ are given by [103]

$$\begin{aligned} b_{(+,-)} &= 1 - \frac{4 - \Delta_+^2 - \Delta_-^2 + 2\beta^2}{8\beta} \left[\ln\left(\frac{\Delta_+ + \beta}{\Delta_+ - \beta}\right) + \ln\left(\frac{\Delta_- + \beta}{\Delta_- - \beta}\right) \right], \\ F_{(+,-)} &= \frac{\Delta_+}{2\beta} \ln\left(\frac{\Delta_+ + \beta}{\Delta_+ - \beta}\right) + \frac{\Delta_-}{2\beta} \ln\left(\frac{\Delta_- + \beta}{\Delta_- - \beta}\right) + \frac{4 - \Delta_-^2 - \Delta_+^2 + 2\beta^2}{4\beta} \\ &\times \left[\text{Re}\left\{ \text{Li}_2\left(-\frac{\beta}{\Delta_-}\right) - \text{Li}_2\left(\frac{\beta}{\Delta_-}\right) + \frac{1}{2}\text{Li}_2\left(\frac{\Delta_- + \beta}{2\Delta_-}\right) - \frac{1}{2}\text{Li}_2\left(\frac{\Delta_- - \beta}{2\Delta_-}\right) \right\} \right. \\ &\left. - \frac{\ln 2}{2} \ln\left(\frac{\Delta_- + \beta}{\Delta_- - \beta}\right) + \frac{1}{4} \ln^2\left(1 + \frac{\beta}{\Delta_-}\right) - \frac{1}{4} \ln^2\left(1 - \frac{\beta}{\Delta_-}\right) + (\Delta_- \rightarrow \Delta_+) \right], \quad (7.6) \end{aligned}$$

where here $\beta \equiv \sqrt{(1 - (r_L + r_D)^2)(1 - (r_L - r_D)^2)}$, with the ratios $r_L \equiv m_L/m_B$, $r_D \equiv m_D/m_B$, and $\Delta_{\pm} \equiv 1 \pm r_L^2 \mp r_D^2$. In Ref. [103] an analogous function $G_{12}(E)$ is computed (see (5)), which agrees with our result when dropping the virtual contributions N_{12} and H_{12} , and setting $\mu = m_B$ in our result. The conceptual differences between the approach adopted here and in Ref. [103] are extensively discussed at the end of Section 6 in Ref. [99]. In the double-logarithmic approximation \mathcal{S}_{\otimes} exponentiates to [104]

$$\mathcal{S}_{\otimes} = \exp\left(\frac{\alpha_{\text{em}}}{4\pi} \mathcal{S}_{\otimes}^{(1)}\right), \quad (7.7)$$

which we will use below.

The scale dependence of \mathcal{S}_{\otimes} has to cancel with the IR scale dependence of the non-radiative amplitude, which comes from the IR divergences of the generalized LCDA and form factor. In order to have finite and well defined objects the generalized LCDA and form factor have to be understood as properly IR subtracted, which nevertheless introduces a μ_{IR} dependence. With perturbative methods we can extract only the UV scale dependence of these objects, related to the factorization scale μ present in the hard-scattering kernels. For this reason we are forced to set $\mu_{\text{IR}} = \mu_s \sim \mathcal{O}(\Lambda_{\text{QCD}})$, where μ_s is the collinear scale, such that no large IR logarithms are introduced in $\zeta^{BD^{(*)}}$ and $\Phi_L(u)$. We restrict ourselves to the resummation of double logarithms, except for those in ΔE [99]. The definition (6.34) with the soft rearrangement factor eliminates the double logarithms from the form factors, allowing us to consider only the two Sudakov factors for the hard-scattering kernels (S_H) and Φ_L ($S_{\bar{C}}$) [98]

$$\begin{aligned} S_H(\mu, \mu_b) &= \exp\left\{-\frac{\alpha_{\text{em}}}{2\pi} Q_L^2 \ln^2 \frac{\mu}{\mu_b}\right\}, \\ S_{\bar{C}}(\mu, \mu_s; E_L) &= \exp\left\{-\frac{\alpha_{\text{em}}}{2\pi} Q_L^2 \left(\ln^2 \frac{\mu_s}{2E_L} - \ln^2 \frac{\mu}{2E_L}\right)\right\}, \quad (7.8) \end{aligned}$$

which sum double logarithms between the factorization scale and the hard scale $\mu_b \sim \mathcal{O}(m_b)$ in the first case, and between the factorization scale and the collinear scale μ_s in the latter. Combining the two factors, restricting to the double logarithmic approximation, the factorization scale dependence drops and we obtain the universal factor

$$S_L(\mu_b, \mu_s) = \exp\left\{-\frac{\alpha_{\text{em}}}{2\pi} Q_L^2 \ln^2 \frac{\mu_s}{\mu_b}\right\}, \quad (7.9)$$

summing all the double logarithms between Λ_{QCD} and m_b . We can therefore define a scale independent ‘‘ultrasoft function’’ by combining (7.7) with $\mu_{\text{IR}} = \mu_s$ and the square of (7.9) coming from the modulus square of the non-radiative amplitude

$$U(D^{(*)}L) = |S_L(\mu_b, \mu_s)|^2 \exp\left(\frac{\alpha_{\text{em}}}{4\pi} \mathcal{S}_{\otimes}^{(1)}\right) = \left(\frac{2\Delta E}{m_B}\right)^{-\frac{\alpha_{\text{em}}}{\pi} 2b_{\otimes}} t_{\otimes}(\mu_s), \quad (7.10)$$

with

$$t_{\otimes}(\mu_s) = \exp\left\{\frac{\alpha_{\text{em}}}{\pi} \left[2b_{\otimes} \ln \frac{\mu_s}{m_B} - Q_L^2 \ln^2 \frac{\mu_s}{\mu_b} + F_{\otimes}\right]\right\}, \quad (7.11)$$

where a fictitious m_B dependence has been introduced, which cancels between $t_{\otimes}(\mu_s)$ and the other factor in $U(D^{(*)}L)$. As discussed, we restrict ourselves to the double-logarithmic approximation (except for logarithms in ΔE), and we now proceed to show explicitly that in this approximation $t_{(+,-)} = 1$. Expanding up to leading order in $m_L/m_B \sim \mathcal{O}(\Lambda_{\text{QCD}}/m_B)$ we obtain from (7.6)

$$\begin{aligned} b_{(+,-)} &= 1 + \ln\left(\frac{m_D m_L}{m_B^2 - m_D^2}\right), \\ F_{(+,-)} &= -\ln^2 \frac{m_L m_B}{m_B^2 - m_D^2}, \end{aligned} \quad (7.12)$$

where in the expression for $F_{(+,-)}$ we only kept the double-logarithmic terms. With these approximations, and setting the hard scale to $\mu_b = m_B$, (7.11) reduces to

$$t_{(+,-)}(\mu_s) = \exp\left\{\frac{\alpha_{\text{em}}}{\pi} \left[-\ln^2 \left(\frac{m_L}{\mu_s} \frac{m_B^2}{m_B^2 - m_D^2}\right)\right]\right\}. \quad (7.13)$$

which is indeed free from large double logarithms as $m_L \sim \mathcal{O}(\mu_s)$, and as expected, the μ_s dependence in $U(D^{(*)}L)$ drops.

In this way the ultrasoft-photon inclusive decay rate can be factorized into two scale-independent parts

$$\Gamma[\bar{B} \rightarrow D^{(*)}L + X_s](\Delta E) = \Gamma^{(0)}[\bar{B} \rightarrow D^{(*)}L]U(D^{(*)}L), \quad (7.14)$$

where the non-radiative scale-independent decay rate is defined as $\Gamma^{(0)}[\bar{B} \rightarrow D^{(*)}L] = |\mathcal{A}(\bar{B} \rightarrow D^{(*)}L)/S_L(\mu_b, \mu_s)|^2$, and

$$U(DL) = \left(\frac{2\Delta E}{m_B}\right)^{-\frac{2\alpha_{\text{em}}}{\pi} \left(1 + \ln \frac{m_D m_L}{m_B^2 - m_D^2}\right)}, \quad (7.15)$$

with obvious replacement for $U(D^*L)$.

A complete treatment of sub-leading logarithms would require a non-perturbative matching from HQET \times SCET to a theory of point-like mesons, which currently is not clear how to implement. Therefore to include an uncertainty on $U(D^{(*)}L)$, we evaluate (7.10) with the non-expanded t_\otimes from (7.11), evaluated at $\mu_s = 1$ GeV, and take the difference with respect to (7.15), using it then as a double-sided conservative uncertainty. For $\Delta E = 60$ MeV [98,99] we get

$$\begin{aligned} U(D^+K^-) &= 0.959 \pm 0.001, \\ U(D^+\pi^-) &= 0.938 \pm 0.005, \\ U(D^{*+}K^-) &= 0.961 \pm 0.001, \\ U(D^{*+}\pi^-) &= 0.939 \pm 0.005, \end{aligned} \tag{7.16}$$

where the electromagnetic coupling constant is also evaluated at μ_s . Note that in the following we refer to these as ultrasoft effects. We take the opportunity to remark that also the semi-leptonic rate will get an ultrasoft correction $U(D^{(*)}\ell)$, where m_L is replaced by m_ℓ . In the case of the semi-leptonic decay with a muon in the final state we get

$$U(D^+\mu^-) = 0.933 \pm 0.007, \quad U(D^{*+}\mu^-) = 0.934 \pm 0.007. \tag{7.17}$$

7.2 Numerical Analysis

In this section we proceed to evaluate the numerical impact of the $\mathcal{O}(\alpha_{\text{em}})$ corrections computed in Chapter 6 and Section 7.1. The decay rate receives QED corrections from three different physical scales:

- Corrections from scales above m_b , encoded in the WET Wilson coefficients,
- Corrections from scales between m_b and Λ_{QCD} , coming from the hard-scattering kernels, the form factors and the light-meson LCDA,
- Corrections to the decay rate from ultrasoft real radiation at scales below Λ_{QCD} .

The first two sources are responsible for virtual corrections at the amplitude level and will be discussed in Section 7.2.1, while the numerical impact of ultrasoft radiation will be addressed in Section 7.2.2

7.2.1 QED Corrections to Non-Radiative Amplitude

We parametrize the non-radiative amplitude as

$$\mathcal{A}(\bar{B} \rightarrow D^{(*)+}L^-) = A_{BD^{(*)}} \left(\frac{\hat{\mathcal{F}}^{BD^{(*)}}}{F_0^{\bar{B}D^{(*)}}} \right) a_1(D^{(*)+}L^-), \tag{7.18}$$

with $F_0^{\bar{B}D^*} \equiv A_0^{\bar{B}D^*}$, and the QCD prefactors

$$\begin{aligned} A_{BD} &= i \frac{G_F}{\sqrt{2}} V_{uq}^* V_{cb} f_L (m_B^2 - m_D^2) F_0^{\bar{B}D}(m_L^2), \\ A_{BD^*} &= -i \frac{G_F}{\sqrt{2}} V_{uq}^* V_{cb} f_L 2m_{D^*} (\varepsilon^* \cdot p_B) A_0^{\bar{B}D^*}(m_L^2). \end{aligned} \quad (7.19)$$

The colour-allowed tree-amplitude is parametrized by

$$a_1(D^{(*)+}L^-) = \sum_{i=1}^2 \frac{C_i}{C_{\text{sl}}} \int_0^1 du T_i^{(*)}(u, z) \frac{\Phi_L(u)}{Z_\ell}, \quad (7.20)$$

where the hard-scattering kernels are known in QCD at NNLO [95], and at NLO in QED from (6.51). We split (7.20) as $a_1(D^{(*)}L) = a_1^{\text{QCD}}(D^{(*)}L) + \delta a_1(D^{(*)}L)$, where the QED effects are encoded in

$$\delta a_1(D^{(*)}L) = \delta a_1^{\text{WC}}(D^{(*)}L) + \delta a_1^{\text{K}}(D^{(*)}L) + \delta a_1^{\text{L}}(D^{(*)}L), \quad (7.21)$$

respectively coming from the Wilson coefficients (δa_1^{WC}), hard-scattering kernels (δa_1^{K}) and the light-meson LCDA (δa_1^{L}). Note that due to the substitution of the HQET form factor $\zeta^{BD^{(*)}}$ with the physical form factor (6.48), the QED corrections (7.21) also contain corrections from C_{sl} , H_{sl} and Z_ℓ according to (6.49). This is a convenient parametrization of the QED corrections since when computing ratios of non-leptonic to semi-leptonic decay rates, the QED corrections from the ratio $\mathcal{F}^{BD^{(*)}}/F_0^{\bar{B}D^{(*)}}$ in (7.18) cancel completely.

For consistency we recompute the NNLO QCD coefficients with our inputs [95]

$$\begin{aligned} a_1^{\text{QCD}}(D^+K^-) &= 1.008 + [0.023 + 0.009i]_{\text{NLO}} + [0.029 + 0.028i]_{\text{NNLO}} \\ &= 1.061_{-0.013}^{+0.015} + 0.037_{-0.012}^{+0.023}i, \end{aligned} \quad (7.22)$$

where the uncertainty is fully dominated by the scale variation $m_b/2 < \mu < 2m_b$ around the central value $\mu = m_b$. We used the Gegenbauer coefficients from Ref. [105] evolved to m_b with NLL accuracy, as reported in Appendix A. The uncertainty coming from the quark masses is negligible. In fact by varying both masses in the conservative ranges $1.3 \text{ GeV} < m_c < 1.7 \text{ GeV}$ and $4.5 \text{ GeV} < m_b < 4.9 \text{ GeV}$, we find the error to be one order of magnitude smaller than the one from the scale variation in (7.22). We emphasize that, differently from Ref. [95], we do not re-expand the Wilson coefficients as series in α_s , but treat their numerical values (at NNLO accuracy) as inputs. Numerical values of $|a_1(D^{(*)+}L^-)|$, at different orders in perturbation theory, are summarized in Table 7.1. Differences between D and D^* final states are numerically small.

By using [99]

$$C_2 = C_2^{(0)} + \frac{\alpha_{\text{em}}}{4\pi} C_2^{(1)}, \quad C_{\text{sl}} = 1 + \frac{\alpha_{\text{em}}}{4\pi} C_{\text{sl}}^{(1)}, \quad (7.23)$$

with $C_2^{(0)} = 1.008$, $C_2^{(1)} = 5.68$ and $C_{\text{sl}}^{(1)} = 11.78$ the QED corrections to the amplitude coming from the Wilson coefficients is

$$\delta a_1^{\text{WC}}(D^{(*)}L) = \frac{\alpha_{\text{em}}}{4\pi} (C_2^{(1)} - C_2^{(0)} C_{\text{sl}}^{(1)}) \int_0^1 du T^{(*) (0)}(u, z) \phi_L(u)$$

$ a_1(D^{(*)+}L^-) $	LO	NLO	NNLO	+QED NLO
$ a_1(D^+\pi^-) $	$1.008_{-0.006}^{+0.012}$	$1.032_{-0.016}^{+0.023}$	$1.063_{-0.014}^{+0.018}$	$1.058_{-0.014}^{+0.018}$
$ a_1(D^{*+}\pi^-) $	$1.008_{-0.006}^{+0.012}$	$1.031_{-0.016}^{+0.022}$	$1.062_{-0.014}^{+0.018}$	$1.058_{-0.014}^{+0.018}$
$ a_1(D^+K^-) $	$1.008_{-0.006}^{+0.012}$	$1.032_{-0.016}^{+0.023}$	$1.061_{-0.013}^{+0.016}$	$1.057_{-0.013}^{+0.016}$
$ a_1(D^{*+}K^-) $	$1.008_{-0.006}^{+0.012}$	$1.031_{-0.016}^{+0.021}$	$1.061_{-0.013}^{+0.017}$	$1.056_{-0.013}^{+0.016}$

Table 7.1: Results for $|a_1(D^+L^-)|$ at LO, NLO and NNLO using the results of Ref. [95] for the NNLO expressions of the hard-scattering kernels. In the last column, we added the QED NLO corrections $\delta a_1 = \delta a_1^{\text{WC}} + \delta a_1^{\text{K}} + \delta a_1^{\text{L}}$.

$$= \frac{\alpha_{\text{em}}}{4\pi} (C_2^{(1)} - C_2^{(0)} C_{\text{sl}}^{(1)}) = -0.37 \cdot 10^{-2}. \quad (7.24)$$

The QED corrections to the light-meson LCDA change its normalization from 1, which have to be intended as the corrections to the decay constant, since we have normalized the generalized LCDA by the QCD decay constant. With this in mind, the evolution from the soft scale 1 GeV to the hard scale m_b produces¹ [83]

$$\delta a_1^{\text{L}}(D^{(*)}L) = C_2^{(0)} \int_0^1 du \left(\frac{\Phi_L(u)}{Z_\ell} - \phi_L(u) \right) = 0.35 \cdot 10^{-2}, \quad (7.25)$$

but QED corrections from at the soft scale to the LCDA are unknown and would have to be determined by non-perturbative methods. Finally the corrections to the hard-scattering kernels give

$$\delta a_1^{\text{K}}(D^{(*)}L) = \frac{\alpha_{\text{em}}}{4\pi} C_2^{(0)} \int_0^1 du T^{(*) (1)}(u, z) \phi_L(u), \quad (7.26)$$

where we truncate the Gegenbauer expansion of the QCD LCDA at second order. We write the convolution in the form

$$\int_0^1 du T^{(*) (1)}(u, z) \phi_L(u) = V_0^{(*) (1)}(z) + V_1^{(*) (1)}(z) a_1^L(\mu) + V_2^{(*) (1)}(z) a_2^L(\mu), \quad (7.27)$$

with the analytical expressions for the convoluted kernels $V_i^{(*) (1)}(z)$ given in Appendix C.2. Setting the factorization scale and the scale of the Wilson coefficients to $\mu = \nu = \mu_b = 4.8$ GeV, we get

$$\delta a_1^{\text{K}}(D^+L^-) = \frac{\alpha_{\text{em}}(\mu_b)}{4\pi} \left[-7.06 - 8.71i - (2.07 + 1.18i) a_1^L(\mu_b) - (2.81 + 1.97i) a_2^L(\mu_b) \right],$$

¹Notice that this contribution was not included originally in Ref. [29], instead the factorization scale was set to $\mu = 1$ GeV.

$$\delta a_1^K(D^{*+}L^-) = \frac{\alpha_{\text{em}}(\mu_b)}{4\pi} \left[-6.94 - 7.30i - (1.51 + 0.76i)a_1^L(\mu_b) - (2.40 + 1.95i)a_2^L(\mu_b) \right]. \quad (7.28)$$

For $L^- = \pi^-, K^-$ we obtain

$$\begin{aligned} \delta a_1^K(D^+\pi^-) &= \frac{\alpha_{\text{em}}(\mu_b)}{4\pi} \left[-7.31 - 8.89i \right] = (-0.44 - 0.53i) \cdot 10^{-2}, \\ \delta a_1^K(D^+K^-) &= \frac{\alpha_{\text{em}}(\mu_b)}{4\pi} \left[-7.38 - 8.92i \right] = (-0.44 - 0.54i) \cdot 10^{-2}, \\ \delta a_1^K(D^{*+}\pi^-) &= \frac{\alpha_{\text{em}}(\mu_b)}{4\pi} \left[-7.16 - 7.47i \right] = (-0.43 - 0.45i) \cdot 10^{-2}, \\ \delta a_1^K(D^{*+}K^-) &= \frac{\alpha_{\text{em}}(\mu_b)}{4\pi} \left[-7.21 - 7.49i \right] = (-0.43 - 0.45i) \cdot 10^{-2}. \end{aligned} \quad (7.29)$$

Comparing to the QCD result (7.22) we notice that the QED corrections to both the real and imaginary part are roughly the 15% of the NNLO QCD corrections. In Table 7.1 we summarize our results adding the QED corrections δa_1 to the NNLO QCD values of a_1^{QCD} obtained with the ancillary files from Ref. [95]. We notice that the QED effects are smaller than the QCD uncertainties, and therefore do not assign an additional uncertainty coming from QED. Our results would apply also to $\bar{B}_s \rightarrow D_s L$ and $\Lambda_b \rightarrow \Lambda_c L$ as the relation

$$a_1(D^+L^-) = a_1(D_s^+L^-) = a_1(\Lambda_c^+L^-), \quad (7.30)$$

holds both in QCD and QED.

7.2.2 Non-Leptonic to Semi-Leptonic Decay Rates Ratios

We finally consider ratios of non-leptonic to semi-leptonic decay rates, such that, as mentioned before, the QED corrections to the form factors cancel in the ratio. These observables are a clean test of factorization as also the QCD form factor largely cancel in the ratio, together with their hadronic uncertainties. Now, as the experimental collaborations might extract the non-radiative rate by correcting for the real ultrasoft radiation with Monte Carlo methods, we define two observables

$$\begin{aligned} R_L^{(0),(*)}(\Delta E) &= \frac{\Gamma[\bar{B} \rightarrow D^{(*)+}L^-](\Delta E)}{d\Gamma^{(0)}(\bar{B} \rightarrow D^{(*)+}\ell^-\bar{\nu}_\ell)/dq^2|_{q^2=m_L^2}}, \\ R_L^{(*)}(\Delta E) &= \frac{\Gamma[\bar{B} \rightarrow D^{(*)+}L^-](\Delta E)}{d\Gamma(\bar{B} \rightarrow D^{(*)+}\ell^-\bar{\nu}_\ell)/dq^2|_{q^2=m_L^2}}, \end{aligned} \quad (7.31)$$

where both have the inclusive non-leptonic rate in the numerator, but the first one has the non-radiative rate in the denominator, while the second one uses the ultrasoft photon inclusive decay rate in the denominator. The two definitions are related by $R_L^{(*)} =$

$R_L^{(0),(*)}/U(D^{(*)}\ell)$. The observable can be related to the $a_1(D^{(*)+}L^-)$ factorization coefficient through

$$\begin{aligned} R_L^{(*)}(\Delta E) &= 6\pi^2 |V_{uq}|^2 \frac{U(D^{(*)}L)}{U(D^{(*)}\ell)} f_L^2 \left| a_1^{\text{QCD}}(D^{(*)}L) + \delta a_1(D^{(*)}L) \right|^2 X_L^{(*)} \\ &= R_L^{(*)} \Big|_{\text{QCD}} \left(1 + \delta_{\text{QED}}(D^{(*)}L) + \delta_{\text{U}}(\Delta E) \right). \end{aligned} \quad (7.32)$$

where

$$\delta_{\text{QED}} = \frac{2\text{Re}[\delta a_1^{\text{WC}} + \delta a_1^{\text{K}} + \delta a_1^{\text{I}}] C_2}{|a_1^{\text{QCD}}|^2}, \quad (7.33)$$

and the ultrasoft effects are encoded in $\delta_{\text{U}} = U(D^{(*)}L)/U(D^{(*)}\ell) - 1$. For the observable $R_L^{(0),(*)}$ only the ultrasoft corrections change to $\delta_{\text{U}}^{(0)} = U(D^{(*)}L) - 1$. The factor $X_L^{(*)}$ in (7.32) encodes the QCD form factors leftover dependence

$$\begin{aligned} X_L &= \frac{(m_B^2 - m_D^2)^2}{[m_B^2 - (m_D - m_L)^2][m_B^2 - (m_D + m_L)^2]} \left| \frac{F_0(m_L^2)}{F_1(m_L^2)} \right|^2, \\ X_L^* &= [m_B^2 - (m_{D^*} - m_L)^2][m_B^2 - (m_{D^*} + m_L)^2] \frac{|A_0(m_L^2)|^2}{m_L^2 \sum_{i=0,\pm} |\mathcal{H}_i(m_L^2)|^2}, \end{aligned} \quad (7.34)$$

where $\mathcal{H}_0(q^2)$ and $\mathcal{H}_{\pm}(q^2)$ are the helicity amplitudes defined in the Appendix of Ref. [106]. The factors $X_L^{(*)}$ can be approximated in an expansion in m_L^2/m_B^2 , using the large-recoil relations for the form factors [107], giving [106]

$$\begin{aligned} X_L &= 1 + \frac{4m_L^2 m_B m_D}{(m_B^2 - m_D^2)^2}, \\ X_L^* &= 1 + \frac{4m_L^2 m_B m_{D^*}}{(m_B^2 - m_{D^*}^2)^2} - \frac{4m_L^2}{(m_B - m_{D^*})^2}. \end{aligned} \quad (7.35)$$

The approximation (7.35) gives the numerical factors

$$X_{\pi} = 1.00 (1.00), \quad X_K = 1.02 (1.01), \quad X_{\pi}^* = 0.99 (1.00), \quad X_K^* = 0.93 (0.95). \quad (7.36)$$

In brackets we give the numerical results obtained with the full expressions (7.34) using the QCD sum-rule results for the form factors from Ref. [96]. For $B \rightarrow D^*$ decays the corrections are at the percent-level. Given the general agreement between the two obtained values, in our numerical analysis we take the first number as the central value and add the difference as an additional uncertainty. In fact we note that the uncertainty coming from this choice is the same as the one propagated on the full expression (7.34) from the form factors [96].

The virtual QED corrections, where again the corrections to $\mathcal{F}^{BD^{(*)}}$ have cancelled in the ratio, are given by

$$\delta_{\text{QED}}(D\pi) = -0.82 \cdot 10^{-2}, \quad \delta_{\text{QED}}(DK) = -0.83 \cdot 10^{-2},$$

$R_L^{(*)}$	LO	QCD NNLO	$+\delta_{\text{QED}}$	$+\delta_U (\delta_U^{(0)})$
R_π	$0.969_{-0.016}^{+0.026}$	$1.077_{-0.031}^{+0.040}$	$1.068_{-0.031}^{+0.040}$	$1.074_{-0.033}^{+0.040} (1.001_{-0.029}^{+0.040})$
R_π^*	$0.962_{-0.016}^{+0.026}$	$1.067_{-0.031}^{+0.040}$	$1.059_{-0.030}^{+0.040}$	$1.064_{-0.032}^{+0.040} (0.994_{-0.029}^{+0.040})$
$R_K \cdot 10^2$	$7.48_{-0.11}^{+0.19}$	$8.28_{-0.22}^{+0.27}$	$8.22_{-0.21}^{+0.26}$	$8.45_{-0.23}^{+0.28} (7.88_{-0.21}^{+0.25})$
$R_K^* \cdot 10^2$	$6.82_{-0.18}^{+0.23}$	$7.54_{-0.26}^{+0.30}$	$7.48_{-0.25}^{+0.29}$	$7.70_{-0.27}^{+0.31} (7.19_{-0.24}^{+0.28})$

Table 7.2: Theoretical predictions for $R_L^{(*)}$ expressed in GeV^2 at LO, NNLO QCD and subsequently adding δ_{QED} given in (7.37) and the ultrasoft effects δ_U (or in brackets $\delta_U^{(0)}$). The last column presents our final results for $R_L^{(*)}(R_L^{(0),(*)})$.

$$\delta_{\text{QED}}(D^*\pi) = -0.80 \cdot 10^{-2}, \quad \delta_{\text{QED}}(D^*K) = -0.81 \cdot 10^{-2}, \quad (7.37)$$

where we notice that the process dependence is quite mild. Since we choose the muon channel in the semi-leptonic decay, the ultrasoft corrections in $R_L^{(*)}$ also vastly cancel between the non-leptonic and the semi-leptonic rate, resulting in

$$\begin{aligned} \delta_U(D\pi) &= \delta_U(D^*\pi) = 0.005 \pm 0.009, \\ \delta_U(DK) &= \delta_U(D^*K) = 0.028 \pm 0.008, \end{aligned} \quad (7.38)$$

for the benchmark value $\Delta E = 60 \text{ GeV}$.

We finally list in Table 7.2 the new predictions for $R_L^{(*)}$ where we used the tree level and NNLO QCD results for $|a_1(D^{(*)}L)|$ from Table 7.1. The last column contains the final results including all the available corrections, differing between the definition $R_L^{(*)}$ and, in brackets, $R_L^{(0),(*)}$. We include uncertainties coming from a_1^{QCD} , CKM factors, f_L and $X_L^{(*)}$. The total uncertainty is dominated by the a_1^{QCD} one. When adding the ultrasoft corrections in the last column, we also add in quadrature the uncertainties from (7.16) with the NNLO QCD ones. Overall the uncertainties are rather conservative and therefore we do not include other uncertainties from the virtual QED contributions, which are by themselves small.

We conclude this chapter by noting that the virtual QED corrections computed in this work are at the sub-percent level. However on top of those, ultrasoft photon real radiation is responsible for downsizing effects of about 5%. The last column of Table 7.2 indeed points out that, when comparing to experimental results, it is essential to understand if and how real QED corrections were treated. Only a precise theoretical definition of the measured quantity allows for a meaningful comparison with Standard Model predictions, resulting in a sensible test of the factorization approach. For this reason we do not report the experimental measurements on $R_L^{(*)}$ as the precise treatment of real radiation, usually implemented using the Monte Carlo code PHOTOS [108] (see e.g. Refs. [109, 110] for dedicated studies in \bar{B} decays), is still unclear.

Part IV

Baryon Number Violation

Chapter 8

Possibility of Observing Baryon Number Violating B Decays?

The matter-antimatter asymmetry of the Universe requires the presence of baryon number violation (BNV) [111]. This motivated several experimental searches for proton decay, which so far were only able to set lower bounds on the proton lifetime $\tau_p \geq 10^{30} - 10^{34}$ yr [24]. Such stringent constraints can be interpreted as a lower bound on the physical scale Λ_{BNV} at which the accidental baryon number symmetry of the SM is explicitly violated. The scale associated with BNV turns out to be of order $\mathcal{O}(10^{15} - 10^{16}$ GeV), typically referred to as the Grand Unification Theories (GUTs) scale.

Nevertheless, it is not excluded that BNV is realized with quark- and lepton-flavour dependent couplings, which could hence drastically modify the scale estimate given the fact that the valence quarks in the nucleons belong exclusively to the first family. In fact anomalies in B -physics, mentioned in the introduction, are often explained through NP scenarios with highly generation-dependent interactions taking place at scales of order $\mathcal{O}(1.5 - 5$ TeV). One might therefore speculate that, if BNV is restricted to occur only through third family quarks, it could be related to scales of the order of the flavour anomalies scale. Explicit models have been built in this direction [112–114].

In this situation it is hence natural to wonder if such a NP sector could induce detectable b -hadron BNV decay rates. In this chapter we answer this question indirectly by studying proton decays induced by virtual b quarks, which will result in bounds on Λ_{BNV} excluding this possibility by a large margin. In particular we look at the three simplest and dominant decay channels: the purely leptonic $p \rightarrow \ell^+ \nu_\ell \bar{\nu}$ and the two-body semi-leptonic $p \rightarrow \pi^+ \bar{\nu}$ and $p \rightarrow \pi^0 \ell^+$. The first one is mediated by a combination of the charged weak current $u \rightarrow b^* \ell^+ \nu_\ell$ and a BNV interaction involving the b quark, while the semi-leptonic channels are mediated by the same BNV interaction together with the charged weak current $u \rightarrow b^* u \bar{d}$. Since we are not aiming at describing the UV model responsible for BNV, we will employ the dimension-6 BNV operator basis from the SMEFT reviewed in Section 2.7, which is valid at scales below Λ_{BNV} . Example tree-level diagrams of proton decay mediated by a virtual bottom quark are shown in Figure 8.1.

As explained in Section 2.7, the operators (2.127) arise from an hypothetical matching

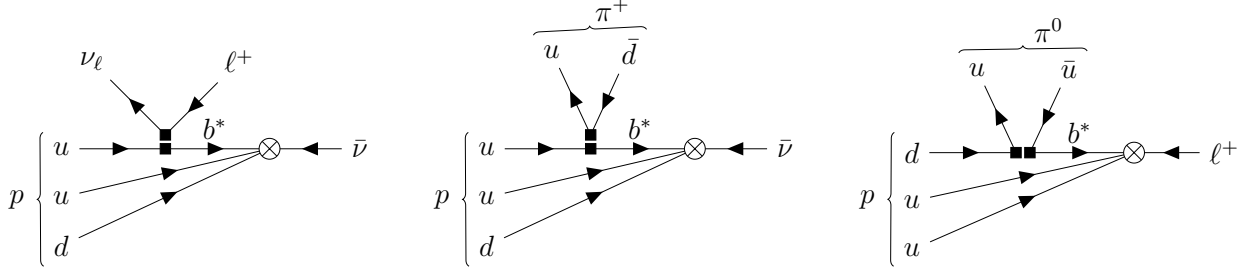


Figure 8.1: Examples of tree-level partonic diagrams for the decays $p \rightarrow \ell^+ \nu_\ell \bar{\nu}$, $p \rightarrow \pi^+ \bar{\nu}$ and $p \rightarrow \pi^0 \ell^+$. The square dots represent the weak effective vertices while \otimes stands for the four-fermion BNV operator insertion.

of an unknown UV theory onto SMEFT at a scale $\mathcal{O}(\Lambda_{\text{BNV}})$. They come with unknown and, in principle, generation-dependent Wilson coefficients C_{duu}^{prst} , C_{duq}^{prst} , C_{quq}^{prst} and C_{qqq}^{prst} . Since we want to study the effect of these BNV operators on low-energy physics, we evolve and match them onto the weak effective theory (WET) at the electroweak scale. The presence of the dimension-6 operators in the SMEFT Lagrangian generates new BNV dimension-6 operators in the WET through a leading power matching. The one-loop renormalization group evolution of the BNV operators in SMEFT is known [115], as well as their one-loop matching to the WET [116]. At the electroweak scale spontaneous symmetry breaking takes place, and the fundamental fermionic degrees of freedom are the (non-chiral) fields u , d , ℓ and ν appropriately rotated to the mass basis¹, which identifies what we mean by “third generation”. Since our interest relies purely on the phenomenology of the BNV interactions, the WET Hamiltonian will be our starting point, and the working assumptions, as well as the results, will be formulated on the WET Wilson coefficients at the electroweak scale.

The WET dimension-6 operator basis² is [116]

$$\begin{aligned}
Q_{RR} &= \varepsilon^{abc} [\tilde{d}_p^a P_R u_r^b] [\tilde{u}_s^c P_R \ell_t] & \left[= \mathcal{O}_{duu}^{S,RR} \right], \\
Q_{RL} &= \varepsilon^{abc} [\tilde{d}_p^a P_R u_r^b] [\tilde{u}_s^c P_L \ell_t] & \left[= \mathcal{O}_{duu}^{S,RL} \right], \\
Q_{LR} &= \varepsilon^{abc} [\tilde{d}_p^a P_L u_r^b] [\tilde{u}_s^c P_R \ell_t] & \left[= \mathcal{O}_{duu}^{S,LR} \right], \\
Q_{LL} &= \varepsilon^{abc} [\tilde{d}_p^a P_L u_r^b] [\tilde{u}_s^c P_L \ell_t] & \left[= \mathcal{O}_{duu}^{S,LL} \right], \\
Q_{R\nu} &= \varepsilon^{abc} [\tilde{d}_p^a P_R u_r^b] [\tilde{d}_s^c P_L \nu_t] & \left[= \mathcal{O}_{dud}^{S,RL} \right], \\
Q_{L\nu} &= \varepsilon^{abc} [\tilde{d}_p^a P_L u_r^b] [\tilde{d}_s^c P_L \nu_t] & \left[= -\mathcal{O}_{udd}^{S,LL} \right],
\end{aligned} \tag{8.1}$$

¹We do not consider the PMNS matrix for neutrinos, as their flavour is irrelevant for our discussion.

²Table 4 in Ref. [116] shows many more BNV operators. However, most of them have vanishing Wilson coefficients at one-loop dimension-6 matching, hence are not listed here. The last equality in brackets refers to the notation of Table 4 in Ref. [116].

where the generation indices p, r, s, t on the left-hand side are omitted for simplicity. The BNV part of the WET Hamiltonian can be expressed compactly as

$$\mathcal{H}_{\text{BNV}} = \frac{1}{\Lambda_{\text{BNV}}^2} \sum_{p,r,s,t} \sum_{X=L,R} \sum_{Y=L,R,\nu} C_{XY}^{prst} Q_{XY}^{prst}, \quad (8.2)$$

where the generation sums do not include top quarks, as they are removed from the theory and their effect is encoded in the Wilson coefficients. The dimensionless Wilson coefficients C_{XY}^{prst} are linear combinations of the SMEFT Wilson coefficients C_k^{prst} evaluated at the electroweak scale [116].

Before moving on we summarize the experimental bounds (90% CL) on proton partial lifetimes that we will use in this chapter [117–119]

$$\begin{aligned} \tau_{p \rightarrow \pi^0 e^+} &> 2.4 \cdot 10^{34} \text{ yr}, \\ \tau_{p \rightarrow \pi^0 \mu^+} &> 1.6 \cdot 10^{34} \text{ yr}, \\ \tau_{p \rightarrow \pi^+ \bar{\nu}} &> 3.9 \cdot 10^{32} \text{ yr}, \\ \tau_{p \rightarrow e^+ \nu \nu} &> 1.7 \cdot 10^{32} \text{ yr}, \\ \tau_{p \rightarrow \mu^+ \nu \nu} &> 2.2 \cdot 10^{32} \text{ yr}, \end{aligned} \quad (8.3)$$

where the partial lifetimes are defined as the inverse decay rate

$$\tau_{p \rightarrow f} = \frac{1}{\Gamma(p \rightarrow f)}, \quad (8.4)$$

and we will use the unit conversion factor $1 \text{ yr} = 4.79434 \cdot 10^{31} \text{ GeV}^{-1}$.

8.1 Constraints on Light-Flavoured BNV Operators

Having set the stage for our analysis, we begin with a quick review of the tree-level constraints on operators made by the light quarks (u, d, s). We define the “light-BNV” operators as

$$\begin{aligned} Q_{XY}^{111} &= \varepsilon^{abc} [\tilde{d}^a P_X u^b] [\tilde{u}^c P_Y \ell], \\ Q_{XY}^{211} &= \varepsilon^{abc} [\tilde{s}^a P_X u^b] [\tilde{u}^c P_Y \ell], \end{aligned} \quad (8.5)$$

and we consider as a reference value the constraint from $p \rightarrow \pi^0 \ell^+$ measurements [118]. The branching ratio is computed at tree-level, with the help of (2.130), as

$$\langle \pi^0 \ell^+(q) | Q_{XY}^{111} | p(p) \rangle = i [v^T(q) \mathcal{C} P_Y \left(W_{XY}^0 + \frac{\not{q}}{m_p} W_{XY}^1 \right) u_p(p)], \quad (8.6)$$

where u_p (v) is the proton (anti-lepton) spinor. The proton to pion form factor is encoded in the W_{XY}^i structure constants, whose numerical values are obtained from light-cone sum-rules [120]

$$\begin{aligned} W_{LL}^0 &= W_{RR}^0 = +0.084 \pm 0.021 \text{ GeV}^2, & W_{LL}^1 &= W_{RR}^1 = -0.068 \pm 0.023 \text{ GeV}^2, \\ W_{LR}^0 &= W_{RL}^0 = -0.118 \pm 0.030 \text{ GeV}^2, & W_{LR}^1 &= W_{RL}^1 = +0.14 \pm 0.06 \text{ GeV}^2, \end{aligned} \quad (8.7)$$

Assuming one operator dominating over the others at a time, the decay rate is

$$\Gamma(p \rightarrow \pi^0 \ell^+) = \frac{|C_{XY}^{111}|^2}{32\pi\Lambda_{\text{BNV}}^4} m_p (W_{XY}^0)^2 + \mathcal{O}\left(\frac{m_\ell^2}{m_p^2}, \frac{m_\pi^2}{m_p^2}\right). \quad (8.8)$$

Using the measurements summarized in (8.3) [118], and restoring the lepton generation index, we get the bounds

$$\begin{aligned} \frac{\Lambda_{\text{BNV}}}{\sqrt{|C_{LL}^{1111}|}} &= \frac{\Lambda_{\text{BNV}}}{\sqrt{|C_{RR}^{1111}|}} > 3.0 \cdot 10^{15} \text{ GeV}, & \frac{\Lambda_{\text{BNV}}}{\sqrt{|C_{LR}^{1111}|}} &= \frac{\Lambda_{\text{BNV}}}{\sqrt{|C_{RL}^{1111}|}} > 3.5 \cdot 10^{15} \text{ GeV}, \\ \frac{\Lambda_{\text{BNV}}}{\sqrt{|C_{LL}^{1112}|}} &= \frac{\Lambda_{\text{BNV}}}{\sqrt{|C_{RR}^{1112}|}} > 2.7 \cdot 10^{15} \text{ GeV}, & \frac{\Lambda_{\text{BNV}}}{\sqrt{|C_{LR}^{1112}|}} &= \frac{\Lambda_{\text{BNV}}}{\sqrt{|C_{RL}^{1112}|}} > 3.2 \cdot 10^{15} \text{ GeV}, \end{aligned} \quad (8.9)$$

implying, as explained above, $\Lambda_{\text{BNV}} \sim \mathcal{O}(\Lambda_{\text{GUT}})$ for the BNV scale, when the Wilson coefficients are thought of as $\mathcal{O}(1)$.

The two operators $Q_{L\nu}$ and $Q_{R\nu}$ of (8.1), involving the neutrino, mediate the decay $p \rightarrow \pi^+ \bar{\nu}$ at tree-level, which is experimentally less constrained by two orders of magnitude. However since $\Gamma \propto \Lambda_{\text{BNV}}^{-4}$, the difference at the level of the BNV scale is much less pronounced. Assuming the hadronic form factor for $p \rightarrow \pi^+$ to be of the same order as for $p \rightarrow \pi^0$, the bounds (8.9) only have to be rescaled by the factor

$$\left[\frac{\Gamma(p \rightarrow \pi^0 e^+)}{\Gamma(p \rightarrow \pi^+ \bar{\nu})} \Big|_{\text{exp}} \right]^{1/4} = 0.36, \quad (8.10)$$

to be translated to bounds on $Q_{L\nu}$ and $Q_{R\nu}$. This allows us to treat the two operators containing the neutrino on the same level as the other four with the charged lepton.

Similar bounds would apply to operators with the strange quark, Q_{XY}^{211} , since the decays $p \rightarrow K^0 \ell^+$ and $p \rightarrow K^+ \bar{\nu}$ are also severely constrained by data [121, 122]

$$\begin{aligned} \tau_{p \rightarrow K^0 e^+} &> 1.0 \cdot 10^{33} \text{ yr}, \\ \tau_{p \rightarrow K^0 \mu^+} &> 3.6 \cdot 10^{33} \text{ yr}, \\ \tau_{p \rightarrow K^+ \bar{\nu}} &> 2.3 \cdot 10^{33} \text{ yr}. \end{aligned} \quad (8.11)$$

Very comprehensive analyses on bounds on light-BNV operators have been presented recently in Refs. [123, 124], agreeing with our crude estimates performed in this section.

8.2 Third Family BNV Operators

The results of Section 8.1 show that if we want to explore the possibility of having $\Lambda_{\text{BNV}} \ll \Lambda_{\text{GUT}}$, we have to assume that the Wilson coefficients of light-BNV operators are negligible at the electroweak scale. We hence formulate our assumption on the Wilson coefficients of the operators (8.1) as

$$C_{XY}^{prst} = 0, \quad \text{for } p, r, s \neq 3, \quad (8.12)$$

namely we postulate the existence of BNV interactions at the low scale only if the operator contains (at least) one bottom quark field (as the top quark has been integrated out). The purpose is then to scan the operator basis and pin down the set that, given the bounds (8.3), would produce the largest possible branching fraction of a BNV b -hadron decay. What we are looking for are hence the BNV operators with the least constrained Wilson coefficients.

Before proceeding we have to mention that the case of operators including a b and a τ field needs to be taken into account separately. This is because the proton is lighter than the τ , forbidding its decay into final states with τ leptons. We will outline the strategy for constraining such operators in Section 8.3.4, together with an estimate of the resulting bounds. From now on we will hence drop the lepton flavour index and consider $\ell = e, \mu$, where the difference between electrons and muons will be encoded in the lepton mass corrections and different experimental bounds.

We will consider operators with two first family quarks and a left-handed or right-handed b field in Sections 8.2.1 and 8.2.2 respectively. In Section 8.2.3 we extend the analysis to operators with second family quarks alongside with a b field.

8.2.1 Operators with Left-Handed b Quark

We start by considering operators where the b quark is left-handed. At tree-level, the matching from the SMEFT operators (2.127) to the WET ones (8.1) simply consists in the rotation of the left-handed down-type quarks with the CKM matrix, due to the choice of the basis in the unbroken phase. This in the WET unavoidably introduces a correlation between the coefficients of operators with a left-handed b quark and operators with only light quarks. In particular, consider the operator $Q_{R\nu}^{113}$ generated by Q_{duq}^{prs} in the SMEFT. The tree-level matching of the SMEFT operators generates two dimension-6 WET operators with coefficients

$$C_{RL}^{prs} = C_{duq}^{prs}, \quad C_{R\nu}^{prs} = -C_{duq}^{prv} V_{vs}, \quad (8.13)$$

with implied sum over the flavour index v . This implies that in the WET the Wilson coefficient of the operator with the left-handed b quark, $Q_{R\nu}^{113}$, depends on the same SMEFT building blocks as the coefficients of light-BNV operators, in particular Q_{RL}^{111} , $Q_{R\nu}^{111}$ and $Q_{R\nu}^{112}$. In other words one can write down the system of equations

$$\begin{aligned} C_{RL}^{111} &= C_{duq}^{111}, \\ C_{R\nu}^{111} &= -V_{ud} C_{duq}^{111} - V_{cd} C_{duq}^{112} - V_{td} C_{duq}^{113}, \\ C_{R\nu}^{112} &= -V_{us} C_{duq}^{111} - V_{cs} C_{duq}^{112} - V_{ts} C_{duq}^{113}, \end{aligned}$$

$$C_{R\nu}^{113} = -V_{ub}C_{duq}^{111} - V_{cb}C_{duq}^{112} - V_{tb}C_{duq}^{113}, \quad (8.14)$$

which for $C_{R\nu}^{111} = C_{R\nu}^{112} = C_{RL}^{111} = 0$ (from our assumption (8.12)) implies $C_{R\nu}^{113} = 0$. Now, for the case of the other WET operators with a left-handed b quark the number of equations is smaller than the number of SMEFT Wilson coefficients involved. Even though this would allow in principle for large non-vanishing Wilson coefficients in the WET, one would need the SMEFT Wilson coefficients to satisfy highly fine-tuned relations to escape the bounds from the light-BNV operators. Such severe cancellations also need to be preserved by evolution [115], requiring an ad-hoc UV model of flavour which is not the purpose of this work. For this reason we exclude this possibility and focus on operators with a right-handed b quark.

8.2.2 Operators with Right-Handed b Quark

The WET operators with a right-handed b quark and two first generation quarks are

$$\begin{aligned} Q_{RR}^{311} &= \varepsilon^{abc} [\tilde{b}^a P_R u^b] [\tilde{\ell} P_R u^c], \\ Q_{RL}^{311} &= \varepsilon^{abc} [\tilde{b}^a P_R u^b] [\tilde{\ell} P_L u^c], \\ Q_{R\nu}^{311} &= \varepsilon^{abc} [\tilde{b}^a P_R u^b] [\tilde{\nu} P_L d^c]. \end{aligned} \quad (8.15)$$

Their Wilson coefficients are related to the SMEFT ones by the tree-level matching [116]

$$\begin{aligned} C_{RR}^{311} &= C_{duu}^{311}, \\ C_{RL}^{311} &= C_{duq}^{311}, \\ C_{R\nu}^{311} &= -V_{ud}C_{duq}^{311} - V_{cd}C_{duq}^{312} - V_{td}C_{duq}^{313}. \end{aligned} \quad (8.16)$$

Differently with respect to the case of left-handed b quark WET operators analyzed in Section 8.2.1, here the Wilson coefficients are not correlated to those of light-BNV operators. However this is true only for the matching at dimension-6.

Considering matching at higher orders, the SMEFT operators generating the left-hand sides of (8.16), \mathcal{Q}_{duu}^{311} and \mathcal{Q}_{duq}^{311} , also generate light-BNV WET operators through W -boson exchange. We now show that this happens at dimension-8, hence suppressing the Wilson coefficients by two powers of the expansion parameter of the WET. To estimate parametrically the suppression, we consider one-loop electroweak matching of \mathcal{Q}_{duu}^{311} and \mathcal{Q}_{duq}^{311} to light-BNV operators in the WET, given by the diagrams in Figure 8.2. We want to match an operator with the b quark to operators containing only light quarks, hence we must consider flavour-changing weak interactions. The right-handed b quark from the operator turns into an external up quark with the emission of a W boson, with the weak coupling carrying the CKM matrix element V_{ub}^* . This in turn requires a bottom-mass insertion to turn the b quark left-handed. The W have then to be attached to one of the remaining three fermions from the BNV operator, closing the loop. One of the three attachments is ruled out by charge conservation.

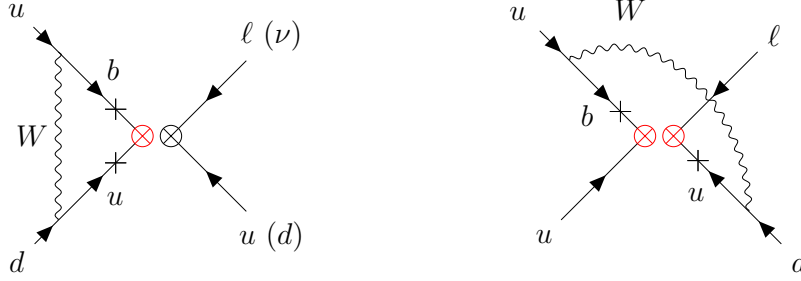


Figure 8.2: Two types of diagrams relevant for the dimension-8 matching of the operators \mathcal{Q}_{duu}^{311} (left and right) and \mathcal{Q}_{duq}^{311} (only left) into light-BNV operators. The red crosses \otimes correspond to right-handed currents, while the black cross \otimes stands for both right- and left-handed ones. Crosses on the propagators stand for mass insertions inducing the chirality flip required to convert the right-handed quarks in the BNV operator to left-handed ones.

In the case of \mathcal{Q}_{duu}^{311} there are two possible diagrams (left and right in Figure 8.2), where the W is attached to one of the two remaining right-handed up quarks in the operator, introducing a second chirality suppression proportional to m_u . The u is hence changed by the weak current into a d , carrying the factor³ V_{ud} . In the case of \mathcal{Q}_{duq}^{311} only the diagram on the left of Figure 8.2 contributes, because if the W couples to the left-handed fermions of the operator the loop integral in the hard region will be odd in the loop momentum and vanish. Summarizing, in all cases the internal right-handed quark legs will bring the factor $m_u m_b / m_W^2$ due to the double chirality flip needed by the weak interaction (depicted as crosses on the propagators in Figure 8.2), showing that it is effectively a dimension-8 matching in the WET counting.

Including CKM and SU(2) coupling factors, the matching coefficient C_i^{EW} of light-BNV operators from \mathcal{Q}_{duq}^{311} and \mathcal{Q}_{duu}^{311} is of the form

$$C_i^{\text{EW}}(\mu) = V_{ud} V_{ub}^* \frac{m_u m_b}{4\pi^2 v^2} F_i\left(\ln \frac{\mu}{m_W}\right) \approx 2 \cdot 10^{-11} F_i\left(\ln \frac{\mu}{m_W}\right), \quad (8.17)$$

where F_i are $\mathcal{O}(1)$ functions and we expressed the SU(2) coupling $g_2^2 = 4m_W^2/v^2$ through the Higgs vev. This parametric suppression, using the results of Section 8.1, leads to constraints of the order

$$\frac{\Lambda_{\text{BNV}}}{\sqrt{|C_{RY}^{311}|}} \gtrsim \sqrt{|C_i^{\text{EW}}|} \cdot 10^{15} \text{ GeV} \gtrsim \mathcal{O}(10^9) \text{ GeV}, \quad Y = L, R, \nu, \quad (8.18)$$

demonstrating that the effective scale of right-handed b -quark BNV can be five to six orders of magnitude below the GUT scale, but still much higher than the new flavour physics scale $\mathcal{O}(\text{TeV})$. In Section 8.3 we will compare such indirect, loop-induced, constraints with the ones coming from the direct computation of tree-level proton decays mediated by the same set of operators.

³Considering the matching into an operator with an s quark instead of d one would only obtain a slightly weaker bound due to the substitution $V_{ud} \rightarrow V_{us}$.

Before moving on we want to quickly investigate the stability of the assumption (8.12) under RG evolution. In other words we want to make sure that the coefficients set to zero do not acquire large values when the renormalization scale $\mu \sim m_W$ is changed for example by a factor of two. We however in practice investigate this point from the SMEFT point of view, as the one-loop evolution is known [115]. Since the Wilson coefficients of the selected WET BNV operators come from the SMEFT coefficients C_{duu}^{311} and C_{duq}^{311} , up to CKM factors according to (8.16), we check the magnitude of the mixing of \mathcal{Q}_{duu}^{311} , \mathcal{Q}_{duq}^{311} into the other SMEFT operators which generate the strongly constrained light-BNV operators Q_{XY}^{111} after matching. We therefore single out the presence of C_{duu}^{311} and C_{duq}^{311} in the RGE of the four first-family BNV Wilson coefficients C_k^{111} ($k = duu, duq, qqu, qqg$), which are the dominant contribution to C_{XY}^{111} . We obtain⁴ [115]

$$\begin{aligned}
\mu \frac{dC_{duu}^{111}}{d\mu} &= \dots, \\
\mu \frac{dC_{duq}^{111}}{d\mu} &= -V_{ud}V_{ub}^* \frac{m_d m_b}{8\pi^2 v^2} C_{duq}^{311} + \dots, \\
\mu \frac{dC_{qqu}^{111}}{d\mu} &= V_{ub}^* \frac{m_\ell m_b}{8\pi^2 v^2} C_{duq}^{311} - 3V_{ub}^* \frac{m_u m_b}{8\pi^2 v^2} C_{duu}^{311} + \dots, \\
\mu \frac{dC_{qqg}^{111}}{d\mu} &= V_{ub}^* \frac{m_u m_b}{2\pi^2 v^2} C_{duq}^{311} + \dots,
\end{aligned} \tag{8.19}$$

where the dots denote the other Wilson coefficients we are not interested in. The parametric suppression is the same as the one for the dimension-8 matching (8.17). As by a small change in the renormalization scale one generates at most a fraction $\mathcal{O}(10^{-11})$ of Wilson coefficients C_{duq}^{311} and C_{duu}^{311} for the light-flavoured operators, the assumption (8.12) is consistent with RG evolution, if the scale of the right-handed b -quark BNV operators is larger than (8.18). Or in other words, as could have been expected, the mixing under renormalization induces bounds on the operators with a right-handed b of the same order as (8.18).

We anyways conclude that among the ones containing a b quark, two first family quarks and a light lepton, the operators (8.15) are the least affected by the light-BNV operator constraints, as the ones with a left-handed b could have a scale lower than (8.9) only by a factor $\sqrt{|V_{td}|}$ or $\sqrt{|V_{ub}|}$.

8.2.3 Operators Including Second Family Quarks

In this section we address the strategies for constraining operators including second family quarks and the right-handed b . Such operators could contribute to BNV B_s/B_c meson decays and B decays to final states with strangeness or charm.

The case of operators with an s field is simple. The only operator with a right-handed b quark and a strange quark is $Q_{R\nu}^{312} = \varepsilon^{abc} [\bar{b}^a P_R u^b] [\tilde{\nu} P_L s^c]$. This operator would mediate

⁴Ref. [115] uses the opposite convention for the Yukawa matrices $Y^d|_{\text{this work}} \rightarrow Y^{d\dagger}|_{\text{Alonso et al.}}$. Therefore in the convention of Ref. [115] the only non-diagonal matrices in flavour space are Y^d , $Y^{d\dagger}$ and $Y^{d\dagger} Y^d$.

the decay $p \rightarrow K^+\bar{\nu}$, as the operator $Q_{R\nu}^{311}$ does for $p \rightarrow \pi^+\bar{\nu}$ in Figure 8.1. However, the experimental constraint (8.11) [125] on $p \rightarrow K^+\bar{\nu}$ is 15 times stronger than the one on $p \rightarrow \pi^+\bar{\nu}$ (8.3) [119]. We can therefore discard this operator as the theoretical calculation follows the same lines as the one for $p \rightarrow \pi^+\bar{\nu}$ which we will present in Section 8.3.2, and focus only on the less constrained $Q_{R\nu}^{311}$, which would allow for larger BNV b -hadron decay rates.

We now focus on charmed operators. The proton is too light to decay into final states with the charm quark. Hence both the b and the c must be virtual, and the dominant constraint will come from electroweak mixing into the dimension-8 WET operators as discussed in Section 8.2.2, where one has to substitute $m_u V_{ud} \rightarrow m_c V_{cd}$. This would imply an enhancement by the factor $V_{cd}m_c/(V_{ud}m_u) \sim 10^2$ in (8.17) which would lead to the constraint $\mathcal{O}(10^{10} \text{ GeV})$ on the scale of these operators. We can conclude that B decays into charmed hadrons are constrained more strongly than those to light hadrons. For this reason we focus only on the operators (8.15) for the rest of this chapter.

8.2.4 Weak Effective Hamiltonian

From the results of Sections 8.2.1, 8.2.2 and 8.2.3 we can finally write down a weak effective Hamiltonian including the relevant BNV operators

$$\mathcal{H}_{\text{BNV}} = \frac{1}{\Lambda_{\text{BNV}}^2} \left(C_L Q_{RL}^{311} + C_R Q_{RR}^{311} + C_\nu Q_{R\nu}^{311} \right) + \text{h.c.}, \quad (8.20)$$

where we renamed the Wilson coefficients for convenience. On the other hand we also have to consider the standard Hamiltonian for semi-leptonic $u \rightarrow b\ell^+\nu_\ell$ and hadronic $u \rightarrow b\bar{u}\bar{d}$ transitions

$$\begin{aligned} \mathcal{H}_W = 4 \frac{G_F}{\sqrt{2}} V_{ub}^* & \left([\bar{b}\gamma^\mu P_L u] [\bar{\nu}_\ell \gamma_\mu P_L \ell] + V_{ud} C_1 [\bar{b}\gamma^\mu P_L T^A u] [\bar{u}\gamma_\mu P_L T^A d] \right. \\ & \left. + V_{ud} C_2 [\bar{b}\gamma^\mu P_L u] [\bar{u}\gamma_\mu P_L d] \right) + \text{h.c.}, \end{aligned} \quad (8.21)$$

responsible for the creation of a virtual b quark in the proton. The quark colour and spinor indices are summed within the squared brackets. Here we consider only the dominant charged-current operators, and neglect the loop-suppressed penguin operators.

8.2.5 Local Six-Fermion Operators

The operators from (8.20) and (8.21) are then evolved to the scale m_b where the virtual b quark in the diagrams of Figure 8.1 is integrated out. The result is in the form of local six-fermion operators

$$\begin{aligned} \mathcal{O}_{\nu,\text{sl}} &= \varepsilon^{abc} [\tilde{u}^a \gamma^\mu P_L u^b] [\tilde{\nu} P_L d^c] [\bar{\nu}_\ell \gamma_\mu P_L \ell], \\ \mathcal{O}_{\nu,1} &= \varepsilon^{abc} [\tilde{u}^a \gamma^\mu P_L T_{bi}^A u^i] [\tilde{\nu} P_L d^c] [\bar{u}^f \gamma_\mu P_L T_{fj}^A d^j], \end{aligned}$$

$$\begin{aligned}
\mathcal{O}_{\nu,2} &= \varepsilon^{abc} [\tilde{u}^a \gamma^\mu P_L u^b] [\tilde{\nu} P_L d^c] [\bar{u}^f \gamma_\mu P_L d^f], \\
\mathcal{O}_{X,1} &= \varepsilon^{abc} [\tilde{u}^a \gamma^\mu P_L T_{bi}^A u^i] [\tilde{\ell} P_X u^c] [\bar{u}^f \gamma_\mu P_L T_{fj}^A d^j], \\
\mathcal{O}_{X,2} &= \varepsilon^{abc} [\tilde{u}^a \gamma^\mu P_L u^b] [\tilde{\ell} P_X u^c] [\bar{u}^f \gamma_\mu P_L d^f],
\end{aligned} \tag{8.22}$$

for the processes $p \rightarrow \ell^+ \nu_\ell \bar{\nu}$, $p \rightarrow \pi^+ \bar{\nu}$ and $p \rightarrow \pi^0 \ell^+$. The subscripts refer to the BNV and weak currents respectively, and $X = L, R$. All the operators have a tree-level matching coefficient $1/m_b$.

As a further simplification, for the colour-singlet current with two up quarks in $\mathcal{O}_{\nu,\text{sl}}$, $\mathcal{O}_{\nu,2}$ and $\mathcal{O}_{X,2}$ only the vectorial part contributes. The term with γ^5 identically vanish due to the identity

$$\varepsilon^{abc} [u^{aT} \mathcal{C} \gamma^\mu P_L u^b] = \varepsilon^{abc} [u^{aT} \mathcal{C} \gamma^\mu P_L u^b]^T = -\varepsilon^{abc} [u^{bT} P_L \gamma^{\mu T} \mathcal{C}^T u^a] = \varepsilon^{abc} [u^{aT} \mathcal{C} \gamma^\mu P_R u^b]. \tag{8.23}$$

We therefore write the final Hamiltonian relevant for the three processes of interest as

$$\mathcal{H}_{6f} = \mathcal{H}_{p \rightarrow \ell^+ \nu_\ell \bar{\nu}} + \mathcal{H}_{p \rightarrow \pi^+ \bar{\nu}} + \mathcal{H}_{p \rightarrow \pi^0 \ell^+}, \tag{8.24}$$

with

$$\begin{aligned}
\mathcal{H}_{p \rightarrow \ell^+ \nu_\ell \bar{\nu}} &= -2\sqrt{2} \frac{G_F C_\nu V_{ub}^*}{m_b \Lambda_{\text{BNV}}^2} \mathcal{O}_{\nu,\text{sl}} + \text{h.c.}, \\
\mathcal{H}_{p \rightarrow \pi^+ \bar{\nu}} &= -2\sqrt{2} \frac{G_F C_\nu V_{ub}^* V_{ud}}{m_b \Lambda_{\text{BNV}}^2} (C_1 \mathcal{O}_{\nu,1} + C_2 \mathcal{O}_{\nu,2}) + \text{h.c.}, \\
\mathcal{H}_{p \rightarrow \pi^0 \ell^+} &= -2\sqrt{2} \frac{G_F V_{ub}^* V_{ud}}{m_b \Lambda_{\text{BNV}}^2} \sum_{X=L,R} C_X (C_1 \mathcal{O}_{X,1} + C_2 \mathcal{O}_{X,2}) + \text{h.c.}
\end{aligned} \tag{8.25}$$

8.3 Proton Decay Rate

The standard formula to compute the decay rate in the proton rest frame is

$$\Gamma(p \rightarrow f) = \frac{1}{2m_p} \int d\Pi_{\text{LIPS}} \frac{1}{2} \sum_{\text{spins}} |\langle f | \mathcal{H}_{6f} | p \rangle|^2, \tag{8.26}$$

for a generic final state f , while the factor $1/2$ is for averaging over the proton spin orientations. The Lorentz-invariant phase space is

$$d\Pi_{\text{LIPS}} = (2\pi)^4 \delta^4 \left(p_{in} - \sum_{\text{final } j} p_j \right) \prod_{\text{final } j} \frac{d^4 p_j}{(2\pi)^3} \delta(p_j^2 - m_j^2) \theta(p_j^0). \tag{8.27}$$

For later convenience we summarize here the parametrizations of the relevant hadronic matrix elements, where all the fields are evaluated at $x = 0$ and the spinor indices α, β, γ are uncontracted:

$$\delta^{ab} \Pi_{\beta\alpha}(p) \equiv \langle \pi^+(p) | \bar{u}_\alpha^a d_\beta^b | 0 \rangle = \frac{i}{4N_c} \delta^{ab} f_\pi (\not{p} \gamma^5 - \mu_\pi \gamma^5)_{\beta\alpha},$$

$$\begin{aligned}
G_{\alpha\beta\gamma}(p) &\equiv \langle 0 | \varepsilon^{abc} \tilde{u}_\alpha^a u_\beta^b d_\gamma^c | p(p) \rangle = -\frac{f_p}{4} \left(\not{p}_{\beta\alpha} [\gamma^5 u_p(p)]_\gamma + i p^\nu [\sigma_{\rho\nu}]_{\beta\alpha} [\gamma^\rho \gamma^5 u_p(p)]_\gamma \right) \\
&+ \frac{m_p}{16} (\lambda_1 - f_p) [\gamma_\rho]_{\beta\alpha} [\gamma^\rho \gamma^5 u_p(p)]_\gamma + \frac{m_p}{96} (\lambda_2 - 6f_p) [\sigma_{\rho\sigma}]_{\beta\alpha} [\sigma^{\rho\sigma} \gamma^5 u_p(p)]_\gamma. \quad (8.28)
\end{aligned}$$

The proton spinor is denoted with $u_p(p)$, and the derivation of (8.28) can be found in Appendix D. The matrix elements are determined with three non-perturbative parameters for the proton and the pion decay constant, together with

$$\mu_\pi = \frac{m_\pi^2}{m_u + m_d}. \quad (8.29)$$

The proton decay constants f_p , λ_1 and λ_2 numerical values are summarized in Appendix A, and for later convenience we define

$$\Omega_p \equiv \frac{1}{4} (\lambda_1 - f_p). \quad (8.30)$$

8.3.1 Leptonic Decay: $p \rightarrow \ell^+ \nu_\ell \bar{\nu}$

In the case of the leptonic three-body decay the formula (8.26) becomes

$$\Gamma(p \rightarrow \ell^+ \nu_\ell \bar{\nu}) = \frac{4G_F^2 |V_{ub}|^2 |C_\nu|^2}{m_p m_b^2 \Lambda_{\text{BNV}}^4} \int d\Pi_{\text{LIPS}} \frac{1}{2} \sum_{\text{spins}} |\langle \ell^+ \nu_\ell \bar{\nu} | \mathcal{O}_{\nu,\text{sl}} | p \rangle|^2. \quad (8.31)$$

We split the six-fermion operator in hadronic and leptonic parts as

$$\mathcal{O}_{\nu,\text{sl}} = \frac{1}{2} [\bar{\nu}_\ell \gamma_\mu P_L \ell] [\bar{\nu} P_L]_\alpha [\mathcal{O}_q^\mu]_\alpha, \quad \mathcal{O}_{\nu,\text{sl}}^\dagger = \frac{1}{2} [\bar{\ell} \gamma_\nu P_L \nu_\ell] [\bar{\mathcal{O}}_q^\nu]_\beta [P_R \nu^c]_\beta, \quad (8.32)$$

where we used (8.23) to write the hadronic parts as

$$\mathcal{O}_q^\mu = \varepsilon^{abg} [\tilde{u}^a \gamma^\mu u^b] d^g, \quad \bar{\mathcal{O}}_q^\nu = \varepsilon^{abg} [\bar{u}^b \gamma^\nu (u^c)^a] \bar{d}^g. \quad (8.33)$$

The matrix element squared reduces then to

$$\frac{1}{2} \sum_{\text{spins}} |\langle \ell^+ \nu_\ell \bar{\nu} | \mathcal{O}_{\nu,\text{sl}} | p \rangle|^2 = \frac{1}{4} L_{\mu\nu} \sum_p \text{Tr} \left[\langle 0 | \mathcal{O}_q^\mu | p \rangle \langle p | \bar{\mathcal{O}}_q^\nu | 0 \rangle \not{q} P_L \right], \quad (8.34)$$

where q is the momentum of the anti-neutrino $\bar{\nu}$. The leptonic tensor from the lepton pair $\nu_\ell(p_n) \ell^+(p_\ell)$ is

$$L^{\mu\nu} = p_\ell^\mu p_n^\nu - p_\ell \cdot p_n g^{\mu\nu} + p_\ell^\nu p_n^\mu + i \varepsilon^{\mu\nu\alpha\beta} p_{\ell\alpha} p_{n\beta}. \quad (8.35)$$

Finally the hadronic matrix element, using (8.28), can be written as

$$\langle 0 | \mathcal{O}_q^\mu | p(p) \rangle = -f_p p^\mu [\gamma^5 u_p(p)] + m_p \Omega_p [\gamma^\mu \gamma^5 u_p(p)]. \quad (8.36)$$

Carrying out the contraction with the leptonic tensor we find for the six-fermion operator matrix element (8.34)

$$\frac{1}{2} \sum_{\text{spins}} |\langle \ell^+(p_\ell) \nu_\ell(p_n) \bar{\nu}(q) | \mathcal{O}_{\nu,sl} | p(p) \rangle|^2 = m_p^6 \left[\hat{\mathcal{M}}_{ff} f_p^2 + \hat{\mathcal{M}}_{f\Omega} f_p \Omega_p + \hat{\mathcal{M}}_{\Omega\Omega} \Omega_p^2 \right], \quad (8.37)$$

with coefficient functions

$$\begin{aligned} \hat{\mathcal{M}}_{ff} &= \frac{1}{2} \hat{E}_q (2\hat{E}_\ell \hat{E}_n - \hat{p}_\ell \cdot \hat{p}_n), \\ \hat{\mathcal{M}}_{f\Omega} &= \hat{E}_\ell \hat{q} \cdot \hat{p}_n + \hat{E}_n \hat{q} \cdot \hat{p}_\ell - \hat{E}_q \hat{p}_\ell \cdot \hat{p}_n, \\ \hat{\mathcal{M}}_{\Omega\Omega} &= 2\hat{E}_n \hat{q} \cdot \hat{p}_\ell, \end{aligned} \quad (8.38)$$

where we used the fact that we are in the proton rest frame ($p = (m_p, 0, 0, 0)$). In this chapter hatted variables refer to the quantities normalized by appropriate powers of the proton mass: $\hat{E}_\ell = E_\ell/m_p$, $\hat{E}_n = E_n/m_p$ and $\hat{E}_q = E_q/m_p$ for the charged lepton, neutrino and anti-neutrino energies, respectively. Later we will also use $\hat{m}_\ell = m_\ell/m_p$ and $\hat{m}_\pi = m_\pi/m_p$.

The Lorentz invariant phase-space integration can be reduced to a two-dimensional integration over the charged lepton and anti-neutrino energies

$$\begin{aligned} \int d\Pi_{\text{LIPS}} &= \frac{1}{4(2\pi)^3} \int_0^\infty dE_q \int_{m_\ell}^\infty dE_\ell \theta\left(m_p - E_\ell - E_q - |E_q - \sqrt{E_\ell^2 - m_\ell^2}|\right) \\ &\quad \times \theta\left(2E_q + E_\ell + \sqrt{E_\ell^2 - m_\ell^2} - m_p\right). \end{aligned} \quad (8.39)$$

The resulting integrated decay rate is

$$\begin{aligned} \Gamma(p \rightarrow \ell^+ \nu_\ell \bar{\nu}) &= |V_{ub}|^2 |C_\nu|^2 \frac{G_F^2 m_p^7}{7680 \pi^3 m_b^2 \Lambda_{\text{BNV}}^4} \\ &\quad \times \left[(1 - \hat{m}_\ell^2)^5 f_p^2 + \frac{5}{8} (1 - 8\hat{m}_\ell^2 + 8\hat{m}_\ell^6 - \hat{m}_\ell^8 - 24\hat{m}_\ell^4 \ln \hat{m}_\ell) (\lambda_1^2 - f_p^2) \right]. \end{aligned} \quad (8.40)$$

As anticipated, for the proton decay constants we use the numerical values evolved to 1 GeV reported in Appendix A, together with the other numerical inputs. Converting the experimental limits on the partial lifetimes $\tau_{p \rightarrow e^+ \nu e \bar{\nu}}$, $\tau_{p \rightarrow \mu^+ \nu \mu \bar{\nu}}$ from (8.3) we then obtain the following lower limits on the BNV scale

$$\begin{aligned} \frac{\Lambda_{\text{BNV}}}{\sqrt{|C_\nu|}} \Big|_{p \rightarrow e^+ \nu e \bar{\nu}} &> 6.59 \cdot 10^9 \text{ GeV}, \\ \frac{\Lambda_{\text{BNV}}}{\sqrt{|C_\nu|}} \Big|_{p \rightarrow \mu^+ \nu \mu \bar{\nu}} &> 6.86 \cdot 10^9 \text{ GeV}. \end{aligned} \quad (8.41)$$

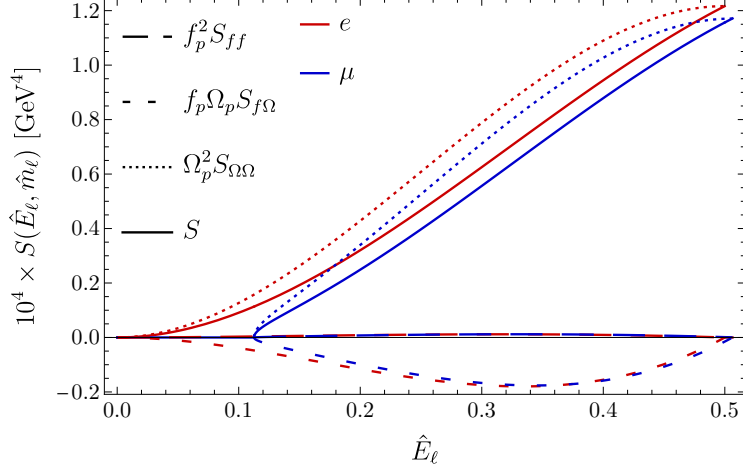


Figure 8.3: Lepton energy spectrum (solid) for an electron (red) or a muon (blue) in the final state. Different dashed lines represent the three separate contributions of (8.43) weighted by their prefactors.

We can study the spectrum in the lepton energy by integrating only over the anti-neutrino energy E_q ,

$$\begin{aligned}
\frac{d\Gamma}{d\hat{E}_\ell} &= |V_{ub}|^2 |C_\nu|^2 \frac{G_F^2 m_p^7}{(2\pi)^3 \Lambda_{\text{BNV}}^4 m_b^2} \int_0^\infty d\hat{E}_q \left[\hat{\mathcal{M}}_{ff} f_p^2 + \hat{\mathcal{M}}_{f\Omega} f_p \Omega_p + \hat{\mathcal{M}}_{\Omega\Omega} \Omega_p^2 \right] \\
&\quad \times \theta \left(1 - \hat{E}_\ell - \hat{E}_q - \left| \hat{E}_q - \sqrt{\hat{E}_\ell^2 - \hat{m}_\ell^2} \right| \right) \theta \left(2\hat{E}_q + \hat{E}_\ell + \sqrt{\hat{E}_\ell^2 - \hat{m}_\ell^2} - 1 \right) \\
&= |V_{ub}|^2 |C_\nu|^2 \frac{G_F^2 m_p^7}{192\pi^3 \Lambda_{\text{BNV}}^4 m_b^2} \theta(\hat{E}_\ell - \hat{m}_\ell) \theta \left(\frac{1 + \hat{m}_\ell^2}{2} - \hat{E}_\ell \right) \\
&\quad \times \left[S_{ff}(\hat{E}_\ell, \hat{m}_\ell) f_p^2 + S_{f\Omega}(\hat{E}_\ell, \hat{m}_\ell) f_p \Omega_p + S_{\Omega\Omega}(\hat{E}_\ell, \hat{m}_\ell) \Omega_p^2 \right], \tag{8.42}
\end{aligned}$$

with functions $S_{ij}(\hat{E}_\ell, \hat{m}_\ell)$ given by

$$\begin{aligned}
S_{ff}(\hat{E}_\ell, \hat{m}_\ell) &= \sqrt{\hat{E}_\ell^2 - \hat{m}_\ell^2} \left(4\hat{E}_\ell^3 - 8\hat{E}_\ell^2 + \hat{E}_\ell (3 - \hat{m}_\ell^2) + 2\hat{m}_\ell^2 \right), \\
S_{f\Omega}(\hat{E}_\ell, \hat{m}_\ell) &= 12\hat{E}_\ell \sqrt{\hat{E}_\ell^2 - \hat{m}_\ell^2} (1 - 2\hat{E}_\ell + \hat{m}_\ell^2), \\
S_{\Omega\Omega}(\hat{E}_\ell, \hat{m}_\ell) &= 4\sqrt{\hat{E}_\ell^2 - \hat{m}_\ell^2} \left(3\hat{E}_\ell (1 + \hat{m}_\ell^2) - 4\hat{E}_\ell^2 - 2\hat{m}_\ell^2 \right). \tag{8.43}
\end{aligned}$$

The lepton energy spectra

$$S(\hat{E}_\ell, \hat{m}_\ell) \equiv \left[S_{ff}(\hat{E}_\ell, \hat{m}_\ell) f_p^2 + S_{f\Omega}(\hat{E}_\ell, \hat{m}_\ell) f_p \Omega_p + S_{\Omega\Omega}(\hat{E}_\ell, \hat{m}_\ell) \Omega_p^2 \right], \tag{8.44}$$

for the electron and muon are displayed with solid lines in Figure 8.3, while the three terms separately in dashed. The term proportional to Ω_p^2 dominates over the others, as one could expect from the numerical values of the proton decay constants.

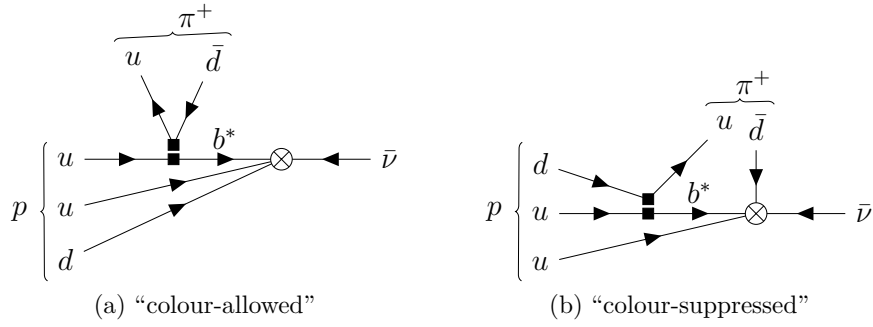


Figure 8.4: Factorizable tree topologies contributing to $p \rightarrow \pi^+ \bar{\nu}$. The virtual b -quark propagator is integrated out but displayed for clarity. For $p \rightarrow \pi^0 \ell^+$ the colour-allowed topology is absent.

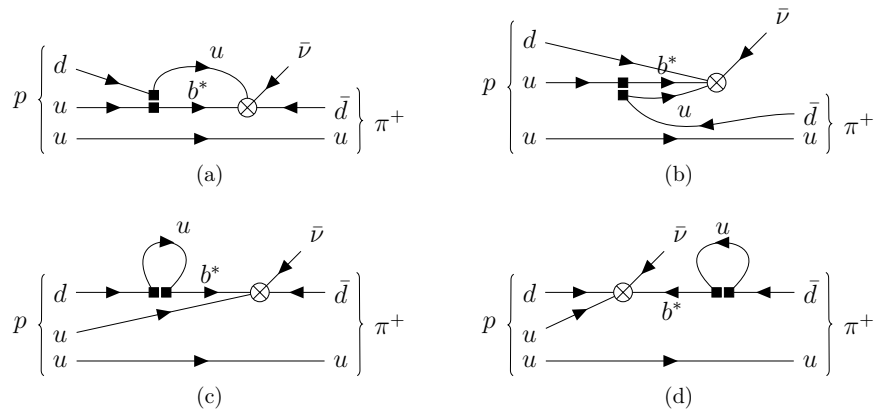


Figure 8.5: Non-factorizable contributions to $p \rightarrow \pi^+ \bar{\nu}$. The virtual b -quark propagator is integrated out but displayed for clarity. Identical topologies exist for the $p \rightarrow \pi^0 \ell^+$ with appropriate substitutions.

8.3.2 Two-Body Decay: $p \rightarrow \pi^+ \bar{\nu}$

We now focus on the two-body proton decay into a charged pion and an anti-neutrino, with the relevant Feynman diagrams displayed in Figure 8.4. With respect to the leptonic decay of Section 8.3.1 the calculation of the hadronic matrix element here is more complicated as it involves an additional hadron in the final state. Since we are basically interested in the order of magnitude of such contributions, we adopt the naive factorization approximation, neglecting soft-gluon exchanges between the pion and the proton constituents. For proton decays the factorization assumption receives $\mathcal{O}(1)$ corrections, differently with respect to the case of heavy hadrons considered in the previous parts of this thesis. Under this assumption the matrix element will be expressed in terms of the proton and pion decay constants.

There are however four “non-factorizable” loop diagrams, displayed in Figure 8.5, on top of the two factorizable contributions of Figure 8.4. In this case one would have to parametrize the matrix element in terms of a BNV proton to pion form factor. However diagrams (c) and (d) are identically zero because the loop integrand is odd in the loop momentum. The remaining first two diagrams are proportional to the up-quark mass, and

hence parametrically of the same order of the dimension-8 contributions (8.17). In the end we are then allowed to consider the two factorizable diagrams of Figure 8.4, as the loop-level ones would give at most a bound of the same order as (8.18).

From (8.26) the decay rate reads

$$\Gamma(p \rightarrow \pi^+ \bar{\nu}) = \frac{4G_F^2 |V_{ub}|^2 |V_{ud}|^2 |C_\nu|^2}{m_p m_b^2 \Lambda_{\text{BNV}}^4} \int d\Pi_{\text{LIPS}} \frac{1}{2} \sum_{\text{spins}} |\langle \pi^+ \bar{\nu} | C_1 \mathcal{O}_{\nu,1} + C_2 \mathcal{O}_{\nu,2} | p \rangle|^2. \quad (8.45)$$

The two diagrams contributing to the matrix element of the operator $\mathcal{O}_{\nu,2}$ can be computed simultaneously by using (8.28)

$$\begin{aligned} \langle \pi^+(p_\pi) \bar{\nu}(q) | \mathcal{O}_{\nu,2} | p(p) \rangle &= \frac{1}{2} [v^T(q) \mathcal{C} P_L]_\gamma \left\{ N_c G_{\alpha\beta\gamma}(p) [\gamma^\mu]_{\alpha\beta} \text{Tr}[\Pi(p_\pi) \gamma_\mu P_L] \right. \\ &\quad \left. - G_{\alpha\beta\rho}(p) [\gamma^\mu]_{\alpha\beta} [\Pi(p_\pi) \gamma_\mu P_L]_{\gamma\rho} \right\} \\ &= \frac{i}{8N_c} m_p^2 f_\pi \left\{ (2N_c \hat{E}_\pi - 1) f_p + (2N_c - 4) \Omega_p \right\} [v^T(q) \mathcal{C} P_L u_p(p)], \end{aligned} \quad (8.46)$$

where again $\hat{E}_\pi = E_\pi/m_p$ is the normalized pion energy in the proton rest frame. The matrix element of the colour-octet operator $\mathcal{O}_{\nu,1}$ receives contribution only from the ‘‘colour-suppressed’’ topology (as the ‘‘color-allowed’’ vanishes for colour algebra), giving

$$\begin{aligned} \langle \pi^+(p_\pi) \bar{\nu}(q) | \mathcal{O}_{\nu,1} | p(p) \rangle &= \frac{N_c + 1}{4N_c} [v^T(q) \mathcal{C} P_L]_\gamma \left\{ G_{\alpha\beta\rho}(p) [\gamma^\mu (1 - \gamma^5)]_{\alpha\beta} [\Pi(p_\pi) \gamma_\mu P_L]_{\gamma\rho} \right\} \\ &= \frac{N_c + 1}{4N_c^2} \frac{i}{4} m_p^2 f_\pi^2 (f_p + 4\Omega_p) [v^T(q) \mathcal{C} P_L u_p(p)]. \end{aligned} \quad (8.47)$$

We use

$$\begin{aligned} \sum_{\text{spins}} |v^T(q) \mathcal{C} P_L u_p(p)|^2 &= \sum_{\text{spins}} \text{Tr}[\mathcal{C}(v(q) \bar{\nu}(q))^T \mathcal{C} P_L u_p(p) \bar{u}_p(p) P_R] \\ &= \text{Tr}[\not{q} P_L (\not{p} + m_p) P_R] = 2m_p^2 \hat{E}_q = m_p^2 (1 - \hat{m}_\pi^2) \end{aligned} \quad (8.48)$$

when squaring the matrix element and summing over the spins. The result for the matrix element square is

$$\begin{aligned} \frac{1}{2} \sum_{\text{spins}} |\langle \pi^+ \bar{\nu} | C_1 \mathcal{O}_{\nu,1} + C_2 \mathcal{O}_{\nu,2} | p \rangle|^2 &= \frac{m_p^6}{64N_c^2} f_\pi^2 \hat{E}_q \left\{ C_2 \left[(2N_c \hat{E}_\pi - 1) f_p + (2N_c - 4) \Omega_p \right] \right. \\ &\quad \left. + C_1 \frac{N_c + 1}{2N_c} (f_p + 4\Omega_p) \right\}^2. \end{aligned} \quad (8.49)$$

Including the standard two-body phase-space integral

$$\int d\Pi_{\text{LIPS}} = \frac{1}{8\pi} (1 - \hat{m}_\pi^2), \quad (8.50)$$

we get from (8.45)

$$\begin{aligned} \Gamma(p \rightarrow \pi^+ \bar{\nu}) &= |V_{ud}|^2 |V_{ub}|^2 |C_\nu|^2 \frac{G_F^2 m_p^5 f_\pi^2}{1024 \pi m_b^2 \Lambda_{\text{BNV}}^4} (1 - \hat{m}_\pi^2)^2 \\ &\times \left[\left((1 + 2\hat{m}_\pi^2) f_p + \frac{\lambda_1}{3} \right) C_2 + \frac{4}{9} \lambda_1 C_1 \right]^2. \end{aligned} \quad (8.51)$$

The WET Wilson coefficients C_1 and C_2 are evaluated at the scale 1 GeV with two-loop running [40], as reported in Appendix A. We finally get the bound

$$\left. \frac{\Lambda_{\text{BNV}}}{\sqrt{|C_\nu|}} \right|_{p \rightarrow \pi^+ \bar{\nu}} > 3.34 \cdot 10^9 \text{ GeV} \quad (8.52)$$

on the third-generation BNV scale. Notice that the leptonic decay is sensitive to the same WET operator $Q_{R\nu}^{311}$ and provides a stronger bound (8.41), although the value (8.52) has to be seen as an order of magnitude since it is affected by $\mathcal{O}(1)$ non-factorizable contributions.

8.3.3 Two-Body Decay: $p \rightarrow \pi^0 \ell^+$

The last process we investigate is the two-body decay of a proton into a neutral pion and a charged lepton. This process is interesting as it is subject to the most stringent experimental constraints on proton decays [118]. The decay rate

$$\Gamma(p \rightarrow \pi^0 \ell^+) = \frac{4G_F^2 |V_{ub}|^2 |V_{ud}|^2}{m_p m_b^2 \Lambda_{\text{BNV}}^4} \int d\Pi_{\text{LIPS}} \frac{1}{2} \sum_{\text{spins}} \left| \sum_{X=L,R} \sum_{i=1,2} C_X C_i \langle \pi^0 \ell^+ | \mathcal{O}_{X,i} | p \rangle \right|^2 \quad (8.53)$$

is now sensitive to two BNV operators, different from the one contributing to $p \rightarrow \ell^+ \nu_\ell \bar{\nu}$ and $p \rightarrow \pi^+ \bar{\nu}$. Now the phase-space factor with two massive particles is

$$\int d\Pi_{\text{LIPS}} = \frac{1}{8\pi} \sqrt{(1 - \hat{m}_\pi^2)^2 - 2\hat{m}_\ell^2(1 + \hat{m}_\pi^2) + \hat{m}_\ell^4}. \quad (8.54)$$

The six-fermion operators matrix elements are given by

$$\begin{aligned} \langle \pi^0(p_\pi) \ell^+(q) | \mathcal{O}_{X,2} | p(p) \rangle &= -\frac{1}{2\sqrt{2}} \left\{ [v^T(q) \mathcal{C} P_X \Pi(p_\pi) \gamma_\mu P_L]_\gamma G_{\alpha\beta\gamma}(p) [\gamma^\mu]_{\alpha\beta} \right. \\ &\quad \left. + 2[v^T(q) \mathcal{C} P_X]_\delta G_{\alpha\delta\gamma}(p) [\gamma^\mu \Pi(p_\pi) \gamma_\mu P_L]_{\alpha\gamma} \right\} \\ &= \frac{i}{16\sqrt{2} N_c} m_p^2 f_\pi \left[A_2^{XL} M_L + A_2^{XR} M_R \right], \end{aligned} \quad (8.55)$$

and

$$\langle \pi^0(p_\pi) \ell^+(q) | \mathcal{O}_{X,1} | p(p) \rangle = \frac{1}{3\sqrt{2}} \left\{ [v^T(q) \mathcal{C} P_X \Pi(p_\pi) \gamma_\mu P_L]_\gamma G_{\alpha\beta\gamma}(p) [\gamma^\mu]_{\alpha\beta} \right.$$

$$\begin{aligned}
& + 2[v^T(q)\mathcal{C}P_X]_\delta G_{\alpha\delta\gamma}(p)[\gamma^\mu(P_R - 2P_L)\Pi(p_\pi)\gamma_\mu P_L]_{\alpha\gamma} \Big\} \\
& = \frac{i}{16\sqrt{2}N_c} m_p^2 f_\pi \left[A_1^{XL} M_L + A_1^{XR} M_R \right]. \tag{8.56}
\end{aligned}$$

The factor $1/\sqrt{2}$ is coming from the π^0 flavour wave-function normalization. We defined the real coefficient functions A_i^{XY} of mass dimension 2, which depend on \hat{m}_π , \hat{m}_ℓ , $\hat{\mu}_\pi$, and the three proton decay constants. They are given by

$$\begin{aligned}
A_1^{XL} &= \frac{4}{3} \left[(f_p (1 - 2\hat{m}_\ell^2 + 2\hat{m}_\pi^2) + \lambda_2 \hat{\mu}_\pi) \delta_{XL} + 2f_p \hat{m}_\ell \delta_{XR} \right], \\
A_1^{XR} &= \frac{4}{3} \left[f_p \hat{m}_\ell \delta_{XL} + (2f_p (1 - 2\hat{m}_\ell^2 + 2\hat{m}_\pi^2) - 3\lambda_1 \hat{\mu}_\pi) \delta_{XR} \right], \\
A_2^{XL} &= (f_p (1 - 2\hat{m}_\ell^2 + 2\hat{m}_\pi^2) - 3\lambda_1 - 2\lambda_2 \hat{\mu}_\pi) \delta_{XL} + 2f_p \hat{m}_\ell \delta_{XR}, \\
A_2^{XR} &= (2f_p (1 - 2\hat{m}_\ell^2 + 2\hat{m}_\pi^2) + 6\lambda_1 \hat{\mu}_\pi) \delta_{XR} + (f_p \hat{m}_\ell + 3\lambda_1 \hat{m}_\ell) \delta_{XL}. \tag{8.57}
\end{aligned}$$

For simplicity, we also defined

$$M_X \equiv [v^T(q)\mathcal{C}P_X u_p(p)]. \tag{8.58}$$

The sum over the proton and lepton spins gives

$$\begin{aligned}
\frac{1}{2} \sum_{\text{spins}} M_L^\dagger M_L &= \frac{1}{2} \sum_{\text{spins}} M_R^\dagger M_R = m_p^2 \hat{E}_\ell, \\
\frac{1}{2} \sum_{\text{spins}} M_L^\dagger M_R &= \frac{1}{2} \sum_{\text{spins}} M_R^\dagger M_L = m_p^2 \hat{m}_\ell, \tag{8.59}
\end{aligned}$$

where $\hat{E}_\ell = (1 - \hat{m}_\pi^2 + \hat{m}_\ell^2)/2$ is the lepton energy in the proton rest frame, normalized by the proton mass.

From (8.53) we get

$$\begin{aligned}
\Gamma(p \rightarrow \pi^0 \ell^+) &= \frac{G_F^2 |V_{ub}|^2 |V_{ud}|^2 f_\pi^2 m_p^5}{9216 \pi m_b^2 \Lambda_{\text{BNV}}^4} \sqrt{(1 - \hat{m}_\pi^2)^2 - 2\hat{m}_\ell^2(1 + \hat{m}_\pi^2) + \hat{m}_\ell^4} \sum_{X,Y=L,R} C_X C_Y^* \\
&\times \sum_{i,j=1,2} C_i C_j \left[(A_i^{XL} A_j^{YL} + A_i^{XR} A_j^{YR}) \hat{E}_\ell + (A_i^{XR} A_j^{YL} + A_i^{XL} A_j^{YR}) \hat{m}_\ell \right]. \tag{8.60}
\end{aligned}$$

For the bounds on Λ_{BNV} , after inserting out numerical inputs⁵, we obtain

$$\Lambda_{\text{BNV}} \Big|_{p \rightarrow \pi^0 e^+} > 6.23 \cdot 10^{10} \text{ GeV} \left(|C_R^e|^2 + 0.0014 \text{Re}[C_L^{e*} C_R^e] + 0.304 |C_L^e|^2 \right)^{1/4},$$

⁵Notice that the numerical results slightly differ from Ref. [30] where a different value for the π^0 mass was used.

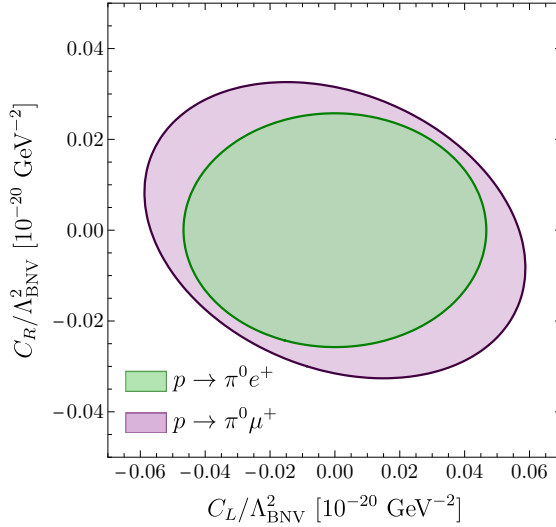


Figure 8.6: Allowed regions for the Wilson coefficients C_L and C_R setting the reference value $\Lambda_{\text{BNV}} = 10^{10}$ GeV. In green the $p \rightarrow \pi^0 e^+$ constraint and in purple the $p \rightarrow \pi^0 \mu^+$ constraint.

$$\Lambda_{\text{BNV}} \Big|_{p \rightarrow \pi^0 \mu^+} > 5.63 \cdot 10^{10} \text{ GeV} \left(|C_R^\mu|^2 + 0.283 \text{Re}[C_L^{\mu*} C_R^\mu] + 0.308 |C_L^\mu|^2 \right)^{1/4}, \quad (8.61)$$

where the lepton-flavour dependence of the Wilson coefficients has been made explicit. Assuming real Wilson coefficients, the results of (8.61) are shown in the C_L - C_R plane in Figure 8.6 as allowed regions in units of $(10^{10} \text{ GeV})^{-2}$. As expected from (8.3), these bounds are stronger by an order of magnitude with respect to the ones on C_ν (8.41) and (8.52). We can therefore state that C_ν is the largest BNV Wilson coefficient (for the light leptons, e and μ) allowed by proton lifetime limits.

8.3.4 Estimate of τ Mediated $p \rightarrow \ell^+ \nu_\ell \bar{\nu}_\tau$ Decay

At the beginning of Section 8.2 we mentioned the fact that operators with τ leptons need a separate treatment. In particular such operators are interesting since they would induce BNV B decays into final states with the τ . For this reason we have to consider constraints from proton decay on the BNV operators (8.15) involving b and τ . On the other hand, experimentally detecting τ leptons is a more complicated task than detecting light leptons, severely reducing the efficiency and precision in such searches. For this reason we only provide here a simple estimate for constraining such operators.

An efficient way of estimating the constraints on these operators is to use the light-BNV operators with a τ generated from the dimension-8 electroweak matching to WET operators discussed in Section 8.2.2. For clarity the process is shown in Figure 8.7, with all the propagators not contracted. This in practice means that we consider a light-BNV operator with a τ and coefficient given by the product of C_{RX}^{3113} and the matching coefficient (8.17). Then, by integrating out the virtual τ propagator, we compute the decay rate of $p \rightarrow \ell^+ \nu_\ell \bar{\nu}_\tau$ as a matrix element of a local six-fermion operator. This six-fermion operator has a different

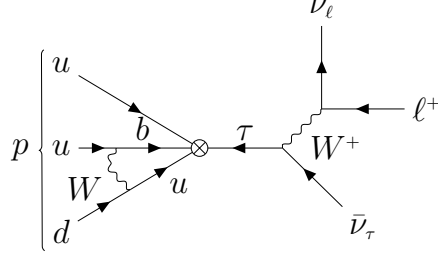


Figure 8.7: Proton decay $p \rightarrow \ell^+ \nu_\ell \bar{\nu}_\tau$ mediated by a Q_{RX}^{3113} operator and a virtual τ lepton. The W propagators and the loop are effectively integrated out in the WET, but displayed for clarity.

Exp. constraint	C	$\Lambda_{\text{BNV}}/\sqrt{ C }$ [10^9 GeV]
dim-8 matching	C_Y	$> \mathcal{O}(1)$
$p \rightarrow e^+ \nu_e \bar{\nu}$	C_ν	> 6.59
$p \rightarrow \mu^+ \nu_\mu \bar{\nu}$	C_ν	> 6.86
$p \rightarrow \pi^+ \bar{\nu}$	C_ν	> 3.34
$p \rightarrow \pi^0 e^+$	C_R^e	> 62.3
$p \rightarrow \pi^0 e^+$	C_L^e	> 46.3
$p \rightarrow \pi^0 \mu^+$	C_R^μ	> 56.3
$p \rightarrow \pi^0 \mu^+$	C_L^μ	> 42.0
$p \rightarrow \ell^+ \nu_\ell \bar{\nu}_\tau$	C_{RX}^{3113}	$> (0.4 \div 1.8) \cdot 10^{-3}$

Table 8.1: Summary of limits on the scale of right-handed BNV operators containing a b quark, assuming single operator dominance, with $Y = L, R, \nu$ and $X = L, R$.

Dirac structure from $\mathcal{O}_{\nu,sl}$ in (8.22), since the diagrams in Figure 8.7 and Figure 8.1 (left) have a different ordering of the BNV and weak vertex. The computation, with the exception of the hadronic matrix element, follows the same steps as above for the leptonic decay, with the virtual b propagator $1/m_b$ replaced by the virtual τ propagator $m_\tau/(m_\tau^2 - m_p^2)$ where we keep the proton mass since $m_p \ll m_\tau$ is not a very good numerical approximation.

Therefore the constraint on C_{RX}^{3113} can be estimated by multiplying the bound (8.41) by the dimension-8 matching factor (8.17) (except for V_{ub} which is already present in the weak effective Hamiltonian for the leptonic decay) and by the propagator ratio $m_b m_\tau/(m_\tau^2 - m_p^2)$. We allow for an uncertainty factor $(0.2 \div 4)$ to account for the uncomputed $\mathcal{O}(1)$ function in C_i^{EW} and the different hadronic matrix element. The estimate gives

$$\frac{\Lambda_{\text{BNV}}}{\sqrt{|C_{RX}^{3113}|}} \approx \left((0.2 \div 4) \frac{|V_{ud}| m_b^2 m_u m_\tau}{4\pi^2 v^2 (m_\tau^2 - m_p^2)} \right)^{1/2} \frac{\Lambda_{\text{BNV}}}{\sqrt{|C_\nu|}} \Big|_{p \rightarrow \ell^+ \nu_\ell \bar{\nu}_\tau} \gtrsim (0.4 \div 1.8) \cdot 10^6 \text{ GeV}, \quad (8.62)$$

which we can now use to estimate the magnitude of BNV B decays into τ final states.

8.4 Inclusive BNV B Decays Estimates

With the results of the previous sections, summarized in Table 8.1, we are now able to estimate the magnitude of BNV B decays. The BaBar [126] and LHCb [127] collaborations have already performed direct searches for exclusive two-body B decays into a baryon and a lepton. The resulting experimental upper bounds on the investigated branching ratios are of about 10^{-9} , which with further studies could in principle improve by a few orders of magnitude.

On the other hand, inclusive decays of b -hadrons could also be studied experimentally, since they offer the clear signature of a single charge lepton in the final state. What makes these channels potentially interesting is that by tagging a baryon in the final state, there is a kinematical window of lepton energy E_ℓ at the higher end of the spectrum allowed only by BNV decays

$$\frac{m_B}{2} \left(1 + \frac{m_\ell^2 - 4m_N^2}{m_B^2} \right) \leq E_\ell \leq \frac{m_B}{2} \left(1 + \frac{m_\ell^2 - m_N^2}{m_B^2} \right), \quad (8.63)$$

where m_N is the mass of the lightest baryon in the final state. This is due to the fact that a baryon-number conserving decay would always need a baryon and an anti-baryon in the final state. The width of such window

$$\Delta E_\ell|_{\text{BNV}} = \frac{3m_N^2}{2m_B} \approx 250 \text{ MeV} \quad (8.64)$$

is quite large, potentially increasing the experimental sensitivity.

A rough estimate of the branching ratio of the inclusive process $\bar{B} \rightarrow X\ell$, can be performed through

$$\Gamma(\bar{B} \rightarrow X\ell) = \frac{1}{2m_B} \int d\Pi_{\text{LIPS}} |\langle X\ell | \mathcal{H}_{\text{BNV}} | \bar{B} \rangle|^2 \approx \frac{4\pi}{2m_B(2\pi)^3} \int_0^{E_\ell^{\text{max}}} dE_\ell \frac{E_\ell [L \cdot W]}{2 \Lambda_{\text{BNV}}^4}, \quad (8.65)$$

where we used the standard technique for inclusive B decays applying the optical theorem [44], and the maximal lepton energy $E_\ell^{\text{max}} \approx m_B/2$. We estimate $L \sim E_\ell$ and $W \sim \pi m_B^3 / (16\pi^2)$ from dimensional analysis for the leptonic and hadronic tensors, respectively. In the latter we also included the loop factor $1/(16\pi^2)$ and a factor of π coming from the imaginary part of the one-loop amplitude when employing the optical theorem.

In the absence of any further suppression by small couplings ($C_{\text{BNV}}^j \sim 1$), and by choosing a benchmark conservative bound $\Lambda_{\text{BNV}} > 6 \cdot 10^9 \text{ GeV}$ suggested by Table 8.1, we find the following upper bound on BNV decays of B mesons into light leptons

$$\mathcal{B}(\bar{B} \rightarrow X\ell) = \frac{\Gamma(\bar{B} \rightarrow X\ell)}{\Gamma_{\bar{B}}} \approx \frac{m_b^5}{2^{10} 3\pi^3 \Lambda_{\text{BNV}}^4 \Gamma_{\bar{B}}} \approx (8|V_{cb}|G_F\Lambda_{\text{BNV}}^2)^{-2} \lesssim \mathcal{O}(5 \cdot 10^{-29}), \quad (8.66)$$

where $\Gamma_{\bar{B}}$ is the total \bar{B} meson decay width reported in Appendix A with all the other inputs. Using the heavy-quark expansion we confirmed this simple estimate for one of the SMEFT operators. The result (8.66) excludes any possibility of direct measurement of

BNV in B decays (to light leptons) in the next decades, as similar bounds would apply for B decays involving second family quarks, following from the discussion of Section 8.2.3.

As estimated in Section 8.3.4 the case of BNV B decays into τ leptons is different. In that case the scale of third-generation BNV involving b -quarks and τ -leptons is much less constrained, allowing for much larger B meson branching fractions

$$\mathcal{B}(\bar{B} \rightarrow X\tau) \lesssim \mathcal{O}(10^{-13} \div 10^{-15}). \quad (8.67)$$

Although these values are closer to the smallest measured branching fractions for any particle decay, the smaller experimental efficiency in detecting τ -leptons still makes the observation of these decay modes quite unrealistic in the near future.

Part V
Conclusions

Chapter 9

Summary and Outlook

In this work we have shown several applications of factorization, and effective field theories in general, in the context of flavour physics. In particular a factorization formula relating the QCD and HQET LCDAs of a heavy meson was derived, allowing to resum large logarithms between Λ_{QCD} , the heavy meson mass and the hard scale of the process at which the highly energetic meson was produced. We have computed the one-loop matching function in QCD, which encodes all the perturbative information from the heavy quark mass scale. Using input models for the universal leading-twist HQET LCDA at the soft scale 1 GeV, we derived the QCD LCDAs for a \bar{B} and a D meson written in terms of Gegenbauer moments. As an example of a three scales process, we proceeded to apply this formula to the branching ratio of $W^\pm \rightarrow B^\pm \gamma$, finding new theoretical predictions implementing the resummation of all the large logarithms. Furthermore, employing the power counting $\Lambda_{\text{QCD}} \ll m_c \ll m_b$, we were able to write down a QCD factorization formula for colour-suppressed tree amplitudes in $\bar{B} \rightarrow DL$, which necessitates a D meson LCDA. In this context we compared theoretical predictions for colour-allowed and colour-suppressed amplitudes to data, showing a consistent picture which could be improved by a better determination of the D meson LCDA.

We have also extended factorization in $\bar{B} \rightarrow DL$ to include QED effects, applying the framework of Ref. [99] to the case of heavy-light final states. The charm mass dependent QED hard-scattering kernels were computed at one-loop in this work. Considering also real ultrasoft photon radiation, we provided numerical results for the $\mathcal{O}(\alpha_{\text{em}})$ corrections to non-leptonic to semi-leptonic decay rates ratios. We found that QED virtual corrections to the amplitude are at the sub-percent level, smaller than the current QCD uncertainties, while ultrasoft effects are responsible for a downward shift of the branching ratios of about 5%.

Finally, motivated by the B -anomalies in recent years, we entertained the idea that baryon number violation could be generation dependent and only takes place when third family quarks are involved. However this does not mean that experimental limits on the proton lifetime do not affect such interactions, since under these assumptions the proton could still decay through a virtual b quark. Therefore we examined the simple processes $p \rightarrow \ell^+ \nu_\ell \bar{\nu}$, $p \rightarrow \pi^+ \bar{\nu}$, $p \rightarrow \pi^0 \ell^+$ mediated by a combination of charged weak current and

baryon number violating SMEFT operator with a b quark.

We found that the very strong constraints on proton lifetime from the Super-Kamiokande collaboration set lower bounds on the new physics scale related to baryon number violation of about 10^9 GeV, incompatible with the scale of new physics suggested by the flavour anomalies. The derived limit on Λ_{BNV} sets an upper bound on the branching ratios of BNV B decays or order $\mathcal{O}(5 \cdot 10^{-29})$, excluding the possibility of any direct detection of such decays.

As the proton cannot decay into a final state with a τ lepton, the case of operators involving a b quark and a τ deserves special treatment. From the process $p \rightarrow \ell^+ \nu_\ell \bar{\nu}_\tau$ mediated by a virtual b and a virtual τ we were able to estimate a bound for the BNV scale around 10^6 GeV. The latter translates into much weaker constraints for $\bar{B} \rightarrow X\tau$ branching ratios of $\mathcal{O}(10^{-13} \div 10^{-15})$, but still far from the current experimental sensitivities due to the reduced efficiency in detecting τ leptons with respect to light leptons.

To conclude, with the LHC at CERN completing its Run-3 and approaching the High-Luminosity phase, the LHCb experiment, alongside with Belle II at SuperKEKB, will provide new interesting results in B -physics in the next few years. In this thesis we have shown the power of factorization in several contexts, being the modern tool allowing to systematically improve the precision of theoretical predictions. Together, these sustained efforts will further develop the intriguing story of the flavour anomalies and of particle physics in general.

Part VI
Appendices

Appendix A

Numerical Inputs

We collect in this appendix the relevant numerical inputs used in this thesis. We start from the coupling constants [24]

$$\alpha_s^{(5)}(m_Z) = 0.1179, \quad \alpha_{\text{em}}(m_Z) = \frac{1}{127.96}, \quad G_F = 1.1663788 \cdot 10^{-5} \text{ GeV}^{-2}, \quad (\text{A.1})$$

where the electromagnetic coupling constant is then evolved and used at the scales μ_b and μ_s

$$\alpha_{\text{em}}(\mu_b) = \frac{1}{132.24}, \quad \alpha_{\text{em}}(\mu_s) = \frac{1}{134.05}. \quad (\text{A.2})$$

Throughout the thesis we defined the scales

$$\mu_b = 4.8 \text{ GeV}, \quad \mu_{\text{hc}} = \mu_c = 1.6 \text{ GeV}, \quad \mu_s = 1 \text{ GeV}, \quad (\text{A.3})$$

where μ_b is typically the hard scale for \bar{B} decays, μ_{hc} the hard-collinear scale, which we chose to be numerically the same as the scale μ_c related to the charm quark mass. Finally μ_s is associated to either the soft or the collinear scale, which are also numerically equivalent.

The QCD beta function is defined as

$$\beta(\alpha_s) = \mu \frac{d\alpha_s}{d\mu} = -2\alpha_s \sum_{n=0}^{\infty} \beta_n \left(\frac{\alpha_s}{4\pi} \right)^{n+1}, \quad (\text{A.4})$$

with the first two coefficients

$$\beta_0 = 11 - \frac{2}{3}n_f, \quad \beta_1 = 102 - \frac{38}{3}n_f. \quad (\text{A.5})$$

For the evaluation and running of the QCD coupling constant $\alpha_s(\mu)$ in the $\overline{\text{MS}}$ scheme, we use the code `RunDec` [128] with three-loop running. We decouple the heavy quarks at their $\overline{\text{MS}}$ masses. We hence have $\alpha_s^{(5)}(\mu_b) = 0.215$.

In Chapter 8 we set the threshold for integrating out the charm quark at 3 GeV such that $n_f = 3$ is constant between 1 and 2 GeV. The quark masses in $\overline{\text{MS}}$ are evolved with

$$m_q(\mu) = \left(\frac{\alpha_s(\mu)}{\alpha_s(\mu_0)} \right)^{4/\beta_0} m_q(\mu_0). \quad (\text{A.6})$$

Masses of elementary particles [GeV]			
Light quarks ($\overline{\text{MS}}$ at 2 GeV)	Heavy quarks	Leptons	Electroweak
$m_u = 2.16 \cdot 10^{-3}$	$m_c = 1.67$	$m_e = 0.511 \cdot 10^{-3}$	$m_W = 80.377$
$m_d = 4.67 \cdot 10^{-3}$	$m_b = 4.8$	$m_\mu = 105.66 \cdot 10^{-3}$	$m_Z = 91.1876$
$m_s = 93.4 \cdot 10^{-3}$	$m_t = 172.7$	$m_\tau = 1.777$	$v = 246.22$

Table A.1: Inputs for the masses of elementary particles in the on-shell scheme, except where stated otherwise. We have replaced the Higgs boson mass by the Higgs vev v .

Meson masses and decay constants [GeV]			
$m_{\pi^\pm} = 0.13957$	$m_{D^\pm} = 1.870$	$m_B = 5.279$	$f_\pi = 0.1302(8)$
$m_{\pi^0} = 0.13498$	$m_{D^0} = 1.865$	$m_{B_s} = 5.367$	$f_K = 0.1557(3)$
$m_{K^\pm} = 0.49368$	$m_{D^{*\pm}} = 2.010$	$f_B = 0.1900(13)$	$f_D = 0.2120(7)$
$m_{K^0} = 0.49761$	$m_{D_s^\pm} = 1.968$	$f_{B_s} = 0.2303(13)$	$f_{D_s} = 0.2499(5)$

Table A.2: Inputs for the meson masses [24] and decay constants [130] with uncertainties in brackets.

In Table A.1 we collect the masses for the elementary particles, where we traded the Higgs boson mass with the Higgs vacuum expectation value v . In Table A.2 we report the meson masses and the decay constants used in this thesis. We also used the \bar{B} lifetime [24]

$$\tau_{\bar{B}} = 1.517 \cdot 10^{-12} \text{ s}, \quad \Gamma_{\bar{B}} = 4.33 \cdot 10^{-13} \text{ GeV}, \quad (\text{A.7})$$

also translated into the \bar{B} meson total decay rate $\Gamma_{\bar{B}}$.

The CKM matrix elements relevant for us are [24, 31, 129]

$$\begin{aligned} |V_{ud}| &= 0.97370 \pm 0.00014, & |V_{us}| &= 0.2245 \pm 0.0008, \\ |V_{ub}| &= (3.77 \pm 0.15) \cdot 10^{-3}, & |V_{cb}| &= (41.97 \pm 0.48) \cdot 10^{-3}. \end{aligned} \quad (\text{A.8})$$

The first two Gegenbauer moments of the pion and kaon QCD LCDAs at 2 GeV are taken from [105]

$$\begin{aligned} a_1^\pi(2 \text{ GeV}) &= 0, & a_2^\pi(2 \text{ GeV}) &= 0.116_{-0.020}^{+0.019}, \\ a_1^{\bar{K}}(2 \text{ GeV}) &= 0.0525_{-0.0033}^{+0.0031}, & a_2^{\bar{K}}(2 \text{ GeV}) &= 0.106_{-0.016}^{+0.015}, \end{aligned} \quad (\text{A.9})$$

where for a K^0 or a K^+ one has to change the sign of the odd Gegenbauer moments. These moments evolved to the scale μ_b with NLL accuracy give

$$\begin{aligned} a_1^\pi(\mu_b) &= 0, & a_2^\pi(\mu_b) &= 0.090, \\ a_1^{\bar{K}}(\mu_b) &= 0.0450, & a_2^{\bar{K}}(\mu_b) &= 0.082, \end{aligned} \quad (\text{A.10})$$

$F_0^{\bar{B}P}(q^2)$	m_π^2	m_K^2	m_D^2
$\bar{B} \rightarrow \pi$	0.196(21)	0.198(21)	0.221(21)
$\bar{B} \rightarrow \bar{K}$	0.329(28)	0.331(28)	0.363(28)
$\bar{B} \rightarrow D$	0.681(28)	0.684(28)	—

Table A.3: Table of the form factors $F_0^{\bar{B}P}(q^2)$ with their uncertainties from Ref. [96].

where we do not quote uncertainties since they will be negligible in our applications. Notice that the NLL evolution is not diagonal in the Gegenbauer moments, hence higher moments are generated by the evolution, however without exceeding the 10^{-4} order of magnitude. For the Gegenbauer moments of the D meson LCDA in Chapter 5 we use as default inputs at the scale μ_c the first four values in (3.108) derived from the matching to HQET.¹ Evolved to the scale μ_b with NLL accuracy we get

$$a_n^D(\mu_b) = \{0.5363, 0.1481, 0.0348, 0.0221\}, \quad n = 1, \dots, 4, \quad (\text{A.11})$$

where the higher moments have values of the order 10^{-3} or less.

For the inverse moment of the HQET LCDA defined in (3.18) we take the input value $\lambda_B(\mu_s) = 350 \pm 150$ MeV at the soft scale μ_s . In Chapter 5 we employ its LL evolution in the form [131]

$$\lambda_B(\mu) = e^{-V-2\gamma_E a} \frac{\mu_s^{-a}}{\Gamma(1+a)} [\lambda_B(\mu_s)]^{1+a}, \quad (\text{A.12})$$

where $a(\mu, \mu_s)$ and $V(\mu, \mu_s)$ are defined in (3.103). This form is derived using the simple exponential model for $\varphi_+(\omega; \mu)$, which we justify given the large uncertainty on the input value for λ_B . For the two values of scales, other than the input one, used in the calculation of the spectator scattering term in Section 5.4 we get

$$\lambda_B(\mu_{\text{hc}}) = 0.40 \pm 0.15 \text{ GeV}, \quad \lambda_B(2 \text{ GeV}) = 0.42 \pm 0.16 \text{ GeV}. \quad (\text{A.13})$$

For the Wilson coefficients of the weak effective Hamiltonian in the CMM basis we implemented the initial conditions and two-loop running from Ref. [40]. At the scale μ_b we find

$$C_1(\mu_b) = -0.257227, \quad C_2(\mu_b) = 1.00844, \quad (\text{A.14})$$

while at 1 GeV

$$C_1(1 \text{ GeV}) = -0.829400, \quad C_2(1 \text{ GeV}) = 1.05009. \quad (\text{A.15})$$

In Chapter 5 we use the form factors for $\bar{B} \rightarrow P$ transitions reported in Table A.3, where P is a pseudoscalar meson.

¹Notice that we have changed the sign of the odd moments because of the different definition of the LCDA in Chapter 3 which was more practical for the connection to HQET.

In Chapter 8 we use the proton mass $m_p = 0.938$ GeV. The proton decay constants values from lattice QCD at 2 GeV are [132]

$$\begin{aligned} f_p(2 \text{ GeV}) &= 3.54_{-0.04}^{+0.06} \cdot 10^{-3} \text{ GeV}^2, \\ \lambda_1(2 \text{ GeV}) &= -(44.9_{-4.1}^{+4.2}) \cdot 10^{-3} \text{ GeV}^2, \\ \lambda_2(2 \text{ GeV}) &= 93.4_{-4.8}^{+4.8} \cdot 10^{-3} \text{ GeV}^2, \end{aligned} \tag{A.16}$$

and we evolve them to 1 GeV with the relations [133, 134]

$$f_p(\mu) = \left(\frac{\alpha_s(\mu)}{\alpha_s(\mu_0)} \right)^{\frac{2}{3\beta_0}} f_p(\mu_0), \quad \lambda_i(\mu) = \left(\frac{\alpha_s(\mu)}{\alpha_s(\mu_0)} \right)^{-\frac{2}{\beta_0}} \lambda_i(\mu_0), \tag{A.17}$$

for $i = 1, 2$, obtaining the values

$$\begin{aligned} f_p(1 \text{ GeV}) &= 3.67 \cdot 10^{-3} \text{ GeV}^2, \\ \lambda_1(1 \text{ GeV}) &= -40.5 \cdot 10^{-3} \text{ GeV}^2, \\ \lambda_2(1 \text{ GeV}) &= 84.2 \cdot 10^{-3} \text{ GeV}^2. \end{aligned} \tag{A.18}$$

The parameter μ_π appearing in the pion-to-vacuum matrix element of the local pseudoscalar current takes the value

$$\begin{aligned} \mu_{\pi^\pm} &= \frac{m_{\pi^\pm}^2}{m_u(1 \text{ GeV}) + m_d(1 \text{ GeV})} = 2.315 \text{ GeV}, \\ \mu_{\pi^0} &= \frac{m_{\pi^0}^2}{m_u(1 \text{ GeV}) + m_d(1 \text{ GeV})} = 2.166 \text{ GeV}. \end{aligned} \tag{A.19}$$

Appendix B

Details of the SCET to bHQET Matching

In this appendix we collect the details on the calculation of the matrix elements in SCET and bHQET for the LCDA matching. We provide analytical results for the individual diagrams of Figure 3.1 as well as a region analysis of the matching.

B.1 SCET Matrix Element

The external momenta for the computation of $\langle h(p_h)\bar{q}(p_q)|\mathcal{O}_C(u)|0\rangle$ are

$$p_h^\mu = m_h v^\mu = \bar{s} n_+ p_H \frac{n_-^\mu}{2} + \frac{m_h^2}{\bar{s} n_+ p_H} \frac{n_+^\mu}{2}, \quad p_q^\mu = n_+ p_q \frac{n_-^\mu}{2} + p_{q\perp}^\mu = s n_+ p_H \frac{n_-^\mu}{2} + p_{q\perp}^\mu, \quad (\text{B.1})$$

where we defined $n_+ p_H = n_+ p_h + n_+ p_q$. The perpendicular component of p_q has to be kept at an early stage of the computation not to miss the loop induced Dirac structure, as explained below (3.40). After having performed the numerator algebra and identified the two Dirac structures, $p_{q\perp}$ is set to zero as it is power suppressed. At this moment we are not yet assigning a scaling to s (namely $n_+ p_q$) and u , as we want to compute the full result (3.45) presented in the main text. Full here means that it includes the peak ($u \sim \lambda_h$) and tail ($u \sim 1$) regions simultaneously. In Sections B.3 and B.4 we will present the results for the two regions obtained by imposing the respective scalings from the start.

Referring to the decomposition (3.38), with (3.41), the results of the three diagrams of Figure 3.1 computed in dimensional regularization ($d = 4 - 2\epsilon$) are

$$W_h(u, s) = \left(\frac{\mu^2}{m_h^2}\right)^\epsilon 2e^{\epsilon\gamma_E} \Gamma(\epsilon) \left\{ \frac{\delta(u-s)}{2\epsilon(1-2\epsilon)} + \frac{\bar{u}}{\bar{s}^{1-2\epsilon}} \frac{\theta(u-s)}{(u-s)^{1+2\epsilon}} \right\}, \quad (\text{B.2})$$

$$W_q(u, s) = 0, \quad (\text{B.3})$$

$$V_+(u, s) = \left(\frac{\mu^2}{m_h^2}\right)^\epsilon 2e^{\epsilon\gamma_E} \Gamma(\epsilon) \left\{ \theta(s-u) e^{i\pi\epsilon} \frac{u}{s} \left(\frac{\bar{s}}{u(s-u)}\right)^\epsilon \left(1 - \epsilon + \frac{1}{s-u}\right) \right\}$$

$$+ \theta(u-s) \left(1 - \frac{\bar{u}}{s}\right)^{-2\epsilon} \left[(1-\epsilon) \frac{\bar{u}}{s} - \frac{u}{s} \left(1 - \epsilon + \frac{1}{s-u}\right) \left(1 - \left(\frac{u-s}{u\bar{s}}\right)^\epsilon\right) \right] \Big\}, \quad (\text{B.4})$$

$$V_-(u, s) = - \left(\frac{\mu^2}{m_h^2}\right)^\epsilon 2e^{\epsilon\gamma_E} \Gamma(\epsilon) (1-\epsilon) \frac{u^{1-\epsilon}}{s\bar{s}^{1-\epsilon}} \left\{ e^{i\pi\epsilon} \frac{\theta(s-u)}{(s-u)^\epsilon} + \frac{\theta(u-s)}{(u-s)^\epsilon} \left(1 - \left(\frac{\bar{s}u}{u-s}\right)^\epsilon\right) \right\}, \quad (\text{B.5})$$

where the Wilson line diagrams W_h and W_q contribute only to the amplitude $M_+^{(1)}(u, s)$, while $M_-^{(1)}(u, s) = V_-(u, s)$ since this term is free from UV and IR divergences.

To renormalize the amplitude we need to extract the UV poles. For this we have to perform the expansion in ϵ , requiring the introduction of the plus-distributions defined in (3.5). We regulate the IR divergences by keeping a small off-shellness. We find

$$W_h^{\text{UV}}(u, s) = \frac{2}{\epsilon} \left[\frac{\bar{u} \theta(u-s)}{\bar{s} u-s} \right]_{u_+}, \quad (\text{B.6})$$

$$W_q^{\text{UV}}(u, s) = \frac{2}{\epsilon} \left[\frac{u \theta(s-u)}{s s-u} \right]_{u_+}, \quad (\text{B.7})$$

$$V_+^{\text{UV}}(u, s) = \frac{2}{\epsilon} \left(\frac{u}{s} \theta(s-u) + \frac{\bar{u}}{\bar{s}} \theta(u-s) \right), \quad (\text{B.8})$$

$$V_-^{\text{UV}}(u, s) = 0. \quad (\text{B.9})$$

Taking into account the $\overline{\text{MS}}$ field strength renormalization $Z_\xi^{(1)} = -1/\epsilon$ in

$$\begin{aligned} Z_{\mathcal{O}_C}(u, s) &= \left[Z_\xi^{-1/2} \right]^2 \left(\delta(u-s) - \frac{\alpha_s C_F}{4\pi} [M_+^{(1)}(u, s)]^{\text{UV}} + \mathcal{O}(\alpha_s^2) \right) \\ &= \delta(u-s) - \frac{\alpha_s C_F}{4\pi} \left([M_+^{(1)}(u, s)]^{\text{UV}} + Z_\xi^{(1)} \delta(u-s) \right) + \mathcal{O}(\alpha_s^2), \end{aligned} \quad (\text{B.10})$$

we get

$$Z_{\mathcal{O}_C}^{(1)}(u, s) = -\frac{2}{\epsilon} \left[\theta(s-u) \frac{u}{s} \left(1 + \frac{1}{s-u}\right) + \theta(u-s) \frac{\bar{u}}{\bar{s}} \left(1 + \frac{1}{u-s}\right) \right]_{u_+}, \quad (\text{B.11})$$

which agrees with the standard ERBL evolution kernel [73–75], as expected.

B.2 bHQET Matrix Element

The external momenta for the bHQET matrix element $\langle h(p_h) \bar{q}(p_q) | \mathcal{O}_h(\omega) | 0 \rangle$ are parameterized as

$$p_h^\mu = m_h v^\mu, \quad v^\mu = n_+ v \frac{n_-^\mu}{2} + \frac{1}{n_+ v} \frac{n_+^\mu}{2}, \quad p_q^\mu = \nu n_+ v \frac{n_-^\mu}{2}. \quad (\text{B.12})$$

We have rescaled the dimensionful variables ω and ν by n_+v such that they correspond to the variables in the heavy meson rest frame. The results for the bare bHQET diagrams in dimensional regularization are

$$W_{h,\text{bHQET}}(\omega, \nu) = \mu^{2\epsilon} 2e^{\epsilon\gamma_E} \Gamma(\epsilon) \frac{\theta(\omega - \nu)}{(\omega - \nu)^{1+2\epsilon}}, \quad (\text{B.13})$$

$$W_{q,\text{bHQET}}(\omega, \nu) = 0, \quad (\text{B.14})$$

$$\begin{aligned} V_{\text{bHQET}}(\omega, \nu) &= \mu^{2\epsilon} 2e^{\epsilon\gamma_E} \Gamma(\epsilon) \frac{\omega}{\nu} \left\{ e^{i\pi\epsilon} \omega^{-\epsilon} \frac{\theta(\nu - \omega)}{(\nu - \omega)^{1+\epsilon}} \right. \\ &\quad \left. + \frac{\theta(\omega - \nu)}{(\omega - \nu)^{1+\epsilon}} ((\omega - \nu)^{-\epsilon} - \omega^{-\epsilon}) \right\}, \end{aligned} \quad (\text{B.15})$$

where now the one-loop amplitude is always proportional to the tree level Dirac structure. The UV poles of (B.13)–(B.15) are again obtained by regulating the IR divergences by an off-shellness $p_q^2 \neq 0$. We find

$$W_{h,\text{bHQET}}^{\text{UV}}(\omega, \nu) = \frac{2\omega}{\epsilon} \left[\frac{\theta(\omega - \nu)}{\omega(\omega - \nu)} \right]_{\omega_+} - \delta(\omega - \nu) \left(\frac{1}{\epsilon^2} + \frac{2}{\epsilon} \ln \frac{\mu}{\nu} \right), \quad (\text{B.16})$$

$$W_{q,\text{bHQET}}^{\text{UV}}(\omega, \nu) = \frac{2\omega}{\epsilon} \left[\frac{\theta(\nu - \omega)}{\nu(\nu - \omega)} \right]_{\omega_+} + \frac{2}{\epsilon} \delta(\omega - \nu), \quad (\text{B.17})$$

$$V_{\text{bHQET}}^{\text{UV}}(\omega, \nu) = 0, \quad (\text{B.18})$$

where the plus-distributions are defined in (3.21).

The renormalization kernel of the bHQET matrix element, in analogy to (B.10), is then obtained as

$$Z_{\mathcal{O}_h}^{(1)}(\omega, \nu) = -W_{Q,\text{bHQET}}^{\text{UV}}(\omega, \nu) - W_{q,\text{bHQET}}^{\text{UV}}(\omega, \nu) - \frac{\delta(\omega - \nu)}{2} (Z_\xi^{(1)} + Z_{h_n}^{(1)}), \quad (\text{B.19})$$

with the bHQET field renormalization constant in $\overline{\text{MS}}$ $Z_{h_n}^{(1)} = 2/\epsilon$. Overall this leads to [77]

$$Z_{\mathcal{O}_h}^{(1)}(\omega, \nu) = -\frac{2\omega}{\epsilon} \left[\frac{\theta(\omega - \nu)}{\omega(\omega - \nu)} + \frac{\theta(\nu - \omega)}{\nu(\nu - \omega)} \right]_{\omega_+} + \delta(\omega - \nu) \left(\frac{1}{\epsilon^2} + \frac{1}{\epsilon} \left[2 \ln \frac{\mu}{\nu} - \frac{5}{2} \right] \right), \quad (\text{B.20})$$

where the plus-distribution can also be intended in the variable ν as the function inside the plus-distribution is symmetric under the exchange $\omega \leftrightarrow \nu$.

B.3 Peak Region

In this section we present the results for the individual diagrams of the SCET matrix element, computed directly in the peak region $u \sim \lambda_h$ at leading power with the external

soft-collinear momentum forcing $s \sim \lambda_h$. The leading power contribution to $M_{\pm}(u, s)$ scales like $1/\lambda_h$, hence as commented in the main text we notice that $M_-(u, s)$ from (B.5) is power suppressed.

The diagram V receives contribution only from the soft-collinear region $k \sim \lambda_h(1, \beta, \beta^2)Q$, reducing to

$$V_+(u, s)\Big|_{sc} = \left(\frac{\mu^2}{m_h^2}\right)^\epsilon 2e^{\epsilon\gamma_E}\Gamma(\epsilon)\frac{u}{s} \left\{ e^{i\pi\epsilon}u^{-\epsilon}\frac{\theta(s-u)}{(s-u)^{1+\epsilon}} + \frac{\theta(u-s)}{(u-s)^{1+\epsilon}}\left((u-s)^{-\epsilon}-u^{-\epsilon}\right) \right\}, \quad (\text{B.21})$$

which as expected coincides with the bHQET result $m_h V_{\text{bHQET}}(\omega, \nu)$ in (B.15) of Section B.2 with $\omega = um_h$ and $\nu = sm_h$. In diagram W_h both the hard- and soft-collinear regions are present, yielding respectively to

$$W_h(u, s)\Big|_{hc} = \left(\frac{\mu^2}{m_h^2}\right)^\epsilon 2e^{\epsilon\gamma_E}\Gamma(\epsilon)\frac{\delta(u-s)}{2\epsilon(1-2\epsilon)}, \quad (\text{B.22})$$

$$W_h(u, s)\Big|_{sc} = \left(\frac{\mu^2}{m_h^2}\right)^\epsilon 2e^{\epsilon\gamma_E}\Gamma(\epsilon)\frac{\theta(u-s)}{(u-s)^{1+2\epsilon}}. \quad (\text{B.23})$$

Again soft-collinear region coincides, as it should, with the bHQET result $m_h W_{h\text{bHQET}}(\omega, \nu)$ in (B.13) with $\omega = um_h$ and $\nu = sm_h$.

We are assured that no other regions exist as expanding to leading power the full expressions for $V_+(u, s)$ and $W_h(u, s)$ given in (B.4) and (B.2) we find

$$\begin{aligned} V_+(u, s) &\xrightarrow{u\sim\lambda_h} V_+(u, s)\Big|_{sc}, \\ W_h(u, s) &\xrightarrow{u\sim\lambda_h} W_h(u, s)\Big|_{sc} + W_h(u, s)\Big|_{hc}. \end{aligned} \quad (\text{B.24})$$

From this we understand that in the peak region the one-loop SCET amplitude is not only given by soft-collinear interactions, but still contains information from the perturbative hard-collinear scale. The hard-collinear region will be encoded in the matching function $\mathcal{J}_p(u, \omega)$ defined in (3.35).

B.4 Tail Region

In Section 3.3.2 we noted that the tail region, defined by $u \sim 1$ and $s \sim \lambda_h$, is power suppressed with respect to the peak region as expected from (3.29). In fact the leading power contribution scales as $\mathcal{O}(1)$. The results for the coefficients of the two Dirac structures contributing to the diagram V are

$$\begin{aligned} V_+(u)\Big|_{hc} &= \left(\frac{\mu^2}{u^2 m_h^2}\right)^\epsilon 2e^{\epsilon\gamma_E}\Gamma(1+\epsilon)\bar{u}\left(\frac{(1-\epsilon)^2}{\epsilon} + \frac{1}{u}\right), \\ V_-(u)\Big|_{hc} &= \left(\frac{\mu^2}{u^2 m_h^2}\right)^\epsilon 2e^{\epsilon\gamma_E}\Gamma(1+\epsilon)\bar{u}(1-\epsilon), \end{aligned} \quad (\text{B.25})$$

with UV poles again computed using an off-shellness to regulate the diagram in the IR

$$\begin{aligned} V_+^{\text{UV}}(u) \Big|_{hc} &= \frac{2\bar{u}}{\epsilon}, \\ V_-^{\text{UV}}(u) \Big|_{hc} &= 0. \end{aligned} \tag{B.26}$$

The corresponding results for the diagram W_h are

$$W_h(u) \Big|_{hc} = \left(\frac{\mu^2}{m_h^2} \right)^\epsilon 2e^{\epsilon\gamma_E} \Gamma(\epsilon) \frac{\bar{u}}{u^{1+2\epsilon}}, \tag{B.27}$$

$$W_h^{\text{UV}}(u) \Big|_{hc} = \frac{2\bar{u}}{\epsilon u}. \tag{B.28}$$

Given the UV poles, and (B.10), the renormalization kernel is

$$Z_{\mathcal{O}_C}^{(1)}(u) \Big|_{hc} = -\frac{2}{\epsilon} \bar{u} \left(1 + \frac{1}{u} \right), \tag{B.29}$$

where there is no need to write it in terms of plus-distribution as the integration domain will be restricted to the region $u \gg \lambda_h$. Again, expanding the full result for V and W_h in (B.4), (B.5) and (B.2) to leading power we find the above computed regions

$$\begin{aligned} V_+(u, s) &\xrightarrow{u \sim 1} V_+(u) \Big|_{hc}, \\ V_-(u, s) &\xrightarrow{u \sim 1} V_-(u) \Big|_{hc}, \\ W_h(u, s) &\xrightarrow{u \sim 1} W_h(u) \Big|_{hc}, \\ Z_{\mathcal{O}_C}^{(1)}(u, s) &\xrightarrow{u \sim 1} Z_{\mathcal{O}_C}^{(1)}(u) \Big|_{hc}, \end{aligned} \tag{B.30}$$

showing that the tail region is dominated by only hard-collinear modes, and that the result is independent on the power-suppressed external momentum fraction $s \ll u$, as argued in Section 3.3.2.

Appendix C

Details on QED Factorization

C.1 Individual Diagrams for One-Loop Matching

We report here the results for the individual one-loop diagrams of Figure 6.1. We use the Dirac structures of (6.14) and the definitions $u = n_{-p_q}/(n_{-p_q} + n_{-p_{\bar{u}}})$, $\bar{u} = 1 - u = n_{-p_{\bar{u}}}/(n_{-p_q} + n_{-p_{\bar{u}}})$ and $z = m_c^2/m_b^2$. For the first four diagrams, the so-called “non-factorizable” ones, we get

$$I_{bq} = -\frac{\alpha_{\text{em}}}{4\pi} Q_d^2 \left(\frac{\mu^2}{m_b^2} \right)^\epsilon \left\{ -\frac{3}{4\epsilon} \mathcal{S}_{E-} + \sqrt{z} \frac{1 - b_q + b_q \ln b_q}{(1 - b_q)^2} \mathcal{S}_+ \right. \\ \left. + \left[\frac{1}{\epsilon^2} + \frac{1}{\epsilon} - \frac{2 \ln b_q}{\epsilon} + \ln^2 b_q + \frac{3b_q - 2}{1 - b_q} \ln b_q - 2\text{Li}_2\left(\frac{b_q - 1}{b_q}\right) + \frac{\pi^2}{12} + 2 \right] \mathcal{S}_- \right\}, \quad (\text{C.1})$$

$$I_{b\bar{u}} = \frac{\alpha_{\text{em}}}{4\pi} Q_u Q_d \left(\frac{\mu^2}{m_b^2} \right)^\epsilon \left\{ \frac{3}{4\epsilon} \mathcal{S}_{E-} \right. \\ \left. + \left[\frac{1}{\epsilon^2} - \frac{2}{\epsilon} - \frac{2 \ln b_{\bar{u}}}{\epsilon} + \ln^2 b_{\bar{u}} - \frac{2 \ln b_{\bar{u}}}{1 - b_{\bar{u}}} - 2\text{Li}_2\left(\frac{b_{\bar{u}} - 1}{b_{\bar{u}}}\right) + \frac{\pi^2}{12} - 3 \right] \mathcal{S}_- \right\}, \quad (\text{C.2})$$

$$I_{c_q} = \frac{\alpha_{\text{em}}}{4\pi} Q_u Q_d \left(\frac{\mu^2}{m_c^2} \right)^\epsilon \left\{ \frac{3}{4\epsilon} \mathcal{S}_{E-} \right. \\ \left. + \left[\frac{1}{\epsilon^2} - \frac{2}{\epsilon} - \frac{2 \ln c_q}{\epsilon} + \ln^2 c_q - \frac{2 \ln c_q}{1 - c_q} - 2\text{Li}_2\left(\frac{c_q - 1}{c_q}\right) + \frac{\pi^2}{12} - 3 \right] \mathcal{S}_- \right\}, \quad (\text{C.3})$$

$$I_{c\bar{u}} = -\frac{\alpha_{\text{em}}}{4\pi} Q_u^2 \left(\frac{\mu^2}{m_c^2} \right)^\epsilon \left\{ -\frac{3}{4\epsilon} \mathcal{S}_{E-} + \frac{1}{\sqrt{z}} \frac{1 - c_{\bar{u}} + c_{\bar{u}} \ln c_{\bar{u}}}{(1 - c_{\bar{u}})^2} \mathcal{S}_+ \right.$$

$$+ \left[\frac{1}{\epsilon^2} + \frac{1}{\epsilon} - \frac{2 \ln c_{\bar{u}}}{\epsilon} + \ln^2 c_{\bar{u}} + \frac{3c_{\bar{u}} - 2}{1 - c_{\bar{u}}} \ln c_{\bar{u}} - 2\text{Li}_2\left(\frac{c_{\bar{u}} - 1}{c_{\bar{u}}}\right) + \frac{\pi^2}{12} + 2 \right] \mathcal{S}_- \Bigg\}, \quad (\text{C.4})$$

where the subscript on $I_{q_1 q_2}$ stand for the quarks interacting with the photon, and we have defined the kinematical variables

$$\begin{aligned} b_q &= \frac{2p_b \cdot p_q}{m_b^2} = u(1 - z), \\ b_{\bar{u}} &= \frac{2p_b \cdot p_{\bar{u}}}{m_b^2} = \bar{u}(1 - z), \\ c_q &= -\frac{2p_b \cdot p_q}{m_c^2} = u\left(1 - \frac{1}{z}\right) - i\eta, \\ c_{\bar{u}} &= -\frac{2p_b \cdot p_{\bar{u}}}{m_c^2} = \bar{u}\left(1 - \frac{1}{z}\right) - i\eta, \end{aligned} \quad (\text{C.5})$$

with η the infinitesimal parameter from the prescription in the propagators.

For the remaining two ‘‘factorizable’’ diagrams we notice that the diagram with the photon connecting the constituents of L^- is scaleless, hence we only need to compute the one with the interaction between the heavy quarks. We get

$$\begin{aligned} I_{q\bar{u}} &= 0, \\ I_{bc} &= \frac{\alpha_{\text{em}}}{4\pi} Q_u Q_d \left(\frac{\mu^2}{m_b^2}\right)^\epsilon \left\{ -\sqrt{z} \frac{\ln z}{1 - z} \mathcal{S}_+ \right. \\ &\quad \left. + \left[\frac{1}{\epsilon} \left(1 - \frac{1 + z}{1 - z} \ln z\right) + \frac{\ln z}{1 - z} \left(\frac{1}{2}(1 + z) \ln z - z - 2\right) \right] \mathcal{S}_- \right\}. \end{aligned} \quad (\text{C.6})$$

For the renormalization of the heavy-to-heavy current in the EFT we extract the UV poles of the three diagrams of Figure 6.2. The first diagram gives the standard

$$\begin{aligned} I_V^{\text{UV}} &= -\frac{\alpha_{\text{em}}}{4\pi} \frac{2Q_u Q_d}{\epsilon} \frac{\omega}{\sqrt{\omega^2 - 1}} \ln(\omega + \sqrt{\omega^2 - 1}) \langle c(v') | \bar{h}_{v'}(0) \not{t}_+(1 - \gamma^5) h_v(0) | b(v) \rangle \\ &= \frac{\alpha_{\text{em}}}{4\pi} \frac{Q_u Q_d}{\epsilon} \frac{1 + z}{1 - z} \ln z \langle c(v') | \bar{h}_{v'}(0) \not{t}_+(1 - \gamma^5) h_v(0) | b(v) \rangle, \end{aligned} \quad (\text{C.7})$$

with $\omega \equiv v \cdot v' = (1 + z)/(2\sqrt{z})$, and in agreement with the QCD result (see e.g. (100) in Ref. [43]). For the other two diagrams the UV poles are

$$\begin{aligned} I_{Sb}^{\text{UV}} &= -\frac{\alpha_{\text{em}}}{4\pi} Q_d Q_L \left(\frac{1}{\epsilon^2} + \frac{2}{\epsilon} \ln \frac{\mu}{-\delta_{\bar{c}}} \right) \langle c(v') | \bar{h}_{v'}(0) \not{t}_+(1 - \gamma^5) h_v(0) | b(v) \rangle, \\ I_{Sc}^{\text{UV}} &= +\frac{\alpha_{\text{em}}}{4\pi} Q_u Q_L \left(\frac{1}{\epsilon^2} + \frac{2}{\epsilon} \ln \frac{\mu}{z\delta_{\bar{c}}} \right) \langle c(v') | \bar{h}_{v'}(0) \not{t}_+(1 - \gamma^5) h_v(0) | b(v) \rangle, \end{aligned} \quad (\text{C.8})$$

with $\text{Im}[\delta_{\bar{c}}] > 0$, and I_{Sb}^{UV} is the diagram where the photon interacts with the b quark, while I_{Sc}^{UV} the one where the photon interacts with the charm.

C.2 Convoluted Kernels

The convoluted one-loop QED hard-scattering kernels are defined as

$$\int_0^1 du T^{(*)^{(1)}}(u, z) \phi_L(u) = \sum_{k=0}^2 a_k^L(\mu) \left[V_{k-}^{(1)}(z) \pm \sqrt{z} V_{k+}^{(1)}(z) \right] \equiv \sum_{k=0}^2 a_k^L(\mu) V_k^{(*)^{(1)}}(z), \quad (\text{C.9})$$

where the hard-scattering kernel $T^{(1)}(u, z)$ can be found in (6.51), while the decomposition of the LCDA in Gegenbauer moments in (3.6). With the logarithms defined in (6.30), we get

$$\begin{aligned} V_{0-}^{(1)}(z) = & -\frac{5L_b}{3} - \frac{2L_\nu}{3} - \frac{2(2z^3 - 6z^2 - 6z + 1)}{3(z-1)^3} \text{Li}_2(z) \\ & - \frac{2(z-3)z^2}{3(z-1)^3} \ln^2 z + \frac{4(z^3 + (-3 - i\pi)z^2 + 3i\pi z + z + 1)z}{3(z-1)^3} \ln z \\ & + \frac{-4z^4 + 15z^3 - 2z^2 + 8z + 1}{3(z-1)^2 z} \ln(1-z) \\ & + \frac{24i\pi z^4 + 4(-19 - 29i\pi + \pi^2)z^3 + 3(45 + 52i\pi - 4\pi^2)z^2}{18(z-1)^3} \\ & + \frac{-6(25 + 18i\pi + 2\pi^2)z + 2\pi^2 + 44i\pi + 91}{18(z-1)^3}, \end{aligned} \quad (\text{C.10})$$

$$\begin{aligned} V_{1-}^{(1)}(z) = & -\frac{L_b}{2} + \frac{2z(8z^2 + 12z + 5)}{(z-1)^4} \text{Li}_2(z) + \frac{2z^2(4z + 3)}{(z-1)^4} \ln^2 z \\ & + \frac{2z(-5z^3 + 6i(4\pi + 5i)z^2 + 3(11 + 6i\pi)z + 2)}{3(z-1)^4} \ln z \\ & + \frac{(23z^3 + 145z^2 + 127z + 5)}{6(z-1)^3} \ln(1-z) \\ & - \frac{101z^4 + 1688z^3 + 54z^2 + 24\pi^2(8z^2 + 12z + 5)z}{72(z-1)^4} \\ & - \frac{24i\pi(11z^4 + 56z^3 - 60z^2 - 8z + 1) - 1976z + 133}{72(z-1)^4}, \end{aligned} \quad (\text{C.11})$$

$$\begin{aligned} V_{2-}^{(1)}(z) = & -\frac{3L_b}{5} + \frac{12z(4z^2 + 6z + 1)}{(z-1)^5} \text{Li}_2(z) + \frac{12z^2(z+1)}{(z-1)^5} \ln^2 z \\ & - \frac{4z(z^3 + (9 - 6i\pi)z^2 + (-9 - 6i\pi)z - 1)}{(z-1)^5} \ln z \end{aligned}$$

$$\begin{aligned}
& + \frac{(3z^4 + 23z^3 + 463z^2 + 163z + 8)}{5(z-1)^4} \ln(1-z) \\
& + \frac{-861z^5 + 1580z^4 - 33610z^3 + 27060z^2 - 600\pi^2(4z^2 + 6z + 1)z}{300(z-1)^5} \\
& + \frac{-120i\pi(z^5 + 5z^4 + 100z^3 - 100z^2 - 5z - 1) + 5095z + 736}{300(z-1)^5}, \quad (C.12)
\end{aligned}$$

$$\begin{aligned}
V_{0+}^{(1)}(z) &= \frac{2(4z^2 + 10z + 1)}{3(z-1)^3} \text{Li}_2(z) + \frac{4z(z+2)}{3(z-1)^3} \ln^2 z \\
& + \frac{4((-5 + 2i\pi)z^2 + (4 + 4i\pi)z + 1)}{3(z-1)^3} \ln z + \frac{(20z^3 + 12z^2 - 3z + 1)}{3(z-1)^2 z^2} \ln(1-z) \\
& + \frac{-(93 + 120i\pi + 8\pi^2)z^3 + 4\pi(-5\pi + 24i)z^2 + (99 + 24i\pi - 2\pi^2)z - 6}{18(z-1)^3 z}, \quad (C.13)
\end{aligned}$$

$$\begin{aligned}
V_{1+}^{(1)}(z) &= -\frac{2(4z^3 + 22z^2 + 13z + 1)}{(z-1)^4} \text{Li}_2(z) - \frac{4z(z^2 + 5z + 2)}{(z-1)^4} \ln^2 z \\
& + \frac{4((19 - 6i\pi)z^3 + (9 - 30i\pi)z^2 + (-27 - 12i\pi)z - 1)}{3(z-1)^4} \ln z \\
& - \frac{77z^2 + 140z + 23}{3(z-1)^3} \ln(1-z) + \frac{259z^3 + 771z^2 + 6\pi^2(4z^3 + 22z^2 + 13z + 1)}{18(z-1)^4} \\
& + \frac{24i\pi(19z^3 + 9z^2 - 27z - 1) - 879z - 151}{18(z-1)^4}, \quad (C.14)
\end{aligned}$$

$$\begin{aligned}
V_{2+}^{(1)}(z) &= \frac{4(4z^4 + 42z^3 + 60z^2 + 18z + 1)}{(z-1)^5} \text{Li}_2(z) + \frac{8z(z^3 + 10z^2 + 12z + 2)}{(z-1)^5} \ln^2 z \\
& + \frac{4((-45 + 12i\pi)z^4 + 8i(15\pi + 17i)z^3 + 36(3 + 4i\pi)z^2 + 24(3 + i\pi)z + 1)}{3(z-1)^5} \ln z \\
& + \frac{(181z^3 + 797z^2 + 473z + 49)}{3(z-1)^4} \ln(1-z) + \frac{-1003z^4 - 8068z^3 + 1602z^2}{36(z-1)^5} \\
& + \frac{-2\pi^2(4z^4 + 42z^3 + 60z^2 + 18z + 1) - 4i\pi(45z^4 + 136z^3 - 108z^2 - 72z - 1)}{3(z-1)^5} \\
& + \frac{7012z + 457}{36(z-1)^5}. \quad (C.15)
\end{aligned}$$

Appendix D

Pion and Proton Decay Matrix Elements

In this appendix we rederive known results for the matrix elements of local operators between an hadronic state and the vacuum. In particular we consider the two relevant cases of a pseudoscalar meson and a proton which we used in the calculations of Chapter 8.

D.1 Pseudoscalar Meson

We consider the positively charged pion as an example for a generic pseudoscalar meson. We would like to parametrize the matrix element of the local (i.e. evaluated at $x = 0$) field product $\bar{u}_\alpha d_\beta$ between the vacuum and the π^+ state in terms of the general Dirac structures

$$M_{\beta\alpha}(p) \equiv \langle \pi^+(p) | \bar{u}_\alpha d_\beta | 0 \rangle = S \mathbb{1}_{\beta\alpha} + V \not{p}_{\beta\alpha} + P \gamma_{\beta\alpha}^5 + A [\not{p} \gamma^5]_{\beta\alpha}, \quad (\text{D.1})$$

where the antisymmetric tensor term with $\sigma_{\mu\nu}$ vanishes since there is only one Lorentz vector to contract the indices.

To further constrain the basis, we then apply a parity transformation

$$\begin{aligned} M_{\beta\alpha}(p) &= \langle \pi^+(p) | P^{-1} P \bar{u}_\alpha P^{-1} P d_\beta P^{-1} P | 0 \rangle \\ &= -\langle \pi^+(\tilde{p}) | [\bar{u} \gamma^0]_\alpha [\gamma^0 d]_\beta | 0 \rangle = -[\gamma^0 M(\tilde{p}) \gamma^0]_{\beta\alpha}, \end{aligned} \quad (\text{D.2})$$

using the fact that pseudoscalar mesons have negative parity and defining $\tilde{p}^\mu = (p^0, -\vec{p})$. For the condition (D.2) to be satisfied, we need $S = 0$ and $V = 0$. The matrix element is usually written in terms of the meson decay constant, defined by

$$\langle \pi^+(p) | \bar{u}(x) \gamma^\mu \gamma^5 d(x) | 0 \rangle = -i f_\pi p^\mu e^{ip \cdot x}, \quad (\text{D.3})$$

implying $A = \frac{i}{4} f_\pi$. To see that f_π is the only independent non-perturbative parameter we take the derivative of (D.3) on both sides, and apply the equation-of-motion of the fields

$$\langle \pi^+(p) | \bar{u}(x) (\overleftarrow{\not{D}} \gamma^5 - \gamma^5 \not{D}) d(x) | 0 \rangle = i(m_d + m_u) \langle \pi^+(p) | \bar{u}(x) \gamma^5 d(x) | 0 \rangle = f_\pi m_\pi^2 e^{ip \cdot x}, \quad (\text{D.4})$$

giving

$$\langle \pi^+(p) | \bar{u}(x) \gamma^5 d(x) | 0 \rangle = -i f_\pi \mu_\pi e^{ip \cdot x}, \quad (\text{D.5})$$

where $\mu_\pi = m_\pi^2 / (m_d + m_u)$. From this relation we get $P = -\frac{i}{4} f_\pi \mu_\pi$. Since the meson is a colour singlet, for uncontracted colour indices the matrix element has to be proportional to δ^{ab} . Therefore the final result for the matrix element is

$$\langle \pi^+(p) | \bar{u}_\alpha^a(0) d_\beta^b(0) | 0 \rangle = \frac{i \delta^{ab}}{4 N_c} f_\pi (\not{p} \gamma^5 - \mu_\pi \gamma^5)_{\beta\alpha}. \quad (\text{D.6})$$

We recall that the expression of μ_π applies also to the neutral pion, contrary to the naive expectation (see Section 3.7.2 of Ref. [71]).

D.2 Proton

We now turn to the proton decay matrix element. It can be parametrized as

$$G_{\alpha\beta\gamma}(p) \equiv \langle 0 | \varepsilon^{abc} \tilde{u}_\alpha^a u_\beta^b d_\gamma^c | p(p) \rangle = \sum_{i,j} f^{ij} M_{\beta\alpha}^i(p) [\Gamma^j u_p(p)]_\gamma, \quad (\text{D.7})$$

where we denote the proton spinor with $u_p(p)$ while i, j label all the possible independent Dirac structures, as done in Section D.1

$$\begin{aligned} \Gamma^j &= \{ \mathbb{1}, \gamma^5, \gamma_\mu, i \gamma_\mu \gamma^5, \sigma_{\mu\nu} \}, \\ M^i(p) &= \{ \mathbb{1}, \gamma^5, \not{p}, \not{p} \gamma^5, \gamma^\mu, \gamma^\mu \gamma^5, \sigma^{\mu\nu}, p_\nu \sigma^{\mu\nu}, \varepsilon^{\mu\nu\rho\sigma} \sigma_{\rho\sigma} \}, \end{aligned} \quad (\text{D.8})$$

keeping in mind that the contraction between M^i and Γ^j must be a Lorentz scalar. We stress that Γ^j is independent of p since we are able to use the equation-of-motion of the spinor $u_p(p)$. In complete generality, each term is multiplied by a non-perturbative parameter f^{ij} . Notice that in (D.7) one could also expect further terms with permuted indices α, β, γ on the right-hand side. Nevertheless, those terms can be reabsorbed in the present term by using the closure relation (i.e. Fierz transformation)

$$\delta_{\alpha\beta} \delta_{\gamma\delta} = \frac{1}{4} \sum_{j \neq \sigma_{\mu\nu}} \Gamma_{\alpha\delta}^j \Gamma_{\gamma\beta}^j + \frac{1}{8} [\sigma^{\mu\nu}]_{\alpha\delta} [\sigma_{\mu\nu}]_{\gamma\beta}, \quad (\text{D.9})$$

where the Lorentz indices are contracted between the two Γ^j .

Similarly to Section D.1 we can constrain the building blocks through a parity transformation, by inserting PP^{-1} between the fields in the matrix element defining $G_{\alpha\beta\gamma}$. Using $u_p(\tilde{p}) = \gamma^0 u_p(p)$, we find

$$M_{\beta\alpha}^i(p) [\Gamma^j u(p)]_\gamma = -[\gamma^0 M^i(\tilde{p}) \gamma^0]_{\beta\alpha} [\gamma^0 \Gamma^j \gamma^0 u_p(p)]_\gamma, \quad (\text{D.10})$$

where the relative minus sign comes from the parity transformation on the field \tilde{u} . Moreover we can use the fact that $G_{\alpha\beta\gamma}$ contains two identical anticommuting up-quark fields, which implies the relation

$$G_{\alpha\beta\gamma} = \mathcal{C}_{\alpha\rho} G_{\sigma\rho\gamma} \mathcal{C}_{\sigma\beta}, \quad (\text{D.11})$$

with the charge conjugation matrix \mathcal{C} obeying the properties (2.129). Since the Dirac structures labelled by j are independent, we can write

$$M^i(p) = \mathcal{C}M^i(p)^T\mathcal{C}, \quad (\text{D.12})$$

forcing M^i in (D.8) to be either the vector or the tensor Dirac structures.

We are ready to exploit the conditions (D.10) and (D.12) to restrict the basis of allowed Dirac structures contributing to $G_{\alpha\beta\gamma}(p)$. The elements of $M^i_{\beta\alpha}(p)$ satisfying the constraint (D.12) are

$$\not{p}, \gamma^\mu, p_\nu\sigma^{\mu\nu}, \sigma^{\mu\nu}, \varepsilon^{\mu\nu\rho\sigma}\sigma_{\mu\nu}. \quad (\text{D.13})$$

Lets now, for each of these structures, identify the possible Γ^j fulfilling the constraint (D.10) and forming a Lorentz scalar with $M^i(p)$. Using $\not{p} = \not{p}^\dagger$ and the short-hand $M^i(p) \otimes \Gamma^j = M^i_{\beta\alpha}(p)\Gamma^j_{\gamma\delta}$, we find that for each allowed $M^i(p)$ there is only one allowed Γ^j , namely

$$M^i(p) \otimes \Gamma^j = \{\not{p} \otimes \gamma^5, \gamma^\mu \otimes \gamma_\mu\gamma^5, p_\nu\sigma^{\mu\nu} \otimes \gamma_\mu\gamma^5, \varepsilon^{\mu\nu\rho\sigma}\sigma_{\mu\nu} \otimes \sigma_{\rho\sigma}\}. \quad (\text{D.14})$$

Therefore, after renaming the f_{ij} , the general decomposition for the proton projector reads

$$G_{\alpha\beta\gamma}(p) = V_P\not{p}_{\beta\alpha}[\gamma^5u(p)]_\gamma + \left(V_A\gamma_\rho + T_AP^\sigma\sigma_{\rho\sigma}\right)_{\beta\alpha}[\gamma^\rho\gamma^5u(p)]_\gamma + T_T[\sigma_{\rho\sigma}]_{\beta\alpha}[\sigma^{\rho\sigma}\gamma^5u(p)]_\gamma, \quad (\text{D.15})$$

where we used

$$\frac{i}{2}\varepsilon^{\mu\nu\rho\sigma}\sigma_{\rho\sigma} = \sigma^{\mu\nu}\gamma^5. \quad (\text{D.16})$$

The structures agree with Eq. (3.11) of [135].

The parameters V_P , V_A , T_A and T_T are related to the commonly used decay constants $f_p, f_p^T, \lambda_1, \lambda_2$ computed by the RQCD lattice collaboration [132] (see numerical values in (A.16)) by

$$\begin{aligned} V_P &= -\frac{f_p}{4}, & V_A &= \frac{m_p}{16}(\lambda_1 - f_p), \\ T_A &= -\frac{i}{4}f_p^T, & T_T &= \frac{m_p}{96}(\lambda_2 - 6f_p^T). \end{aligned} \quad (\text{D.17})$$

Isospin symmetry implies $f_p^T = f_p$, reducing to only three the number of independent parameters. The full proton matrix projector, in terms of the three parameters, is hence given by

$$\begin{aligned} G_{\alpha\beta\gamma}(p) &= -\frac{f_p}{4}\left(\not{p}_{\beta\alpha}[\gamma^5u_p(p)]_\gamma + ip^\nu[\sigma_{\rho\nu}]_{\beta\alpha}[\gamma^\rho\gamma^5u_p(p)]_\gamma\right) \\ &+ \frac{m_p}{16}(\lambda_1 - f_p)[\gamma_\rho]_{\beta\alpha}[\gamma^\rho\gamma^5u_p(p)]_\gamma + \frac{m_p}{96}(\lambda_2 - 6f_p)[\sigma_{\rho\sigma}]_{\beta\alpha}[\sigma^{\rho\sigma}\gamma^5u_p(p)]_\gamma. \end{aligned} \quad (\text{D.18})$$

Bibliography

- [1] S. L. Glashow, *Partial Symmetries of Weak Interactions*, *Nucl. Phys.* **22** (1961) 579–588.
- [2] S. Weinberg, *A Model of Leptons*, *Phys. Rev. Lett.* **19** (1967) 1264–1266.
- [3] A. Salam, *Weak and Electromagnetic Interactions*, *Conf. Proc. C* **680519** (1968) 367–377.
- [4] G. 't Hooft and M. J. G. Veltman, *Regularization and Renormalization of Gauge Fields*, *Nucl. Phys. B* **44** (1972) 189–213.
- [5] ATLAS collaboration, G. Aad et al., *Observation of a new particle in the search for the Standard Model Higgs boson with the ATLAS detector at the LHC*, *Phys. Lett. B* **716** (2012) 1–29, [1207.7214].
- [6] CMS collaboration, S. Chatrchyan et al., *Observation of a New Boson at a Mass of 125 GeV with the CMS Experiment at the LHC*, *Phys. Lett. B* **716** (2012) 30–61, [1207.7235].
- [7] D. Clowe, M. Bradac, A. H. Gonzalez, M. Markevitch, S. W. Randall, C. Jones et al., *A direct empirical proof of the existence of dark matter*, *Astrophys. J. Lett.* **648** (2006) L109–L113, [astro-ph/0608407].
- [8] B. T. Cleveland, T. Daily, R. Davis, Jr., J. R. Distel, K. Lande, C. K. Lee et al., *Measurement of the solar electron neutrino flux with the Homestake chlorine detector*, *Astrophys. J.* **496** (1998) 505–526.
- [9] SUPER-KAMIOKANDE collaboration, Y. Fukuda et al., *Measurements of the solar neutrino flux from Super-Kamiokande's first 300 days*, *Phys. Rev. Lett.* **81** (1998) 1158–1162, [hep-ex/9805021].
- [10] D. J. Gross and F. Wilczek, *Ultraviolet Behavior of Nonabelian Gauge Theories*, *Phys. Rev. Lett.* **30** (1973) 1343–1346.
- [11] BABAR collaboration, D. Boutigny et al., *The BABAR physics book: Physics at an asymmetric B factory*. SLAC, 10, 1998, 10.2172/979931.

- [12] BABAR, BELLE collaboration, A. J. Bevan et al., *The Physics of the B Factories*, *Eur. Phys. J. C* **74** (2014) 3026, [1406.6311].
- [13] BELLE-II collaboration, W. Altmannshofer et al., *The Belle II Physics Book*, *PTEP* **2019** (2019) 123C01, [1808.10567].
- [14] LHCb collaboration, S. Amato et al., *LHCb technical proposal: A Large Hadron Collider Beauty Experiment for Precision Measurements of CP Violation and Rare Decays*, .
- [15] J. Albrecht, D. van Dyk and C. Langenbruch, *Flavour anomalies in heavy quark decays*, *Prog. Part. Nucl. Phys.* **120** (2021) 103885, [2107.04822].
- [16] M. Bordone, N. Gubernari, T. Huber, M. Jung and D. van Dyk, *A puzzle in $\bar{B}_{(s)}^0 \rightarrow D_{(s)}^{(*)+} \{\pi^-, K^-\}$ decays and extraction of the f_s/f_d fragmentation fraction*, *Eur. Phys. J. C* **80** (2020) 951, [2007.10338].
- [17] C. Cornella, D. A. Faroughy, J. Fuentes-Martin, G. Isidori and M. Neubert, *Reading the footprints of the B-meson flavor anomalies*, *JHEP* **08** (2021) 050, [2103.16558].
- [18] B. Capdevila, A. Crivellin and J. Matias, *Review of Semileptonic B Anomalies*, *Eur. Phys. J. ST* **1** (2023) 20, [2309.01311].
- [19] LHCb collaboration, R. Aaij et al., *Test of lepton universality in beauty-quark decays*, *Nature Phys.* **18** (2022) 277–282, [2103.11769].
- [20] LHCb collaboration, R. Aaij et al., *Test of lepton universality in $b \rightarrow s\ell^+\ell^-$ decays*, *Phys. Rev. Lett.* **131** (2023) 051803, [2212.09152].
- [21] LHCb collaboration, R. Aaij et al., *Measurement of lepton universality parameters in $B^+ \rightarrow K^+\ell^+\ell^-$ and $B^0 \rightarrow K^{*0}\ell^+\ell^-$ decays*, *Phys. Rev. D* **108** (2023) 032002, [2212.09153].
- [22] HFLAV collaboration, Y. S. Amhis et al., *Averages of b-hadron, c-hadron, and τ -lepton properties as of 2021*, *Phys. Rev. D* **107** (2023) 052008, [2206.07501].
- [23] F.-M. Cai, W.-J. Deng, X.-Q. Li and Y.-D. Yang, *Probing new physics in class-I B-meson decays into heavy-light final states*, *JHEP* **10** (2021) 235, [2103.04138].
- [24] PARTICLE DATA GROUP collaboration, R. L. Workman and Others, *Review of Particle Physics*, *PTEP* **2022** (2022) 083C01.
- [25] A. A. Petrov and A. E. Blechman, *Effective Field Theories*. WSP, 2016, 10.1142/8619.
- [26] A. V. Manohar, *Introduction to Effective Field Theories*, 1804.05863.

- [27] T. Cohen, *As Scales Become Separated: Lectures on Effective Field Theory*, PoS **TASI2018** (2019) 011, [1903.03622].
- [28] M. Beneke, G. Finauri, K. K. Vos and Y. Wei, *QCD light-cone distribution amplitudes of heavy mesons from boosted HQET*, *JHEP* **09** (2023) 066, [2305.06401].
- [29] M. Beneke, P. Böer, G. Finauri and K. K. Vos, *QED factorization of two-body non-leptonic and semi-leptonic B to charm decays*, *JHEP* **10** (2021) 223, [2107.03819].
- [30] M. Beneke, G. Finauri and A. A. Petrov, *Indirect constraints on third generation baryon number violation*, 2404.09642.
- [31] G. Finauri and P. Gambino, *The q^2 moments in inclusive semileptonic B decays*, *JHEP* **02** (2024) 206, [2310.20324].
- [32] BELLE collaboration, R. van Tonder et al., *Measurements of q^2 Moments of Inclusive $B \rightarrow X_c \ell^+ \nu_\ell$ Decays with Hadronic Tagging*, *Phys. Rev. D* **104** (2021) 112011, [2109.01685].
- [33] BELLE-II collaboration, F. Abudinén et al., *Measurement of lepton mass squared moments in $B \rightarrow X_c \ell \nu \bar{\ell}$ decays with the Belle II experiment*, *Phys. Rev. D* **107** (2023) 072002, [2205.06372].
- [34] G. Buchalla, A. J. Buras and M. E. Lautenbacher, *Weak decays beyond leading logarithms*, *Rev. Mod. Phys.* **68** (1996) 1125–1144, [hep-ph/9512380].
- [35] E. Fermi, *Tentativo di una Teoria dei Raggi β* , *Nuovo Cim.* **11** (1934) 1–19.
- [36] K. G. Chetyrkin, M. Misiak and M. Munz, *Weak radiative B meson decay beyond leading logarithms*, *Phys. Lett. B* **400** (1997) 206–219, [hep-ph/9612313].
- [37] K. G. Chetyrkin, M. Misiak and M. Munz, *$|\Delta F| = 1$ nonleptonic effective Hamiltonian in a simpler scheme*, *Nucl. Phys. B* **520** (1998) 279–297, [hep-ph/9711280].
- [38] N. Cabibbo, *Unitary Symmetry and Leptonic Decays*, *Phys. Rev. Lett.* **10** (1963) 531–533.
- [39] M. Kobayashi and T. Maskawa, *CP Violation in the Renormalizable Theory of Weak Interaction*, *Prog. Theor. Phys.* **49** (1973) 652–657.
- [40] M. Gorbahn and U. Haisch, *Effective Hamiltonian for non-leptonic $|\Delta F| = 1$ decays at NNLO in QCD*, *Nucl. Phys. B* **713** (2005) 291–332, [hep-ph/0411071].
- [41] H. Georgi, *An Effective Field Theory for Heavy Quarks at Low-energies*, *Phys. Lett. B* **240** (1990) 447–450.

- [42] B. Grinstein, *The Static Quark Effective Theory*, *Nucl. Phys. B* **339** (1990) 253–268.
- [43] M. Neubert, *Heavy quark effective theory*, *Subnucl. Ser.* **34** (1997) 98–165, [[hep-ph/9610266](#)].
- [44] A. V. Manohar and M. B. Wise, *Heavy quark physics*, vol. 10. Cambridge University Press, 2000.
- [45] E. Eichten and B. R. Hill, *An Effective Field Theory for the Calculation of Matrix Elements Involving Heavy Quarks*, *Phys. Lett. B* **234** (1990) 511–516.
- [46] C. W. Bauer, S. Fleming and M. E. Luke, *Summing Sudakov logarithms in $B \rightarrow X_s \gamma$ in effective field theory.*, *Phys. Rev. D* **63** (2000) 014006, [[hep-ph/0005275](#)].
- [47] C. W. Bauer, S. Fleming, D. Pirjol and I. W. Stewart, *An Effective field theory for collinear and soft gluons: Heavy to light decays*, *Phys. Rev. D* **63** (2001) 114020, [[hep-ph/0011336](#)].
- [48] C. W. Bauer and I. W. Stewart, *Invariant operators in collinear effective theory*, *Phys. Lett. B* **516** (2001) 134–142, [[hep-ph/0107001](#)].
- [49] C. W. Bauer, D. Pirjol and I. W. Stewart, *Soft collinear factorization in effective field theory*, *Phys. Rev. D* **65** (2002) 054022, [[hep-ph/0109045](#)].
- [50] M. Beneke, A. P. Chapovsky, M. Diehl and T. Feldmann, *Soft collinear effective theory and heavy to light currents beyond leading power*, *Nucl. Phys. B* **643** (2002) 431–476, [[hep-ph/0206152](#)].
- [51] M. Beneke and T. Feldmann, *Multipole expanded soft collinear effective theory with nonAbelian gauge symmetry*, *Phys. Lett. B* **553** (2003) 267–276, [[hep-ph/0211358](#)].
- [52] R. J. Hill and M. Neubert, *Spectator interactions in soft collinear effective theory*, *Nucl. Phys. B* **657** (2003) 229–256, [[hep-ph/0211018](#)].
- [53] T. Becher, A. Broggio and A. Ferroglia, *Introduction to Soft-Collinear Effective Theory*, vol. 896. Springer, 2015, 10.1007/978-3-319-14848-9.
- [54] T. Becher, *Soft-Collinear Effective Theory*, 1803.04310.
- [55] M. Beneke, P. Hager and R. Szafron, *Soft-Collinear Gravity and Soft Theorems*, 2210.09336.
- [56] V. A. Smirnov, *Asymptotic expansions in momenta and masses and calculation of Feynman diagrams*, *Mod. Phys. Lett. A* **10** (1995) 1485–1500, [[hep-th/9412063](#)].
- [57] M. Beneke and V. A. Smirnov, *Asymptotic expansion of Feynman integrals near threshold*, *Nucl. Phys. B* **522** (1998) 321–344, [[hep-ph/9711391](#)].

- [58] T. Becher and M. Neubert, *Drell-Yan Production at Small q_T , Transverse Parton Distributions and the Collinear Anomaly*, *Eur. Phys. J. C* **71** (2011) 1665, [1007.4005].
- [59] J.-Y. Chiu, A. Jain, D. Neill and I. Z. Rothstein, *A Formalism for the Systematic Treatment of Rapidity Logarithms in Quantum Field Theory*, *JHEP* **05** (2012) 084, [1202.0814].
- [60] T. Becher and G. Bell, *Analytic Regularization in Soft-Collinear Effective Theory*, *Phys. Lett. B* **713** (2012) 41–46, [1112.3907].
- [61] M. Beneke, M. Garny, R. Szafron and J. Wang, *Anomalous dimension of subleading-power N -jet operators. Part II*, *JHEP* **11** (2018) 112, [1808.04742].
- [62] S. Fleming, A. H. Hoang, S. Mantry and I. W. Stewart, *Jets from massive unstable particles: Top-mass determination*, *Phys. Rev. D* **77** (2008) 074010, [hep-ph/0703207].
- [63] S. Fleming, A. H. Hoang, S. Mantry and I. W. Stewart, *Top Jets in the Peak Region: Factorization Analysis with NLL Resummation*, *Phys. Rev. D* **77** (2008) 114003, [0711.2079].
- [64] L. Dai, C. Kim and A. K. Leibovich, *Heavy quark jet production near threshold*, *JHEP* **09** (2021) 148, [2104.14707].
- [65] A. Hardmeier, E. Lunghi, D. Pirjol and D. Wyler, *Subleading collinear operators and their matrix elements*, *Nucl. Phys. B* **682** (2004) 150–182, [hep-ph/0307171].
- [66] M. E. Luke and A. V. Manohar, *Reparametrization invariance constraints on heavy particle effective field theories*, *Phys. Lett. B* **286** (1992) 348–354, [hep-ph/9205228].
- [67] A. V. Manohar, T. Mehen, D. Pirjol and I. W. Stewart, *Reparameterization invariance for collinear operators*, *Phys. Lett. B* **539** (2002) 59–66, [hep-ph/0204229].
- [68] B. Grzadkowski, M. Iskrzynski, M. Misiak and J. Rosiek, *Dimension-Six Terms in the Standard Model Lagrangian*, *JHEP* **10** (2010) 085, [1008.4884].
- [69] J. D. Bjorken and S. D. Drell, *Relativistic Quantum Mechanics*. International Series In Pure and Applied Physics. McGraw-Hill, New York, 1965.
- [70] M. Beneke, G. Buchalla, M. Neubert and C. T. Sachrajda, *QCD factorization for $B \rightarrow \pi\pi$ decays: Strong phases and CP violation in the heavy quark limit*, *Phys. Rev. Lett.* **83** (1999) 1914–1917, [hep-ph/9905312].
- [71] M. Beneke, G. Buchalla, M. Neubert and C. T. Sachrajda, *QCD factorization for exclusive, nonleptonic B meson decays: General arguments and the case of heavy light final states*, *Nucl. Phys. B* **591** (2000) 313–418, [hep-ph/0006124].

- [72] M. Beneke, G. Buchalla, M. Neubert and C. T. Sachrajda, *QCD factorization in $B \rightarrow \pi K$, $\pi\pi$ decays and extraction of Wolfenstein parameters*, *Nucl. Phys. B* **606** (2001) 245–321, [[hep-ph/0104110](#)].
- [73] G. P. Lepage and S. J. Brodsky, *Exclusive Processes in Quantum Chromodynamics: Evolution Equations for Hadronic Wave Functions and the Form-Factors of Mesons*, *Phys. Lett.* **87B** (1979) 359–365.
- [74] G. P. Lepage and S. J. Brodsky, *Exclusive Processes in Perturbative Quantum Chromodynamics*, *Phys. Rev.* **D22** (1980) 2157.
- [75] A. V. Efremov and A. V. Radyushkin, *Factorization and Asymptotical Behavior of Pion Form-Factor in QCD*, *Phys. Lett.* **94B** (1980) 245–250.
- [76] V. M. Braun, A. N. Manashov, S. Moch and M. Strohmaier, *Three-loop evolution equation for flavor-nonsinglet operators in off-forward kinematics*, *JHEP* **06** (2017) 037, [[1703.09532](#)].
- [77] B. O. Lange and M. Neubert, *Renormalization group evolution of the B meson light cone distribution amplitude*, *Phys. Rev. Lett.* **91** (2003) 102001, [[hep-ph/0303082](#)].
- [78] V. M. Braun, Y. Ji and A. N. Manashov, *Two-loop evolution equation for the B-meson distribution amplitude*, *Phys. Rev. D* **100** (2019) 014023, [[1905.04498](#)].
- [79] Z. L. Liu and M. Neubert, *Two-Loop Radiative Jet Function for Exclusive B-Meson and Higgs Decays*, *JHEP* **06** (2020) 060, [[2003.03393](#)].
- [80] A. M. Galda, M. Neubert and X. Wang, *Factorization and Sudakov resummation in leptonic radiative B decay — a reappraisal*, *JHEP* **07** (2022) 148, [[2203.08202](#)].
- [81] S. J. Lee and M. Neubert, *Model-independent properties of the B-meson distribution amplitude*, *Phys. Rev. D* **72** (2005) 094028, [[hep-ph/0509350](#)].
- [82] A. G. Grozin and M. Neubert, *Asymptotics of heavy meson form-factors*, *Phys. Rev. D* **55** (1997) 272–290, [[hep-ph/9607366](#)].
- [83] M. Beneke, P. Böer, J.-N. Toelstede and K. K. Vos, *Light-cone distribution amplitudes of light mesons with QED effects*, *JHEP* **11** (2021) 059, [[2108.05589](#)].
- [84] S. Ishaq, Y. Jia, X. Xiong and D.-S. Yang, *Factorization Theorem Connecting the Light-Cone Distribution Amplitudes of Heavy-Flavor Mesons in QCD and Heavy-Quark Effective Theory*, *Phys. Rev. Lett.* **125** (2020) 132001, [[1905.06930](#)].
- [85] S. Zhao, *Heavy quark expansion for heavy-light light-cone operators*, *Phys. Rev. D* **101** (2020) 071503, [[1910.03470](#)].
- [86] M. Beneke, V. M. Braun, Y. Ji and Y.-B. Wei, *Radiative leptonic decay $B \rightarrow \gamma \ell \nu_\ell$ with subleading power corrections*, *JHEP* **07** (2018) 154, [[1804.04962](#)].

- [87] M. Beneke, P. Böer, J.-N. Toelstede and K. K. Vos, *Light-cone distribution amplitudes of heavy mesons with QED effects*, *JHEP* **08** (2022) 020, [2204.09091].
- [88] T. Feldmann, B. O. Lange and Y.-M. Wang, *B -meson light-cone distribution amplitude: Perturbative constraints and asymptotic behavior in dual space*, *Phys. Rev. D* **89** (2014) 114001, [1404.1343].
- [89] G. Bell, T. Feldmann, Y.-M. Wang and M. W. Y. Yip, *Light-Cone Distribution Amplitudes for Heavy-Quark Hadrons*, *JHEP* **11** (2013) 191, [1308.6114].
- [90] Y. Grossman, M. König and M. Neubert, *Exclusive Radiative Decays of W and Z Bosons in QCD Factorization*, *JHEP* **04** (2015) 101, [1501.06569].
- [91] S. Ishaq, Y. Jia, X. Xiong and D.-S. Yang, *W radiative decay to heavy-light mesons in HQET factorization through $\mathcal{O}(\alpha_s)$* , *Phys. Rev. D* **100** (2019) 054027, [1903.12627].
- [92] A. Pak and A. Smirnov, *Geometric approach to asymptotic expansion of Feynman integrals*, *Eur. Phys. J. C* **71** (2011) 1626, [1011.4863].
- [93] B. Jantzen, A. V. Smirnov and V. A. Smirnov, *Expansion by regions: revealing potential and Glauber regions automatically*, *Eur. Phys. J. C* **72** (2012) 2139, [1206.0546].
- [94] M. Beneke, T. Huber and X.-Q. Li, *NNLO vertex corrections to non-leptonic B decays: Tree amplitudes*, *Nucl. Phys. B* **832** (2010) 109–151, [0911.3655].
- [95] T. Huber, S. Kräinkl and X.-Q. Li, *Two-body non-leptonic heavy-to-heavy decays at NNLO in QCD factorization*, *JHEP* **09** (2016) 112, [1606.02888].
- [96] N. Gubernari, A. Kokulu and D. van Dyk, *B \rightarrow P and B \rightarrow V Form Factors from B-Meson Light-Cone Sum Rules beyond Leading Twist*, *JHEP* **01** (2019) 150, [1811.00983].
- [97] M. Beneke, C. Bobeth and R. Szafron, *Enhanced electromagnetic correction to the rare B-meson decay $B_{s,d} \rightarrow \mu^+ \mu^-$* , *Phys. Rev. Lett.* **120** (2018) 011801, [1708.09152].
- [98] M. Beneke, C. Bobeth and R. Szafron, *Power-enhanced leading-logarithmic QED corrections to $B_q \rightarrow \mu^+ \mu^-$* , *JHEP* **10** (2019) 232, [1908.07011].
- [99] M. Beneke, P. Böer, J.-N. Toelstede and K. K. Vos, *QED factorization of non-leptonic B decays*, *JHEP* **11** (2020) 081, [2008.10615].
- [100] C. Cornella, M. König and M. Neubert, *Structure-dependent QED effects in exclusive B decays at subleading power*, *Phys. Rev. D* **108** (2023) L031502, [2212.14430].

- [101] P. Böer and T. Feldmann, *Structure-dependent QED effects in exclusive B-meson decays*, 2312.12885.
- [102] J. Fuentes-Martín, M. König, J. Pagès, A. E. Thomsen and F. Wilsch, *Evanescent operators in one-loop matching computations*, *JHEP* **02** (2023) 031, [2211.09144].
- [103] E. Baracchini and G. Isidori, *Electromagnetic corrections to non-leptonic two-body B and D decays*, *Phys. Lett. B* **633** (2006) 309–313, [hep-ph/0508071].
- [104] S. Weinberg, *The Quantum theory of fields. Vol. 1: Foundations*. Cambridge University Press, 6, 2005, 10.1017/CBO9781139644167.
- [105] RQCD collaboration, G. S. Bali, V. M. Braun, S. Bürger, M. Göckeler, M. Gruber, F. Hutzler et al., *Light-cone distribution amplitudes of pseudoscalar mesons from lattice QCD*, *JHEP* **08** (2019) 065, [1903.08038].
- [106] M. Neubert and B. Stech, *Nonleptonic weak decays of B mesons*, *Adv. Ser. Direct. High Energy Phys.* **15** (1998) 294–344, [hep-ph/9705292].
- [107] M. Beneke and T. Feldmann, *Symmetry breaking corrections to heavy to light B meson form-factors at large recoil*, *Nucl. Phys. B* **592** (2001) 3–34, [hep-ph/0008255].
- [108] P. Golonka and Z. Was, *PHOTOS Monte Carlo: A Precision tool for QED corrections in Z and W decays*, *Eur. Phys. J. C* **45** (2006) 97–107, [hep-ph/0506026].
- [109] G. Isidori, S. Nabeebaccus and R. Zwicky, *QED corrections in $\bar{B} \rightarrow \bar{K}\ell^+\ell^-$ at the double-differential level*, *JHEP* **12** (2020) 104, [2009.00929].
- [110] G. Isidori, D. Lancierini, S. Nabeebaccus and R. Zwicky, *QED in $\bar{B} \rightarrow \bar{K}\ell^+\ell^-$ LFU ratios: theory versus experiment, a Monte Carlo study*, *JHEP* **10** (2022) 146, [2205.08635].
- [111] A. D. Sakharov, *Violation of CP Invariance, C asymmetry, and baryon asymmetry of the universe*, *Pisma Zh. Eksp. Teor. Fiz.* **5** (1967) 32–35.
- [112] I. Baldes, N. F. Bell and R. R. Volkas, *Baryon Number Violating Scalar Diquarks at the LHC*, *Phys. Rev. D* **84** (2011) 115019, [1110.4450].
- [113] A. E. Nelson and H. Xiao, *Baryogenesis from B Meson Oscillations*, *Phys. Rev. D* **100** (2019) 075002, [1901.08141].
- [114] G. Elor, M. Escudero and A. Nelson, *Baryogenesis and Dark Matter from B Mesons*, *Phys. Rev. D* **99** (2019) 035031, [1810.00880].

- [115] R. Alonso, H.-M. Chang, E. E. Jenkins, A. V. Manohar and B. Shotwell, *Renormalization group evolution of dimension-six baryon number violating operators*, *Phys. Lett. B* **734** (2014) 302–307, [1405.0486].
- [116] W. Dekens and P. Stoffer, *Low-energy effective field theory below the electroweak scale: matching at one loop*, *JHEP* **10** (2019) 197, [1908.05295].
- [117] SUPER-KAMIOKANDE collaboration, V. Takhistov et al., *Search for Trilepton Nucleon Decay via $p \rightarrow e^+\nu\nu$ and $p \rightarrow \mu^+\nu\nu$ in the Super-Kamiokande Experiment*, *Phys. Rev. Lett.* **113** (2014) 101801, [1409.1947].
- [118] SUPER-KAMIOKANDE collaboration, A. Takenaka et al., *Search for proton decay via $p \rightarrow e^+\pi^0$ and $p \rightarrow \mu^+\pi^0$ with an enlarged fiducial volume in Super-Kamiokande I-IV*, *Phys. Rev. D* **102** (2020) 112011, [2010.16098].
- [119] SUPER-KAMIOKANDE collaboration, K. Abe et al., *Search for Nucleon Decay via $n \rightarrow \bar{\nu}\pi^0$ and $p \rightarrow \bar{\nu}\pi^+$ in Super-Kamiokande*, *Phys. Rev. Lett.* **113** (2014) 121802, [1305.4391].
- [120] U. Haisch and A. Hala, *Light-cone sum rules for proton decay*, *JHEP* **05** (2021) 258, [2103.13928].
- [121] SUPER-KAMIOKANDE collaboration, R. Matsumoto et al., *Search for proton decay via $p \rightarrow \mu^+K^0$ in 0.37 megaton-years exposure of Super-Kamiokande*, *Phys. Rev. D* **106** (2022) 072003, [2208.13188].
- [122] SUPER-KAMIOKANDE collaboration, K. Kobayashi et al., *Search for nucleon decay via modes favored by supersymmetric grand unification models in Super-Kamiokande-I*, *Phys. Rev. D* **72** (2005) 052007, [hep-ex/0502026].
- [123] A. B. Beneito, I. J. Gargalionis, J. Herrero-Garcia, A. Santamaria and M. A. Schmidt, *An EFT approach to baryon number violation: lower limits on the new physics scale and correlations between nucleon decay modes*, 2312.13361.
- [124] J. Gargalionis, J. Herrero-Garcia and M. A. Schmidt, *Model-independent estimates for loop-induced baryon-number-violating nucleon decays*, 2401.04768.
- [125] SUPER-KAMIOKANDE collaboration, K. Abe et al., *Search for proton decay via $p \rightarrow \nu K^+$ using 260 kiloton-year data of Super-Kamiokande*, *Phys. Rev. D* **90** (2014) 072005, [1408.1195].
- [126] BABAR collaboration, P. del Amo Sanchez et al., *Searches for the baryon- and lepton-number violating decays $B^0 \rightarrow \Lambda_c^+\ell^-$, $B^- \rightarrow \Lambda\ell^-$, and $B^- \rightarrow \bar{\Lambda}\ell^-$* , *Phys. Rev. D* **83** (2011) 091101, [1101.3830].
- [127] LHCb collaboration, R. Aaij et al., *Search for the baryon- and lepton-number violating decays $B^0 \rightarrow p\mu^-$ and $B_s^0 \rightarrow p\mu^-$* , *Phys. Rev. D* **108** (2023) 012021, [2210.10412].

- [128] F. Herren and M. Steinhauser, *Version 3 of RunDec and CRunDec*, *Comput. Phys. Commun.* **224** (2018) 333–345, [1703.03751].
- [129] D. Leljak, B. Melić and D. van Dyk, *The $\bar{B} \rightarrow \pi$ form factors from QCD and their impact on $|V_{ub}|$* , *JHEP* **07** (2021) 036, [2102.07233].
- [130] FLAVOUR LATTICE AVERAGING GROUP (FLAG) collaboration, Y. Aoki et al., *FLAG Review 2021*, *Eur. Phys. J. C* **82** (2022) 869, [2111.09849].
- [131] G. Bell and T. Feldmann, *Modelling light-cone distribution amplitudes from non-relativistic bound states*, *JHEP* **04** (2008) 061, [0802.2221].
- [132] RQCD collaboration, G. S. Bali et al., *Light-cone distribution amplitudes of octet baryons from lattice QCD*, *Eur. Phys. J. A* **55** (2019) 116, [1903.12590].
- [133] I. V. Anikin, V. M. Braun and N. Offen, *Nucleon Form Factors and Distribution Amplitudes in QCD*, *Phys. Rev. D* **88** (2013) 114021, [1310.1375].
- [134] S. Kränkl and A. Manashov, *Two-loop renormalization of three-quark operators in QCD*, *Phys. Lett. B* **703** (2011) 519–523, [1107.3718].
- [135] V. Braun, R. J. Fries, N. Mahnke and E. Stein, *Higher twist distribution amplitudes of the nucleon in QCD*, *Nucl. Phys. B* **589** (2000) 381–409, [hep-ph/0007279].

“Mo, sta fisica, co è c’saria?”
— *Nonna Franca*

Acknowledgements

First of all I would like to express my immense gratitude to Martin Beneke, for his brilliant guidance over these years. His endless passion was contagious, and our discussions were always pleasant, helpful and inspiring. My second big thank you goes to Matthias and Philipp, for their patience in answering too many questions, helping me growing in the context of physics, but, more importantly, for being invaluable friends.

Furthermore I would like to thank my collaborators Paolo Gambino, Alexey Petrov and Keri Vos, for showing me different ways of approaching and overcoming the difficulties of a given project. For a lot of interesting, helpful, diverse, light and funny discussions over lunch (and coffee/tea) I would like to thank collectively all the people that were part of T31 over these three and a half years.

My PhD in Munich could not have been more enjoyable, and this is undoubtedly because of my friends here: Javier, Andrea, Lollo, Mar, Nico, Konstantin, Raúl, Damiano, Matthias, Cesare, Giacomo, Francesco, Alberto. I could thank each of them for many specific reasons, but I’ll keep it simple, they already know! I also cannot avoid to thank Music, which is, and will always be, the best thing humans are capable of.

A warm thank you goes to my family, for never doubting on my life choices. The unfortunately too restricted time we spent together during these years was extremely restoring and priceless.

Finally, I thank Francesca, for all those long nights under pale neon lights, and the rest, which words cannot describe.